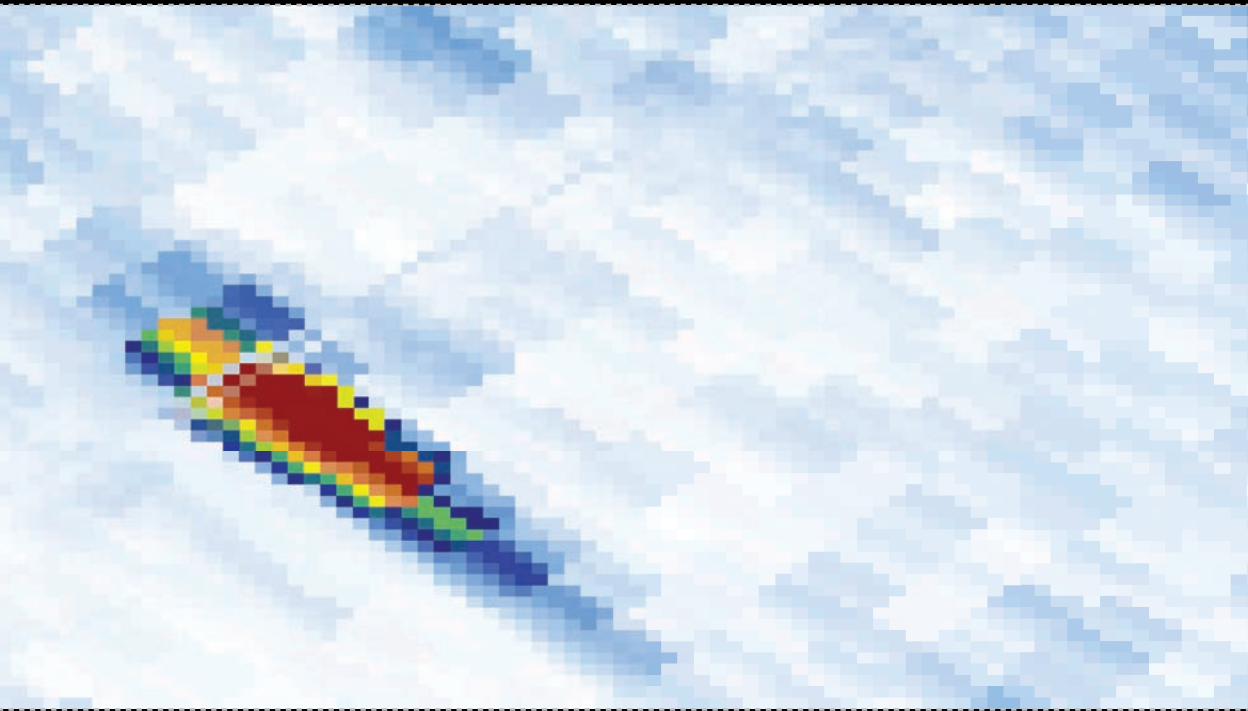


# INTRODUCTION TO **PHASED ARRAY** ULTRASONIC TECHNOLOGY APPLICATIONS



**ADVANCED PRACTICAL NDT SERIES**

**OLYMPUS<sup>®</sup>**



Introduction to Phased Array  
Ultrasonic Technology Applications  
Olympus Guideline





# Introduction to Phased Array Ultrasonic Technology Applications Olympus Guideline

Olympus

Advanced Practical NDT Series

*Introduction to Phased Array Ultrasonic Technology Applications: Olympus Guideline*

Series coordinator: Noël Dubé

Technical reviewers and advisers:

Dr. Michael D. C. Moles (Olympus, Canada)  
Colin R. Bird (TWI Ltd, UK)  
Pamela Herzog (USAF, USA)  
Tim Armitt (Lavender International Ltd., UK)  
Petru Ciorau (OPG, Canada)  
Ron Roberts (Iowa State University, USA)  
Mark Davis (Davis NDE, Inc.)

Layout, graphics, editing, proofreading, and indexing: Olympus Technical Communications Service.

Published by: Olympus, 48 Woerd Avenue, Waltham, MA 02453, USA

Marketing and distribution: Olympus

This guideline and the products and programs it describes are protected by the Copyright Law of the United States, by laws of other countries, and by international treaties, and therefore may not be reproduced in whole or in part, whether for sale or not, without the prior written consent from Olympus. Under copyright law, copying includes translation into another language or format.

The information contained in this document is subject to change or revision without notice.

Olympus part number: DUMG068D

© 2004, 2005, 2007, 2017 by Olympus  
All rights reserved. Published 2004.

Printed in the United States of America

Second printing 2005. Third printing 2007. Fourth printing 2017

ISBN 0-9735933-0-X

**Library and Archives Canada Cataloguing in Publication**

Introduction to phased array ultrasonic technology applications : R/D Tech guideline

Includes bibliographical references and index.  
ISBN 0-9735933-0-X

1. Ultrasonic testing. 2. Nondestructive testing. 3. Materials--Testing. I. R/D Tech

TA417.4.I58 2004

620.1'1274

C2004-904731-0

**Notice**

To the best of our knowledge, the information in this publication was accurate at the time of first printing (2004); however, the Publisher does not assume any responsibility or liability for the accuracy or completeness of, or consequences arising from, such information. This book is intended for informational purposes only. Final determination of the suitability of any information or product for use contemplated by any user, and the manner of that use, is the sole responsibility of the user. The Publisher recommends that anyone intending to rely on any recommendation of materials or procedures mentioned in this publication should satisfy himself or herself as to such suitability, and that he or she can meet all applicable safety and health standards.

All brands are trademarks or registered trademarks of their respective owners and third party entities.

---

---

# Table of Contents

---

<b>Foreword</b> .....	<b>xi</b>
<b>Preface</b> .....	<b>xiii</b>
<b>Acknowledgements</b> .....	<b>xv</b>
<b>Introduction</b> .....	<b>1</b>
References to Introduction .....	6
<b>1. Basic Concepts of Phased Array Ultrasonic Technology</b> .....	<b>9</b>
1.1 Principles .....	9
1.2 Delay Laws, or Focal Laws .....	13
1.3 Basic Components of a Phased Array System .....	16
1.4 Basic Scanning and Imaging .....	16
References to Chapter 1 .....	21
<b>2. Main Formulas and Ultrasonic Reference Data</b> .....	<b>23</b>
2.1 Physics of Ultrasonics—Definitions .....	23
2.2 Some Common Velocities and Wavelengths .....	25
2.3 Sound Pressure Formulas .....	29
2.4 Example of Temperature Effects .....	39
2.5 Circular Transducers .....	39
2.6 Beam Divergence .....	46
2.7 Rectangular Probes .....	48
2.8 Focused Sound Fields .....	51
2.9 Time-Frequency Response .....	57
2.10 Probe Classification Based on <i>BW</i> (Damping) .....	59
2.11 Ultrasonic Beam Interaction with Test Piece / Reflectors .....	61
2.12 Attenuation .....	66
2.13 Defect Sizing Using Diffraction and Mode-Conversion Techniques .....	68
2.13.1 TOFD (Time-of-Flight Diffraction) .....	68
2.13.2 Relative Arrival Time Technique (RATT) .....	78

2.13.3 Absolute Arrival Time Technique (AATT) .....	80
2.13.4 Mode-Converted Techniques .....	81
2.13.5 Pitch-and-Catch and Tandem Techniques .....	86
2.13.6 Satellite Pulse-Echo Technique .....	87
2.14 Testing Round Parts .....	88
2.15 Measuring the Lengths of Small Defects .....	90
2.16 Reliability of Ultrasonic Inspection .....	92
References to Chapter 2 .....	94
<b>3. Probes and Ultrasonic Field Formula .....</b>	<b>97</b>
3.1 Piezocomposite Materials .....	97
3.1.1 Matching Layer and Cable Requirements .....	98
3.1.2 Backing Material .....	98
3.2 Piezocomposite Manufacture .....	99
3.3 Types of Phased Array Probes for Industrial Applications .....	103
3.4 Linear Arrays .....	108
3.4.1 Active Aperture .....	108
3.4.2 Effective Active Aperture .....	109
3.4.3 Minimum Active Aperture .....	110
3.4.4 Passive Aperture .....	110
3.4.5 Elementary Pitch .....	111
3.4.6 Element Gap .....	112
3.4.7 Element Width .....	112
3.4.8 Maximum Element Size .....	112
3.4.9 Sweep Range .....	112
3.4.10 Steering Focus Power .....	113
3.4.11 Gain Compensation .....	114
3.4.12 Beam Length .....	114
3.4.13 Beam Width .....	115
3.4.14 Focal Depth .....	116
3.4.15 Depth of Field .....	117
3.4.16 Focal Range .....	117
3.4.17 Near-Surface Resolution .....	118
3.4.18 Far-Surface Resolution .....	118
3.4.19 Lateral and Axial Resolution .....	118
3.4.20 Angular Resolution .....	119
3.4.21 Main Lobe .....	119
3.4.22 Side Lobes .....	119
3.4.23 Grating Lobes .....	120
3.4.24 Beam Apodization .....	121
3.4.25 Grating Lobe Amplitude .....	121
3.5 Dynamic Depth Focusing .....	122
3.5.1 DDF Beam Divergence .....	123
3.5.2 DDF Advantages .....	124
3.6 Probe on the Wedge .....	125

3.6.1	Wedge Delay .....	125
3.6.2	Index Point Length .....	126
3.6.3	Index Point Migration .....	127
3.7	Beam Deflection on the Wedge .....	127
3.7.1	Azimuthal Deflection .....	128
3.7.2	Lateral Deflection .....	128
3.7.3	Skew Deflection .....	128
3.7.4	Active Axis Offset .....	129
3.7.5	Passive Axis Offset .....	129
3.8	2-D Matrix Phased Array Probes .....	130
3.9	Focal Law Calculator .....	133
3.10	Standard Array Probes .....	137
3.11	Other Array Features .....	138
3.11.1	Sensitivity .....	138
3.11.2	Impedance .....	138
3.11.3	Cross Talk .....	138
3.12	Phased Array Simulation Software (PASS) .....	138
3.13	Probe Design .....	139
3.13.1	Physics Guidelines .....	140
3.13.2	Practical Guidelines .....	143
3.14	Ultrasonic Setup Details .....	144
3.14.1	Pulse Width .....	145
3.14.2	Band-Pass Filters .....	145
3.14.3	Smoothing .....	146
3.14.4	Digitizing Frequency .....	147
3.14.5	Averaging .....	148
3.14.6	Compression .....	148
3.14.7	Repetition Rate (PRF, or Pulse Repetition Frequency) .....	149
3.14.8	Acquisition Rate .....	149
3.14.9	12-Bit Data Versus 8-Bit Data .....	150
3.14.10	Setup File .....	150
3.14.11	Data File Size .....	151
3.15	Probe Identification .....	152
3.16	Probe Characterization and Periodic Checking .....	153
3.16.1	Probe Characterization .....	153
3.16.2	Tolerances .....	155
3.16.3	Curved Wedges .....	156
3.17	Olympus Probes for the OmniScan .....	157
	References to Chapter 3 .....	161

## **4. Scanning Patterns and Views ..... 163**

4.1	Scanning Patterns .....	163
4.1.1	Bidirectional Scan .....	164
4.1.2	Unidirectional Scan .....	164
4.1.3	Linear Scan .....	165

4.1.4	Skewed Scan .....	166
4.1.5	Helical Scan .....	167
4.1.6	Spiral Scan .....	168
4.1.7	Beam Directions .....	169
4.1.8	Other Scanning Patterns .....	170
4.1.9	Time-Base Scanning .....	171
4.2	Ultrasonic Views (Scans) .....	172
4.2.1	A-Scan .....	174
4.2.2	B-Scan .....	176
4.2.3	C-Scan .....	177
4.2.4	D-Scan .....	178
4.2.5	S-Scan .....	178
4.2.6	Polar Views .....	179
4.2.7	Strip Charts .....	180
4.2.8	Multiple Views and Layouts .....	181
4.2.9	TOFD (Time-of-Flight Diffraction) .....	184
4.2.10	Combined TOFD and Pulse-Echo (PE) .....	186
4.2.11	Combined Strip Charts .....	187
4.2.12	Olympus TomoView Cube Views .....	188
	References to Chapter 4 .....	190
<b>5.</b>	<b>Applications .....</b>	<b>193</b>
5.1	Olympus Instruments .....	194
5.2	On-Site Equipment Checking .....	198
5.3	Active Element Integrity Checking .....	199
5.4	Ray Tracing .....	200
5.5	Aerospace .....	201
5.5.1	Inspection of Titanium Billets .....	201
5.5.2	Inspection of Friction Stir Welds .....	205
5.5.3	Inspection of Fastener Holes .....	209
5.5.4	Inspection of Landing Gear Using Manual Phased Arrays .....	211
5.5.5	Corrosion Mapping of Aircraft Fuselage .....	213
5.6	Energy .....	213
5.6.1	Dissimilar Welds Inspection of BWR Core Shroud .....	214
5.6.2	High-Speed Inspection of Stainless Steel and Carbon Steel Pipe Welds .....	216
5.6.3	Inspection of PWR Main Coolant Piping Weld Made of Wrought Stainless Steel Using Phased Arrays .....	219
5.6.4	Reactor Vessel Nozzle-to-Shell Weld .....	220
5.6.5	CANDU Feeder Tube Cracking .....	222
5.6.6	Detection of Stress Corrosion Cracking in Welded Rotor or Single Block Rotor .....	224
5.6.7	Detection of SCC in Disc Keyway and Anti-Rotation Key in Low- Pressure Turbine Rotor .....	224
5.6.8	Boresonic Inspection: Detect and Size SCC in the Rotor Body ...	225

5.6.9	Detection and Sizing of SCC in Low-Pressure Turbine Components .....	226
5.6.10	Detection and Sizing of SCC in Disc Rim-Blade Attachment—GE Style .....	228
5.6.11	Detection and Sizing of Fatigue Cracks in Blade Roots—Axial Entry Style .....	229
5.7	Pressure Vessel Construction Weld Inspection .....	230
5.7.1	Inspection Codes for Pressure Vessels .....	231
5.7.2	PV-100: Linear Scanning Using TOFD and PE .....	233
5.7.3	PV-200: Versatile Phased Array and TOFD System .....	235
5.7.4	PV-300: Premium Inspection System Using Ultrasonics, Phased Arrays, and Eddy Current Arrays .....	237
5.7.5	Typical Pressure Vessel Mechanics .....	239
5.8	Pipeline Phased Arrays .....	243
5.8.1	Standard Pipeline Zone Discrimination .....	243
5.8.2	Seamless Pipe Girth Welds .....	249
5.8.3	Risers and Tendons .....	250
5.8.4	Small Diameter Piping .....	252
5.9	Miscellaneous Applications .....	254
5.9.1	In-Service Inspection of Pipe for Stress Corrosion Cracking .....	254
5.9.2	Seam Weld Inspections of Coiled Tubing for Offshore Petrochemical Applications .....	255
5.9.3	T-Weld Inspection of Bridge Structure .....	257
5.10	Mills and Manufacturing .....	258
5.10.1	ERW Pipes Using Phased Arrays .....	258
5.10.2	Volumetric Phased Array Inspection of Bars .....	261
5.10.3	Phased Array Inspection of Full-Body Pipe (In-line) .....	266
5.10.4	Phased Array Inspection of Copper Canister Weld for Nuclear Waste Fuel .....	270
5.10.5	Phased Array Inspection of Heavy Forgings .....	272
5.11	Railroad Transportation .....	272
5.11.1	Axle (with or without Wheel) .....	272
5.11.2	Rail Inspection .....	273
5.11.3	Wheel Inspection .....	274
5.12	Portable Phased Array Applications .....	277
5.12.1	Construction Welding: T-Joints .....	278
5.12.2	Construction Welding: Butt Weld Inspections .....	279
5.12.3	Small Diameter Austenitic Welds .....	280
5.12.4	Hydrogen-Induced Cracking (HIC) .....	281
5.12.5	Tie-Ins for Pipeline Welds .....	283
5.12.6	Flange Corrosion Under Gasket .....	283
5.12.7	Component Testing: Thread Inspection .....	284
5.12.8	Component Testing: Spindle Inspection .....	286
5.12.9	Aerospace: Laser Weld Inspection .....	287
5.12.10	Aerospace: Composite Inspection .....	288

5.12.11 Aerospace: T-Joint Composite .....	290
5.12.12 Power Generation: Turbine Blade Root Inspection .....	292
5.12.13 Petrochemical Industry: Nozzle Inspection .....	292
5.12.14 Compressor Blade .....	294
5.12.15 Austenitic Welds .....	295
References to Chapter 5 .....	297
<b>6. Conclusions and Recommendations .....</b>	<b>299</b>
6.1 Advantages of Phased Arrays .....	299
6.2 General Phased Array Solutions to Inspection Problems .....	300
6.3 Implementing Phased Array Technology .....	302
<b>Appendix: Unit Conversion .....</b>	<b>305</b>
<b>Glossary .....</b>	<b>307</b>
<b>References .....</b>	<b>315</b>
<b>List of Figures .....</b>	<b>323</b>
<b>List of Tables .....</b>	<b>339</b>
<b>Index .....</b>	<b>341</b>

---

# Foreword

---

For a project of the scope of the *Introduction to Phased Array Ultrasonic Technology Application: Olympus Guideline*, the contribution and support of knowledgeable people is of tremendous help. The following are a few lines from worldwide-recognized institutes and companies that offered their recommendations about the guideline content and presentation.

## **The Welding Institute (TWI) Ltd**

*Industrial application of phased array ultrasonic technology has come of age. Many companies and engineers are employing this new and advantageous technology in a multitude of applications. There has been a need over the last few years for literature on the correct use and application of phased array technology. This book meets that need in published literature and provides a valuable introduction to ultrasonic phased array technology for professional engineers and managers wishing to gain a thorough understanding of its capabilities and methods of application.*

Colin R. Bird  
Principal Consultant NDT  
TWI Ltd, UK

## **US Air Force**

*The knowledge and interest in phased array inspection capabilities has expanded considerably over the past few years, and is expected to continue to expand. This book gives an excellent overview of the broad spectrum of phased array inspection capabilities, and a good look at the variety of equipment and uses that have been created.*

Pamela Herzog  
Materials Engineer  
AF NDI Office  
USAF, USA

## Lavender International NDT Ltd.

*Ultrasonic phased array instruments and applications have been evolving rapidly within the last decade; however, there is a desperate need for reference text to inform and educate engineers on the fundamental principles involved. The intention of this book is to briefly address many aspects of ultrasonic phased array technology as an informative guide, rather than a sequential learning program. To that end, the reader will be confronted with many concepts that likewise will promote numerous questions relating to conceptual applications of the technique. It gives me great pleasure in recommending this text as essential reading for all those interested in learning phased array principles from trainee practitioner to those with NDT level-3 management perspectives.*

Tim Armitt  
Director, Senior Lecturer  
ASNT and EN473 level 3  
Lavender International NDT Ltd., UK

## Ontario Power Generation (OPG)

*The R/D Tech Guideline<sup>1</sup> is a necessary step to fill in the information gap for conventional practitioners (technicians and engineers) to use the new phased array ultrasound technology.*

*The book is well balanced between theory, basic features, and main applications. The chapter dedicated to phased array probes includes a very useful practical guide for probe design. The back-to-basics chapter provides useful formulas, tables, and graphs for a proper application of phased array ultrasound technology.*

Petru Ciorau  
Senior Technical Expert, UT Phased Array Technology  
Inspection and Maintenance Services, Ontario Power Generation, Canada

## Iowa State University

*This book addresses multiple needs of the NDE engineering community. For the practicing ultrasonic NDE technician first encountering phased array technology, this book provides an explanation of ultrasonic phased array operation in terms of familiar ultrasonic principles. For the advanced engineer already familiar with principles of phased array technology, this book provides a useful reference defining scan configurations and measurement parameters upon which R/D Tech instrument operating software is based. Insight is given into a wide spectrum of issues encompassed in phased array application, from probe design to data presentation.*

Ron Roberts  
Senior Scientist  
Center for Nondestructive Evaluation, Iowa State University, USA

---

1. Editor's note at fourth printing: *R/D Tech Guideline* was the document subtitle at the time of first printing; it is now referred to as *Olympus Guideline*.

---

# Preface

---

R/D Tech<sup>1</sup>, as a world leader in ultrasound and eddy current nondestructive test equipment, has developed advanced techniques to diagnose and evaluate the fitness for service of critical components.

Refineries, planes, turbines, nuclear pressure vessels and primary circuits, steam generators, railways, and highway bridges are *aging*, while new products are being built to ever-increasing standards of quality. As part of this trend, NDT (nondestructive testing) must shift from qualitative assessment to quantitative evaluation. Missed cracks and false calls may lead to catastrophic failures, loss of life, costly and unnecessary repairs, and the loss of production capacity or forced outages.

The reliability and credibility of the NDT techniques used is the number one priority for inspection companies involved in life assessment or periodic inspection of critical components. They are faced with very difficult inspections such as anisotropic structures, limited probe access, or other problems.

Other inspection challenges are posed by the new manufacturing facilities designed with built-in NDT systems to perform inspections 24 hours a day and 7 days a week. They are asking us to build systems capable of detecting small defects, regardless of their orientation and at very high scanning speeds. Data analysis and reporting must be optimized for real-time inspections, remote analysis, and third-party evaluation. In many cases, the results must be provided in near real time.

The NDT issues mentioned above have triggered the development of a new technology: phased array ultrasound. R/D Tech, in cooperation with its customers, pioneered the development of the phased array ultrasonic technology in the middle of the 1990s. Over the last decade, the phased array technology has reached a commercially mature status for NDT applications.

---

1. Editor's note at fourth printing: R/D Tech operated at the time of first printing; it was later acquired by Olympus and now operates under the new name.

The phased array technology is an advanced ultrasonic inspection tool that is capable of providing *reliable* quantitative data for the life assessment and fitness for service of vital components in transportation, power generation, petrochemical, aerospace, defense, and pipeline industries, just to name a few important economic sectors. The phased array technology is also used for assuring the quality of new products in pipes, vessels, and other major components.

The advances in microelectronics, computer processing power, remote data transfer, and micromachining of phased array probes have allowed R/D Tech<sup>1</sup> to manufacture battery-operated, portable phased array equipment, and to standardize ultrasonic phased array kits (probes, blocks, wedges, miniscanners) for specific applications.

Ultrasound technicians, through their skill, education, training, and certification, are an integral part of inspection reliability. In order to be rated as a qualified inspection technique, the phased array ultrasonic technology requires formal training and certification of personnel.

This guideline is R/D Tech's first step to help fill the lack of information between conventional and phased array UT technology. This guideline is focused on terminology, principles, useful formulas, tables, and charts. It gives an overview of the phased array technology, including examples of inspection applications. The guideline is an introduction to phased array technology applications, not a training manual.

Our website offers you an opportunity to communicate with our specialists, as well as to make your comments and suggestions in order to improve this guideline.

I hope the first edition of this phased array ultrasonic technology guideline will help enrich your ultrasound terminology knowledge, familiarize you with the phased array inspection tools, and reduce your training time to meet the new challenges brought by the twenty-first century.

Alain Allard  
President and CEO  
R/D Tech  
August 2004

---

1. Editor's note at fourth printing: R/D Tech operated at the time of first printing; it was later acquired by Olympus and now operates under the new name.

---

# Acknowledgements

---

## Technical Reviewers and Advisers

R/D Tech<sup>1</sup> would like to express a special appreciation to the advisers that have contributed to the review of the successive versions of *Introduction to Phased Array Ultrasonic Technology Applications: R/D Tech Guideline*. R/D Tech thanks them for the time and consideration they have put into this advisory task. Their involvement in this project is greatly appreciated.

A great thank-you to our advisers:

- **Colin R. Bird**  
The Welding Institute, UK
- **Pamela Herzog**  
USAF, USA
- **Tim Armitt**  
Lavender International, UK
- **Petru Ciorau**  
Ontario Power Generation, Canada
- **Ron Roberts**  
Iowa State University, USA
- **Mark Davis**  
Davis NDE, Inc., USA

R/D Tech was honored to enlist well-recognized advisers from Europe and North America to participate in the realization of the first phased array book of the NDT community. The broad scope of *Introduction to Phased Array Ultrasonic Technology Applications* made this task a real challenge. All along the lengthy writing and revision process, we received excellent reaction and

---

1. Editor's note at fourth printing: R/D Tech operated at the time of first printing; it was later acquired by Olympus and now operates under the new name.

support from our advisers. They helped guide R/D Tech in the completion of this work. Their contribution touched many aspects: general review, improvement and additions to some sections, and validation of the equations and formulas. In short, they allowed *Introduction to Phased Array Ultrasonic Technology Applications: R/D Tech Guideline*<sup>1</sup> to reach the level of quality everyone expected.

R/D Tech wishes to acknowledge the special contribution of Ontario Power Generation (OPG), Canada. During the 1995–2004 period, OPG has made an important contribution to the development of the phased array technology at R/D Tech. Their strong expertise and continuous support helped R/D Tech in the development of specific phased array hardware and software functions, such as the ones found in the OmniScan instrument and the TomoView software.

## **R/D Tech Personnel**

R/D Tech wishes to thank all personnel involved in the development, manufacturing, sales, and marketing of phased array ultrasonic technology applications and to especially thank everyone at R/D Tech who contributed to the production of this guideline.

## **Customers**

R/D Tech also wants to acknowledge the catalyst role of many customers who have challenged the company with specific inspection problems. The research and development these challenges have inspired has contributed to the advancement of the phased array ultrasonic technology during the last decade.

---

1. Editor's note at fourth printing: The document subtitle is now *Olympus Guideline*.

---

# Introduction

---

The development and application of phased array ultrasonic technology as a stand-alone technique has reached a mature phase at the beginning of the twenty-first century.

Phased array ultrasonic technology moved from the medical field<sup>1</sup> to the industrial sector at the beginning of the 1980s.<sup>2,3</sup> By the mid-1980s, piezocomposite materials were developed and made available to manufacture complex-shaped phased array probes.<sup>4-13</sup>

By the beginning of the 1990s, phased array technology was incorporated as a new NDE (nondestructive evaluation) method in ultrasonic handbooks<sup>14,15</sup> and training manuals for engineers.<sup>16</sup> The majority of the applications from 1985 to 1992 were related to nuclear pressure vessels (nozzles), large forging shafts, and low-pressure turbine components.

Advances in piezocomposite technology,<sup>28,29</sup> micromachining, microelectronics, and computing power (including simulation packages for probe design and beam-component interaction), contributed to the revolutionary development of the phased array technology. Functional software was also developed as computer capabilities increased.

The phased array ultrasonic technology for NDT (nondestructive testing) use was triggered by the following power generation inspection problems:

1. The need to detect cracks located at different depths with random orientations using the same probe in a fixed position
2. The requirement to improve SNR (signal-to-noise ratio) and sizing capability for dissimilar metal welds and centrifugal-cast stainless steel welds
3. The requirement to increase the scanner reliability
4. Increased accessibility requirements for difficult-to-reach PWR/BWR (pressurized water reactor / boiling water reactor) components
5. Decreased setup and inspection time (productivity)

6. Detection and sizing of small SCC (stress corrosion cracking) in turbine components with complex geometries
7. A requirement to decrease the amount of radiation the personnel is exposed to
8. A requirement to increase the accuracy in detection, sizing, location, and orientation of critical defects, regardless of their orientation
9. The need to provide a quantitative, easy-to-interpret report for *fitness for purpose* (also called “engineering critical assessment,” or “life assessment/disposition-inspection interval strategy”)

Other industries—such as aerospace, defense, petrochemical, and manufacturing—required similar improvements, though specific requirements vary for each industry application. However, the requirements center round several main characteristics of phased array ultrasonic technology:

1. *Speed.* The phased array technology allows electronic scanning, which is typically an order of magnitude faster than conventional raster scanning.
2. *Flexibility.* A single phased array probe can cover a wide range of applications, unlike conventional ultrasound probes.
3. *Electronic setups.* Setups are performed by simply loading a file and calibrating. Different parameter sets are easily accommodated by pre-prepared files.
4. *Small probe dimensions.* For some applications, access is a major issue, and one small phased array probe can provide the equivalent of multiple single-transducer probes.

R/D Tech<sup>1</sup> has been developing phased array technology for more than a decade. Since the beginning of the 1990s, R/D Tech has implemented the concept of standardization and transfer of the technology.

The phased array ultrasonic technology reached a commercially viable status by 1997 when the transportable phased array Tomoscan FOCUS instrument could be operated in the field by a single person, and data could be transferred and remotely analyzed in real time.

Many papers have been published on phased array NDT applications.<sup>17-24</sup> For example, the EPRI NDE Center has organized three seminars pertaining to phased array technology.<sup>25-27</sup>

---

1. Editor’s note at fourth printing: R/D Tech operated at the time of first printing; it was later acquired by Olympus and now operates under the new name.

The portable, battery-operated, phased array OmniScan instrument is a quantum leap in the ultrasonic technology. This instrument brings phased array capabilities to everyday inspections such as corrosion mapping, rapid crack detection, imaging, and special applications. The new technology must be validated and endorsed by regulatory bodies, insurance companies, and standardization organizations. As part of the validation process, operators must demonstrate that they can handle the phased array ultrasonic technology.

Training and certification of personnel will be one of the major tasks to generalize the use of the phased array technology, along with performance demonstration and technology transfer process.

R/D Tech has issued this guideline as a first step to fill the gap in phased array ultrasonic technology information and to provide an overview of its many applications.

The guideline includes the following:

- Chapter 1, “Basic Concepts of Phased Array Ultrasonic Technology”  
Describes the phased array ultrasonic technology principles and illustrates the main hardware components, type of beam forming and scanning patterns (linear, sectorial, dynamic depth focusing, 3-D), phased array advantages, defect discrimination, pattern recognition and advanced imaging, and basic system requirements.
- Chapter 2, “Main Formulas and Ultrasonic Reference Data”  
Describes the most commonly used formulas in phased array ultrasonic technology and illustrates the basic requirements to build setups and analyze defects (Snell’s law, attenuation, defect sizing, mode-converted techniques, couplant influence, gain compensation with refracted angle, reflectivity laws from different reflectors, ultrasonics setting formulas).
- Chapter 3, “Probes and Ultrasonic Field Formula”  
Presents the properties of piezocomposite materials, types of phased array probes and their properties, the main field features, guidelines to design a phased array probe, and the minimum features required for certification.
- Chapter 4, “Scanning Patterns and Views”  
Describes the main scanning patterns, data acquisition methods, and the most important views used when inspecting with the phased array ultrasonic technology.
- Chapter 5, “Applications”  
Consists of the following sections:
  - “Olympus Instruments” (scanners, probes, hardware, software)

- “On-Site Equipment Checking”
- “Active Element Integrity Checking”
- “Ray Tracing”
- “Aerospace”
- “Energy”
- “Pressure Vessel Construction Weld Inspection”
- “Pipeline Phased Arrays”
- “Miscellaneous Applications”
- “Mills and Manufacturing”
- “Railroad Transportation”
- “Portable Phased Array Applications”

The applications describe R/D Tech’s solutions for specific inspection problems brought up by our customers.

- Chapter 6, “Conclusions and Recommendations”  
Sums up the main ideas of this guideline and makes specific recommendations to enhance your knowledge about the phased array technology.
- Appendix: “Unit Conversion”  
Provides the metric-English conversions for units used in this book.
- “Web Site Forum”<sup>1</sup>  
Presents the web-hosted discussion forum where you can browse to find or post added information.
- “Glossary”  
Lists abbreviations, acronyms, and symbols used in the guideline, along with short definitions.
- “References”  
Is *selective* to the main R/D Tech manuals and technical papers. Additional standards for probes and ultrasonic flaw detectors (systems) are also mentioned. Major EPRI workshops and worldwide NDT conferences are mentioned at the end of the section.

As the title suggests, this book is an *introduction* to the phased array ultrasonic technology; this R/D Tech guideline<sup>2</sup> is *not* a training manual. Specific problem-solving examples, with different degrees of difficulty, will be issued

---

1. Editor’s note at fourth printing: *Web Site Forum* existed at the time of first printing, but has since been removed. For information on current online discussions, please contact Olympus.

2. Editor’s note at fourth printing: The document subtitle is now *Olympus Guideline*.

in the upcoming R/D Tech training manuals (beginner, level II, advanced, and engineers).

This guideline is the first book issued by R/D Tech to help people, particularly those using conventional ultrasound, comprehend the phased array ultrasonic technology.

As mentioned in chapter 6, “Conclusions and Recommendations,” and in “Web Site Forum,”<sup>1</sup> your support and comments are important. They will help improve on phased array ultrasonic technology and NDT inspection equipment to better fulfill the industry requirements.

R/D Tech is waiting for your input, so the second edition of this guideline will feature contents more adapted to your needs and expectations.

We hope this book will be a worthy contribution to the development of phased array ultrasonic technologies and becomes an integral part of your NDT references.

Noël Dubé  
Business Development Vice-President  
R/D Tech

---

1. Editor’s note at fourth printing: *Web Site Forum* existed at the time of first printing, but has since been removed. For information on current online discussions, please contact Olympus.

## References to Introduction

1. Somer, J. C. "Electronic Sector Scanning for Ultrasonic Diagnosis," *Ultrasonics*, vol. 6 (1968): p. 153.
2. Gebhardt, W., F. Bonitz, and H. Woll. "Defect Reconstruction and Classification by Phased Arrays." *Materials Evaluation*, vol. 40, no. 1 (1982): pp. 90–95.
3. Von Ramm, O. T., and S. W. Smith. "Beam Steering with Linear Arrays." *Transactions on Biomedical Engineering*, vol. 30, no. 8 (August 1983): pp. 438–452.
4. Erhards, A., H. Wüstenberg, G. Schenk, and W. Möhrle. "Calculation and Construction of Phased Array-UT Probes." *Proceedings 3rd German-Japanese Joint Seminar on Research of Structural Strength and NDE Problems in Nuclear Engineering*, Stuttgart, Germany, August 1985.
5. Hosseini, S., S. O. Harrold, and J. M. Reeves. "Resolutions Studies on an Electronically Focused Ultrasonic Array." *British Journal of Non-Destructive Testing*, vol. 27, no. 4 (July 1985): pp. 234–238.
6. Gururaja, T. T. "Piezoelectric composite materials for ultrasonic transducer applications." Ph.D. thesis, The Pennsylvania State University, University Park, PA, May 1984.
7. McNab, A., and I. Stumpf. "Monolithic Phased Array for the Transmission of Ultrasound in NDT Ultrasonics." *Ultrasonics*, vol. 24 (May 1984): pp. 148–155.
8. McNab, A., and M. J. Campbell. "Ultrasonic Phased Array for Nondestructive Testing." *NDT International*, vol. 51, no. 5: pp. 333–337.
9. Hayward, G., and J. Hossack. "Computer models for analysis and design of 1-3 composite transducers." *Ultrasonic International 89 Conference Proceedings*, pp. 532–535, 1989.
10. Poon, W., B. W. Drinkwater, and P. D. Wilcox. "Modelling ultrasonic array performance in simple structures." *Insight*, vol. 46, no. 2 (February 2004): pp. 80–84.
11. Smiths, W. A. "The role of piezocomposites in ultrasonic transducers." *1989 IEEE Ultrasonics Symposium Proceedings*, pp. 755–766, 1989.
12. Hashimoto, K. Y., and M. Yamaguchi. "Elastic, piezoelectric and dielectric properties of composite materials." *1986 IEEE Ultrasonic Symposium Proceedings*, pp. 697–702, 1986.
13. Oakley, C. G. "Analysis and development of piezoelectric composites for medical ultrasound transducer applications." Ph.D. thesis, The Pennsylvania State University, University Park, PA, May 1991.
14. American Society for Nondestructive Testing. *Nondestructive Testing Handbook*. 2nd edition. Vol. 7, *Ultrasonic Testing*, pp. 284–297. Columbus, OH: American Society for Nondestructive Testing, 1991.
15. Krautkramer, J., and H. Krautkramer. *Ultrasonic Testing of Materials*. 4th fully rev. ed., pp. 194–195, 201, and 493. Berlin; New York: Springer-Verlag, c1990.
16. DGZfP [German Society for Non-Destructive Testing]. *Ultrasonic Inspection Training Manual Level III-Engineers*. 1992.  
<http://www.dgzfp.de/en>.

17. Harumi, K., M. Uchida, and H. Okada. *Ultrasonic Defect Sizing - Japanese Tip Echo Handbook*. 2nd version. Edited by K. Harumi, Y. Ogura, and M. Uchida. Translated by D. C. Moles and N. Miura. JSNDI (Japanese Society for Non-Destructive Inspection), 1989.
18. Schelengermann, U. "Sound field structure of plane ultrasonic sources with focusing lenses." *Acustica*, vol. 30, no. 6 (1974): pp. 291–300.
19. Schelengermann, U. "The characterization of focusing ultrasonic transducers by means of single frequency analysis." *Materials Evaluation*, vol. 38, no. 12 (Dec. 1980): pp. 73–79.
20. Wüstenberg, H., E. Schenk, W. Möhrle, and E. Neumann. "Comparison of the performances of probes with different focusing techniques and experiences." *10<sup>th</sup>-WCNDT Proceedings*, vol. 7, pp 563–567.
21. Wüstenberg, H., J. Kutzner, and W. Möhrle. "Focusing probes for the improvement of flaw size in thick-walled reactor components." [In German.] *Materialprüfung*, vol. 18, no. 5 (May 1976): pp. 152–161.
22. Singh, G. P., and J. L. Rose. "A simple model for computing ultrasonic beam behavior of broad-band transducers." *Materials Evaluation*, vol. 40, no. 7 (1982): pp. 880–885.
23. Fowler, K. A., H. C. Hotchkiss, and T. V. Yamartino. "Important characteristics of ultrasonic transducers and their factors related to their applications." Panametrics, USA, 1993.
24. Hotchkiss, F. H., D. R. Patch, and M. E. Stanton. "Examples of ways to evaluate tolerances on transducer manufacturing specifications." *Materials Evaluation*, vol. 45, no. 10 (1987): pp. 1195–1202.
25. Murphy, R. V. "Focussed Ultrasonic Probes for Contact Inspection." *Materials Evaluation*, vol. 38, no. 9 (1980): pp. 53–58.
26. Onozawa, M., and Y. Ishii. "The industrial application of improved narrow-beam probes for ultrasonic inspection." *British Journal of Non-Destructive Testing*, vol. 28, no. 1 (1986): pp. 23–26.
27. Beck, K. H. "Ultrasonic transducers focusing for inspection of cylindrical material." *Materials Evaluation*, vol. 49, no. 7 (July 1991): pp. 875–882.
28. Fleury, G., and C. Gondard. "Improvements of Ultrasonic Inspections through the Use of Piezo Composite Transducers." *6th Eur. Conference on Non Destructive Testing*, Nice, 1994.
29. Ritter, J. "Ultrasonic Phased Array Probes for Non-Destructive Examinations Using Composite Crystal Technology." DGZfP, 1996.

# Chapter Contents

1.1	Principles .....	9
1.2	Delay Laws, or Focal Laws .....	13
1.3	Basic Components of a Phased Array System.....	16
1.4	Basic Scanning and Imaging.....	16
	References to Chapter 1.....	21

---

# 1. Basic Concepts of Phased Array Ultrasonic Technology

---

This chapter describes the principles pertaining to ultrasound, the concepts of time delays (or focal laws) for phased arrays, and Olympus phased array instruments.

## 1.1 Principles

Ultrasonic waves are mechanical vibrations induced in an elastic medium (the test piece) by the piezocrystal probe excited by an electrical voltage. Typical frequencies of ultrasonic waves are in the range of 0.1 MHz to 50 MHz. Most of the industrial applications require frequencies between 0.5 MHz and 15 MHz.

Most conventional ultrasonic inspections use monocrystal probes with divergent beams. The ultrasonic field propagates along an acoustic axis with a single refracted angle. The divergence of this beam is the only “additional” angle, which might contribute to detection and sizing of misoriented small cracks.

Assume the monoblock is cut in many identical elements, each with a width much smaller than its length (elevation [ $e < W$ ]) [for definitions, see “Glossary” on page 307]. Each small crystal may be considered a line source of cylindrical waves. The wavefronts of the new acoustic block will interfere, generating an overall wavefront.

The small wavefronts can be time-delayed and synchronized for phase and amplitude, in such a way as to create an ultrasonic *focused* beam with *steering* capability.

The main feature of phased array ultrasonic technology is the *computer-controlled excitation* (amplitude and delay) of individual elements in a multielement probe. The excitation of piezocomposite elements can generate

an ultrasonic focused beam with the possibility of modifying the beam parameters such as angle, focal distance, and focal spot size through software. The sweeping beam is focused and can detect in specular mode the misoriented cracks. These cracks may be located randomly away from the beam axis. A single crystal probe, with limited movement and beam angle, has a high probability of missing misoriented cracks, or cracks located away from the beam axis (see Figure 1-1).

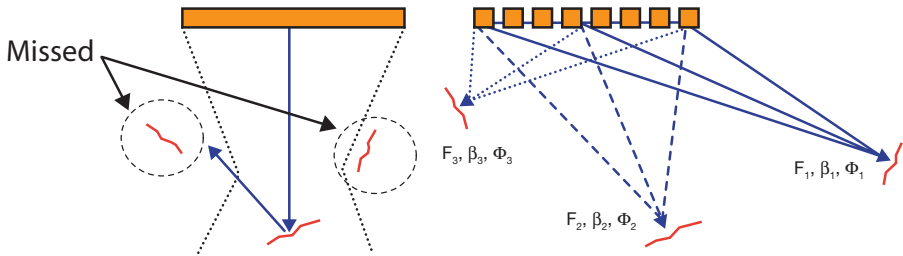


**Figure 1-1** Detection of misoriented cracks by monocrystal (*left*) and multielement probes (*right*). The beam is divergent and unidirectional for the monocrystal probe, while it is focused and multiangled for the phased array probe. Cracks of most orientations can be detected by the phased array probe.

To generate a beam in phase and with a constructive interference, the various active probe elements are pulsed at slightly different times. As shown in Figure 1-2, the echo from the desired focal point hits the various transducer elements with a computable time shift. The echo signals received at each transducer element are time-shifted before being summed together. The resulting sum is an A-scan that emphasizes the response from the desired focal point and attenuates various other echoes from other points in the material.

- During transmission, the acquisition instrument sends a trigger signal to the phased array instrument. The latter converts the signal into a high-voltage pulse with a preprogrammed width and time delay defined in the focal laws. Each element receives one pulse only. This creates a beam with a specific angle and focused at a specific depth. The beam hits the defect and bounces back.
- The signals are received, then time-shifted according to the receiving focal law. They are then reunited together to form a single ultrasonic pulse that is sent to the acquisition instrument.

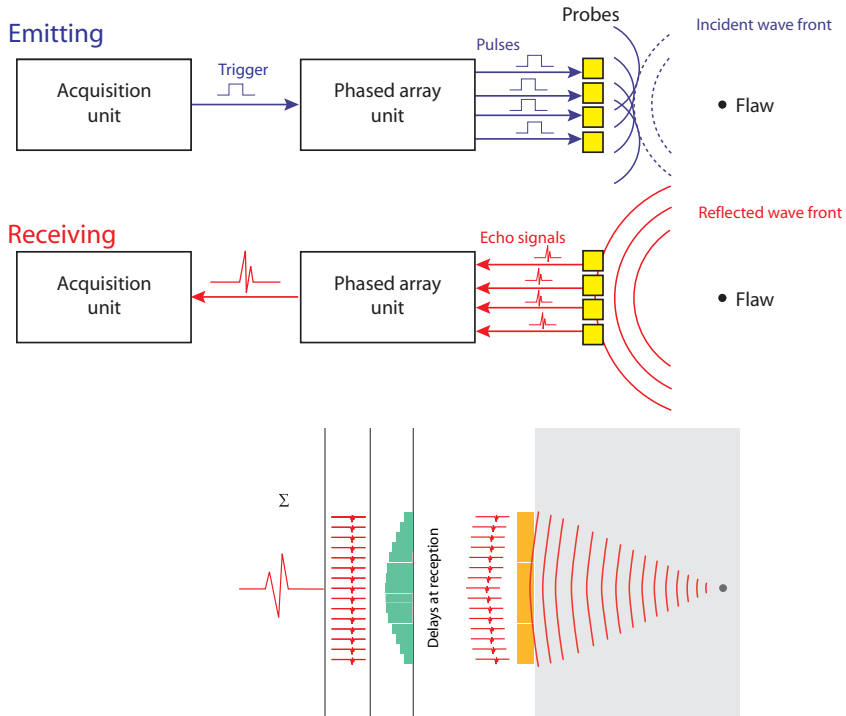


**Figure 1-2** Beam forming and time delay for pulsing and receiving multiple beams (same phase and amplitude).

The beam focusing principle for normal and angled incidences is illustrated in Figure 1-3.

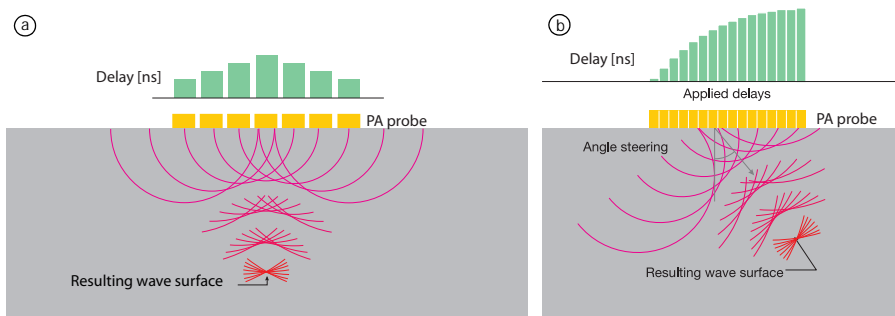


**Figure 1-3** Beam focusing principle for (a) normal and (b) angled incidences.

The delay value on each element depends on the aperture of the phased array probe active element, type of wave, refracted angle, and focal depth.

There are three major computer-controlled beam scanning patterns (see also chapters 3 and 4):

- *Electronic scanning*: the same focal law and delay is multiplexed across a group of active elements (see Figure 1-4); scanning is performed at a constant angle and along the phased array probe length (aperture). This is equivalent to a conventional ultrasonic transducer performing a raster scan for corrosion mapping or shear wave inspection. If an angled wedge is used, the focal laws compensate for different time delays inside the wedge.
- *Dynamic depth focusing*, or *DDF* (along the beam axis): scanning is performed with different focal depths. In practice, a single transmitted focused pulse is used, and refocusing is performed on reception for all programmed depths (see Figure 1-5).
- *Sectorial scanning* (also called *azimuthal* or *angular scanning*): the beam is moved through a sweep range for a specific focal depth, using the same elements; other sweep ranges with different focal depths may be added. The angular sectors may have different values.

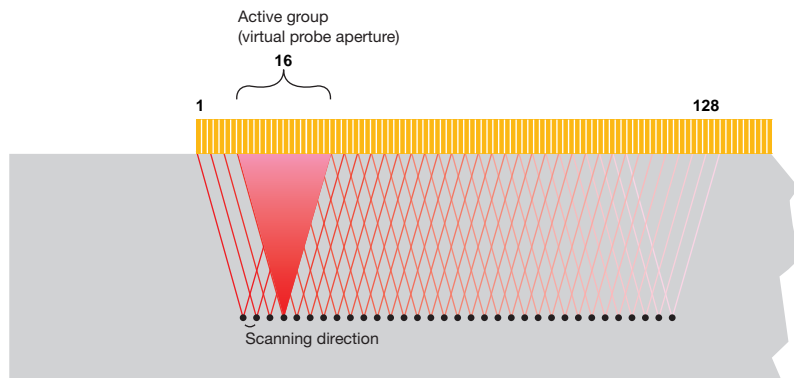


**Figure 1-4** Electronic scanning with normal beam (virtual probe aperture = 16 elements).

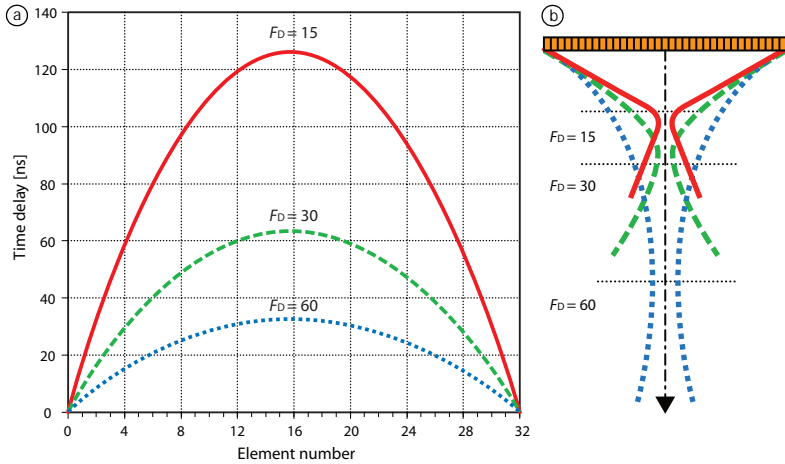


**Figure 1-5** Delay values (*left*) and depth scanning principles (*right*) for a 32-element linear array probe focusing at 15-mm, 30-mm, and 60-mm longitudinal waves. Direct contact, no angled wedge.

## 1.2 Delay Laws, or Focal Laws

The focal law delay for probes without wedge—in direct contact with the test piece—, which were programmed to generate longitudinal waves, has a parabolic shape for depth focusing. The delay increases from the edges of the probe towards the center. The delay will be divisible in half when the focal distance is doubled (see Figure 1-5). The element timing has a linear increase when the element pitch is increasing (see Figure 1-7).

Phased array probes installed on the wedge provide delay laws with different shapes, based on Fermat's principle of minimum arrival time along a specific path (see Figure 1-6). Other types of phased array probes (matrix or conical, for example) may require advanced simulation for delay law values and for beam feature evaluation (see chapters 3 and 5).

If the beam deflection is sectorial (azimuthal), and the probe has no wedge, the delay on identical elements will depend on the element position in the active aperture and on the generated angle (see Figure 1-8). The delay value increases with refracted angle and with element number.

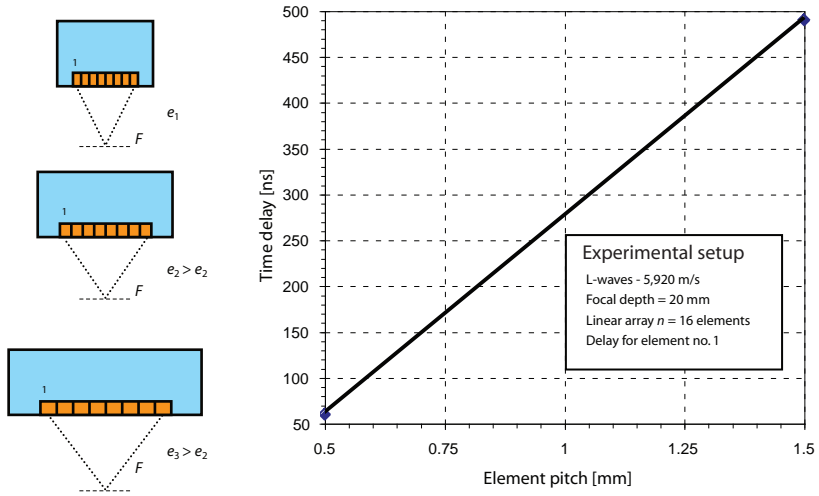


**Figure 1-6** Delay dependence on pitch size for the same focal depth.

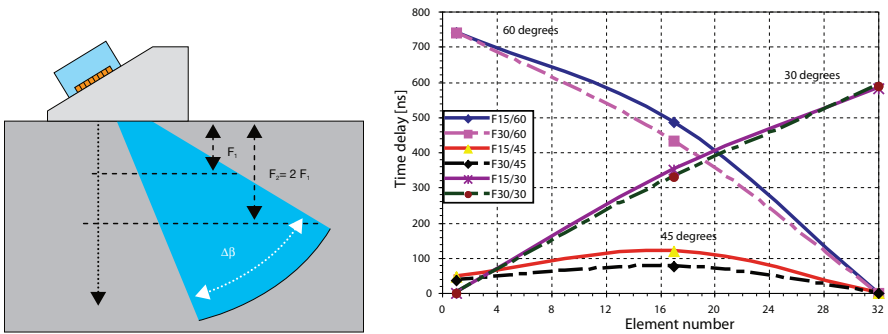


**Figure 1-7** Example of delay dependence on refracted angle and element position for a phased array probe on a 37° Plexiglas wedge ( $H_1 = 5$  mm).

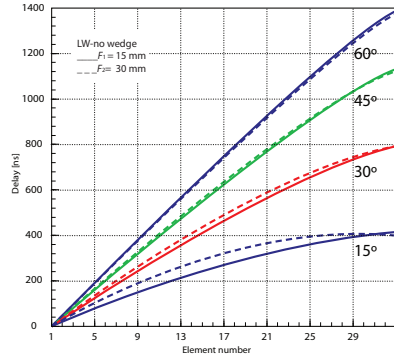
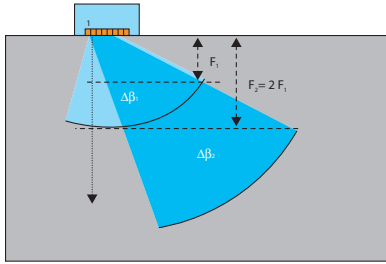


**Figure 1-8** Example of delay dependence on generated angle, and element position and focal depth for a probe with no wedge (longitudinal waves, refracted angle in steel: 15–60°).

If the phased array probe is on a wedge, the delay value depends on element position and programmed refracted angle.

The delay has a parabolic shape for the angle given by Snell's law (45° in Figure 1-7). For angles smaller than one provided by Snell's law, the delay on elements increases from the back towards the front of the probe. For greater angles, the delay is higher for the back elements, because the beam generated by the front elements follows a longer path in the wedge, and thus they have to be excited first.

In all cases, the delay value on each element must be accurately controlled. The minimum delay increment determines the maximum probe frequency that can be used according to the following ratio:

$$\frac{n}{f_c}$$

### 1.3 Basic Components of a Phased Array System

The main components required for a basic scanning system with phased array instruments are presented in Figure 1-9.

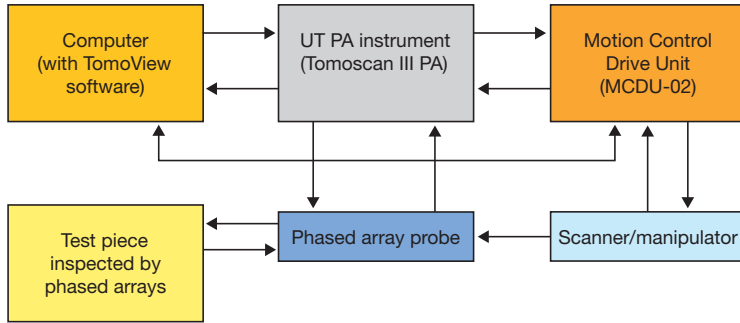


Figure 1-9 Basic components of a phased array system and their interconnectivity.

### 1.4 Basic Scanning and Imaging

During a scan with mechanical device, data is collected based on encoder position. The data is displayed in different views for interpretation.

Typically, phased arrays use multiple stacked A-scans (also called “B-scans,” see details on chapter 4) with different angles, time of flight and time delays on each small piezocomposite crystal (element) of the phased array probe.

The real-time information from the total number of A-scans, which are fired for a specific probe position, are displayed in a *sectorial scan* or *S-scan*, or in a *electronic B-scan* (see chapter 4 for more details).

Both S-scans and electronic scans provide a global image and quick information about the component and possible discontinuities detected in the ultrasonic range at all angles and positions (see Figure 1-10).

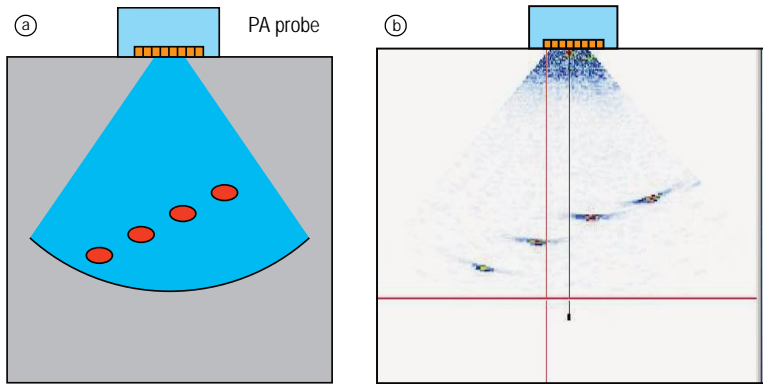


**Figure 1-10** Detection of four side-drilled holes (SDH): (a) sectorial scanning principle; (b) S-scan view using  $\pm 30^\circ$ .

Data plotting into the 2-D layout of the test piece, called “corrected S-scans,” makes the interpretation and analysis of ultrasonic results straightforward. S-scans offer the following benefits:

- Image display during a scan
- True depth representation
- 2-D volumetric reconstruction

Advanced imaging can be achieved by a combination of linear and sectorial scanning with multiple-angle scans during probe movement. S-scan displays in combination with other views (see chapter 4 for more details) lead to a form of defect imaging or recognition. Figure 1-11 illustrates the detection of artificial defects and the comparison between the defect dimensions (including shape) and B-scan data.

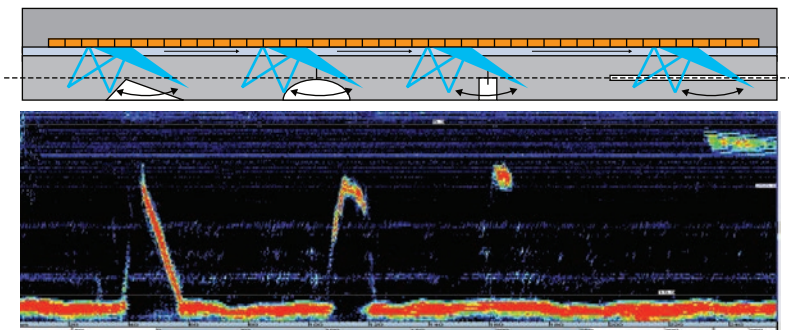


**Figure 1-11** Advanced imaging of artificial defects using merged data: defects and scanning pattern (*top*); merged B-scan display (*bottom*).

A combination of longitudinal wave and shear wave scans can be very useful for detection and sizing with little probe movement (see Figure 1-12). In this setup, the active aperture can be moved to optimize the detection and sizing angles.

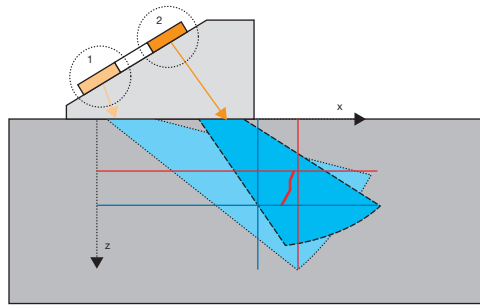


**Figure 1-12** Detection and sizing of misoriented defects by a combination of longitudinal wave (1) and shear wave sectorial scans (2).

Cylindrical, elliptical or spherical focused beams have a better signal-to-noise ratio (discrimination capability) and a narrower beam spread than divergent beams. Figure 1-13 illustrates the discrimination of cluster holes by a cylindrical focused beam.

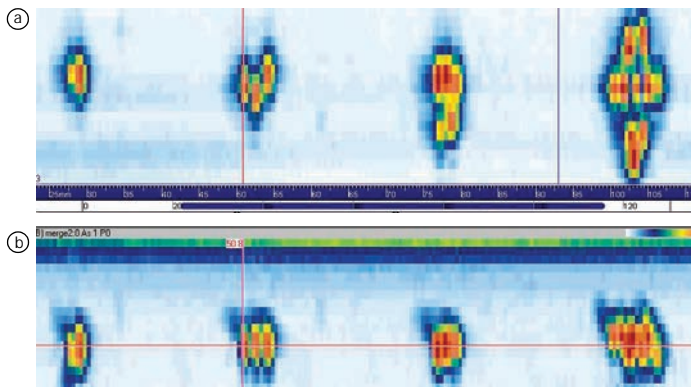


**Figure 1-13** Discrimination (resolution) of cluster holes: (a) top view (C-scan); (b) side view (B-scan).

Real-time scanning can be combined with probe movement, and the data merged into a single view (see Figure 1-14). This feature offers the following benefits:

- High redundancy
- Defect location
- Accurate plotting
- Defect imaging

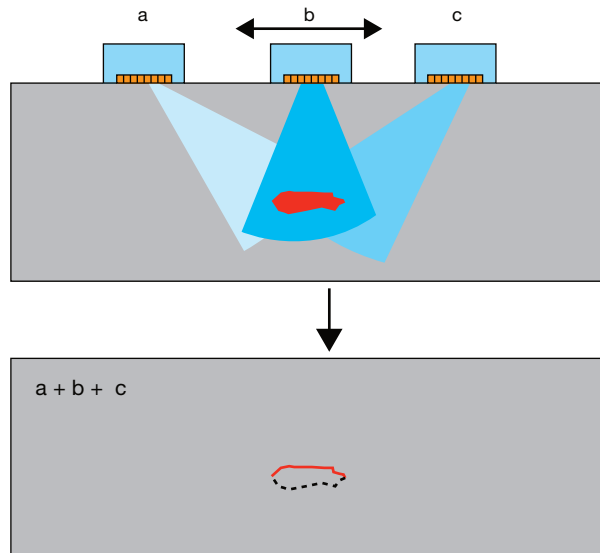


**Figure 1-14** Multiple scan patterns and merged data to show potential imaging techniques for defects.

Figure 1-15 shows sectorial plans in the volume. Each slice presents a section of the defect at a different position. Such slices compare to metallographic multiple slices during defect sizing and characterization.

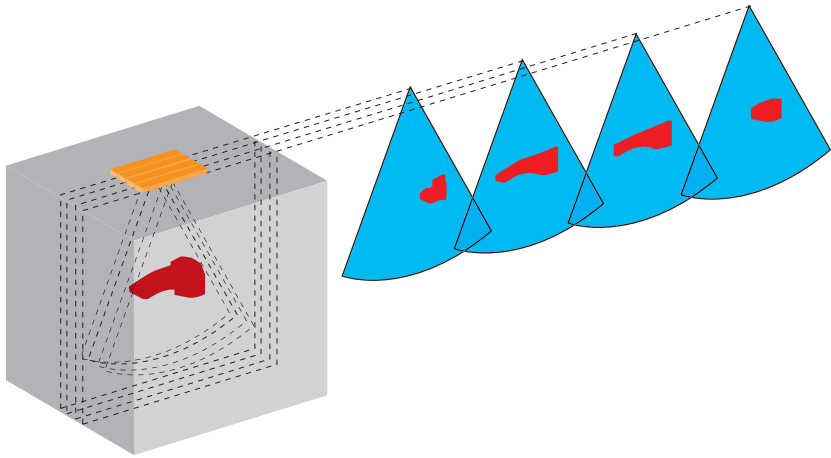


**Figure 1-15** Multiple scan patterns and merged data to show potential imaging techniques for defects.

More details regarding the general concepts of phased array ultrasonic principles may be found in references 1 to 9.

## References to Chapter 1

1. American Society for Nondestructive Testing. *Nondestructive Testing Handbook*. 2nd edition. Vol. 7, *Ultrasonic Testing*, pp. 284–297. Columbus, OH: American Society for Nondestructive Testing, 1991.
2. Spies, M., W. Gebhardt, and M. Kröning (IZFP Saarbrücken). “Recent Developments in Phased Array Technology.” [In German.] *NDT of Welds Conference*, Bamberg, Sept. 7–9, 1998.
3. Wüstenberg, H., A. Erhard, and G. Schenk. “Some Characteristic Parameters of Ultrasonic Phased Array Probes and Equipments.” *The e-Journal of Nondestructive Testing*, vol. 4, no. 4 (April 1999). NDTnet, <http://www.ndt.net/v04n04.htm>.
4. Wüstenberg, H., A. Erhard, and G. Schenk. “Scanning Modes at the Application of Ultrasonic Phased Array Inspection Systems.” *WCNDT*, paper idn 193, Rome, Oct. 2000.
5. Gros, X. E., N. B. Cameron, and M. King. “Current Applications and Future Trends in Phased Array Technology.” *Insight*, vol. 44, no. 11 (Nov. 2002).
6. Bird, C. R. “Ultrasonic phased array inspection technology for the evaluation of friction stir welds.” *Insight*, vol. 46, no. 1 (January 2004): pp. 31–36.
7. Lafontaine, G., and F. Cancre. “Potential of UT Phased Arrays for Faster, Better, and Lower Cost Inspections.”
8. Lamarre, A., M. Moles, and F. Cancre. “Use of state-of-the art phased-array ultrasound for the inspection of Friction Stir Welds (FSW).”
9. R/D Tech. “Ultrasound Phased Array.” *The e-Journal of Nondestructive Testing*, vol. 7, no. 5 (May 2004). NDTnet, <http://www.ndt.net/v07n05.htm>.

# Chapter Contents

2.1	Physics of Ultrasonics—Definitions .....	23
2.2	Some Common Velocities and Wavelengths .....	25
2.3	Sound Pressure Formulas .....	29
2.4	Example of Temperature Effects .....	39
2.5	Circular Transducers.....	39
2.6	Beam Divergence.....	46
2.7	Rectangular Probes .....	48
2.8	Focused Sound Fields .....	51
2.9	Time-Frequency Response .....	57
2.10	Probe Classification Based on BW (Damping).....	59
2.11	Ultrasonic Beam Interaction with Test Piece / Reflectors .....	61
2.12	Attenuation.....	66
2.13	Defect Sizing Using Diffraction and Mode-Conversion Techniques ....	68
2.14	Testing Round Parts .....	88
2.15	Measuring the Lengths of Small Defects .....	90
2.16	Reliability of Ultrasonic Inspection .....	92
	References to Chapter 2.....	94

---

## 2. Main Formulas and Ultrasonic Reference Data

---

This chapter is a brief review of the main formulas used in conventional ultrasonics and in advanced sizing. Specific tables and graphs are useful for phased array ultrasonics (to detail the focal law sectorial scanning range, location of mode-converted signals, gain loss, gain compensation with angle, axial and lateral probe resolution, and beam features).

### 2.1 Physics of Ultrasonics—Definitions

Ultrasonic waves are characterized by:

- Particle deviation,  $\epsilon$  [m]
- Frequency,  $f$  [MHz =  $10^6$  s<sup>-1</sup>]
- Velocity (speed),  $v$  (see Table 2-1) [km/s; mm/ $\mu$ s]
- Wavelength,  $\lambda = v/f$  (see Table 2-2) [mm]
- Angular velocity,  $\omega$  [rad/s<sup>-1</sup>]
- Acoustic impedance,  $Z = v \cdot \rho$  [kg/m<sup>2</sup> s = rayl]
- Intensity of acoustic power,  $J = 0.5 Z\omega^2\xi^2$  [W/m<sup>2</sup>]
- Intensity (amplitude) ratio [dB]
- Sound pressure,  $P$  [Pa = N/m<sup>2</sup>]
- Attenuation coefficient,  $\alpha_{\text{attenuation}}$  [dB/mm]

The following types of waves may be generated in a solid:

- Longitudinal (compression)
- Transverse (shear)
- Creeping (head)
- Surface (Rayleigh)

- Guided (Lamb)
- Edge (diffracted)

**Note:** Longitudinal wave is the only mode that can generally be propagated through liquids and gases.

Solids support many different types of wave modes, unlike liquids and gases. The two main types are longitudinal (L-waves) and shear waves (S-waves). L-waves have the particle motion and propagation in the same direction, while shear waves have particle and propagation at right angles to each other. The other wave modes listed here are typically combinations of these two basic modes. For example, Lamb waves are normally bulk waves in plates using both L and S characteristics. Surface waves are usually a special form of S-wave. Diffracted waves are either L-waves or S-waves (see section 2.13).

The formulas for longitudinal, transverse, and surface waves are:

$$v_L = \left[ \frac{E(1-\mu)}{\rho(1+\mu)(1-2\mu)} \right]^{0.5} \quad (2.1)$$

$$v_T = \left[ \frac{E}{2\rho(1+\mu)} \right]^{0.5} \quad (2.2)$$

$$v_S = \left[ \frac{(0.87 + 1.12\mu)}{(1+\mu)} \right] v_T \quad (2.3)$$

where:

$E$ : modulus of elasticity (Young's modulus) [N/m<sup>2</sup>]

$\mu$ : Poisson's ratio [( $E - 2G$ )/ $2G$ ]

$\rho$ : mass density [kg/m<sup>3</sup>]

The surface (Rayleigh) velocity is about  $0.92 \times$  shear wave velocity.

## 2.2 Some Common Velocities and Wavelengths

The velocities and acoustic impedance for the most common used materials are presented in Table 2-1.

**Table 2-1** Velocities and acoustic impedance for frequently used and tested materials at 20°C.

Material	Mass density	Velocity (LW)	Velocity (SW)	Acoustic impedance
	kg/m <sup>3</sup>	m/s	m/s	10 <sup>6</sup> kg/m <sup>2</sup> s
<b>Liquid couplant / wedge material</b>				
Water (20°C)	1,000	1,480	-	1.48
Heavy water	1,104	1,400	-	1.55
Glycerin (Hamikleer)	1,260	1,920	-	2.42
Motor oil	870	1,740	-	1.51
Acrylic resin	1,180	2,730	1,430	3.22
Lucite	1,180	2,680	1,260	3.16
Plexiglas	1,270	2,730	-	3.51
Polystyrene (Rexolite)	1,056	2,340	-	2.47

**Table 2-1** Velocities and acoustic impedance for frequently used and tested materials at 20°C. (Cont.)

Material	Mass density	Velocity (LW)	Velocity (SW)	Acoustic impedance
	kg/m <sup>3</sup>	m/s	m/s	10 <sup>6</sup> kg/m <sup>2</sup> s
<b>Component material</b>				
Aluminum	2,700	6,320	3,130	17.06
Brass	8,560	4,280	2,030	36.64
Copper	8,930	4,660	2,260	41.61
Gold	19,320	3,240	1,200	62.60
Inconel	8,500	5,820	3,020	49.47
Iron cast–slow	6,950	3,500	2,200	25
Iron cast–fast	7,350	5,600	3,200	40
Monel	8,830	5,350	2,720	47.24
Steel 1020	7,710	5,890	3,240	45.41
Steel, austenitic	7,910	5,740	3,090	45.40
Titanium	4,500	6,070	3,110	27.32
Tungsten	19,250	5,180	2,870	99.72
Zircaloy	6,500	4,686	2,360	30.46

Source: ASNT, *Nondestructive Testing Handbook, 2nd edition, vol. 7, Ultrasonic Testing* (Columbus, OH: American Society for Nondestructive Testing, 1991), p. 836–839.

The wavelengths for the most frequently used couplants, wedge materials, and inspected test pieces are presented in Table 2-2.

**Table 2-2** Wavelengths for the most commonly used couplants, wedges, and materials in industrial ultrasonic inspection at 20°C.

Frequency (MHz)	Wavelength (mm)	
	Longitudinal waves	Shear waves
<b>Water</b>		
1	1.5	-
2	0.75	-
4	0.4	-
5	0.3	-
10	0.15	-
<b>Glycerin (Hamikleer)</b>		
1	1.9	-
2	0.95	-
4	0.48	-
5	0.38	-
10	0.19	-
<b>Plexiglas</b>		
1	2.7	-
2	1.35	-
4	0.75	-
5	0.54	-
10	0.27	-

**Table 2-2** Wavelengths for the most commonly used couplants, wedges, and materials in industrial ultrasonic inspection at 20°C. (Cont.)

Frequency (MHz)	Wavelength (mm)	
	Longitudinal waves	Shear waves
<b>Rexolite</b>		
1	2.3	-
2	1.15	-
4	0.58	-
5	0.46	-
10	0.23	-
<b>Steel</b>		
1	5.9	3.2
2	3	1.6
4	1.5	0.8
5	1.2	0.6
10	0.6	0.3
<b>Aluminum</b>		
1	6.1	3
2	3	1.5
4	1.5	0.8
5	1.2	0.6
10	0.6	0.3

## 2.3 Sound Pressure Formulas

Sound pressure is critical in modeling inspection procedures. The following section gives numerical approaches for modeling. It also includes some aspects of refraction at interfaces, which is essential in modeling ultrasonics.

A co-phasal plane wave has a given phase of the oscillation ( $\omega$ ) moving parallel to itself. The wavefront may be spherical or cylindrical (see Figure 2-1).

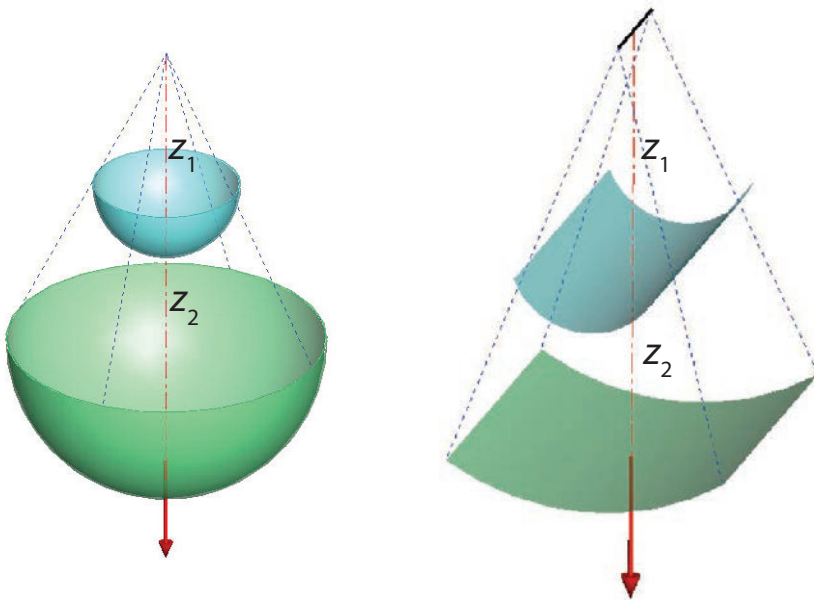


**Figure 2-1** Examples of propagation for spherical (point source) and cylindrical (line source) waves.

The sound pressure at a point for spherical waves depends on distance according to the following law:

$$\left(\frac{P_2}{P_1}\right)_{\text{spherical waves}} = \frac{z_2}{z_1} \quad (2.4)$$

The sound pressure for cylindrical waves changes as a function of the distance:

$$\left(\frac{P_2}{P_1}\right)_{\text{cylindrical waves}} = \left(\frac{z_2}{z_1}\right)^{0.5} \quad (2.5)$$

The ultrasonic waves have the following properties:

- *Reflection.* Energy returning off an interface where the acoustic impedances of the mating materials differ due to inherent acoustic velocity and density values ( $\alpha = \alpha'$  — or angle of incidence = angle of reflection).
- *Refraction.* A change in the direction of propagation when a wave passes from one medium to another of differing velocity (Snell's law:  $\frac{\sin \alpha}{\sin \beta} = \frac{v_1}{v_2}$ ).
- *Attenuation.* Reduction in amplitude, density, or energy as the result of friction absorption and scattering (basically loss of sound as it travels through a material, generally more pronounced as grain size increases). See also section 2.12, "Attenuation," page 66.
- *Dispersion.* Separation of a wave into waves of different frequencies (can be useful in specialized analysis of materials using frequency response analysis).
- *Interference.* Superposition of two or more waves of the same frequency resulting in a single wave (constructive wave fronts accumulating into one wave front).
- *Diffraction.* The ability of waves to spread around edges of small dimensions (such as the tips of cracks).
- *Polarization.* Associated with wave propagation in certain media where the displacement direction of the wave disturbance varies in time (directional property of wave vibration).
- *Mode-conversion.* Change of the vibration mode.

The main reflected/refracted combinations for longitudinal and shear waves in steel are presented in Figure 2-2. Solids can support both L-waves and S-waves (as well as other modes), and these are illustrated in Figure 2-2 (3). If the incident angle is above the "second critical angle," the shear wave is totally reflected. In most cases, extra wave modes (plate or diffracted, for example) are not included for clarity.

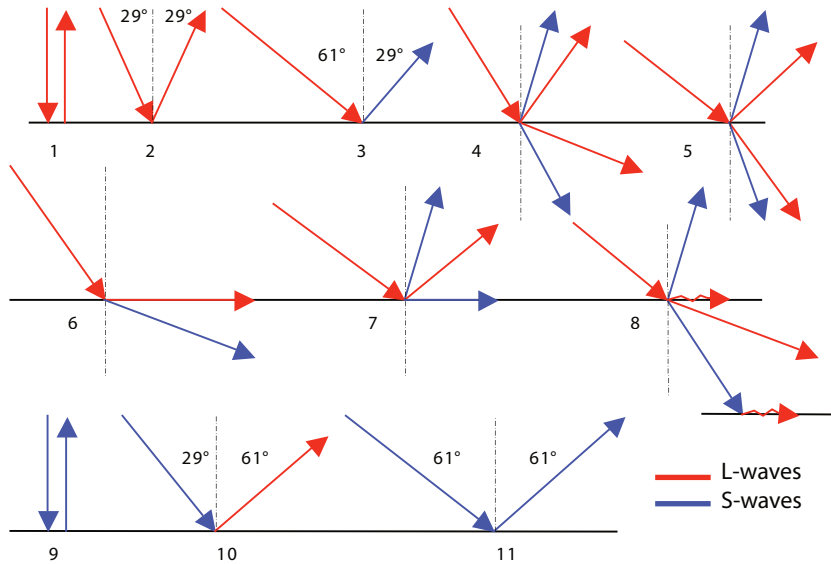


**Figure 2-2** Possible events from longitudinal and shear wave reflection/refraction in steel, with different interfaces (2nd medium) [red line is LW; blue line is SW]: (1) LW at normal incidence steel-air; (2) LW at 29° steel-air; (3) LW at 61° steel-air; (4) LW on the wedge-steel; (5) LW from steel to the wedge; (6) LW at first critical angle 1; (7) LW at second critical angle 2; (8) LW generating creeping waves; (9) SW at normal incidence (honey/viscose resin as couplant) steel-air; (10) SW at 29° steel-air; (11) SW at 61° steel-air.

The reflection coefficient ( $R$ ) is given by formula (2.6):

$$R = \frac{(Z_2 - Z_1)}{(Z_1 + Z_2)} \quad (2.6)$$

The transmission (refracted) coefficient ( $T$ ) is given by formula (2.7):

$$T = \frac{2Z_2}{(Z_1 + Z_2)} \quad (2.7)$$

The influence of the couplant in transmission is given by formula (2.8) [see Figure 2-3 for an example]:

$$T_{\text{couplant}} = \frac{(4Z_1/Z_3)}{[(Z_1/Z_3 + 1)^2 \cos^2 \theta + (Z_1/Z_2 + Z_2/Z_3) \sin^2 \theta]} \quad (2.8)$$

where:

$$\theta = 2\pi t_{\text{couplant}} / \lambda_{\text{couplant}}$$

$T_{\text{couplant}}$  = transmission coefficient through couplant

$Z_1$  = acoustic impedance of medium 1 (wedge)

$Z_2$  = acoustic impedance of the test piece

$Z_3$  = acoustic impedance of the couplant

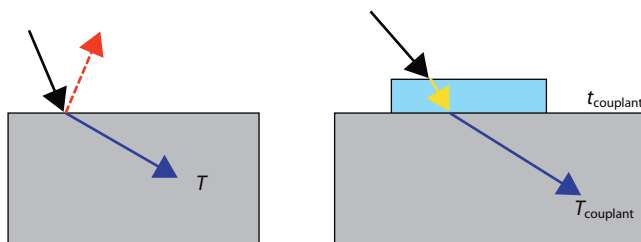


**Figure 2-3** Reflection and transmission coefficients for immersion (*left*) and direct contact (wedge) (*right*), taking the couplant layer into account.

The optimum couplant thickness is less than  $\lambda/2$ , and ideally only a few microns. For a couplant thickness of  $\lambda/4$ , the gain loss is about 5 dB.

The amplitude variation (dB or %FSH) is defined as:

$$\Delta A = 20 \log_{10} \left( \frac{A_1}{A_2} \right)$$

See Figure 2-4 for details.

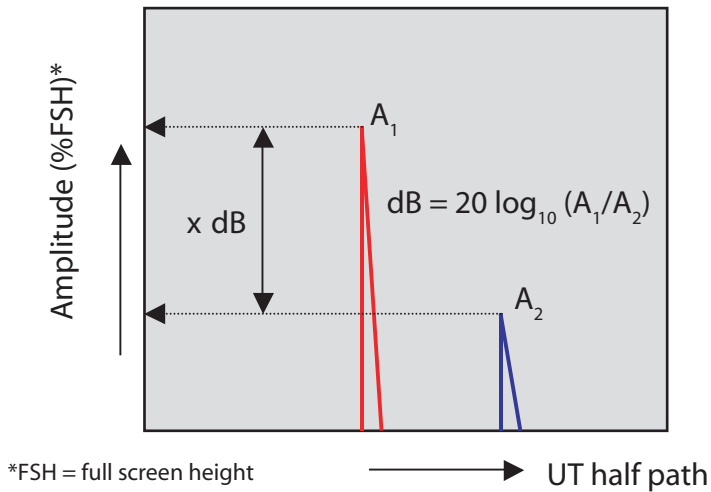


**Figure 2-4** Relationship between the amplitudes of two signals.

The relationship between the amplitude variation in % of FSH (full screen height) and the dB reading is presented in Figure 2-5.

For example, if a small crack signal has an amplitude of 40% from the reference level (which is, say, 100% of FSH) of an EDM (electrical discharged machining) notch, the crack amplitude is  $-8$  dB below this level.

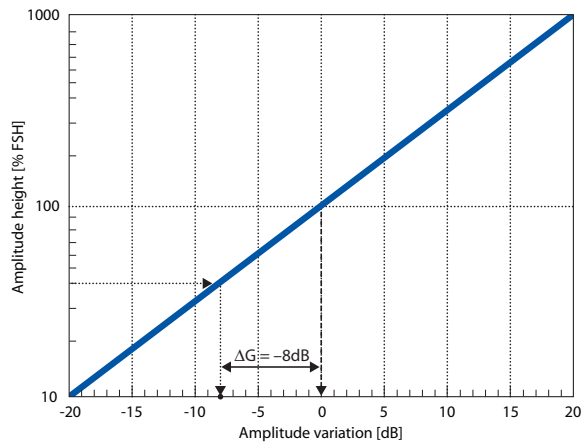


**Figure 2-5** Graph representation between amplitude ratio and dB value. Example for 40% of FSH vs. 100% of FSH;  $\Delta G = -8$  dB.

The transmission loss (in dB) of a wave from medium 1 to medium 2 is given by formula (2.9):

$$\Delta G_{\text{transmission}} = -20 \log_{10} \left[ \frac{Z_1 Z_2}{(Z_1 + Z_2)} \right] \quad (2.9)$$

The reflection loss (in dB) at the boundary between medium 1 and medium 2 is given by formula (2.10):

$$\Delta G_{\text{reflection}} = -20 \log_{10} \left[ \frac{(Z_2 - Z_1)}{(Z_1 + Z_2)} \right] \quad (2.10)$$

Snell's law will be affected by the velocity dependence on temperature. The graphs in Figure 2-6 to Figure 2-9 should be corrected for actual velocities at the test piece temperature. These temperature variations increase with a refracted angle. The velocity variations due to temperature (see Figure 2-10 to Figure 2-13) must be taken into account to avoid any error in detection, sizing, and positioning.

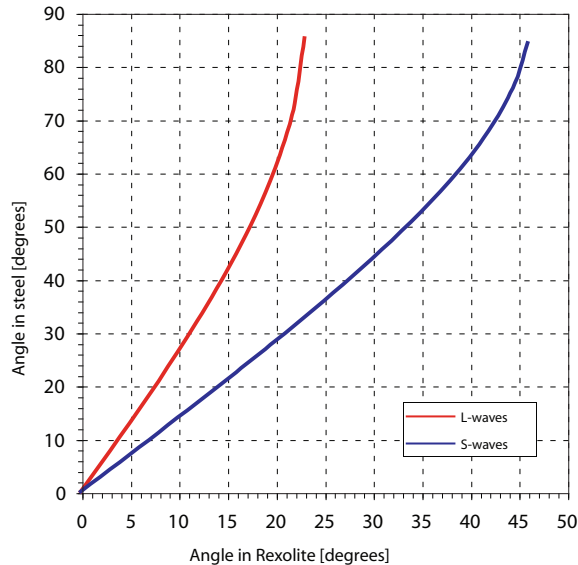


**Figure 2-6** Snell's law for a Rexolite wedge on mild steel.

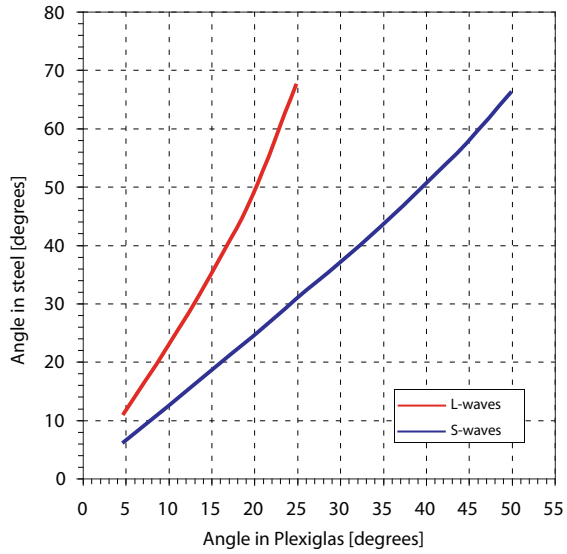


**Figure 2-7** Snell's law for a Plexiglas wedge on mild steel.

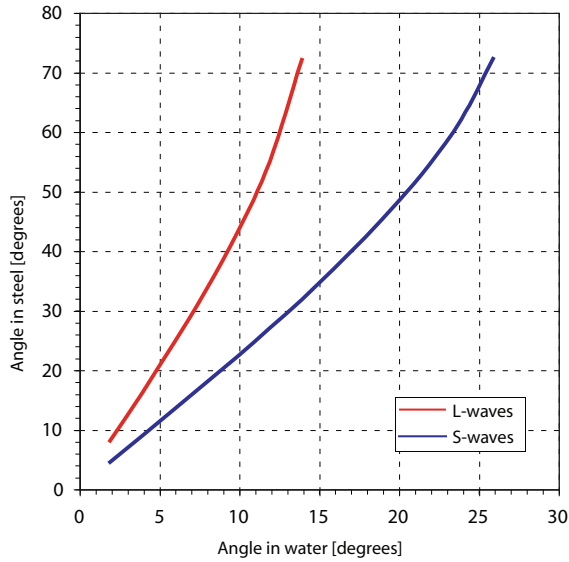


**Figure 2-8** Snell's law for immersion-mild steel.

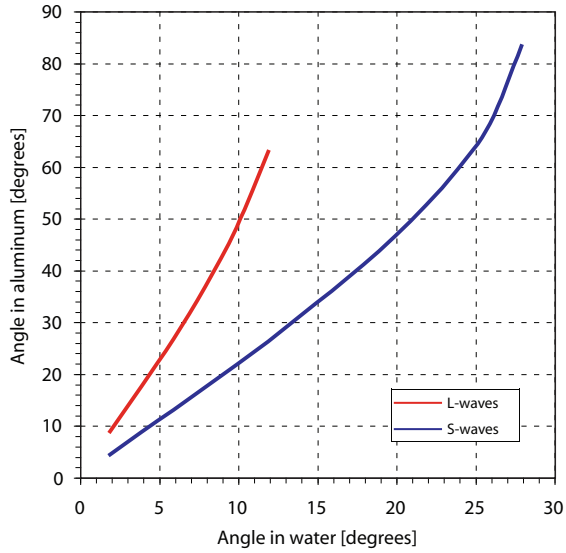


**Figure 2-9** Snell's law for water-aluminum.

The graphs in Figure 2-10 to Figure 2-13 show typical temperature effects on refracted angles. These types of results are important in industrial applications since components are often at a different temperature to the ideal or calibration values. Actual angles can be calculated using Snell's Law.

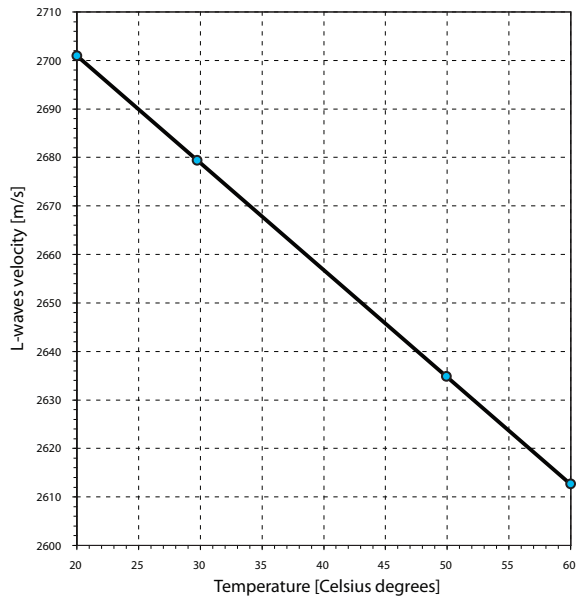


**Figure 2-10** Velocity variation in a Plexiglas wedge in relation to temperature.

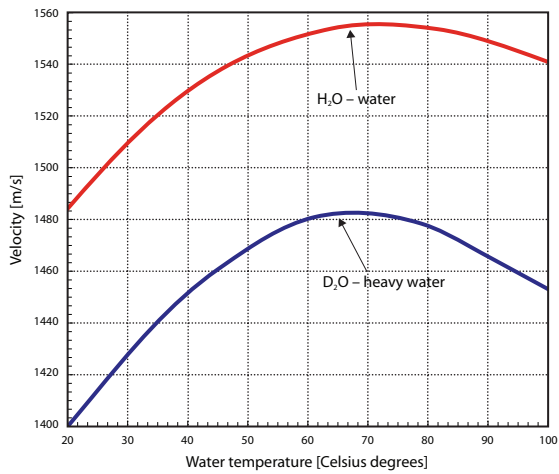


**Figure 2-11** Velocity variation in water and heavy water in relation to temperature.

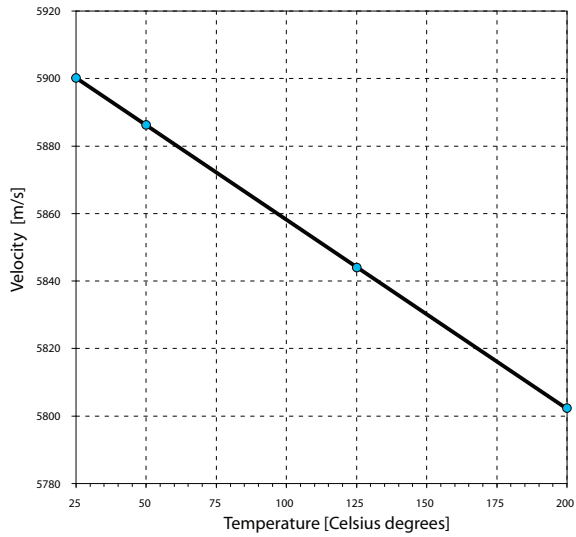


**Figure 2-12** Velocity variation of longitudinal waves in steel in relation to temperature.

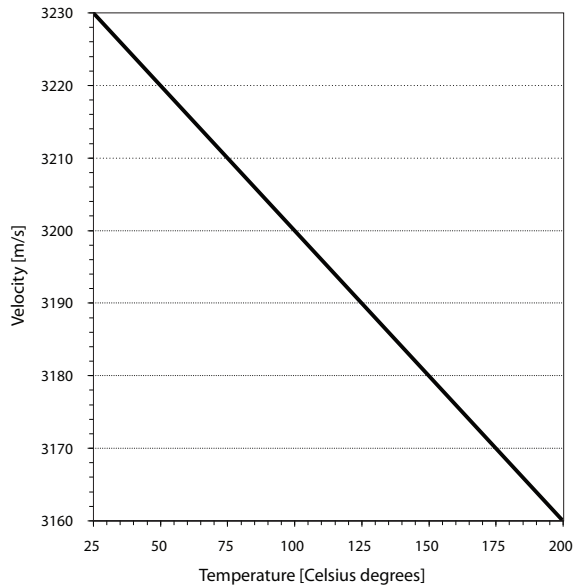


**Figure 2-13** Velocity variation of shear waves in steel in relation to temperature.

## 2.4 Example of Temperature Effects

As mentioned earlier, temperature can be an important factor in inspections if the refracted angles are outside a reasonable range. The following example shows how real refracted angles can be calculated.

Situation: An annular array probe is used in combination with a specially designed mirror to inspect a small bore piping weld. The probe system is immersed in water at 60°C. The sweep range was calibrated at 20°C. The sweep range is from 30° to 60°. What is the actual sweep range at 60°C?

Answer: Input the correction for velocities for 60°C from Figure 2-11 (water) and Figure 2-13 (T-waves—steel). The new velocity values will give you the sweep range in steel at 60°C as lying between 28.4° to 54.4°.

## 2.5 Circular Transducers

The sound pressure produced by a *circular transducer* possesses variations along the propagation axis (acoustic) and along the axis perpendicular to it. The ratio between probe diameter  $D$  and wavelength  $\lambda$  provides an answer to the location of maxima and minima, beam divergence, and beam diameter. For a free-field propagation (same medium, no interaction with defects, no reflection), the distance in front of the probe is divided into three regions (see Figure 2-14).

These results are strictly applicable to one test medium only, and for normal beam applications. In practice, conventional ultrasound produces a range of angles due to beam divergence and wedge refraction effects. However, these are small compared with phased array beam sweeping.

1. Near-field zone, for  $0 \leq z \leq N_0$
2. Transit-field zone, for  $N_0 \leq z \leq 3N_0$
3. Far-field zone, for  $z > 3N_0$

where:

$$N_0 = \frac{(D_{\text{probe}}^2 - \lambda^2)}{(4\lambda)}$$

is the near-field length. Near-field length depends on probe frequency and medium velocity. For probes with  $D_{\text{probe}}/\lambda > 10$ , the near-field length can be

approximated by formula (2.11):

$$N_0 = \frac{D_{\text{probe}}^2 f}{4v} \quad (2.11)$$

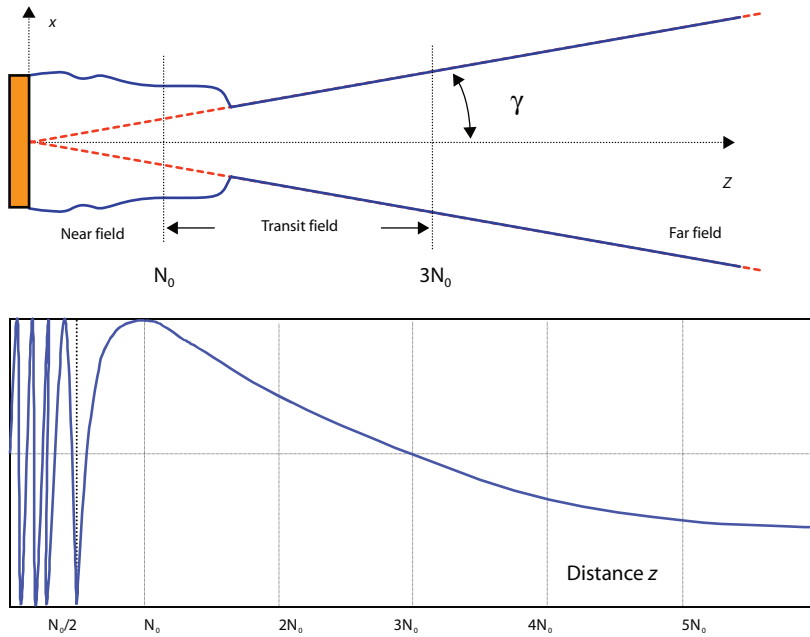


**Figure 2-14** Sound region definition in  $xz$  plane for a circular probe (*top*) and the pressure variation on the acoustic axis with distance (*bottom*) [disc-shaped transducer under continuous and constant excitation]. Note that this figure is for a theoretical monofrequency crystal with a sinusoidal pulse.

If the monofrequency crystal is excited by an electric signal with a different duration, the sound pressure has a different shape<sup>3</sup> (see Figure 2-15).

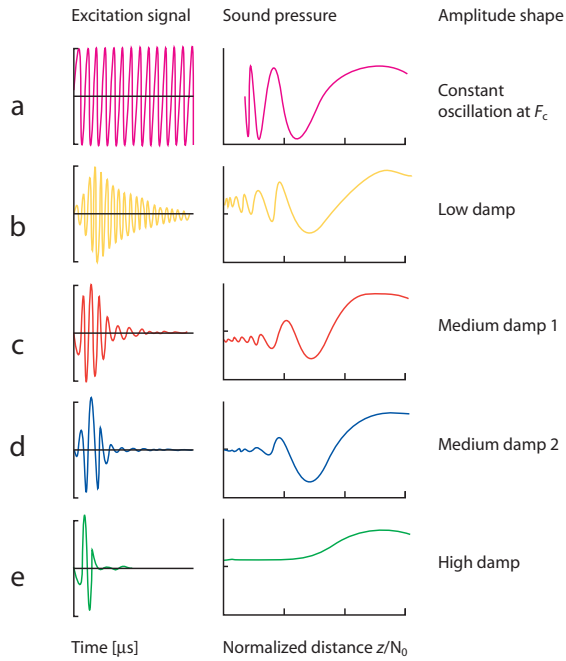


**Figure 2-15** Sound pressure dependence on pulse shape (duration) excitation for plane disc-shaped crystal.<sup>3</sup>

The sound pressure on the z-axis is given by formula (2.12):

$$P(z) = P_0 2 \sin \left\{ \frac{\pi}{\lambda} \left[ \sqrt{\left( \frac{D_{\text{probe}}}{2} \right)^2 + z^2} - z \right] \right\} \quad (2.12)$$

where:  $P_0$  = the sound pressure on the probe surface ( $z = 0$ ).

The sound pressure in the far field may be approximated by formula (2.13):

$$P(z) \approx \frac{P_0 \pi D_{\text{probe}}^2}{4 \lambda z} = \frac{P_0 S_{\text{probe}}}{\lambda z} \quad (2.13)$$

where:  $S_{\text{probe}}$  = probe surface area

Equivalent near-field length in different materials is given by formula (2.14):

$$N_{02} = \frac{N_{01} v_1}{v_2} \quad (2.14)$$

**Note:** This is for contact mode with no coupling path length.

The effective near-field length (see Figure 2-16) is given by formula (2.15):

$$N_{\text{eff}} = N_0 \left( \frac{\cos \beta}{\cos \alpha} \right)^2 \quad (2.15)$$

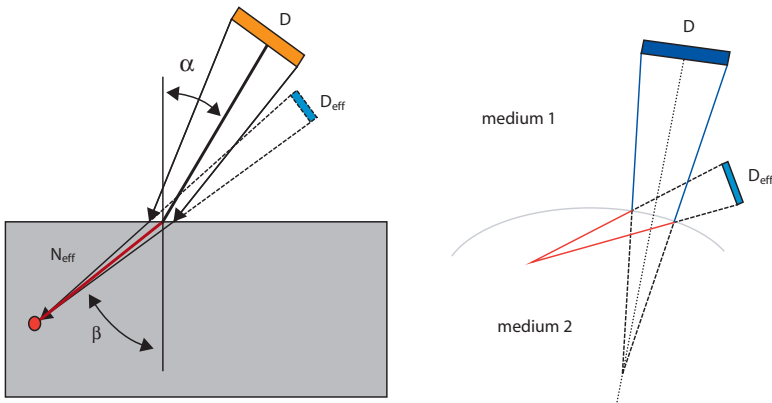


**Figure 2-16** Effective probe diameter and effective near-field length given by refraction law on planar and curved surfaces.

Figure 2-16 shows the shortening of the near-far field transition under angled transmission during immersion testing due to the narrowing effective aperture.

For longitudinal waves, the effective near-field length follows the curve shown in Figure 2-17.

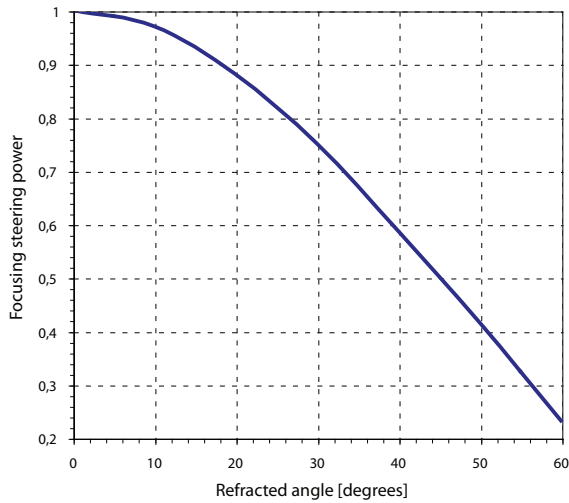


**Figure 2-17** Dependence of effective near-field length on refracted angle; longitudinal waves refracted from a 0° to 60° range.

The near-field length values for the most commonly used circular probes are presented in Table 2-3.

**Table 2-3** Near-field length for circular crystals (in millimeters).

Frequency (MHz)	Crystal diameter (mm)					
	5	6	10	12	20	24
Water; LW; $v = 1.5 \text{ mm}/\mu\text{s}$						
1	4.2	6	17	24	68	96
2	8.4	12	34	48	136	192
4	17	24	68	96	272	384
5	21	30	85	120	340	480
10	42	60	170	240	680	920
Steel; LW; $v = 5.9 \text{ mm}/\mu\text{s}$						
1	1	1.5	4	6	16	24
2	2	3	8	12	32	48
4	4	6	16	24	64	96
5	5	7	20	30	80	120
10	10	15	40	60	160	240
Steel; SW; $v = 3.2 \text{ mm}/\mu\text{s}$						
1	2	3	8	12	32	48
2	4	6	16	24	64	96
4	8	12	32	48	128	192
5	10	15	40	60	160	240
10	20	30	80	120	320	480

**Table 2-3** Near-field length for circular crystals (in millimeters). (Cont.)

Frequency (MHz)	Crystal diameter (mm)					
	5	6	10	12	20	24
Copper; LW; $v = 4.7 \text{ mm}/\mu\text{s}$						
1	1.3	2	5	8	20	32
2	2.6	4	10	16	40	64
4	5	8	20	32	80	128
5	6.5	10	26	40	104	160
10	13	20	52	80	208	320
Aluminum; LW; $v = 6.3 \text{ mm}/\mu\text{s}$						
1	1	1.4	4	6	16	24
2	2	3	8	12	32	48
4	4	6	16	24	64	96
5	5	7	20	30	80	120
10	10	14	40	60	160	240

For circular oscillators, the sound pressure on the transverse axis ( $x$ ) depends on the beam divergence angle, according to formula (2.16) for the far field only:

$$P(z, \gamma) = \frac{2P_z J_1(X)}{X} \quad (2.16)$$

where:

$J_1(X)$  = the first degree Bessel's function

$$X = \pi(D/\lambda) \sin \gamma$$

$\gamma$  = divergence angle

**Note:** For angles of less than  $10^\circ$ ,

$$\sin \gamma \approx \tan \gamma \approx \gamma [\text{in rad}] \quad [1 \text{ rad} = 57.3^\circ].$$

The sound profile in space is given by isometrics and cross sections at specific distances of sound pressure/amplitude (see Figure 2-18).

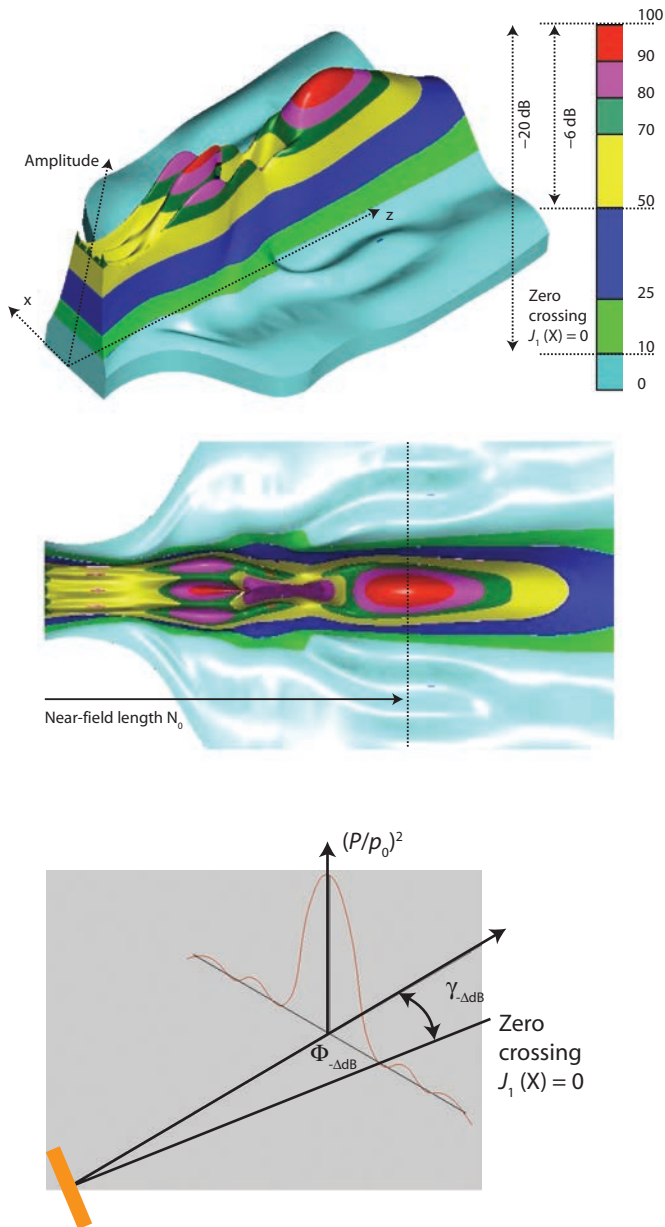


**Figure 2-18** Isometric (*top*), top view isobars display (*middle*), and cross section of sound pressure in the near field (*bottom*) from a circular probe.

## 2.6 Beam Divergence

The beam divergence angle in the far field depends on the probe diameter and frequency. The value for a specific dB drop is given in Table 2-4.

**Table 2-4** Half-angle beam divergence constant:  $\gamma_{-\Delta \text{ dB}} = \arcsin(k\lambda/D_{\text{probe}})$ .

$\Delta$ dB value	$k_{\text{free field}}$
-1.5	0.37
-3	0.51
-6	0.70
-10	0.87
-12	0.93
-24	1.09
Zero crossing ( $J_1 = 0$ )	1.22

The half-angle beam divergence for pulse-echo is linked with the half-angle beam divergence of the free-field using formula (2.17):

$$\gamma_{(2\Delta \text{ dB}) \text{ pulse-echo}} = \gamma_{(\Delta \text{ dB}) \text{ free field}} \quad (2.17)$$

The beam diameter for circular probes at a specific dB drop is obtained by measuring the beam width at the appropriate dB drop (see Figure 2-19).

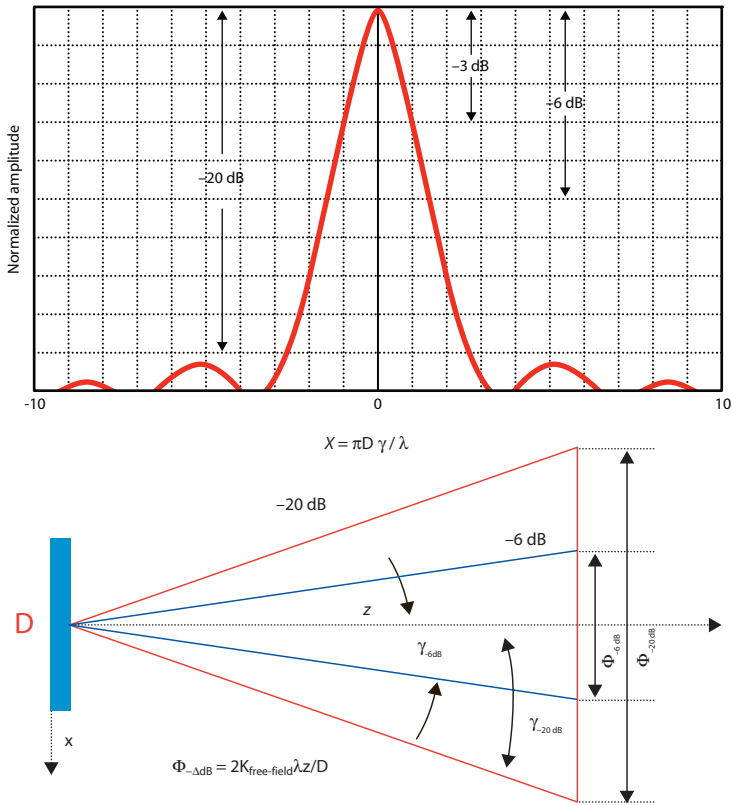


**Figure 2-19** Normalized amplitude dependence on divergence angle (*top*) and beam diameter dependence on distance and dB drop of normalized amplitude for a circular probe (*bottom*).

The beam spread at -6 dB and -20 dB for disc-shaped and rectangular-shaped probe surface is presented in Table 2-5.

**Table 2-5** Beam spread of disc-shaped and rectangular-shaped probes.

Probe	$\Delta$ dB	Beam spread
Disc-shaped	-6 dB	$\gamma_{-6\text{ dB}} = \arcsin\left(\frac{0.51\lambda}{D}\right)$
	-20 dB	$\gamma_{-20\text{ dB}} = \arcsin\left(\frac{0.87\lambda}{D}\right)$

**Table 2-5** Beam spread of disc-shaped and rectangular-shaped probes. (Cont.)

Probe	$\Delta$ dB	Beam spread
Rectangular-shaped	-6 dB	$\lambda_{-6 \text{ dB}} = \arcsin\left(\frac{0.44\lambda}{D}\right)$
	-20 dB	$\lambda_{-20 \text{ dB}} = \arcsin\left(\frac{0.74\lambda}{D}\right)$

The half angle spread in degrees at -6 dB drop in steel is presented in Figure 2-20.

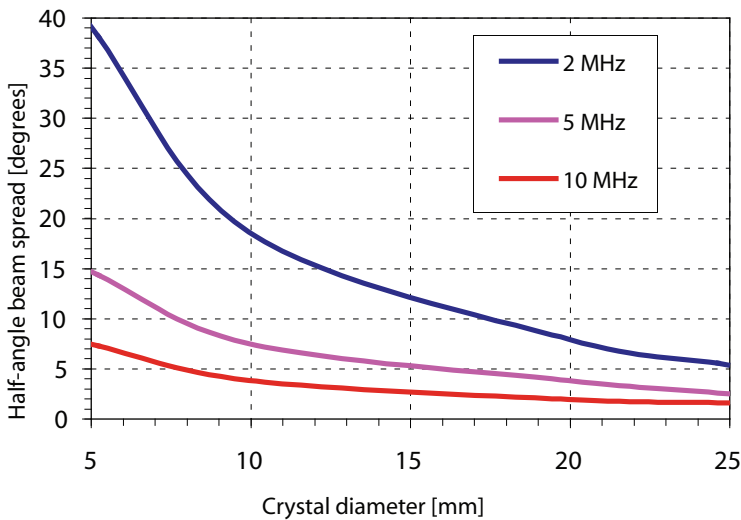


**Figure 2-20** 6 dB half-angle beam spread for longitudinal waves in carbon steel.

## 2.7 Rectangular Probes

Piezoelectric crystal and piezocomposite materials can also be cut as rectangular elements with a specific width/length ratio ( $W_{\text{probe}}/L_{\text{probe}}$ ).

The sound pressure is no longer symmetrical, but elliptical in the far field (see Figure 2-21). Its shape depends on the  $W_{\text{probe}}/L_{\text{probe}}$  ratio and the sound pressure equation is given by formula (2.18):

$$P_{\text{rectangular}} = P_0 \left( \frac{\sin X_1}{X_1} \right) \left( \frac{\sin X_2}{X_2} \right) \quad (2.18)$$

where:

$$X_1 = \pi(L/\lambda) \sin \gamma_{\text{length}}$$

$$X_2 = \pi(W/\lambda) \sin \gamma_{\text{width}}$$

$$L_{\text{crystal}} = \text{crystal length}$$

$$W_{\text{crystal}} = \text{crystal width}$$

$\gamma_{\text{length}}$  = half-angle beam divergence on length direction (xz plane)

$$\gamma_{\text{length}} = \frac{k_{\Delta \text{ dB}} \lambda}{L_{\text{crystal}}} \quad (2.19)$$

$\gamma_{\text{width}}$  = half-angle beam divergence on width direction (yz plane)

$$\gamma_{\text{width}} = \frac{k_{\Delta \text{ dB}} \lambda}{W_{\text{crystal}}} \quad (2.20)$$

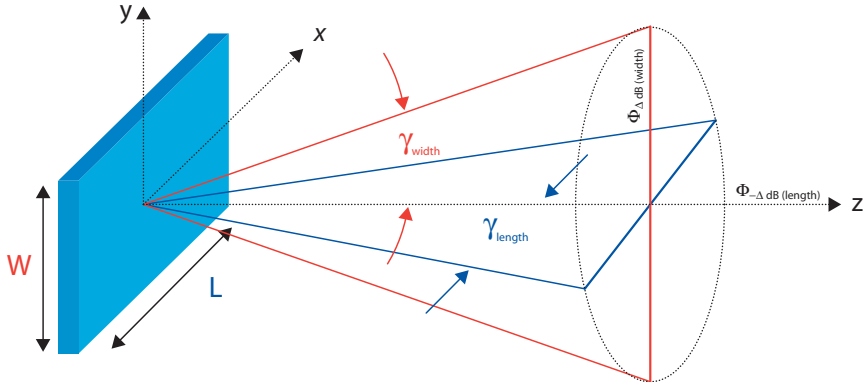


**Figure 2-21** Beam divergence and shape for a rectangular probe.

The half-angle beam divergence has a higher value for the width of the probe (where  $W_{\text{crystal}} < L_{\text{crystal}}$ ).

For a square crystal, the half-beam divergence in a free-field is equal to:

$$\gamma_{(-6 \text{ dB})L} = \arcsin(0.44\lambda/L_{\text{crystal}}) \quad (2.21)$$

$$\gamma_{(-6 \text{ dB})W} = \arcsin(0.44\lambda/W_{\text{crystal}})$$

$$\gamma_{(-20 \text{ dB})L} = \arcsin(0.74\lambda/L_{\text{crystal}})$$

$$\gamma_{(-20 \text{ dB})W} = \arcsin(0.74\lambda/W_{\text{crystal}})$$

The maximum pressure and the longest near-field length is achieved for a square probe ( $L_{\text{probe}} = W_{\text{probe}}$ ). The near-field length formula is shown in equation (2.22):<sup>10</sup>

$$N_{\text{rectangular}} = \frac{k_{\square} L_{\text{probe}}^2 f}{4v} \quad (2.22)$$

where:

$k_{\square}$  = near-field correction factor (see Figure 2-22)

$L_{\text{probe}}$  = probe length (mm)

$W_{\text{probe}}$  = probe width (mm)

$f$  = frequency (MHz)

$v$  = velocity in the test piece (mm/ $\mu$ s)

The effective near-field length is shorter, if the probe is mounted on the wedge, as shown in formula (2.23):

$$N_{\text{effective-rectangular on wedge}} = \frac{k_{\square}(L_{\text{probe}} \cos \beta / \cos \alpha)^2 f}{4v} - \frac{L_{\text{wedge}} v_{\text{test piece}}}{v_{\text{wedge}}} \quad (2.23)$$

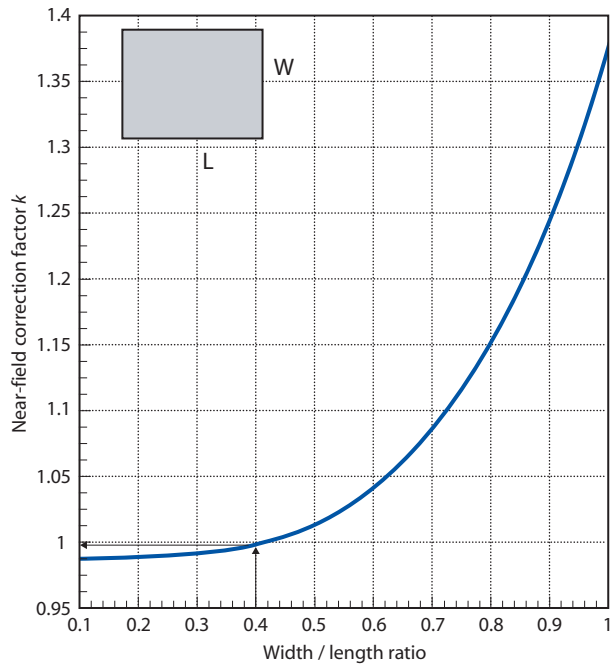


**Figure 2-22** Near-field length correction factor for a rectangular probe.<sup>9</sup>

## 2.8 Focused Sound Fields

The beam divergence in the far field (Fraunhofer region) and the pressure fluctuation in the near field (Fresnel region) have negative effects on defect evaluation and lateral resolution. Lateral resolution depends on beam width (see Figure 2-23).

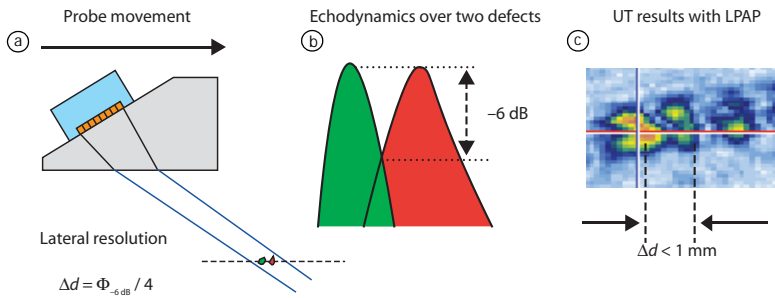


**Figure 2-23** Lateral resolution discrimination of two adjacent defects: (a) probe movement; (b) echo dynamics of two defects; (c) ultrasonic data to resolve volumetric defects (same depth and same angle of detection) spaced apart by a distance of less than 1 mm.

$$\Delta d = \frac{\Phi_{-6\text{dB}}}{4} \tag{2.24}$$

Formula (2.24) provides the discrimination or lateral resolving power. If the code requirements demand a constant lateral resolution over the inspected range (depth), the ultrasonic beam spread must be independent of the ultrasonic path length. Another requirement may be to increase the sensitivity in the near field. The solution may be the controlled focusing of the beam. A focused beam has a smaller diameter than the probe diameter at the focal point. By focusing the beam, the sound pressure is compressed in the near-field zone. Focusing may be obtained through curved crystals, special mirrors, phased arrays, or through the addition of a concave/convex lens (see Figure 2-24).

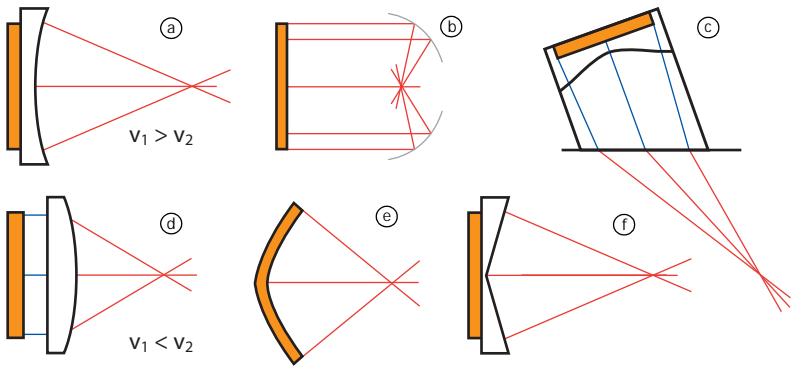


**Figure 2-24** Examples of focusing the ultrasonic beam: (a) concave lens ( $v_1 > v_2$ ); (b) concave mirror in water; (c) with a wedge and a concave lens for angled beam; (d) convex

lens ( $v_1 < v_2$ ); (e) concave crystal; (f) conical lens.<sup>7,8</sup> Note that axion lenses do not make a point focal spot.

The theory of focused beams is detailed in references 14–16 and 20–23. A summary of the theory is presented below:

- The ultrasonic beam may be focused by geometrical means only for  $z < N_0$ .
- A focused beam is characterized by the focusing factor or normalized focus depth:

$$S_{ac} = \frac{F_{ac}}{N_0} \quad (2.25)$$

with  $0 \leq S_{ac} \leq 1$  and  $F_{ac} < N_0$ , and  $F_{ac}$  is the actual focal depth.

- An optical focus point is defined by:

$$F_{opt} = \frac{R}{1 - (v_{test\ piece}/v_{lens})} \quad (2.26)$$

with  $R$  = lens curvature radius

- The optical focusing factor is defined by:

$$S_{opt} = \frac{F_{opt}}{N_0} \quad (2.27)$$

- At any point along the acoustic axis,  $F_{ac} < F_{opt}$ .
- The focused beam may be classified as:<sup>5</sup>
  - a) strong focusing for  $0.1 \leq S_{ac} \leq 0.33$
  - b) medium focusing for  $0.33 < S_{ac} \leq 0.67$
  - c) weak focusing for  $0.67 < S_{ac} \leq 1.0$
- Most of the industrial applications that work with focused beams use  $S_{ac} < 0.6$ .
- The sound pressure of a spherical curved circular crystal is given by:<sup>1</sup>

$$P(z, R, D, \lambda) = \frac{2P_0}{(1 - z/z_0) \sin \{ [(z-h)^2 + (D^2/4)]^{0.5} - (z - hv_2/v_1) \}} \quad (2.28)$$

where:

$$h = R - \left( R^2 - \frac{D^2}{4} \right)^{0.5} ; \quad z_0 = \frac{\{ h^2 [1 - (v_2/v_1)^2] + z^2 \}}{2h [1 - (v_2/v_1)]}$$

- The relationship between  $S_{ac}$  and  $S_{opt}$  is given by the equation:<sup>6</sup>

$$S_{opt} = \frac{(S_{ac} - 0.635S_{ac}^2 + 0.2128S_{ac}^3)}{(1 - S_{ac})} \quad (2.29)$$

- The dependence of  $S_{opt}$  on  $S_{ac}$  is presented in Figure 2-25.
- The constituents of a focused beam are illustrated in Figure 2-26.

The depth of field depends on  $S_{ac}$  according to the formulas above (see also Figure 2-27).

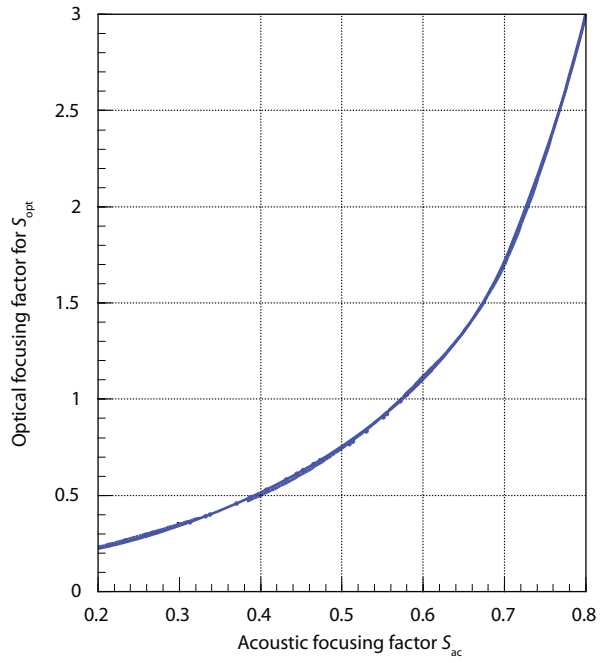


**Figure 2-25** Dependence of  $S_{opt}$  on  $S_{ac}$  for  $0.2 \leq F_{ac} / N_0 \leq 0.8$ .

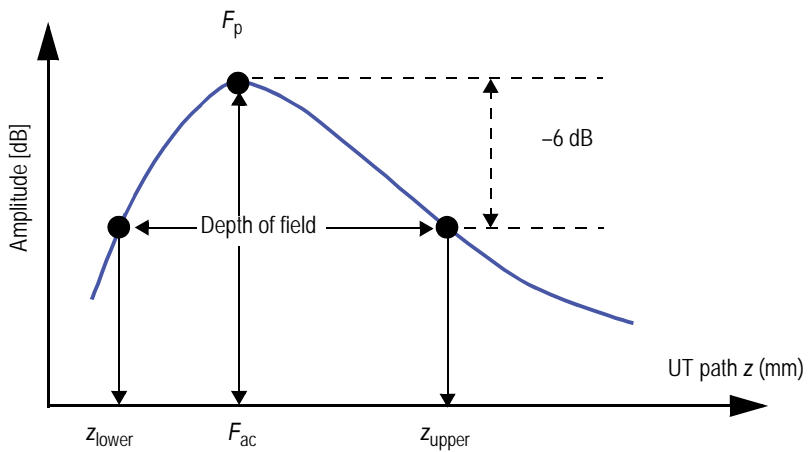


**Figure 2-26** Definition of focal depth and depth of field (focal length).

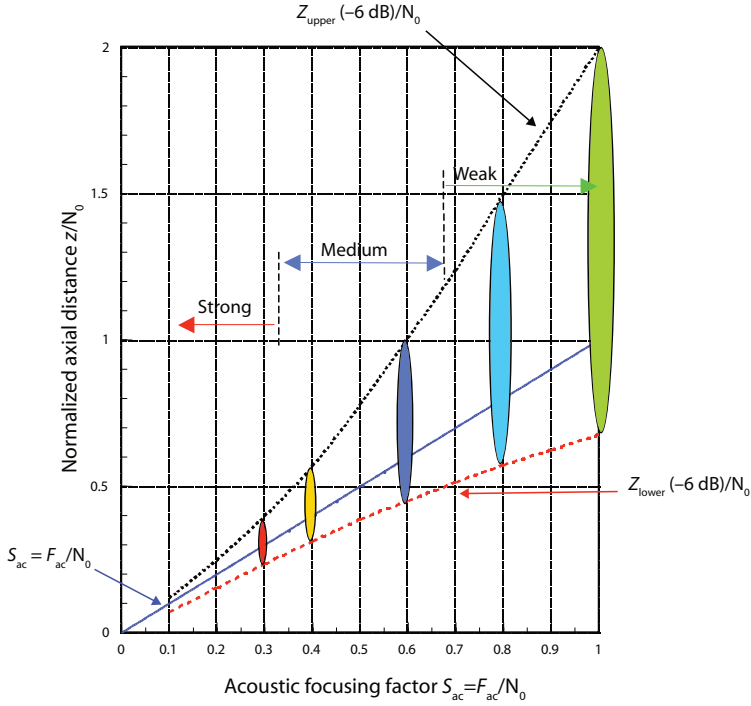


**Figure 2-27** Dependence of depth of field on acoustic focusing factor.

For  $S_{ac} < 0.6$ , the depth of field is computed with the following formula:

$$L_{-6\text{ dB}} = 7\lambda \left( \frac{F_{ac}}{D_{probe}} \right)^2 \quad (2.30)$$

The beam diameter at  $-6$  dB drop is given by:

$$\Phi_{-6\text{ dB}} = \frac{S_{ac} D_{probe}}{4} \quad \text{or} \quad \frac{\lambda F_{ac}}{D_{probe}} \quad (2.31)$$

These formulas may be translated into the following statements:

- A higher-frequency probe with an identical diameter will produce a narrower beam than a probe with a lower frequency.
- The field depth is shorter for a smaller  $S_{ac}$ .
- The beam diameter is smaller for a smaller  $S_{ac}$ .

- A constant lateral resolution over a large ultrasonic range can be achieved only by probes with different  $S_{ac}$  values; this inconvenience is eliminated by phased array probes (annular, linear, matrix) working with dynamic depth focusing (DDF) [see chapter 3].

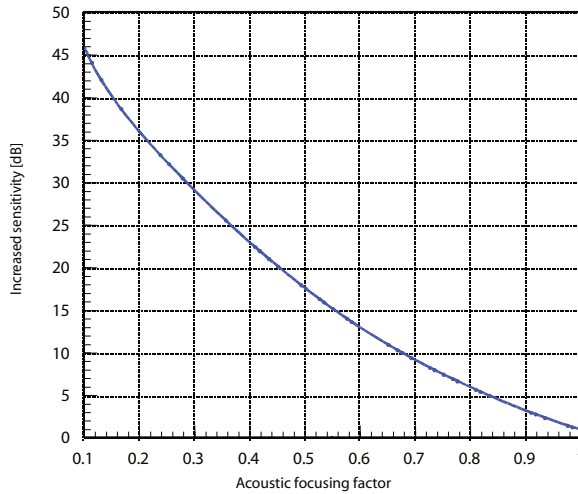


**Figure 2-28** Increased sensitivity for an annular array probe (spherical focused) with  $D_{probe} / \lambda = 15$  in detecting small inclusions with diameter of less than 1 mm in titanium billets.

## 2.9 Time-Frequency Response

The radio frequency (RF) signal from a specific reflector is used to measure the following time-response features (see Figure 2-29):

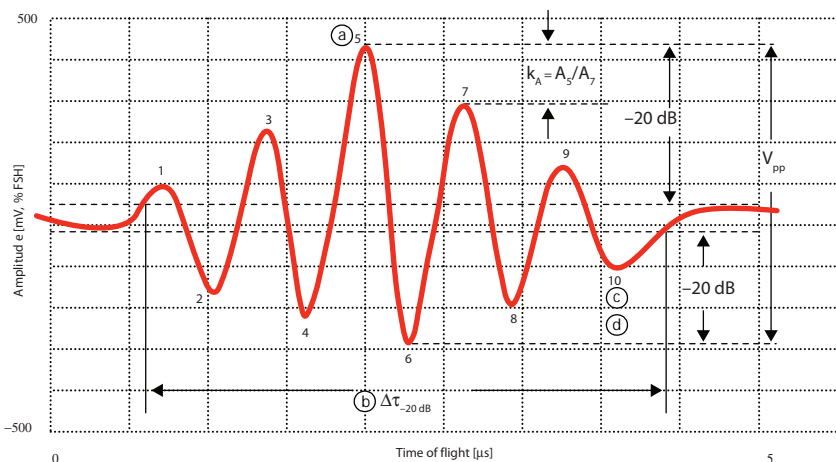


**Figure 2-29** RF signal characteristics: (a)  $V_{pp} = 700$  mV; (b)  $\Sigma\tau_{-20\text{ dB}} = 3.25$   $\mu\text{s}$ ; (c) peak number PN = 10; (d) cycle number CN = 5; (e) damping factor  $k_A = 1.4$ .

- Peak-to-peak amplitude ( $V_{pp}$ ): the maximum deviation (in volts or %) between the largest positive and the largest negative cycle amplitudes of the RF signal.
- Pulse duration, or waveform length ( $\Delta\tau_{-20\text{ dB}}$ ): represents the waveform duration for a cutoff at  $-20$  dB from positive and negative maximum amplitudes.
- Peak number (PN): the number of peaks from the RF signal which cross the  $-20$  dB negative and positive cutoffs.
- Cycle number (CN): the number of peaks divided by two (or the number of wavelengths).
- Damping factor ( $d_A$ ): the ratio between the maximum amplitude and the next highest positive amplitude.

The RF signal is converted into a frequency-response [formula (2.32)] through a fast Fourier transform (FFT), which is characterized by the following features (see Figure 2-30):

- Peak frequency ( $f_{\text{peak}}$ ): the maximum occurring frequency value of the FFT.
- Lower frequency ( $f_{L-6\text{ dB}}$ ): the frequency value on the left portion of the peak frequency, determined by the  $-6$  dB drop horizontal line.
- Upper frequency ( $f_{U-6\text{ dB}}$ ): the frequency value on the right portion of the peak frequency, determined by the  $-6$  dB drop horizontal line.

- Center frequency ( $f_c$ ): the frequency evaluated by the arithmetic or geometric mean<sup>11</sup> of the lower and upper frequencies.

$$f_c = \frac{(f_{L-6\text{ dB}} + f_{U-6\text{ dB}})}{2} \quad \text{or} \quad f_c = (f_{L-6\text{ dB}} \cdot f_{U-6\text{ dB}})^{0.5} \quad (2.32)$$

- Bandwidth (relative) [ $BW_{\text{rel}}$ ]: the frequency range within given limits.

$$BW_{\text{rel}}[\%] = 100\% \cdot \frac{(f_{U-6\text{ dB}} - f_{L-6\text{ dB}})}{f_c} \quad (2.33)$$

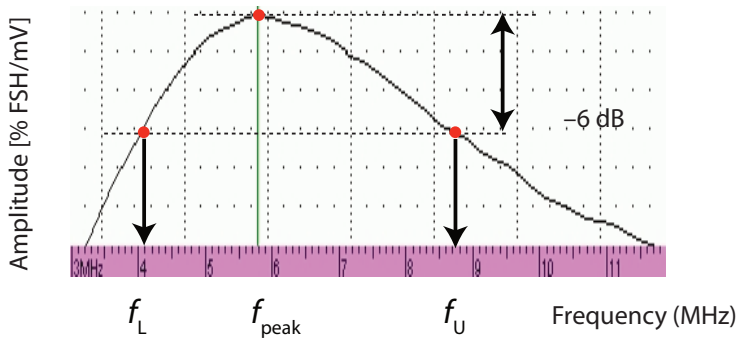


**Figure 2-30** FFT response of a 5-MHz phased array probe;  
 $f_c = (2.539 + 7.813) \text{ MHz} / 2 = 5.2 \text{ MHz}$ ;  
 $BW_{\text{rel}} = (7.813 - 2.539) \text{ MHz} / 5.2 \text{ MHz} \times 100\% = 54\%$ .

## 2.10 Probe Classification Based on $BW$ (Damping)

See Figure 2-31 for a description.

- |                          |           |                      |
|--------------------------|-----------|----------------------|
| • Narrow bandwidth       | (15–30%)  | best for detection   |
| • Medium bandwidth       | (31–75%)  | detection and sizing |
| • Broad (wide) bandwidth | (76–110%) | best for sizing      |

These are general guidelines for ferritic materials and some others. The actual guidelines depend on crack morphology and orientation. These guidelines are true for planar normal incidence, but are not typically valid for austenitic detection and sizing of branched cracks in austenitic and/or dissimilar materials.

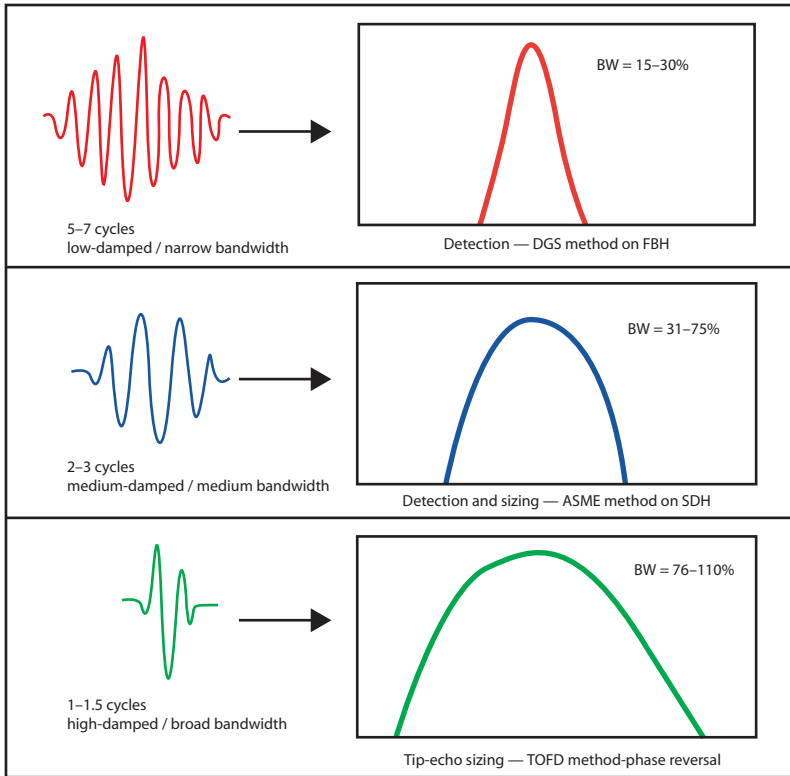


**Figure 2-31** Probe classification based on relative bandwidth.

Pulse shape (duration) has a direct effect on axial resolution (with fixed angle and stationary probe). Axial resolution is the ultrasonic capability of resolving two adjacent defects separated along the acoustic axis through a small  $\Delta z$  ultrasound path. For good axial resolution, reflectors should produce peak amplitudes that are separated by more than 6 dB (peak-valley).

Phased array probes typically have a broad bandwidth, and the piezocomposite material which phased array probes are made of provides high sizing performance. Piezocomposite material also provides high power and good detection, which makes the best compromise.

The axial resolution formula can be given by the following relationship (see also Figure 2-32):

$$\Delta z = \frac{v_{\text{test piece}} [\text{mm}/\mu\text{s}] \cdot \Delta\tau_{-20 \text{ dB}} [\mu\text{s}]}{2} \quad (2.34)$$

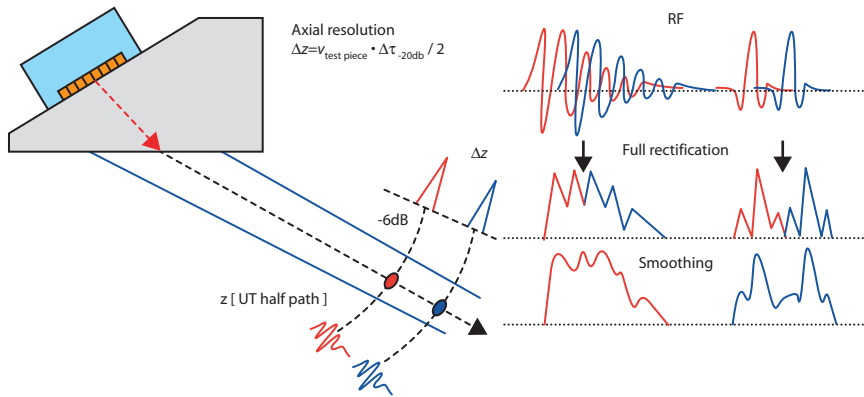


**Figure 2-32** Axial resolution: principle (*left*); poor and good resolution (*right*).

Additional information regarding probe features and test block characteristics can be found in references 14–18, 42, 46, 50–52, 54–57, 59, and 105.

## 2.11 Ultrasonic Beam Interaction with Test Piece / Reflectors

Regardless of whether the inspection is performed in immersion or contact, and whether the probe is a monocrystal or a linear phased array, the interaction between the ultrasound beam and the test piece is governed by the *detectability region*.

The detectability region is the area where one can detect and size specific defects—such as dimensions—with enough gain and with a signal 6 dB greater than competing noise signals, including front surface ring-down or initial components of backwall signals.

The detectability region is defined by the following curves or boundaries (see Figure 2-33):

- a) *backwall (BW) reflectivity curve*: this defines the maximum energy the probe may receive by specular reflection;
- b) *near-surface resolution (NSR)* [or the dead zone]: this defines the minimum distance a defect may be separated from the main bang signal or the interface (immersion) signal, and still be resolved; the higher the gain of the receiver, the longer the dead zone;
- c) *attenuation curve (ATTN)*: the gain in reserve ( $G_{\text{reserve}}$ ) is the maximum gain the electronic instrument can provide. Starting from

that point, the gain is reduced due to attenuation in the test piece; the loss due to attenuation is governed by the equation:

$$\Delta G_{\text{attenuation}} = 2\alpha UT_{\text{path}} \text{ [dB]}$$

d) *noise level* (NOISE) and the *useful gain* ( $G_{\text{useful}}$ ): once the probe is plugged into the ultrasonic instrument and coupled with the test piece, the electronic noise level increases; this noise has a stochastic distribution, with contributions from the probe, wedge, cable, couplant and test piece structure; its amplitude has an identical law to BW, but the starting point is determined by the  $G_{\text{useful}}$ .

Outside the detectability region, any defects are *undetectable*, due to dead-zone influence, increased noise level, and exhaustion of the electronic gain in the amplifier due to attenuation or/and defects being too close to the backwall.

An ideal disc-shaped reflector (flat-bottomed hole, FBH), perpendicular to the beam, has an amplitude given by the DGS method for defects smaller than the beam, and centered:<sup>1</sup>

$$P_{\text{FBH}} = \frac{P_{0 \text{ probe}} (\pi D_{\text{FBH}} D_{\text{probe}})^2}{16\lambda^2 z^2} \quad (2.35)$$

If the normalized features are used:

$$\frac{z}{N_0} = D \text{ [Distance]} , \quad \frac{H_{\text{reflector}}}{H_{\text{probe}}} = G \text{ [amplifier Gain]} ;$$

$$\frac{D_{\text{FBH}}}{D_{\text{probe}}} = S \text{ [reflector normalized Size]} ,$$

generates the DGS diagram.

The reflectivity diagram for the DGS method in the far field leads to the following simple rules:

- double the distance, and the amplitude decreases by  $-12$  dB;
- double the reflector size, and the amplitude increases by  $+12$  dB.

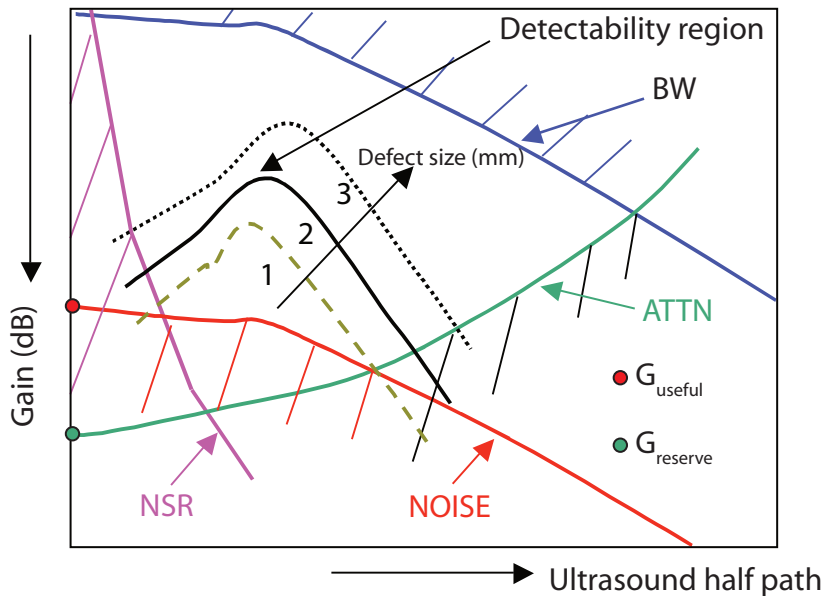


**Figure 2-33** Definition of the detectability region.

Sensitivity settings depend on the reference reflector and its signal-to-noise ratio (SNR). When using the TCG (time-of-flight corrected gain) feature, first establish the SNR for the worst detection case.

The *signal-to-noise ratio* is the difference in decibels (dB) between the amplitude of a reference reflector and the average amplitude of the noise given by electronic, coupling, probe, and test piece contributions. The SNR is evaluated for a specific setup, target size, and UT path [see formula (2.36) and Figure 2-34].

$$\text{SNR} = 20 \log_{10} \left( \frac{\text{Ampl.}_{\text{target}}}{\text{Ampl.}_{\text{noise}}} \right) \quad (2.36)$$

A practical minimum value for SNR is 10 dB or a 3:1 ratio.

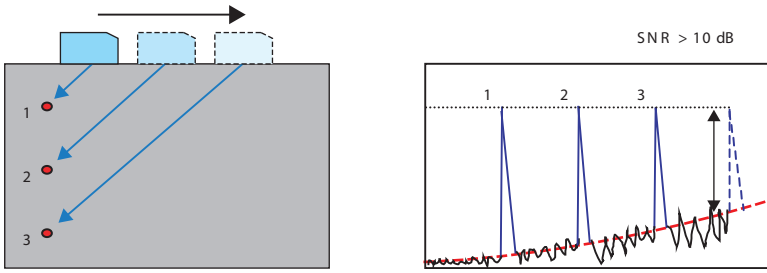


**Figure 2-34** SNR evaluation for TCG feature. SNR typically should be greater than 3:1 (10 dB).

The most commonly used reflectors for sensitivity setting are illustrated in Figure 2-35. Specific reflectivity reflectors (depending on ultrasonic beam path, frequency, and reflector size) for small reflectors, whose size is less than the beam width, are given in Table 2-6.

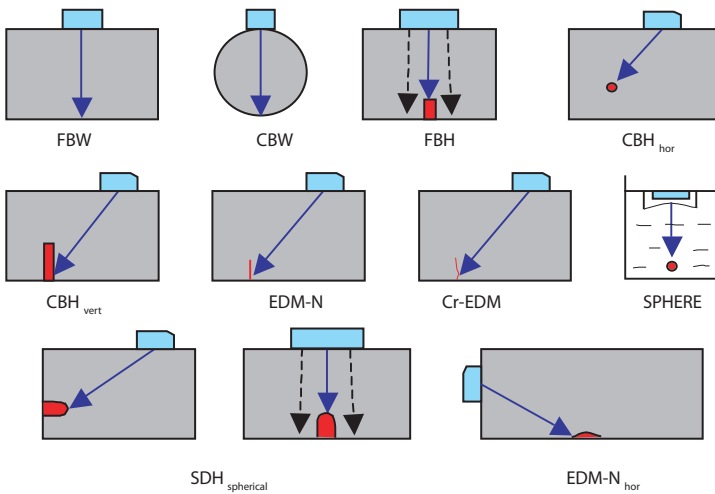


**Figure 2-35** The most commonly used reflectors for sensitivity setting.

The following relationship [see formula (2.37)] between the two artificial reflectors, flat-bottomed holes (FBH) and side-drilled holes (SDH), may be used for equivalent amplitudes when  $z > 1.5N_0$ .

$$D_{\text{FBH}} = (0.2\lambda^2 z D_{\text{SDH}})^{0.25} \quad (2.37)$$

The equivalent FBH diameter versus a spherical-bottomed hole is given by the relationship in formula 2.38:

$$D_{\text{FBH}} = 0.56(\lambda D_{\text{sphere}})^{0.5} \quad (2.38)$$

**Table 2-6** Reflectivity pattern for small reference reflectors.

Reflector type	Reflectivity law (far field)
FBW (counter-bore)	$\lambda^{-1} U_{\text{path}}^{-1}$
SDH (lack of penetration)	$\sqrt{\frac{1}{2} D_{\text{SDH}}^{0.5} \lambda^{-1} U_{\text{path}}^{-1.5}}$
FBH normal (smooth crack)	$D_{\text{FBH}}^2 \lambda^{-2} U_{\text{path}}^{-2}$
Edge from misoriented crack <sup>12</sup>	$K_{(\epsilon)} \lambda^{-1.5} U_{\text{path}}^{-1.5} \left( \frac{0.5a}{a - U_{\text{path}} \cos \epsilon} \right)^{0.5}$
Elliptical EDM notch –normal	$H_{\text{notch}} \lambda^{-1.5} U_{\text{path}}^{-1.5}$
Small sphere (porosity)	$D_{\text{sphere}} \lambda^{-1} U_{\text{path}}^{-2}$

where:

- $U_{\text{path}}$  = half path
- $\lambda$  = wavelength
- $D_{\text{SDH / FBH / sphere}}$  = diameter of (SDH, FBH, or sphere)
- $H_{\text{notch}}$  = notch height
- $a$  = crack edge curvature radius
- $K_{(\epsilon)}$  = diffraction coefficient
- $\epsilon$  = angle between incident ray and crack surface

Figure 2-36 presents the amplitude dependence level on defect size for different reflectors: FBH, SDH, notch, sphere, and detected by shear waves, longitudinal waves, and creeping waves.

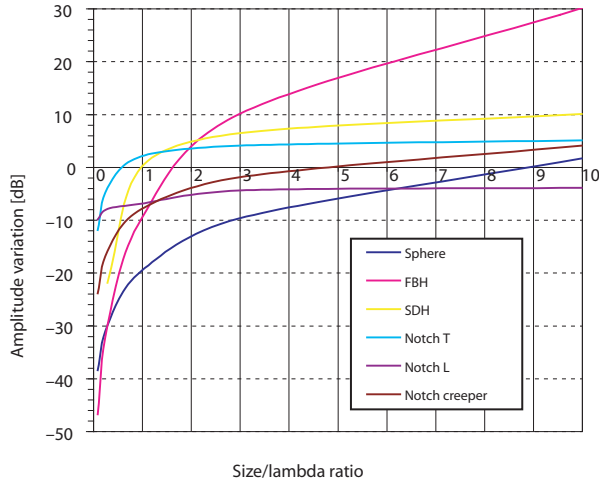


**Figure 2-36** Amplitude dependence on normalized defect size for: sphere; FBH; SDH-SW; N-LW; N-SW; N-Cr.

## 2.12 Attenuation

Attenuation of ultrasonic waves is caused by absorption and scattering (see also definition on page 30). The attenuation depends on frequency ( $f$ ), grain size ( $\Phi_{\text{grain}}$ ), wave type, and anisotropy coefficient.

$$\text{Attenuation} = \text{constant}_{\text{absorption}} f + \text{constant}_{\text{scattering}} f^4 \quad (2.39)$$

The scattering depends on the ratio between the grain size and wavelength:

- for  $\Phi_{\text{grain}} < \lambda \rightarrow$  Rayleigh scattering
- for  $\Phi_{\text{grain}} \approx \lambda \rightarrow$  stochastic scattering
- for  $\Phi_{\text{grain}} > \lambda \rightarrow$  diffuse scattering

When testing coarse-grained parts, the frequency must be chosen according to the following formula:

$$\lambda_{\text{min}} > 6\Phi_{\text{grain}} \quad (2.40)$$

Attenuation dependence on frequency for the most commonly used couplants/wedges and for steel are presented in Figure 2-37 to Figure 2-39.

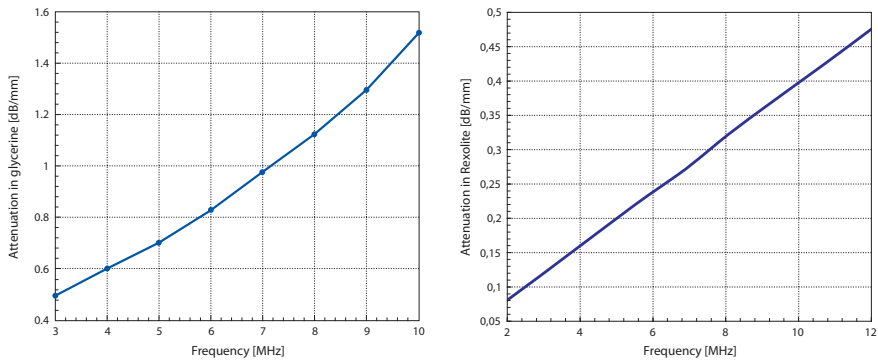


**Figure 2-37** Attenuation dependence on frequency for glycerin/Hamikleer and Rexolite.

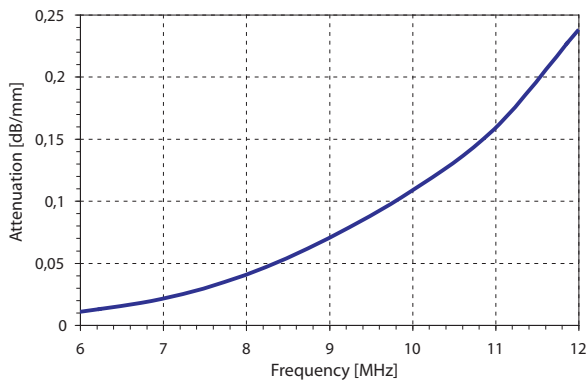


**Figure 2-38** Attenuation in 2.25 Cr-Mo steel for longitudinal waves.

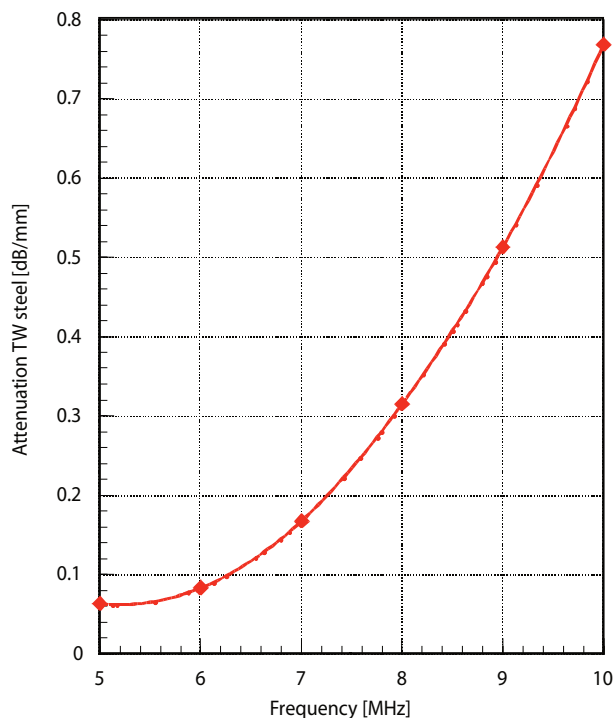


**Figure 2-39** Attenuation in steel for shear waves.

Accurate crack sizing with L-waves or S-waves is based on TOFD or tip-echo back scattering diffraction (see section 2.13 below).

## 2.13 Defect Sizing Using Diffraction and Mode-Conversion Techniques

### 2.13.1 TOFD (Time-of-Flight Diffraction)

TOFD is now becoming a standard technique for both power generation and petrochemical industries. TOFD can also be performed by phased array probes; TOFD is simply a procedure that uses two probes in pitch-and-catch mode. The main difference between power generation and petrochemical applications is that power generation applications typically use raster TOFD, while the petrochemical industry and other industries use linear TOFD. Raster TOFD collects more data and is more accurate, while linear TOFD is

faster. Most of the weld caps in power generation are removed, which permits raster scanning.

**Note:** *Linear scanning* is single-axis scanning parallel to the weld. *Raster scanning* is an *x-y* back-and-forth scanning motion.

TOFD detects and records signals diffracted from defect tips for both detection and sizing. The TOFD data is displayed in a gray-scale B-scan. Modifications to this standard setup are possible.

Four types of waves are used in TOFD:

- The *lateral wave*: A sub-near-surface longitudinal wave generated from the wide beam of the probe.
- The *backwall reflection*: A longitudinal wave reflected from the backwall.
- The *reflected wave*: A longitudinal wave reflected by a lamellar planar defect.
- The *tip diffracted wave*: A circular wave diffracted by the edge of a defect. Both longitudinal and shear waves are normally generated, but L-waves are typically used for TOFD.

The TOFD method is based on the following principles:

- Pitch-and-catch setups are in LW configuration (see Figure 2-40).
- The probes are high-damped ( $1.5 \lambda$ , or white-black-white, with  $BW_{rel} > 90\%$ ) and high-frequenced ( $>6$  MHz).
- The beam divergence is large enough to produce lateral waves and a backwall reflection, so the entire wall thickness is displayed between the lateral waves and backwall (skipped) signals.
- The probes are typically centered over the weld center line.
- For walls thicker than 75 mm, double TOFD pairs should be used.
- Wedge delay, velocity in the test piece, lateral wave TOF, backwall TOF value, thickness, and PCS (probe center separation) must be known (though some can be deduced).
- Upper-tip and lower-tip echoes have phase reversal (see Figure 2-40 for an illustration of the physics).
- Additional defect image recognition can be performed with mode-converted (LT, TL) signals.

- A preamplifier is often required to display the digital signals from defect edges, which are  $-20$  dB to  $-30$  dB lower than a 3 mm side-drilled hole signal at the same range.
- Maximum amplitudes of diffracted signals are obtained at about  $70^\circ$ .
- L-waves are preferred to T-waves for their “first-hit” arrival at the defect edges; they are also less attenuated by test piece structure.
- Linear scanning is performed in a single scan, parallel with the weld center line.

Assuming the defect is symmetrically placed between probes, the following formulas are used to measure defect height  $h$  ( $2a$ ) and the upper ligament ( $d$ ):

$$T_{\text{lat. wave}} = \frac{\text{PCS}}{v_L} = \frac{2S}{v_L} \quad (2.41)$$

$$T_{\text{upper tip}} = \frac{2(S^2 + d^2)^{0.5}}{v_L} \quad (2.42)$$

$$T_{\text{lower tip}} = \frac{2[S^2 + (d + h)^2]^{0.5}}{v_L} \quad (2.43)$$

$$T_{\text{backwall}} = \frac{2(S^2 + t^2)^{0.5}}{v_L} \quad (2.44)$$

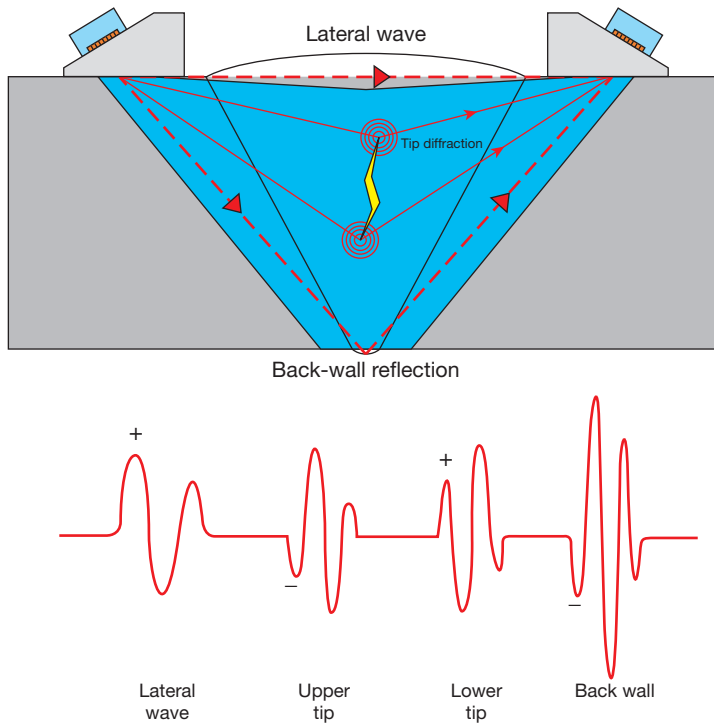


**Figure 2-40** Principle of TOFD and the phase sign of four major signals. The defect is assumed to be symmetrically located between the probes. The phase of each RF signal is marked with "+" and "-".

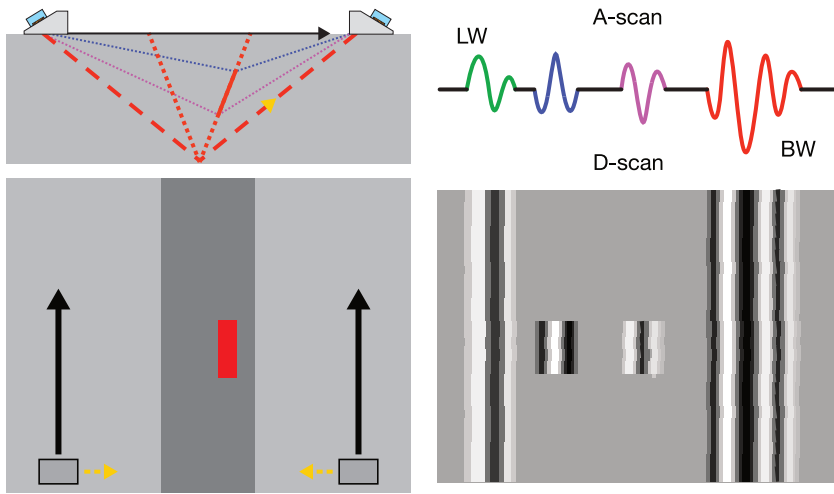


**Figure 2-41** Detection and sizing of a lack of fusion by TOFD D-scan. Phase reversal of upper and lower defect edges is displayed in gray levels.

### *TOFD limitations*

- Defects located at upper surface and inner surface are difficult to detect due to the dead zone of the lateral wave and because of the dead zone of the backwall signal (see Figure 2-42).

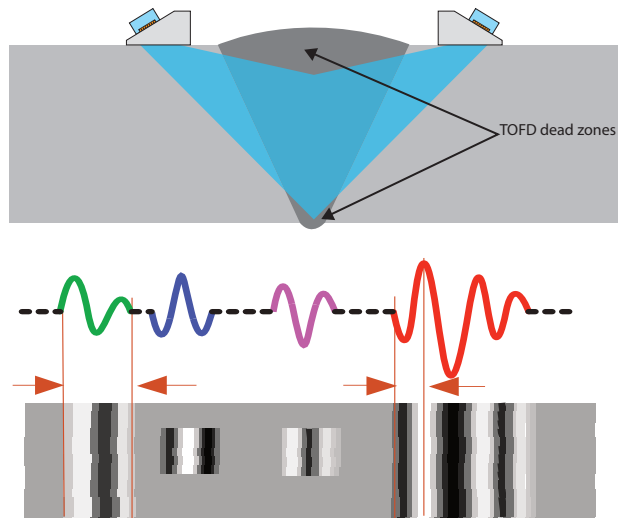


**Figure 2-42** TOFD dead zones due to lateral waves and backwall. Dead zone size depends on frequency, pulse length, probe center separation, material thickness, and velocity. Errors can occur with TOFD if the defect is not symmetrically placed between the two probes.

- Defect location in a linear D-scan has some errors due to TOF locus (see Figure 2-43), since time of arrival of diffracted waves depend on defect position relative to the probes. The location of the defect is estimated by an additional B-scan over the defect position (when probes are moving transverse to the weld).
- Defect interpretation and defect pattern recognition require advanced training and analysis experience.
- Pressure vessel with shells thickness greater than 75 mm require multipass scanning with different PCS.
- Low signal-to-noise ratio.
- Signals sensitive to coarse-grained material.
- Geometry and coupling problems may hamper the propagation of the lateral wave.
- Amplitude is not related to defect size or importance.

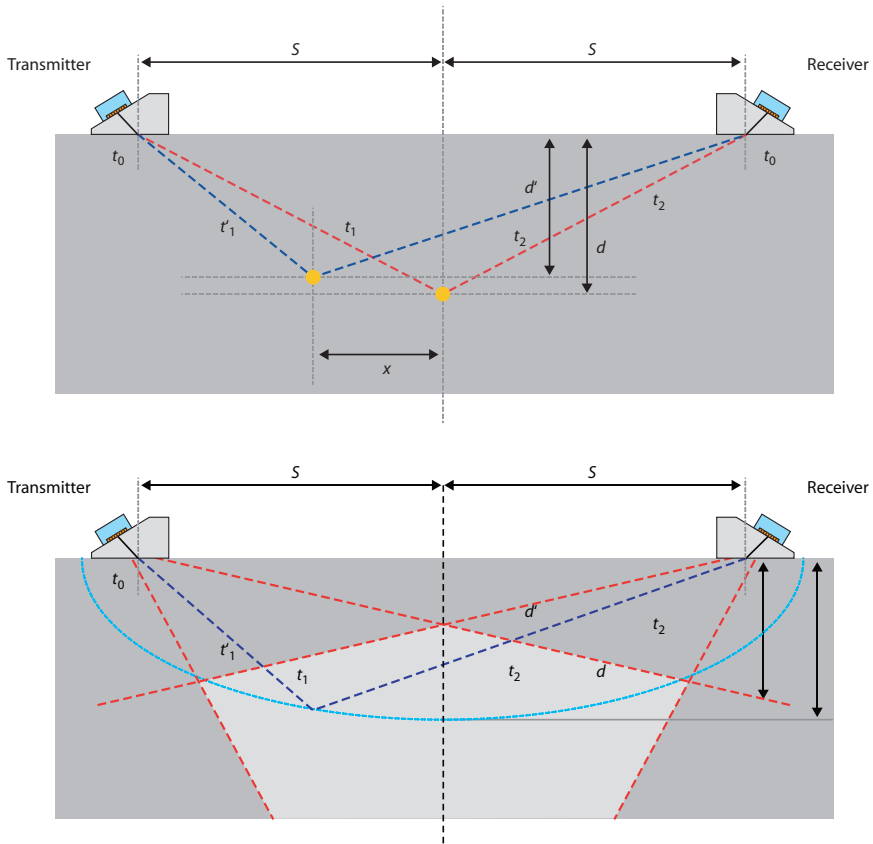
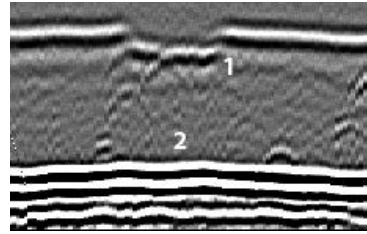
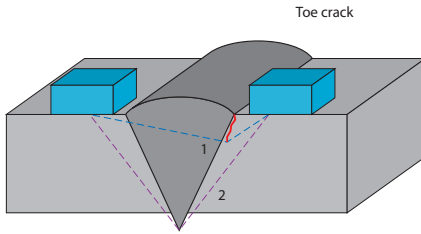


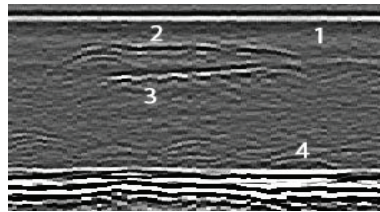
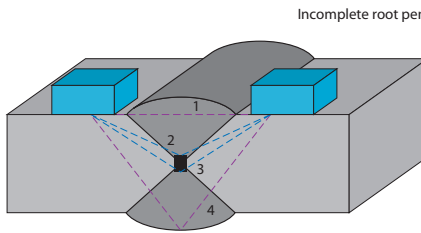
**Figure 2-43** TOFD errors in lateral location and upper ligament caused by the TOF locus of L-waves.

In spite of these limitations, TOFD is *the most accurate* UT technique for crack sizing (both length and specifically height). TOFD was accepted as an alternative to assess the weld quality of pressure vessels in ASME Code Case 2235.

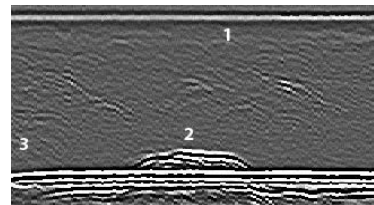
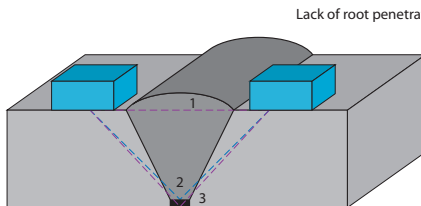
For improved reliability of defect detection, Olympus has proposed a combination of TOFD and pulse-echo, so a real-time display with image recognition is available on a specific layout. Figure 2-44 (a) to Figure 2-44 (h) show typical defects and their corresponding TOFD displays.



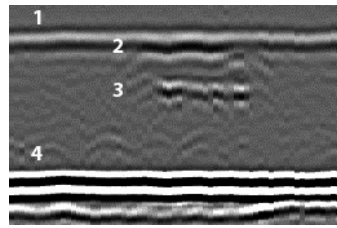
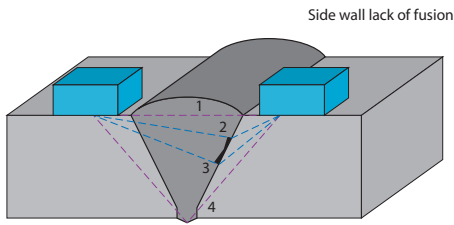
(a) For the toe crack, the lateral wave is disrupted and the bottom of the crack visible. This can be characterized as a surface-breaking crack, and depth measured.



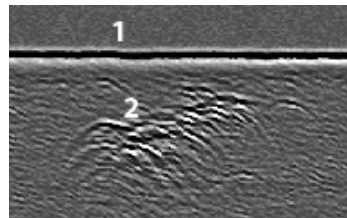
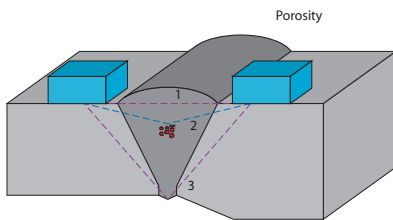
(b) For the incomplete root penetration, the top and bottom diffracted signals are distinguishable, while the uninterrupted lateral and backwall signals indicate a buried defect.



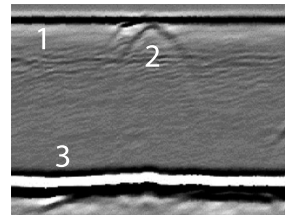
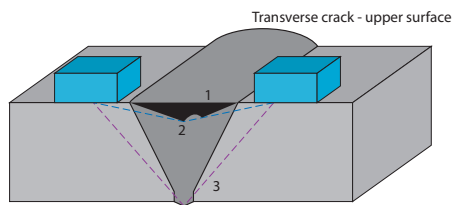
(c) For the lack of root penetration, the backwall is perturbed but not broken, while the top diffracted signal is visible. This indicates a surface-breaking defect.



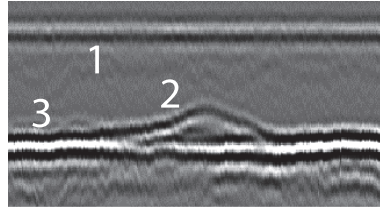
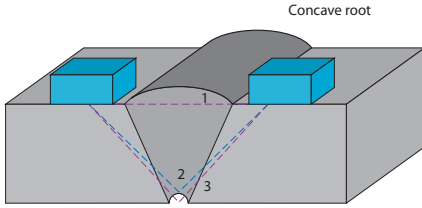
(d) The lack of sidewall fusion shows no lateral or backwall perturbation, so shows a buried defect. The bottom diffracted signal is clear, but the top diffracted signal is partly buried in the lateral wave.



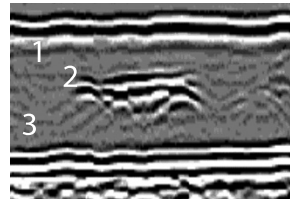
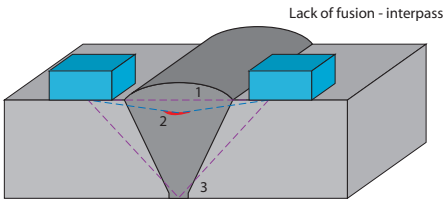
(e) The porosity shows as a series of point defects with associated hyperbolic tails. Multiple porosity is difficult to analyze, but easily characterized. Note that the backwall signal is not displayed in this TOFD image.



(f) The transverse defect shows essentially as a point defect, similar to porosity.



(g) The concave root defect perturbs the backwall signal (showing it is surface breaking), while the tip is visible.



(h) The interpass lack of fusion shows as a single reflected signal of high amplitude, but would not be detectable on the pulse-echo channels.

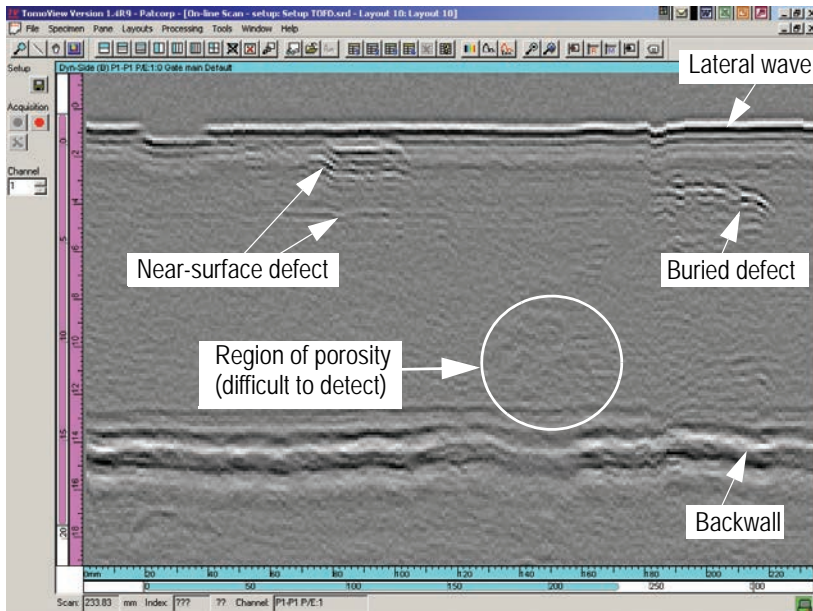


**Figure 2-44** TOFD imaging of defects in weld.

## Benefits

- Single pass
- Real-time A-scans, B-scans, and C-scans
- High-accuracy sizing: TOFD
- High SNR: focused-beam phased array ultrasounds
- High accuracy in defect positioning
- Easy reporting

### 2.13.2 Relative Arrival Time Technique (RATT)

The *relative arrival time technique* (RATT) is a sizing technique based on time-of-flight readings, not on amplitude echo dynamic. This technique is also called *satellite pulse observation time technique* (SPOT).

The RATT (see Figure 2-45) has the following features:

- The crack size is less than the beam spread (divergence).
- The evaluation is relative to the corner trap time-of-flight (TOF) signal.
- The crack corner trap and the crack tip are detected by the same angle at the same position of the probe.
- The relative ultrasound path between the crack corner trap and the crack tip signals is measured with  $\Delta UT$ .
- The crack height is determined by:

$$h_{\text{crack}} = \frac{\Delta UT_{\text{RATT}}}{\cos \beta} = \frac{UT_2 - UT_1}{\cos \beta} \quad (\text{see Figure 2-45}). \quad (2.45)$$

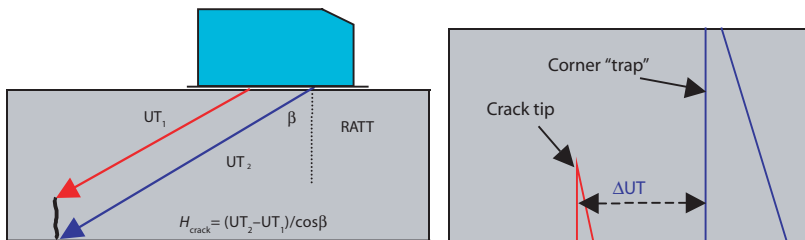


**Figure 2-45** RATT crack height evaluation based on relative measurement of ultrasound path between crack tip and crack corner trap signals.

If the ultrasound beam has enough divergence (a longer ultrasound path and

higher refracted angles), then the tip of the crack is detected by the direct beam and by the skip beam (see Figure 2-46). The RF signals are phased-reversed for direct detection and in phase with the corner-trap signal for skip detection.

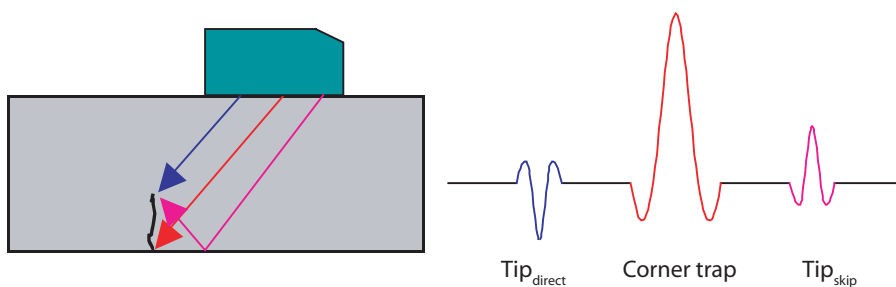


**Figure 2-46** RF display of the crack tip by direct and skip beam.

The height factor dependence on the refracted angle is presented in Figure 2-47. One can conclude that  $\Delta UT_{RATT}$  decreases when the refracted angle is increased. The best separation is achieved for “steeper” refracted angles, such as 30° to 35°.

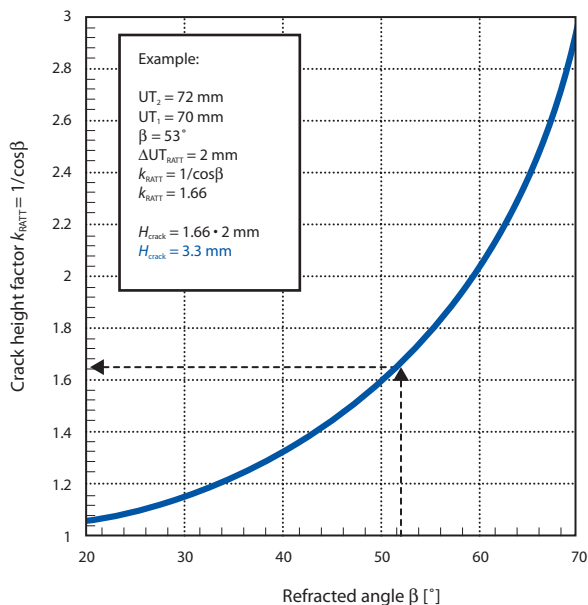


**Figure 2-47** Crack height factor for RATT and a sizing example.

### 2.13.3 Absolute Arrival Time Technique (AATT)

The *absolute arrival time technique* (AATT), also called *pulse arrival time technique* (PATT), has the following features (see Figure 2-48):

- Crack height possibly greater than the beam width.
- Probe movement and two angles required for optimum ultrasonic path reading.
- Reading corrected for angle and ultrasound path.
- The probe is scanned manually over the crack area to detect the root corner signal and maximize the crack tip signal.

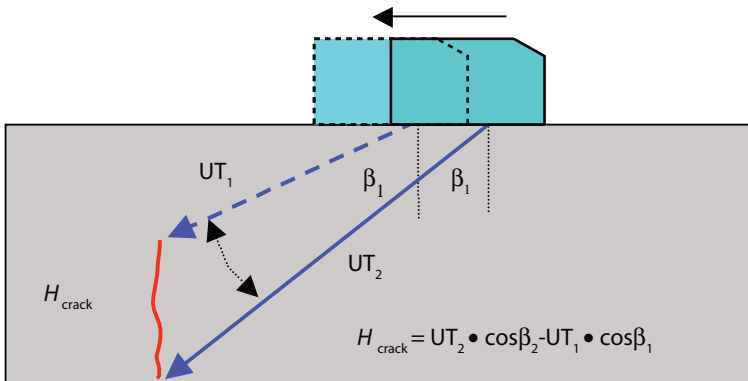


**Figure 2-48** Crack height measurement principle using AATT.

**Note:** In phased array ultrasonics, the beam can sweep over the crack facets using an S-scan and the height is evaluated (see Figure 2-49). Similar approaches use electronic B-scans or raster scans.

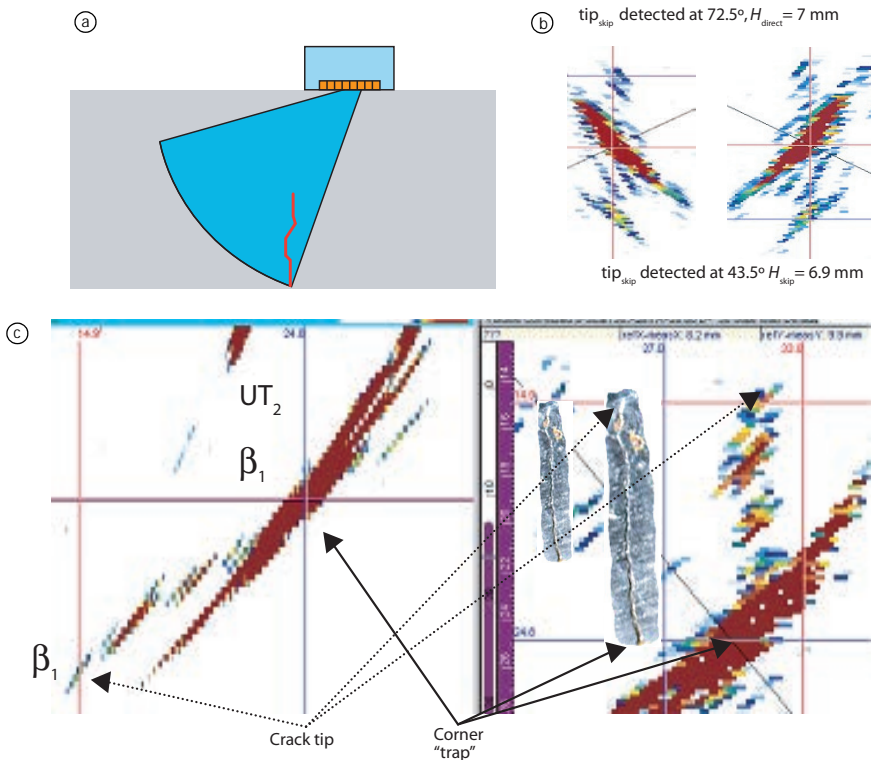


**Figure 2-49** Example of AATT sizing of a fatigue crack with phased array probe in static position and beam sweeping over the crack: (a) principle; (b) sizing a 7.1 mm crack with the skip tip; (c) sizing a  $H_{\text{crack}} = 10.2$  mm crack;  $H_{\text{AATT}} = 9.9$  mm.

A reliable crack sizing capability based on tip-echo techniques depends on suitable specimen thickness, phased array probe frequency, damping, and bandwidth, as well as material quality.

More details regarding tip-echo sizing can be found in references 14–19, 62, 64, 68, and 108.

### 2.13.4 Mode-Converted Techniques

Defect detection based on mode-converted (MC) techniques is illustrated in Figure 2-50 to Figure 2-52. In these figures, blue waves are shear waves, and red waves are longitudinal waves. The many mode conversions are clearly visible.

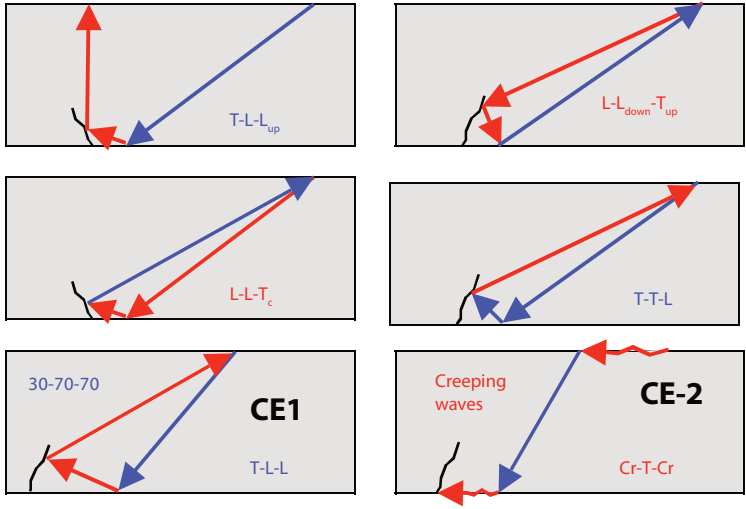


**Figure 2-50** Detection of inner surface-breaking cracks using MC techniques.

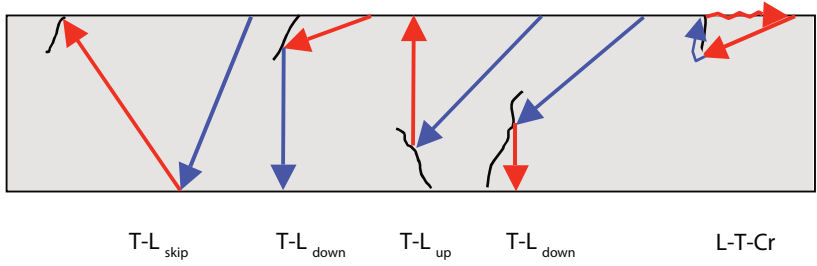


**Figure 2-51** Techniques for detection of outside and inner surface-breaking cracks using mode conversion.

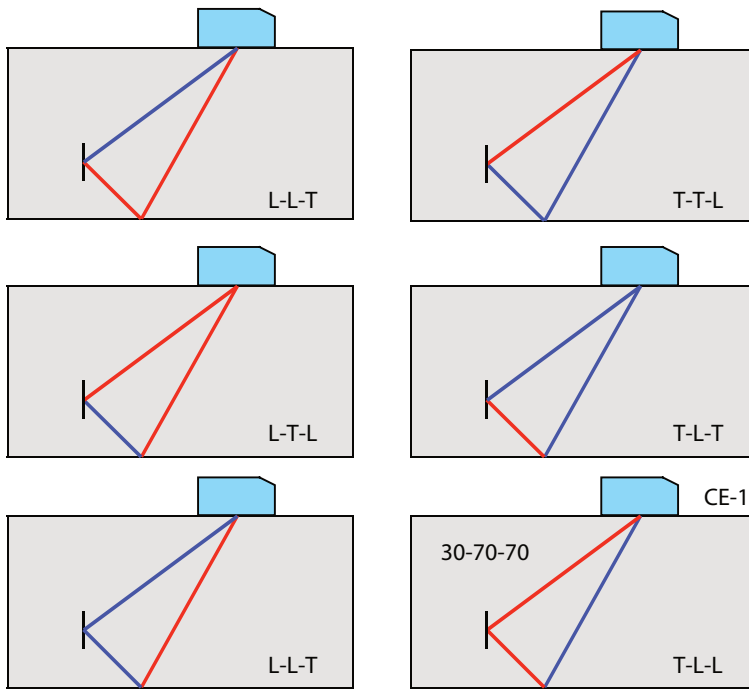


**Figure 2-52** Detection of embedded linear defects using MC techniques.

The *creeping-wave* technique<sup>1-4</sup> is the most common MC application for detection and confirmation of ID surface-breaking defects. The technique may be used to detect and size linear defects from OD to ID regions. This capability is based on the characteristics of the “creeper” probe, which generates the following types of waves (see Figure 2-53):

- Direct creeping waves (OD surface)
- Direct SW of 34°
- Direct LW of 70°
- Indirect MC SW of 31°
- Indirect MC creeping waves (ID surface)

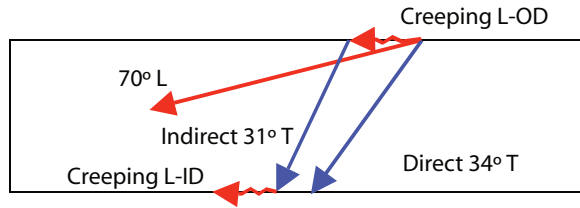


**Figure 2-53** Type of waves generated by "creeper" probe.

The creeping waves have a short surface propagation (2 mm to 13 mm). The propagation occurs within 2 to 3 wavelength thicknesses and depends on plate/pipe parallelism ( $\pm 5^\circ$ ). The shear wave may mode-convert at the back surface to a longitudinal wave at  $70^\circ$ , and be reflected by a vertical defect as a  $70^\circ$  longitudinal wave. This MC detection is called "collateral echo no. 1" (CE 1). Creeping wave detection/confirmation echo is called "collateral echo no. 2" (CE 2). Their ultrasonic path in LW calibration depends on thickness (see Figure 2-54).

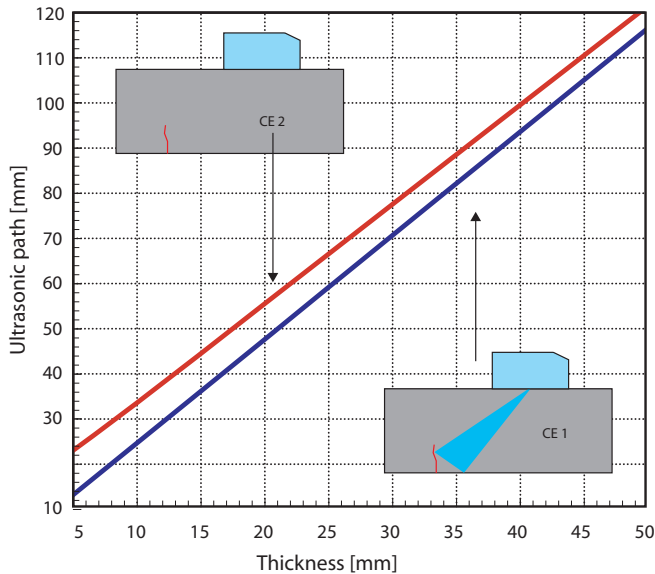


**Figure 2-54** Ultrasound path dependence on thickness for CE 1 ( $30^\circ$ - $70^\circ$ - $70^\circ$ ) and for CE 2 (creeping waves).

A combination of longitudinal wave detection and MC confirmation is obtained for angles between  $55^\circ$  and  $62^\circ$  (see Figure 2-55). Sizing is based on

the LL doublet, and the ligament is evaluated by CE 1 and CE 2 amplitudes. A vertical defect with a ligament greater than 4 mm will reflect only the doublets and CE 1. The signal amplitude of CE 1 varies linearly with crack height. However, if the defect is inclined, CE 1 amplitude is no longer linear.

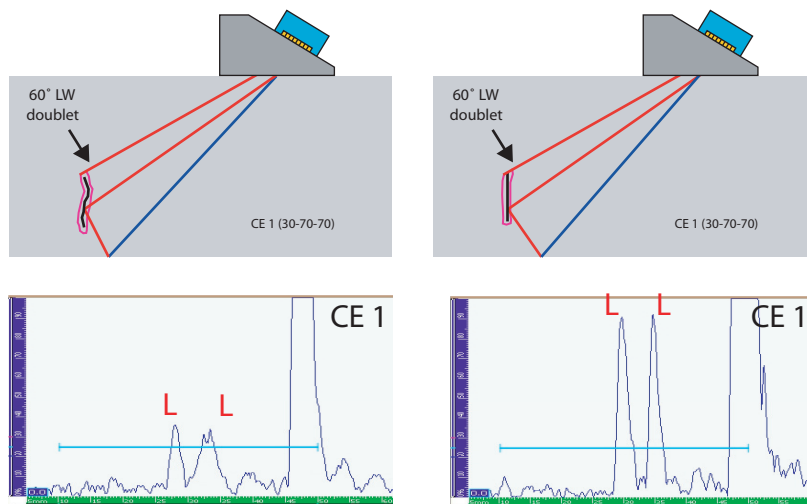


**Figure 2-55** Detection, confirmation, and sizing of a fatigue crack by LL doublet and CE 1 (30°-70°-70°) for a 60° LW probe; *left* = crack signals; *right* = EDM notch signals; ligament = 5 mm; height = 11 mm.

Another MC sizing method is the *delta technique* (see Figure 2-56). The delta technique consists of a combination of a 60° shear wave and a 0° longitudinal wave. The height measurement can be calculated from formula (2.46):

$$\text{TOF}_{\Delta 60} = \frac{(t - h_{\text{crack}})}{v_T[(1/\cos\beta) + (v_T/v_L)]} \quad (2.46)$$

Due to the beam spread, the 60° shear wave detects the crack tip because of a direct hit and of a reflection at the backwall. For steel, the crack height is given by formula (2.47):

$$h_{\Delta 60T} = t - 0.8 \text{CRT}_{\text{TW}} \quad (2.47)$$

where  $\text{CRT}_{\text{TW}}$  is the shear wave time of arrival from the screen.

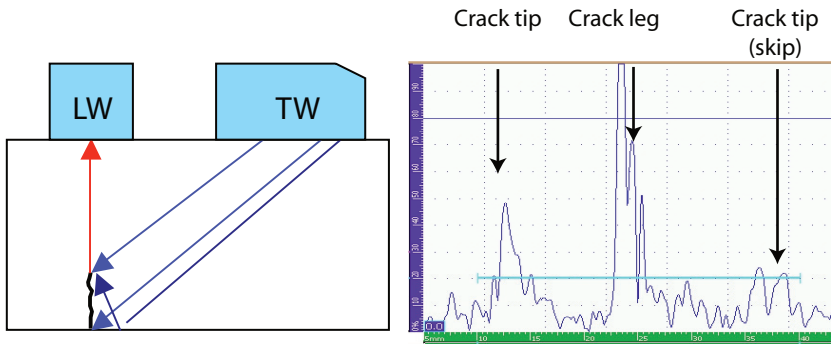


**Figure 2-56** Principle of  $\Delta 60^\circ$  technique and an example of ID-connected crack sizing; note the crack tip detection by skip.

### 2.13.5 Pitch-and-Catch and Tandem Techniques

Detection and sizing of vertical defects by MC techniques may be possible using the pitch-and-catch method with multiple depth zones. Phased arrays are an ideal tool for detection and sizing, because they generate a range of shear-wave and longitudinal-wave angles, which may mode-convert on vertical defects (see Figure 2-57).

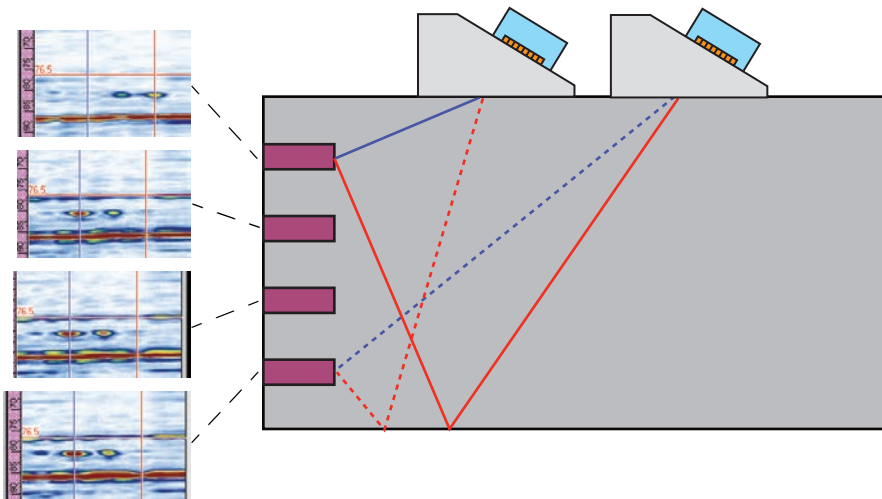


**Figure 2-57** Detection of four vertical FBH with a phased array pitch-and-catch mode-converted setup in a 100-mm test piece. Blue lines show shear waves, and red lines show longitudinal waves.

Mode-converted techniques are very useful for narrow gap welds on thick plates. The most common defect is the sidewall lack of fusion (see Figure 2-58).

A more traditional approach is the “tandem” technique using 45° shear waves (Figure 2-58, *right*). Tandem techniques work well with phased arrays.

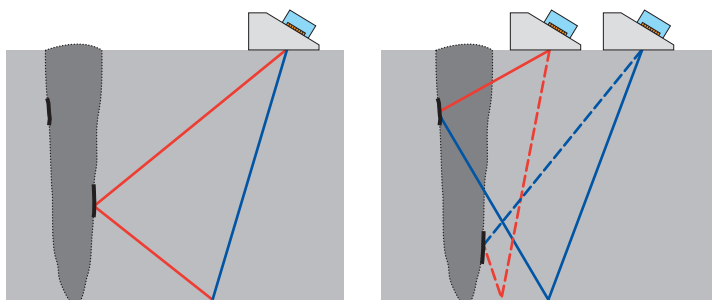


**Figure 2-58** Detection of side lack of fusion in a narrow gap weld by MC techniques with a single (*left*) and double (pitch-and-catch) probe (*right*).

### 2.13.6 Satellite Pulse-Echo Technique

Another mode-converted technique consists of sizing the volumetric rounded inclusions (cylindrical voids) with T-T/T-S-T satellite pulses<sup>14,17</sup> (see Figure 2-59).

$$\Delta t_{\text{void}} = \left[ \left( \pi \frac{1}{2v_T} \right) + \left( \frac{1}{v_s} \right) \right] D_{\text{void}} \quad (2.48)$$

where:

$\Delta t_{\text{void}}$  = time-of-flight difference between T-T and T-S-T signals (see Figure 2-59)

$D_{\text{void}}$  = void diameter

$v_T$  = shear-wave velocity

$v_s$  = surface-wave velocity (Rayleigh's)

For steel, a simplified formula is:  $D_{\text{void}} = 0.7\Delta t_{\text{path}}$ , with the ultrasonic path calibrated in shear wave half distance.

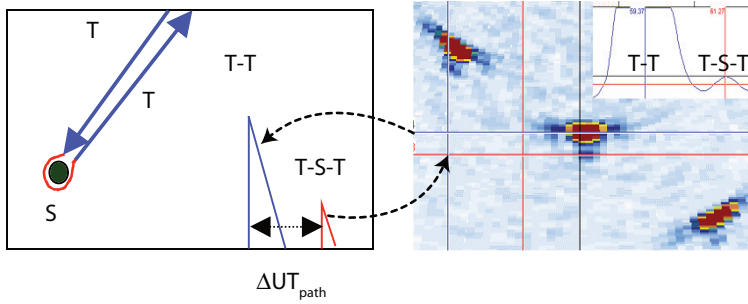


**Figure 2-59** Mode-converted detection and sizing of cylindrical voids; principle (*left*); ultrasonic B-scan display of SDH of  $D_{SDH} = 0.6$  mm (*right*). Blue lines show shear waves, and red lines show longitudinal waves.

## 2.14 Testing Round Parts

Focal law calculations will be inaccurate due to curvature of the component and couplant variations under the wedge. This is caused by the acoustic velocity in liquid coupling media being approximately one quarter the velocity of steels, thus calculated time delays for optimum focusing will be compromised. Profiling the wedge to mate the component curvature will be beneficial; however, this will require recalculating the focal laws taking into account the new geometric profile of the wedge in order to satisfactorily accomplish the desired focusing effect.

Testing round parts (pipes, cylinders) by contact or immersion requires special setups.

It is recommended, for contact inspections, that if the shoe is not shaped the wedge length ( $L_{wedge}$ ) correspond to the following relationship:

$$R_{part} > \frac{L_{wedge}^2}{4} \quad (2.49)$$

The practical height between the wedge extremes and the part must be smaller than 0.5 mm (see Figure 2-60). Wedges must provide sufficient contact area to generate consistent refracted beams in the component. For convex surfaces, typically couplant will leak out, and the value of 0.5 mm is a practical mismatch value.

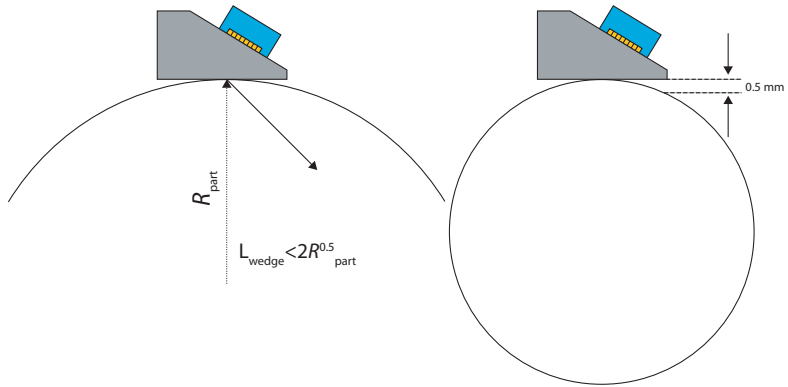


**Figure 2-60** The relationship between wedge length and part radius.

The ultrasonic beam path and the reflected angle on the inner surface are changed when performing an ultrasonic inspection of axial seam welds (or wrought pipe) [see Figure 2-61, where  $D$  is the pipe outside diameter].

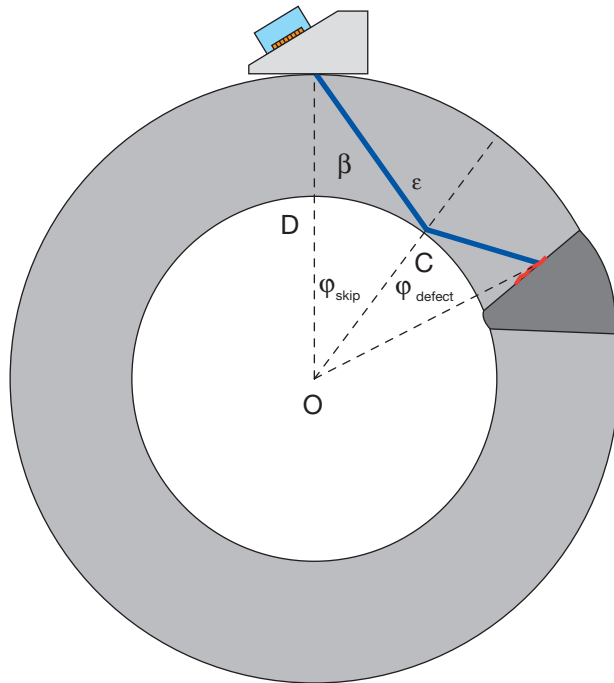


**Figure 2-61** Ultrasonic examination of an axial weld pipe.

$$\beta_{\max} = \sin^{-1}\left(1 - \frac{t}{2D}\right) \quad (2.50)$$

where  $\beta_{\max}$  is the maximum refracted angle.

The reflected angle on the inner surface ( $\epsilon$ ) may be found from a standard nomogram<sup>1</sup> or by the following relationships:

$$\sin \epsilon = \left[ \frac{1}{(1 - 2t/D)} \right] \sin \beta \quad (2.51)$$

$$\varphi = \pi - (\beta + \epsilon) \quad (2.52)$$

where  $\varphi$  is the radial angle.

$$h_{\text{defect}} = OB - 0.5(D - 2t) \quad (2.53)$$

where OB is the distance from the tube center to the top of the defect.

## 2.15 Measuring the Lengths of Small Defects

Images produced using phased array data collection are echo-dynamic envelopes of the peak response received from an A-scan waveform at incremental points along the axis of beam travel. This can be assimilated by utilizing the peak memory function of many contemporary digital A-scan flaw detectors. Data collected by the PA instrument correlates signal amplitude into an amplitude-related color palette allowing the data to be viewed as if the A-scan was observed looking down onto the top edge of the display. This concept is commonly utilized in a number of immersion systems and similarly applied using gray-scale palette in TOFD data imaging.

Estimation of flaw size is therefore a product of gauging amplitude change by moving cursors across the colored echo-dynamic image. The following points have to be considered:

- Is the reflector diffuse or specular (scatters sound or acts like a smooth mirror)?
- Is the image a result of pure reflection or tip diffraction?
- Has the image been formed as a result of mode-converted waves?
- What is the width of the focused beam in the direction of beam travel?
- Was dynamic depth focusing applied or not?

All of the above considerations contribute to amplitude discrepancies during sizing; the list is not exhaustive but still subject to common factors that affect conventional pulse-echo sizing techniques.

Phased array applications do, however, offer more reliable and reproducible sizing than that obtained from manual A-scan ultrasonic applications, which is principally due to the following:

- Focused beams can be much narrower than conventional divergent beams resulting in higher precision during sizing.
- Phased array images compress numerous individual A-scans, allowing the NDT technician to observe all this data in one image.
- Coupling with arrays tends to be more consistent than when scanning with conventional probes.
- Collection of raw digital data in the form of phased array images allows offline sizing and software tools to be used to manipulate, merge, and filter data for enhanced evaluation.

Figure 2-62 shows images generated and sized from a 2-mm diameter spherical SDH using different amplitude thresholds.

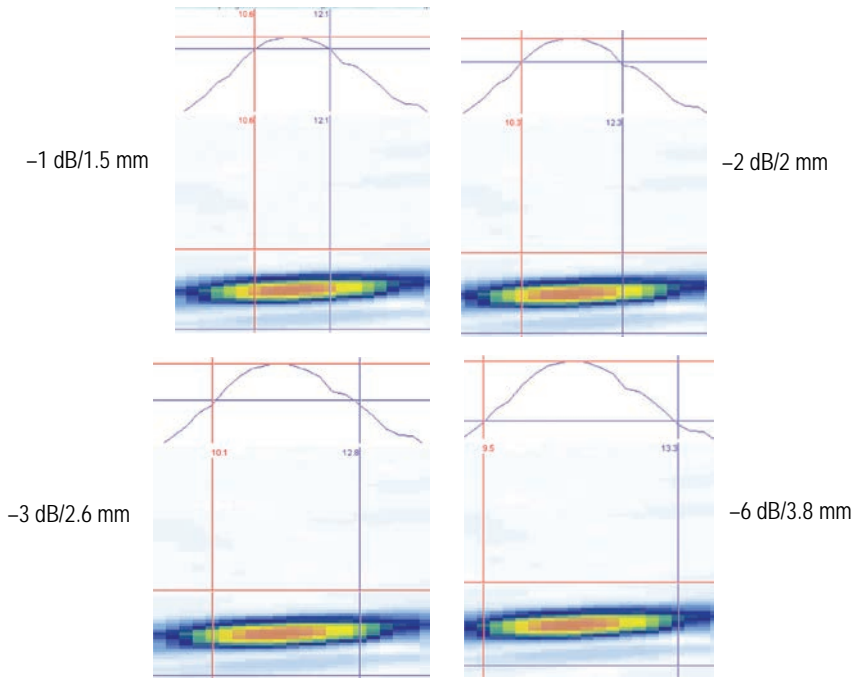


**Figure 2-62** Length sizing of a 2-mm diameter  $SDH_{\text{spherical}}$  using different dB amplitude drops from echo-dynamic single-peak curves.

## 2.16 Reliability of Ultrasonic Inspection

The minimum defect size reliably detected by ultrasonic waves depends on a number of factors, including noise, the probe frequency, and surface roughness, as well as the defect itself:

- $D_{\text{min}} > \frac{\lambda}{4}$
- $h_{\text{min}} > 3R_t$

The couplant layer should have a thickness of a few microns or  $\lambda/2$ . An amplitude increase of 6 dB to 10 dB is produced by a couplant layer optimized to  $\lambda/4$ .<sup>13</sup>

Sources of errors in defect sizing are listed in Table 2-7.<sup>15,16</sup>

**Table 2-7** Example of source of errors; results are from CEGB [UK], after a 6-year experimental program during 1980's.<sup>15,16</sup>

Description	Error type / practical value
Systematic undersizing	Systematic; resolution of the probe beam; 2–3 mm. Also depends on type of defect, probe characteristics, etc. For example, the maximum amplitude sizing technique typically undersizes 2–3 mm, while the 6 dB drop technique has only random sizing errors.
Range calibration	Random/systematic; $\pm 1$ mm
Probe angle and index	Random; $\pm 1^\circ$ for angle; $\pm 1$ mm for index
Probe position measurement	Random; $\pm 2$ mm for manual; $\pm 1$ mm for automatic
Screen reading (UT path)	Random; $\pm 1$ mm
Beam width	Random; $\pm 1^\circ$

More information regarding the reliability of ultrasonic inspection can be found in references 65, 68, 69, and 114–121. For phased arrays, the errors from index point, beam angles, and couplant are minimal. The main errors are range calibration and defect characterization errors.

## References to Chapter 2

1. Krautkramer, J., and H. Krautkramer. *Ultrasonic Testing of Materials*. 4th fully rev. ed., pp. 194–195, 201, and 493. Berlin; New York: Springer-Verlag, c1990.
2. DGZfP [German Society for Non-Destructive Testing]. *Ultrasonic Inspection Training Manual Level III-Engineers*. 1992.  
<http://www.dgzfp.de/en>.
3. EPRI. *Ultrasonic advanced sizing course*. 1987.
4. Davis, J. M. *Advanced Ultrasonic Flaw Sizing Handbook*. USA: The Art Room Corporation, 1998.
5. Schelengermann, U. "The characterization of focusing ultrasonic transducers by means of single frequency analysis." *Materials Evaluation*, vol. 38, no. 12 (Dec. 1980): pp. 73–79.
6. Wüstenberg, H., E. Schenk, W. Möhrle, and E. Neumann. "Comparison of the performances of probes with different focusing techniques and experiences." *10<sup>th</sup>-WCNDT Proceedings*, vol. 7, pp 563–567.
7. Murphy, R. V. "Focussed Ultrasonic Probes for Contact Inspection." *Materials Evaluation*, vol. 38, no. 9 (1980): pp. 53–58.
8. Onozawa, M., and Y. Ishii. "The industrial application of improved narrow-beam probes for ultrasonic inspection." *British Journal of Non-Destructive Testing*, vol. 28, no. 1 (1986): pp. 23–26.
9. Gros, X. E, N. B. Cameron, and M. King. "Current Applications and Future Trends in Phased Array Technology." *Insight*, vol. 44, no. 11 (Nov. 2002).
10. Poguét, J., J. Marguet, F. Pichonnat, and Laurent Chupin. "Phased Array Technology." *The e-Journal of Nondestructive Testing*, vol. 7, no. 5 (May 2004). NDTnet, <http://www.ndt.net/v07n05.htm>.
11. Krimholtz, R., D. Leedom, and G. Matthaei. "New equivalent circuits for elementary piezoelectric transducers." *Electronics Letters*, vol. 6 (June 1970): pp. 398–399.
12. JIS Z 2350:2002: Method for measurement of performance characteristics of ultrasonic probes.
13. McGrath, B. A., R. K. Chapman, and I. Einav. "A study of changes in ultrasonic probe performance due to the thickness of the couplant layer." *12th WCNDT*, Amsterdam, 1988.
14. Gruber, J. G. "Defect identification and sizing by the ultrasonic satellite pulse technique." SwRI, USA, 1979.
15. Chapman, R. K. "Code of practice on the assessment of defect measurement errors in the ultrasonic NDT of welds." CEGB, UK, Report STN-87-2013-R, July 1987.
16. Gardner, W. E., ed. *Improving the Effectiveness and Reliability of Non-Destructive Testing*. Chapters 4 and 8. Oxford; New York: Pergamon Press, 1992.
17. Jacques, F., F. Moreau, and E. Ginzler. "Ultrasonic backscatter sizing using phased array-developments in tip diffraction flaw sizing." *Insight*, vol. 45, no. 11 (Nov. 2003): pp. 724–728.



## Chapter Contents

3.1	Piezocomposite Materials .....	97
3.2	Piezocomposite Manufacture .....	99
3.3	Types of Phased Array Probes for Industrial Applications .....	103
3.4	Linear Arrays .....	108
3.5	Dynamic Depth Focusing.....	122
3.6	Probe on the Wedge .....	125
3.7	Beam Deflection on the Wedge.....	127
3.8	2-D Matrix Phased Array Probes .....	130
3.9	Focal Law Calculator .....	133
3.10	Standard Array Probes .....	137
3.11	Other Array Features .....	138
3.12	Phased Array Simulation Software (PASS) .....	138
3.13	Probe Design .....	139
3.14	Ultrasonic Setup Details .....	144
3.15	Probe Identification.....	152
3.16	Probe Characterization and Periodic Checking .....	153
3.17	Olympus Probes for the OmniScan .....	157
	References to Chapter 3.....	161

---

## 3. Probes and Ultrasonic Field Formula

---

This chapter describes the main aspects of probes and arrays used in phased array and ultrasound inspections.

### 3.1 Piezocomposite Materials

One of the main technical issues for large-scale applications of phased array technology in the late 1970s and mid-1980s was the manufacturing process and acoustic insulation between array elements. The high cross-talk amplitude between elements and the challenge to cut curved-shaped piezoelectric materials led to a setback in industrial development. The common piezoelectric materials are listed in Table 3-1.

**Table 3-1** Main properties of commonly used piezoelectric materials.<sup>1,7</sup>

Symbol / Unit	Quartz	BaTiO <sub>3</sub>	PbNb <sub>2</sub> O <sub>6</sub>	PZT-4	PZT-5A	PVF2
d <sub>33</sub> (pC/N)	2.3	190	85	289	400	20
g <sub>33</sub> 10 <sup>-3</sup> Vm/N	57	12.6	42.5	26.1	26.5	190
d <sub>33</sub> g <sub>33</sub> 10 <sup>-15</sup> N/m	133	2394	3612	7542	10,600	3,800
k <sub>t</sub>	0.095	0.38	0.32	0.51	0.49	0.1
k	5	1700	225	1300	1700	11
Z (10 <sup>6</sup> Rayl)	15.2	25.9	20	30	29	4
Mechanical Q	2,500		24	500	80	3-10

The amount of acoustic energy transferred to the load (test piece) reaches a maximum when the acoustic impedance is matched between the probe and the test piece. Some applications require an immersion technique and some use direct contact with aluminum and/or steel. Most shear-wave and longitudinal-wave applications for weld inspections require phased array probes mounted on a wedge. Impedance matching between the probe/wedge and the test piece may be achieved by mechanical (matching layer) or

electrical (fine tuning with the KLM model) methods. The main properties of matching layers are listed in section 3.1.1, “Matching Layer and Cable Requirements.”

### 3.1.1 Matching Layer and Cable Requirements

The key points of matching layer and cable requirements are:

- Optimization of the mechanical energy transfer
- Influence on the pulse duration
- Contact protection for piezocomposite elements (wear resistance)
- Layer thickness of  $\lambda/4$

The maximum electrical efficiency is obtained when the probe is matched to the electrical impedance of both the transmitter and the receiver. The KLM model<sup>6</sup> takes into account all the steps along the transmission line of electrical signals.

A good cable should have the following properties:

- Minimum gain drop due to cable length
- Low impedance—the ideal is  $50 \Omega$
- Elimination/reduction of the cable reflections (cable speed:  $2/3 v_{\text{light}}$ )
- Mechanical endurance for bending, mechanical pressure, accidental drops
- Water resistance for all wires
- Avoidance of internal wire twists

A high value of  $d_{33} g_{33}$  represents a good transmitting-receiving energy. A low mechanical  $Q$  means that the transducer has a higher bandwidth and better axial resolution. The damping material placed behind the crystal can increase the bandwidth value. The main properties of the backing material are listed in section 3.1.2, “Backing Material.”

### 3.1.2 Backing Material

The key features of backing material are:

- Attenuation of high-amplitude echoes reflected back from the crystal face (high acoustic attenuation)
- Influence on pulse duration (damping)

## 3.2 Piezocomposite Manufacture

Piezocomposite materials were developed in the mid-1980s, primarily in the United States, in order to improve the ultrasonic imaging resolution in biomedical applications.

Piezocomposites used for transducers are fabricated using a 1-3 structure. A *piezocomposite* is made of uniformly oriented piezoelectric rods embedded in an epoxy matrix, as depicted in Figure 3-1. The piezo-ceramic embedded in a polymer resin has a 1-D connectivity (that is, it is oscillating in one dimension towards the test piece), while the polymer has a 3-D connectivity.

For example, PZT (lead zirconate titanate ceramic), in combination with different polymer resins, has a higher  $d_{33}$   $g_{33}$  value than its original parent material (see Table 3-2).

**Table 3-2** Values of  $d_{33}$   $g_{33}$  for different combinations between PZT and polymer resins.<sup>1</sup>

1-3 PZT-polymer matrix combination	$d_{33}$ $g_{33}$ (10–15 N/m)
PZT + silicone rubber	190,400
PZT rods + Spurs epoxy	46,950
PZT rods + polyurethane	73,100
PZT rods + REN epoxy	23,500

The properties of 1-3 piezocomposite materials can be derived from Smith's effective medium theory model<sup>3</sup> and finite element model (FEM)<sup>2</sup> [see Figure 3-1].

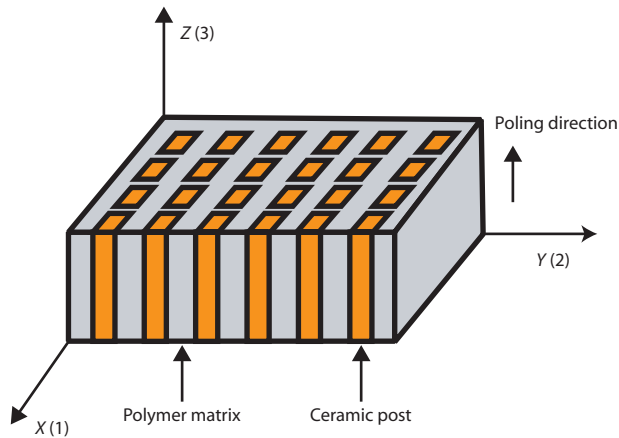


**Figure 3-1** The 1-3 composite coordinates according to Smith's theory.<sup>3,5</sup>

Based on the assumption that the field quantities associated with the  $x(1)$  direction must be equal to those quantities associated with the  $y(2)$  direction, the following main piezocomposite features can be computed:

- Thickness mode electromechanical coupling ( $k_t$ )
- Thickness mode velocity ( $v_{13}$ )—Figure 3-2
- Effective characteristic impedance (for thickness mode)  $[Z_{13}]$ —Figure 3-3

The following advantages are obtained from a 1-3 piezocomposite probe:

- Very low lateral mode vibration; cross-talk amplitudes typically less than  $-34$  dB to 40 dB
- Low value of quality factor  $Q$ —Figure 3-4
- Increased bandwidth (80% to 100%)
- High value of electromechanical coupling
- Higher sensitivity and an increased SNR versus normal PZT probes
- Easy dice-and-fill technology for machining Fermat aspherically focused phased array probes and complex-shaped probes
- Constant properties over a large temperature range
- Easy to change the velocity, impedance, relative dielectric constant, and electromechanical factor as a function of volume fraction of ceramic material
- Easy to match the acoustic impedance of different materials (from water to steel)

- Reduction of the need for multiple matching layers
- Manufacturing costs comparable to those of an equivalent multiprobe system
- Possibility of acoustic sensitivity apodization through the variation of the ceramic volume fraction across the phased array probe aperture (length)

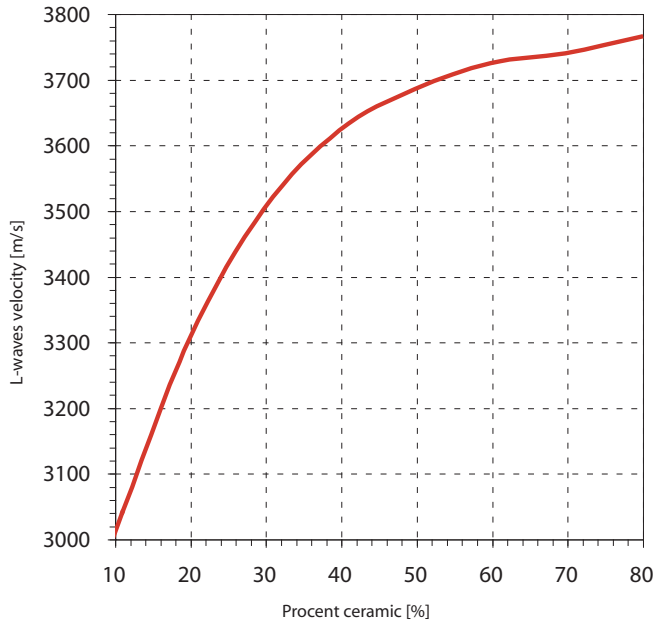


**Figure 3-2** Dependence of longitudinal velocity on ceramic concentration.

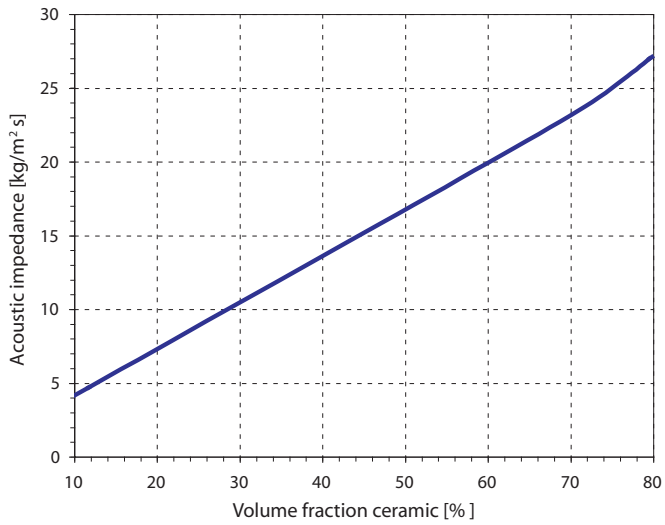


**Figure 3-3** Acoustic impedance dependence on volume fraction of PZT.

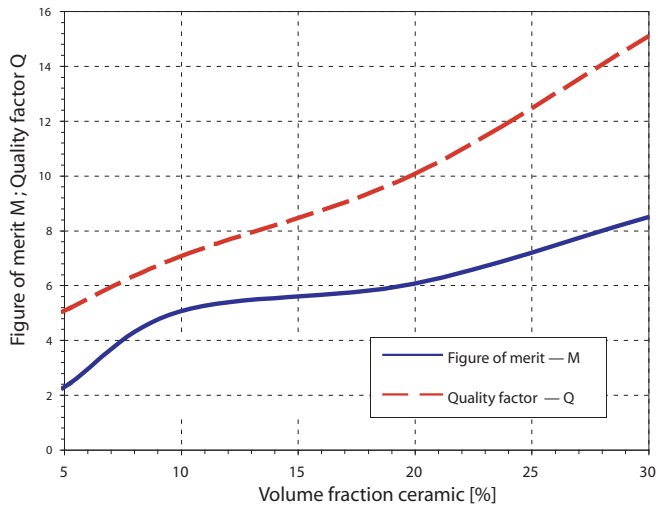


**Figure 3-4** Figure of merit M and quality factor Q dependence on PZT volume for a 1-3 piezocomposite rod of 0.45-mm diameter.

More information regarding piezocomposite materials and their properties can be found in references 3–13 and 31.

### 3.3 Types of Phased Array Probes for Industrial Applications

The phased array probes used for industrial applications and their types of focusing/beam deflections are listed in Table 3-3 and presented in Figure 3-5 to Figure 3-9.

**Table 3-3** Typical phased array probes widely available.

Type	Deflection	Beam shape	Figure
Annular	Depth – $z$	Spherical	Figure 3-5
1-D Linear planar	Depth, angle	Elliptical	Figure 3-6
2-D matrix	Depth, solid angle	Elliptical	Figure 3-7
2-D segmented annular	Depth, solid angle	Spherical/elliptical	Figure 3-8
1.5-D matrix	Depth, small solid angle	Elliptical	Figure 3-9

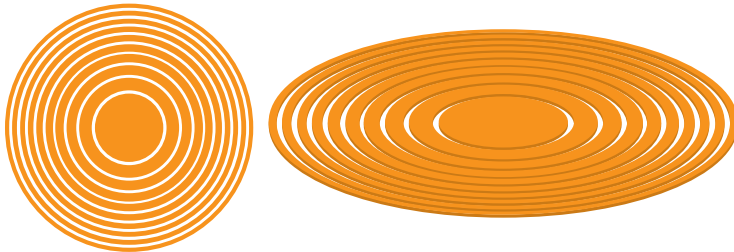


**Figure 3-5** Annular phased array probes of equal Fresnel surfaces.



**Figure 3-6** 1-D linear phased array probe.

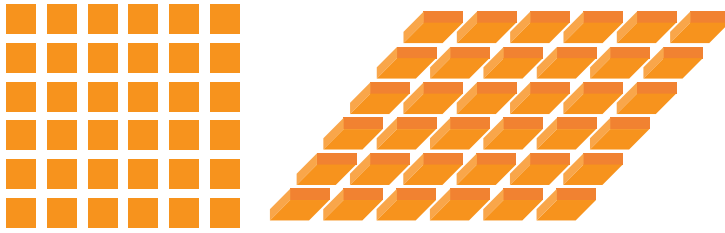


**Figure 3-7** 2-D matrix phased array probe.

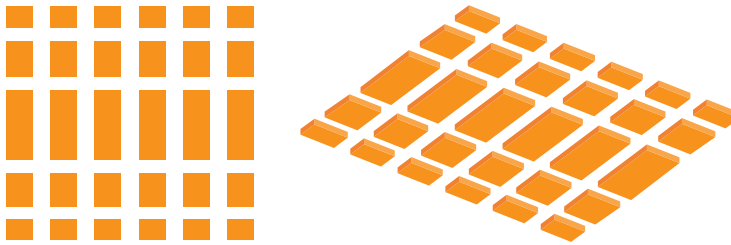


**Figure 3-8** 1.5-D matrix phased array probe.

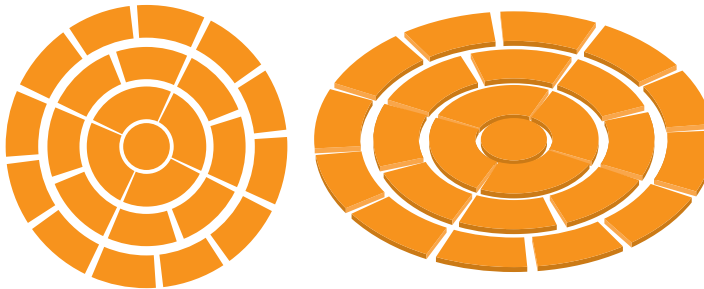


**Figure 3-9** Rho-theta (segmented annular) phased array probe.

Other types of phased array probes are presented in Figure 3-10 to Figure 3-13.

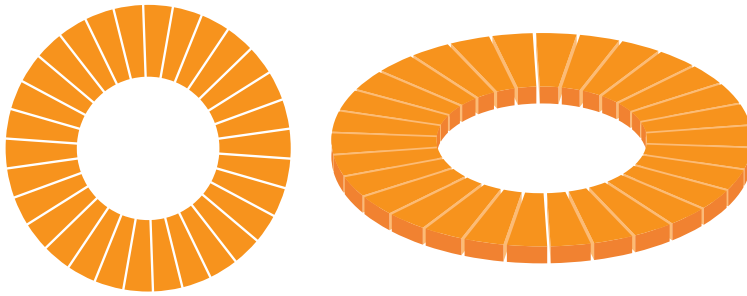


**Figure 3-10** 1-D circular phased array probes (“daisy probes”).

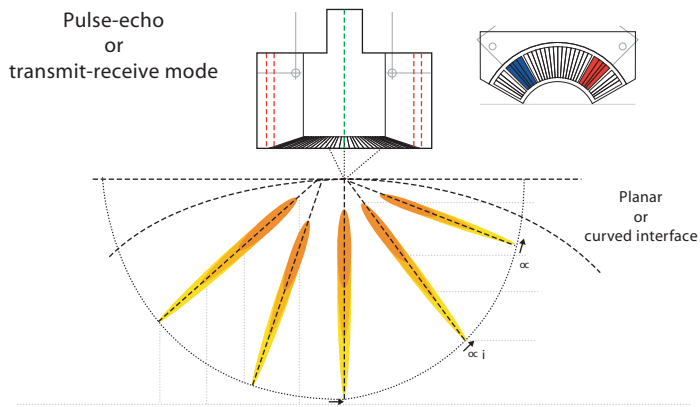
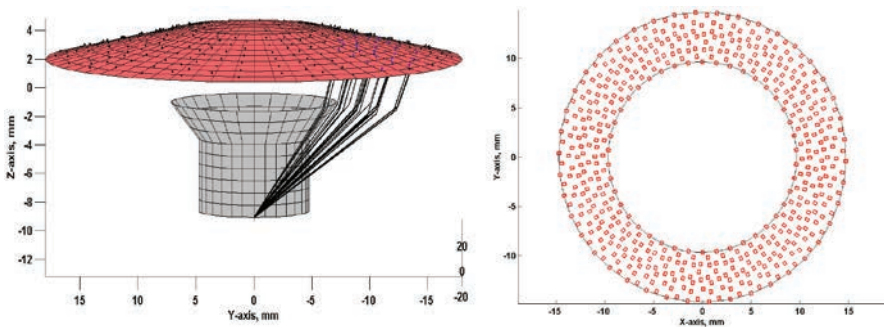


**Figure 3-11** Cluster phased array probe for small diameter pipe/tube inspection showing typical beam angles (R/D Tech U.S. patent 2004/0016299AL).



*Courtesy of Lockheed Martin AS and USAF, USA*

**Figure 3-12** 2-D matrix conical phased array probe (R/D Tech U.S. patent 10-209,298).

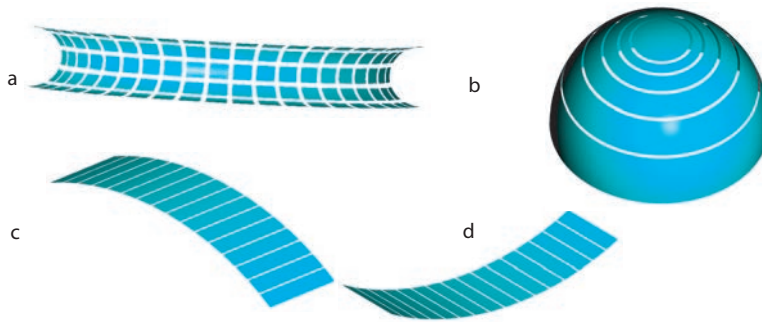


**Figure 3-13** Mechanically focused phased array probes: (a) toroidal convex prefocused; (b) annular concave; (c) linear concave; (d) linear convex.

Examples of focusing patterns for the commonly used probes are presented in Figure 3-14 to Figure 3-16.

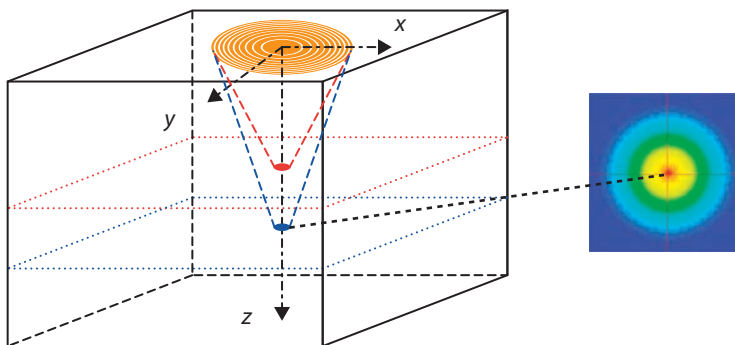


**Figure 3-14** Spherical focusing (1-D depth) pattern and simulation of the beam profile for an annular phased array probe.

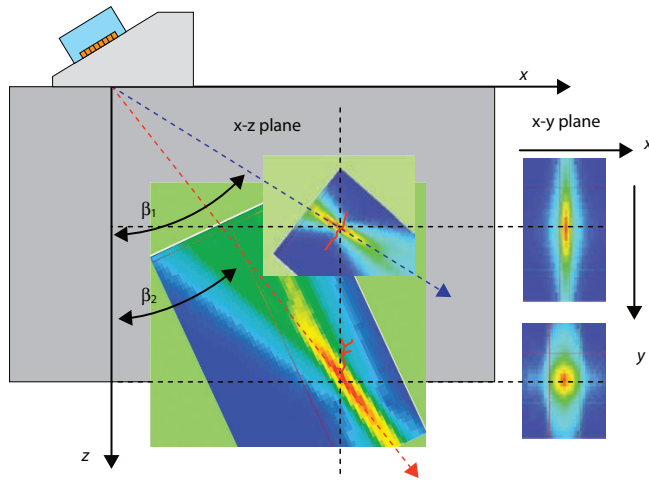


**Figure 3-15** Cylindrical focusing pattern (2-D; depth and angle) of linear phased array probe for detecting a SCC at the inner surface and a fatigue crack at mid-wall; simulation of beam profile for both depths.

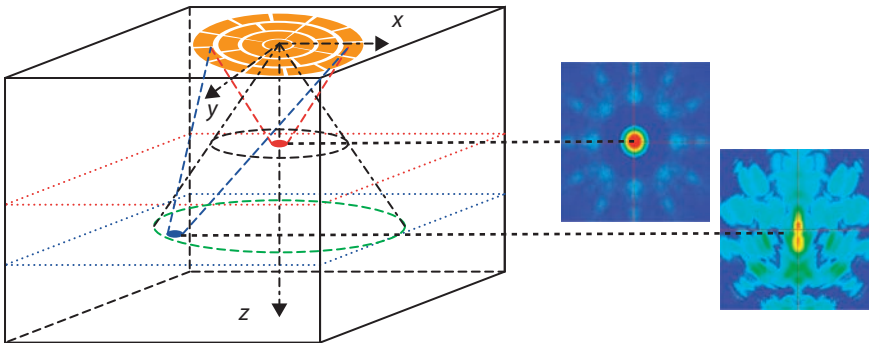


**Figure 3-16** Spherical/elliptical focusing pattern (3-D solid angle) of segmented annular phased array probe and beam simulation at two depths and two angles. Note the noise increase due to the grating lobes.

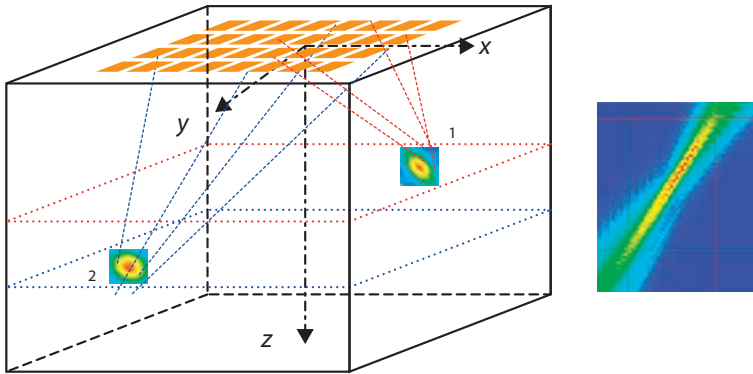


**Figure 3-17** Elliptical focusing pattern (3-D solid angle) of 2-D matrix phased array probe and beam simulation for two depths and two angles.

## 3.4 Linear Arrays

Linear arrays are the most commonly used phased array probes for industrial applications. Their main advantages are:

- Easy design
- Easy manufacturing
- Easy programming and simulation
- Easy applications with wedges, direct contact, and immersion
- Relatively low cost
- Versatile

The characteristic features of linear arrays are detailed in sections 3.4.1, “Active Aperture,” to 3.4.25, “Grating Lobe Amplitude.”

### 3.4.1 Active Aperture

The *active aperture* ( $A$ ) is the total probe active length. Aperture length is given by formula (3.1) [see also Figure 3-18]:

$$A = n \cdot e + g \cdot (n - 1) \quad (3.1)$$

where:

$A$  = active aperture

$g$  = gap between two adjacent elements. A practical value is  $e < \lambda/2$ .

$n$  = number of elements  
 $\lambda$  = wavelength

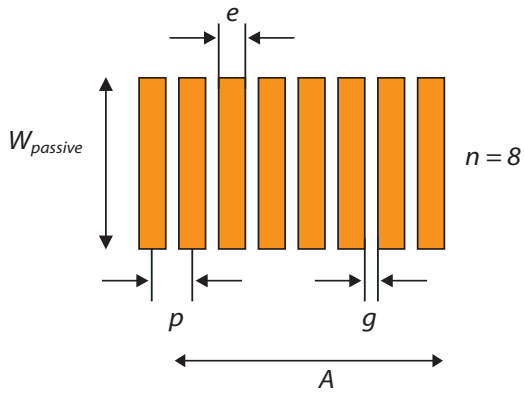


**Figure 3-18** Active and passive aperture.

### 3.4.2 Effective Active Aperture

The *effective active aperture* ( $A_{eff}$ ) is the projected aperture seen along the refracted rays (see Figure 3-19).

$$A_{eff} = \frac{A \cdot \cos \beta_R}{\cos \alpha_I} \quad (3.2)$$

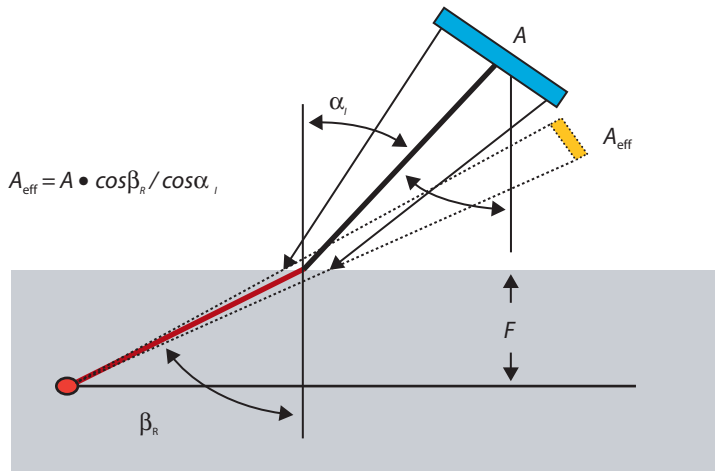


Figure 3-19 Effective aperture definition.

### 3.4.3 Minimum Active Aperture

The *minimum active aperture* ( $A_{\min}$ ) is the minimum active aperture to get an effective focusing at the maximum refracted angle.

$$A_{\min} = 2 \left[ \frac{F(v_R^2 - v_I^2 \cdot \sin^2 \beta_R)}{f \cdot v_R \cdot \cos^2 \beta_R} \right]^{0.5} \quad (3.3)$$

where:

- $v_I$  = velocity in first medium (water, wedge)
- $v_R$  = velocity in test piece
- $f$  = ultrasound frequency
- $F$  = focal depth for maximum refracted angle
- $\beta_R$  = maximum refracted angle in the test piece

### 3.4.4 Passive Aperture

The *passive aperture* ( $W$ ) is the element length or probe width (see Figure 3-18). Recommended passive aperture is determined by probe frequency and the focal depth range:

$$W = 1.4[\lambda(F_{\min} + F_{\max})]^{0.5} \quad (3.4)$$

Its contribution to the focal depth (near-field length) is given (for nonfocused probes) by formula (3.5):

$$N_0 = \frac{(A^2 + W^2)(0.78 - 0.27W/A)}{\pi\lambda} \quad (3.5)$$

A good practical estimation is given by formula (3.6):

$$N_0 \approx \frac{0.25A^2}{\lambda} \quad (3.6)$$

The passive aperture contributes to sensitivity and defect length sizing. The maximum efficiency for a linear array probe is obtained with  $W_{\text{passive}} = A$ .

The passive aperture also affects the beam-diffracted pattern and the beam width (see Figure 3-20). Generally, design phased array probes with  $W_{\text{passive}}/p > 10$  and/or keep  $W_{\text{passive}} = (0.7 \text{ to } 1.0)A$  (applicable to nonfocused probes).

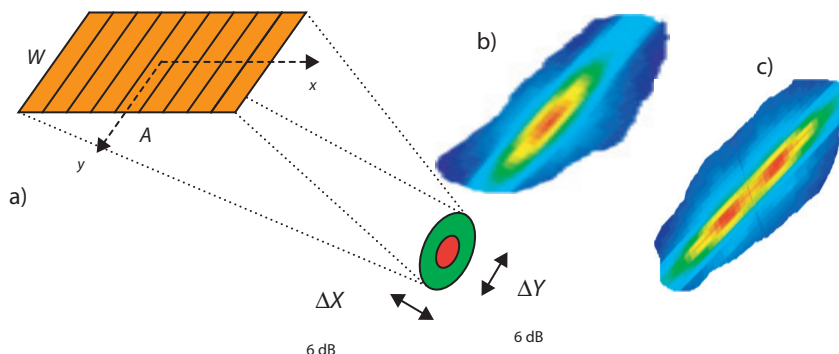


**Figure 3-20** Influence of passive aperture width on beam width and shape: (a) deflection principle and beam dimensions; (b) beam shape for  $W = 10$  mm; (c) beam shape for  $W = 8$  mm, 5 MHz shear wave, pitch  $p = 1$  mm;  $n = 32$ ;  $F = 50$  mm in steel.

### 3.4.5 Elementary Pitch

The *elementary pitch* ( $p$ ) is the distance between the centers of two adjacent elements:

$$p = e + g$$

### 3.4.6 Element Gap

The *element gap* ( $g$ ) [kerf] is the width of acoustic insulation between two adjacent elements.

### 3.4.7 Element Width

The *element width* ( $e$ ) is the width of a single piezocomposite element. The general rule is keep  $p < 0.67 \cdot \lambda$ ; to avoid grating lobes at large steering angles:

$$e_{\text{design}} < \frac{\lambda}{2}$$

New modelling from the UK (see reference 10) and our PipeWIZARD probe design proved the element pitch may be larger than the wave length, but the steering capabilities are limited.

### 3.4.8 Maximum Element Size

The *maximum element size* ( $e_{\text{max}}$ ) is the width of a single piezocomposite crystal, and depends on the maximum refracted angle.

$$e_{\text{max}} = \frac{0.514 \cdot \lambda}{\sin \alpha_{R_{\text{max}}}} \quad (3.7)$$

### 3.4.9 Sweep Range

The *sweep range* ( $\alpha_s$ ) is the difference between the maximum and minimum refracted angles of the focused beam in the test piece (see  $\Delta\beta$  in Figure 3-21).

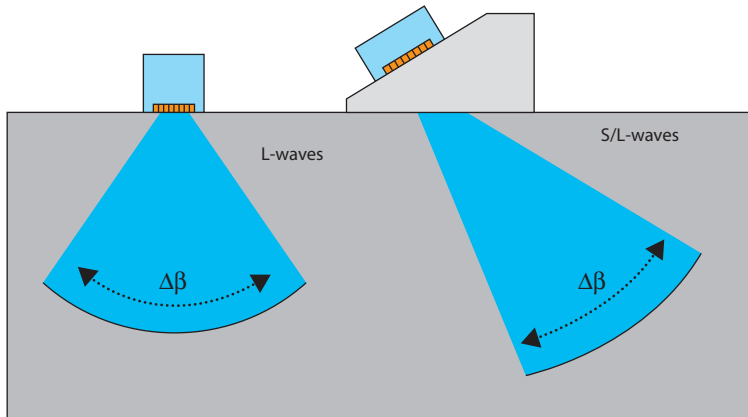


**Figure 3-21** Definition of sweep range for direct contact (longitudinal wave) and wedge (shear/longitudinal wave) inspection.

### 3.4.10 Steering Focus Power

The *steering focus power* [ $F(\beta_R)/F_0$ , where  $\beta_R$  is the refracted angle] is the focal depth dependence on the sweep angle (see Figure 3-22).

$$\frac{F(\beta_R)}{F_0} = \left( \frac{\cos \beta_R}{\cos \alpha_0} \right)^2 \quad (3.8)$$

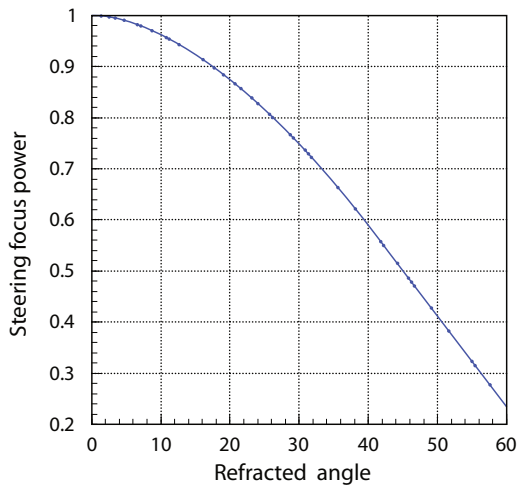


**Figure 3-22** Steering focus power dependence on refracted angle.

### 3.4.11 Gain Compensation

An example of *gain compensation* due to sweep range (effective aperture) is presented in Figure 3-23.

**Note:** When using a refracting wedge, the value referred to is the refracted angle given by Snell's law for the specific wedge material and angle.

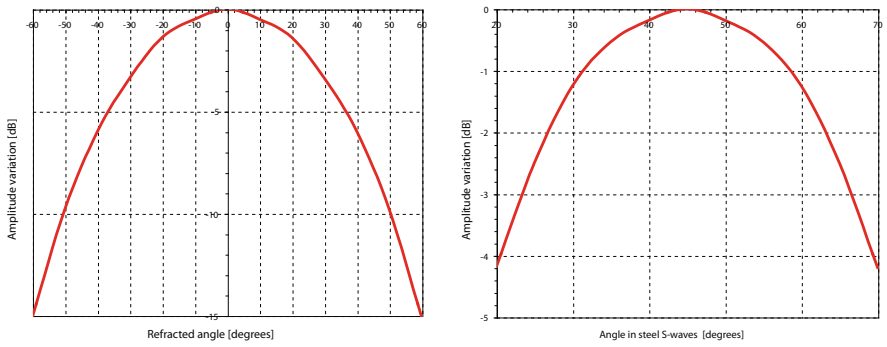


**Figure 3-23** Amplitude dependence on steering angle for longitudinal waves in steel ( $-60^\circ$  to  $+60^\circ$ ) [left], and shear waves with a sweep range:  $20^\circ$  to  $70^\circ$  with a central ray refracted angle of  $45^\circ$  (right).

The cross section of a beam, which is circular at normal incidence, will become elliptical at high-refraction angles. The beam dimensions depend on the active and passive apertures, according to the relationships explained in the following sections.

### 3.4.12 Beam Length

*Beam length* ( $\Delta Y_{-6\text{ dB}}$ ) is the length of the beam in a C-scan display at a specific depth ( $z$ ) in a plane perpendicular to the incident plane (parallel with the passive aperture—see Figure 3-20).

$$\Delta Y_{-6\text{ dB}} \approx \frac{0.884 UT_{\text{path}} \lambda}{W_{\text{passive}}} \quad (3.9)$$

### 3.4.13 Beam Width

*Beam width* ( $\Delta X_{-6\text{ dB}}$ ) is the length of the beam in a C-scan display at a specific depth ( $z$ ) in the incident plane (parallel to the active aperture—see Figure 3-20).

$$\Delta X_{-6\text{ dB}} \approx \frac{0.884UT_{\text{path}}\lambda}{A \cos \beta} \quad (3.10)$$

Relations (3.9) and (3.10) are valid for ultrasound paths outside the focal depth ( $UT_{\text{path}} \neq F$ ). The formulas predict the beam width to within 15% to 30%.

The beam width is measured based on echo dynamics from a SDH. Beam length is evaluated based on echo dynamics from the FBH profiles (see Figure 3-24).

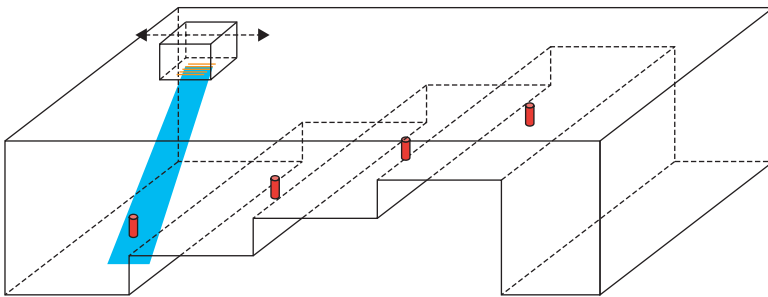


**Figure 3-24** Beam length evaluation on FBH placed on a step block.

Beam width is important for height sizing and for the detection of small defects (see Figure 2-45 on page 78 and Figure 2-48 on page 80, for example). The beam width depends on focal depth and the refracted angle (see Figure 3-25).



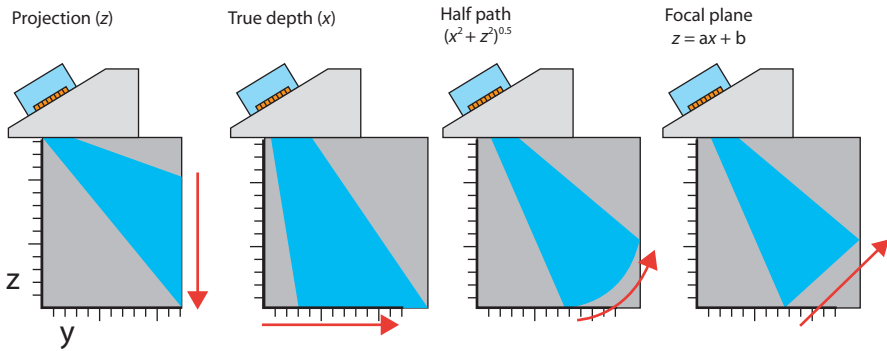


Figure 3-26 Types of focusing for linear phased array probe.

### 3.4.15 Depth of Field

*Depth of field* ( $L_{-6\text{ dB}}$ ), or *focal length*, is the length measured at the  $-6\text{ dB}$  drop along the acoustic axis, taking the focal depth as a reference point.

### 3.4.16 Focal Range

The *focal range* is the scanning distance either in depth or in ultrasonic path for multichannel focal laws or with sweep angles (see Figure 3-27). The cutoff lower value is normally  $-6\text{ dB}$ ; for some applications, the cutoff value is  $-3\text{ dB}$  (see also chapter 2, Figure 2-25 on page 55 and Figure 2-26 on page 55).

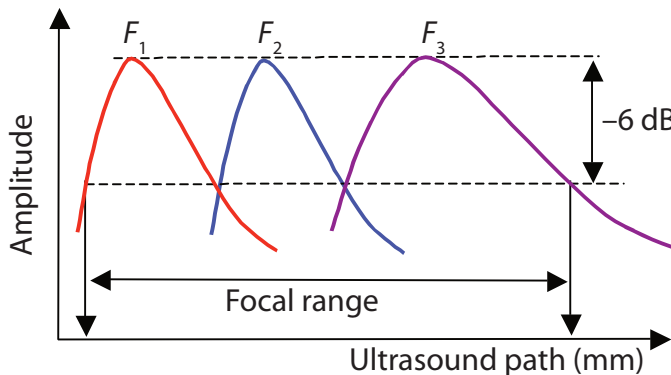


Figure 3-27 Focal range definition for  $-6\text{ dB}$  cutoff (pulse-echo).

### 3.4.17 Near-Surface Resolution

*Near-surface resolution* (dead zone) is the minimum distance from the scanning surface where a reflector (SDH, FBH) amplitude has more than a 6-dB resolution compared with the decay amplitude from the main bang (initial pulse) for normal beam (see Figure 3-28). The dead zone increases along with the gain increase.

### 3.4.18 Far-Surface Resolution

*Far-surface resolution* is the minimum distance from the inner surface where the phased array probe can resolve the amplitude ( $\Delta A > 6$  dB) to specific reflectors (SDH or FBH) located at a height of 1 mm to 5 mm from the flat/cylindrical backwall (see Figure 3-28).

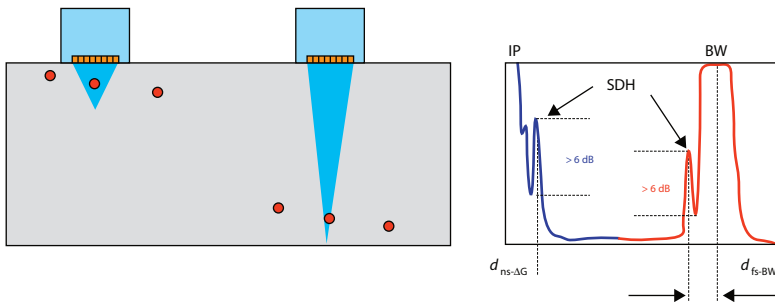


**Figure 3-28** The near-surface and far-surface resolution definitions.

### 3.4.19 Lateral and Axial Resolution

*Lateral resolution* and *axial resolution* are defined below. Note that the phased array probe is moving for lateral resolution and is static for axial resolution. A shorter pulse duration and smaller beam length increases both resolutions.

Lateral resolution:

$$\Delta d = \frac{\Delta X_{-6 \text{ dB}}}{4}$$

Axial resolution:

$$\Delta z = \frac{v_{\text{test piece}} \Delta \tau_{-20 \text{ dB}}}{2}$$

where  $\Delta\tau_{-20\text{ dB}}$  is the time resolution at a  $-20\text{ dB}$  drop-off.

### 3.4.20 Angular Resolution

The *angular resolution* is the minimum angular value between two A-scans where adjacent defects located at the same depth are resolvable (see Figure 3-29).

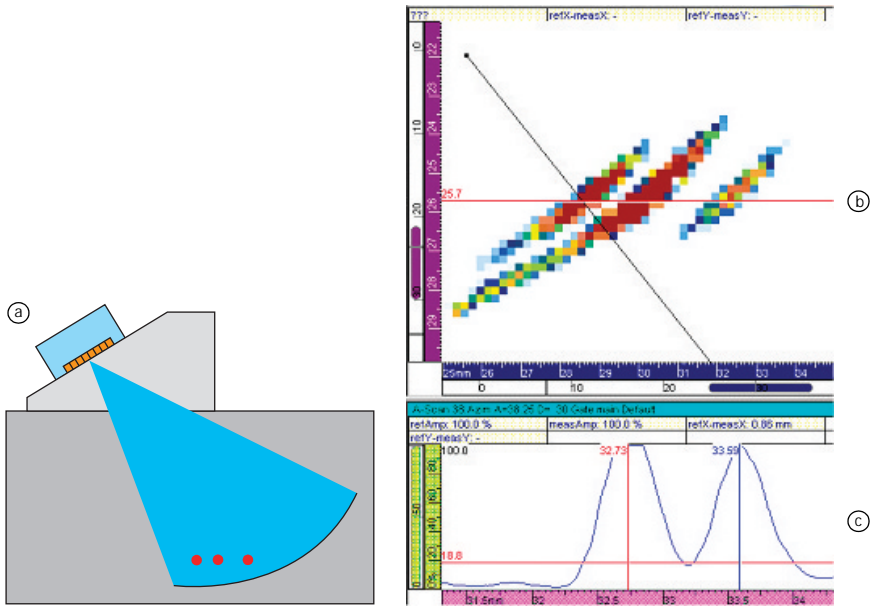


**Figure 3-29** Angular resolution and detection of three 0.5-mm SDHs spaced apart by 0.8 mm and 1.2 mm. SDHs are located at  $z = 25.7\text{ mm}$ . Principle (a); angle-corrected true depth (b); and echo dynamic (c).

### 3.4.21 Main Lobe

The *main lobe* is the acoustic pressure directed towards the programmed angle.

### 3.4.22 Side Lobes

*Side lobes* are produced by acoustic pressure leaking from probe elements at different and defined angles from the main lobe.

### 3.4.23 Grating Lobes

*Grating lobes* are generated by acoustic pressure due to even sampling across the probe elements (see Figure 3-30).

Their locations are given by formula (3.11):

$$\beta_{\text{grating}} = \sin^{-1}(m\lambda/p) \quad (3.11)$$

where:

$$m = \pm 1, \pm 2, \pm 3, \dots$$

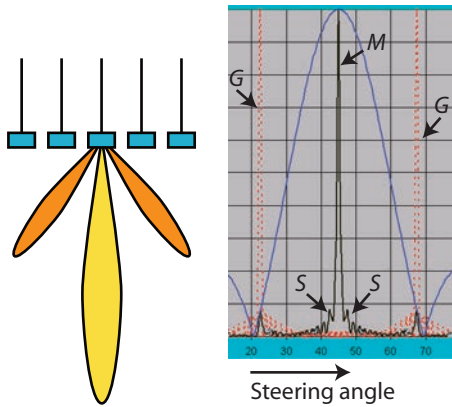


**Figure 3-30** Directivity plot for a phased array probe: *M* = main lobe; *S* = side lobes; *G* = grating lobes.  $\beta_{\text{grating}}$  is shown in orange; the main lobe, in yellow.

**Note:** Probe design optimization is achieved by:

- Minimizing the main lobe width
- Suppressing the side lobes
- Eliminating the grating lobe(s)

### 3.4.24 Beam Apodization

*Beam apodization* is a computer-controlled feature that applies lower voltage to the outside elements in order to reduce the side lobes.

**Note:** The Tomoscan FOCUS beam apodization is performed during the receiving stage. The gain applied to each element of the probe can be adjusted individually, but the pulse voltage is kept the same for each element.

### 3.4.25 Grating Lobe Amplitude

*Grating lobe amplitude* depends on pitch size, number of elements, frequency, and bandwidth (see Figure 3-31 and Figure 3-32).

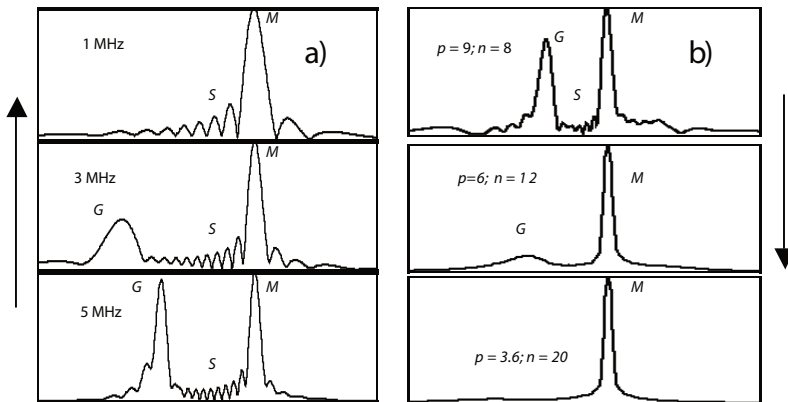


**Figure 3-31** Grating lobe dependence on: (a) frequency; (b) pitch size and number of elements (same aperture of 72 mm).

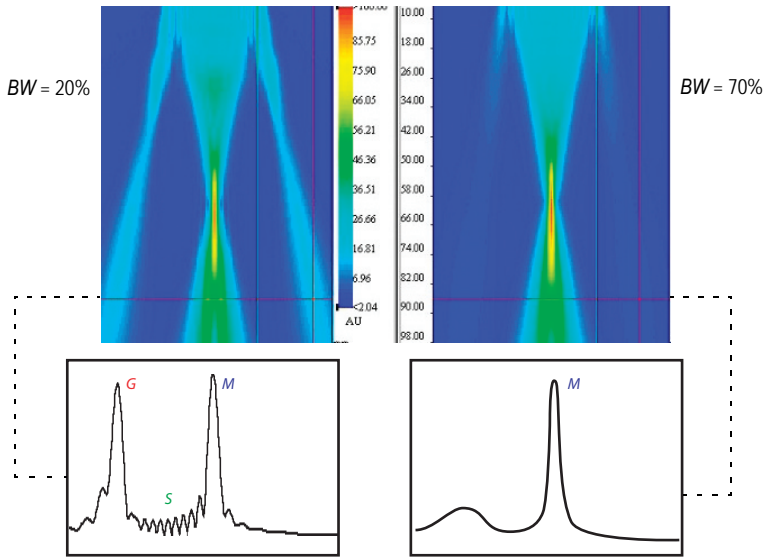


**Figure 3-32** Influence of damping ( $BW_{tel}$ ) on grating lobes for a 1-MHz probe focusing at  $z = 60$  mm (simulation using PASS).

Grating lobes may be reduced though:

- Decreased frequency
- Reduced pitch size
- Increased bandwidth, which spreads out the grating lobes
- Reduced sweeping range (addition of a wedge)
- Subdicging (cutting elements into smaller elements)
- Randomized element spacing (using irregular element positioning to break up the grating lobes)

### 3.5 Dynamic Depth Focusing

*Dynamic depth focusing* (DDF) is a programmable, real-time array response on reception by modifying the delay line, gain, and excitation of each element as a function of time (see Figure 3-33). DDF replaces multiple focal laws for the same focal range by the product of the emitted beam with separate “focused beams” at the receiving stage. In other words, DDF dynamically changes the focal distance as the signal returns to the phased array probe. DDF significantly increases the depth-of-field and SNR.

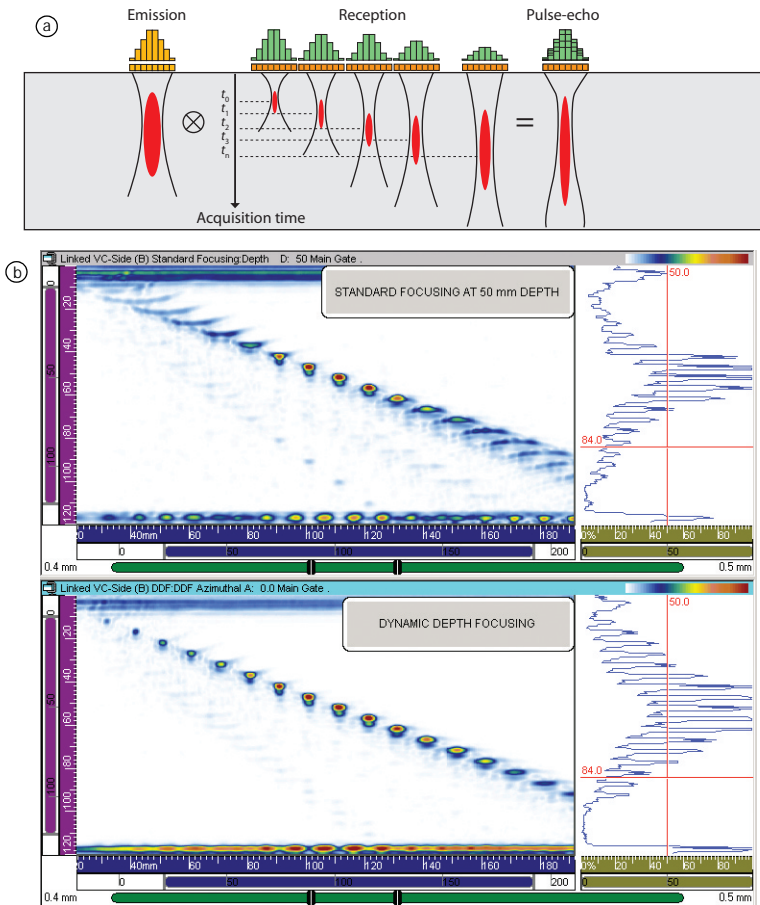


**Figure 3-33** Dynamic depth focusing (DDF): (a) principle—resulting beam by product; (b) comparison between standard phased array focusing (*top*) and DDF on the depth-of-field (*bottom*). Note the detection of two SDHs in the near-surface zone by DDF that are missed by standard phased array focusing.

### 3.5.1 DDF Beam Divergence

The *DDF beam divergence on acoustic axis*  $\Delta X_{-6\text{ dB}}(\text{SDH})$  is the beam width measured using the echo-dynamic amplitude from side-drilled hole reflectors when the DDF board is enabled.

A comparison of DDF with the standard phased array probes is presented in Figure 3-34. Note the narrow beam of the DDF compared to standard phased array focusing.

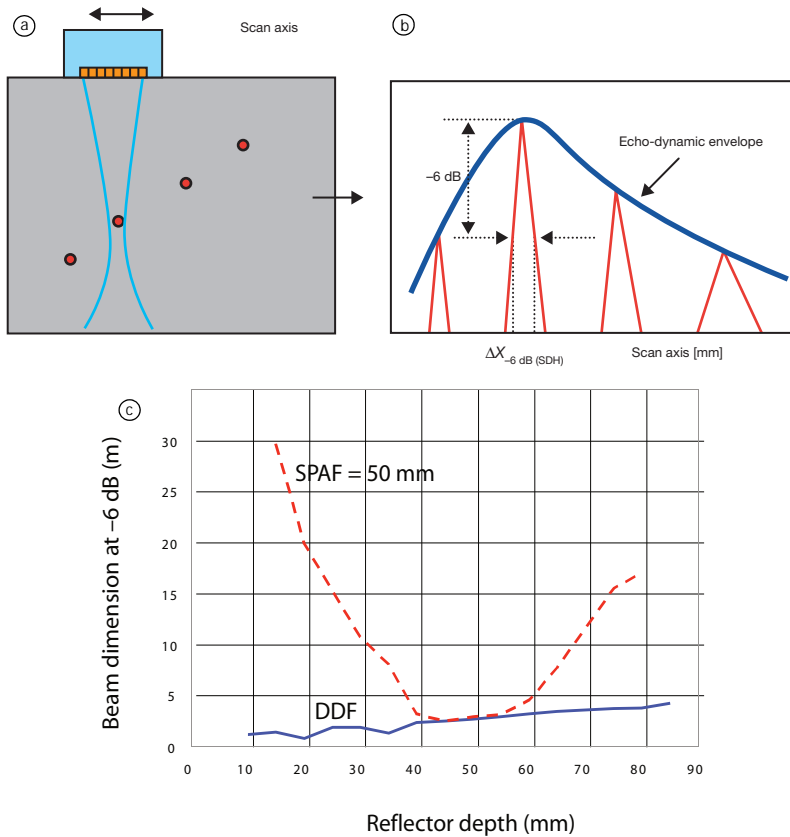


**Figure 3-34** Beam divergence: (a) principle; (b) longitudinal waves at 0°; (c) comparison between standard phased arrays (SPAF) and DDF.

### 3.5.2 DDF Advantages

DDF has the following advantages:

- The depth-of-field generated by an optimized DDF is improved by a factor of four in practical applications with respect to standard focusing.
- The beam spot produced by DDF is always as small as the one produced by standard focusing, or smaller.
- The use of DDF creates very small beam spreads. Half angles as small as 0.30 and 0.14 degrees were obtained with linear and annular array probes.
- DDF diminishes the beam spread without altering the dimension of the beam obtained with the standard phased array.

- The  $SNR_{DDF}$  is greater than the  $SNR_{SPAF}$ .
- File size is greatly reduced because only one A-scan is recorded at each mechanical position.
- Effective PRF is increased because only one A-scan is needed to cover a long sound path instead of multiple pulses from individual transducers.

All of these properties make the use of DDF suitable for applications such as boresonic, titanium billet, and blade root inspections<sup>8</sup> (see chapter 5, "Applications").

## 3.6 Probe on the Wedge

Linear phased array probes are mostly used in combination with a wedge. The probe-wedge features are detailed in section 3.6.1, "Wedge Delay," to section 3.6.3, "Index Point Migration."

### 3.6.1 Wedge Delay

*Wedge delay* ( $D_w$ ) is the time of flight ( $\mu s$ ) for specific angles in the wedge (full path).

The computation is detailed in Figure 3-35.

1. Find the ray angle for a specific refracted angle from Snell's law:

$$\alpha_i = \sin^{-1}\left(\frac{v_{\text{wedge}} \sin \beta_R}{v_{\text{test piece}}}\right)$$

2. Find the height of the middle of the phased array probe (virtual emitting point):

$$E_h = (L_1 + L_2) \cdot \sin \omega = [H_1 + p/2 \cdot (n - 1)] \cdot \sin \omega \quad (3.12)$$

3. Find the ultrasound path ( $P$ ) in the wedge:

$$P_{\text{wedge}} = \frac{E_h}{\cos \alpha_i}$$

4. Find the wedge delay:

$$D_{\text{wedge}} = \frac{2 \bullet P}{v_w} \quad (3.13)$$

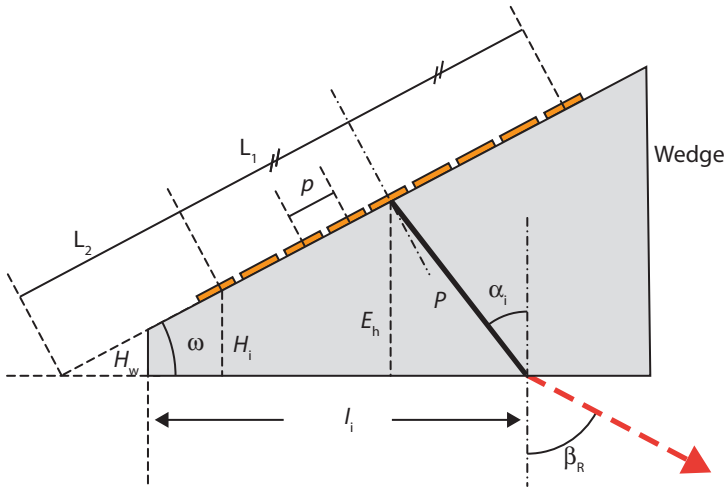


**Figure 3-35** Wedge elements for computation of wedge delay and index.

### 3.6.2 Index Point Length

*Index point length ( $I_i$ ):* the length from the back (or front) of the wedge to the exit point of a specific angle (see Figure 3-35).

$$I_i = (L_1 + L_2) \bullet \cos \omega - H_w \bullet \tan \omega + P \bullet \sin \alpha_i \quad (3.14)$$

where:

- $\omega$  = wedge angle
- $H_i$  = height in the middle of the first element
- $H_w$  = wedge height—back
- $P$  = ultrasound path in wedge (half path)
- $\alpha_i$  = incident angle of ultrasonic ray in the wedge
- $\beta_R$  = refracted angle in test piece
- $E_h$  = height of middle of phased array probe (for virtual emitting point)
- $p$  = element pitch
- $L_1$  = distance from the middle of first element to the emitting point

- $L_2$  = distance from the emitting point to the intersection with horizontal line (wedge contact surface)
- $I_i$  = index point length
- $v_R$  = ultrasonic velocity in test piece
- $v_w$  = ultrasonic velocity in wedge

### 3.6.3 Index Point Migration

*Index point migration* [ $\Delta I(\alpha_i)$ ]: index point change with respect to angle of beam in wedge (see Figure 3-36).

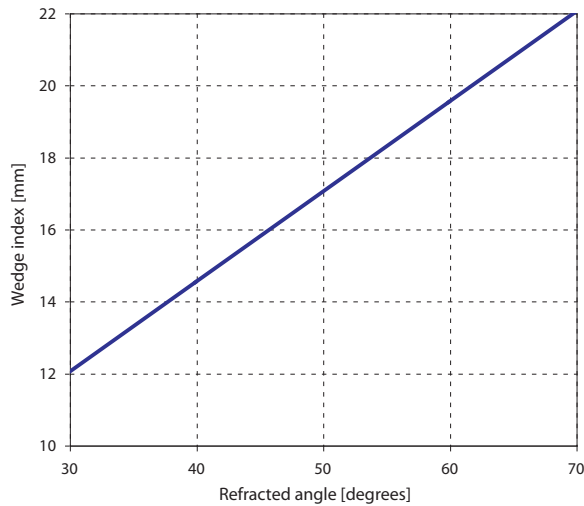


**Figure 3-36** Sample plot of migration of the index point with refraction angle for a linear phased array probe. TomoView software compensates for this migration.

## 3.7 Beam Deflection on the Wedge

This section describes the various types of beam deflection that are possible when using phased arrays. This subject is unique to phased arrays, due to the beam steering capability.

### 3.7.1 Azimuthal Deflection

*Azimuthal (or sectorial) deflection* is defined as beam sweeping along the wedge length [see Figure 3-37 (A)] in the  $xz$  plane (the passive aperture is parallel with the wedge width) [see Figure 3-38 (a)].

### 3.7.2 Lateral Deflection

*Lateral deflection* is defined as beam sweeping along the wedge width [see Figure 3-37 (B)] in the  $yz$  plane (the passive aperture is parallel with wedge length) [see Figure 3-38 (b)]. The deflection is performed at a constant refracted angle given by the wedge angle.

### 3.7.3 Skew Deflection

*Skew deflection* is defined as beam sweeping with the active aperture parallel with the wedge width and tilted [see Figure 3-38 (c)]. This could also be described as an azimuthal deflection with an out-of-plane tilt.

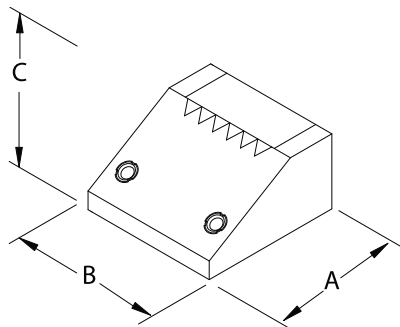


**Figure 3-37** Wedge dimensions: (A) length; (B) width; and (C) height.

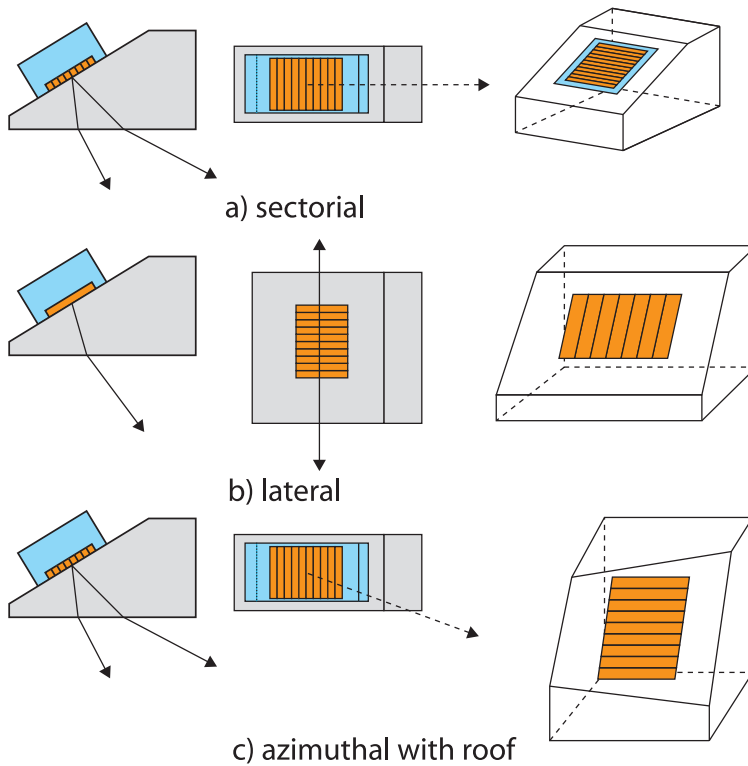


**Figure 3-38** Beam deflection on the wedge: (a) sectorial/azimuthal; (b) lateral; (c) sectorial/azimuthal with a roof (skewed).

### 3.7.4 Active Axis Offset

*Active axis offset* is defined as the offset of the middle of the first element along the active axis (transducer array axis), relative to the reference point (see Figure 3-39).

### 3.7.5 Passive Axis Offset

*Passive axis offset* is defined as the offset of the middle of the first element along the passive axis (the axis that is perpendicular to the transducer array axis), relative to the reference point (see Figure 3-39).

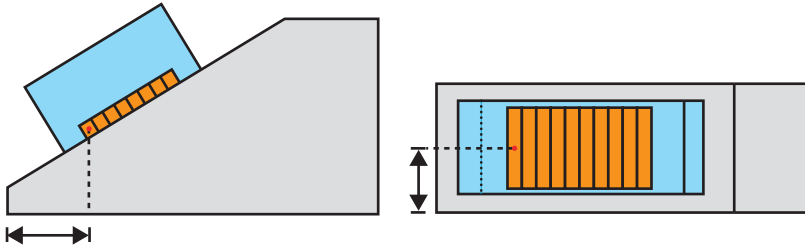


**Figure 3-39** Active (*left*) and passive (*right*) offset definition.

### 3.8 2-D Matrix Phased Array Probes

Two-dimensional phased array probes are used to inspect in pitch-and-catch and/or in pulse-echo mode. The main advantages of 2-D matrix probes are:

- Potential for deflecting the beam in 3-D space
- Potential for focusing in spherical, elliptical, or linear patterns
- Potential for focusing at different depths and skew angles using the same wedge
- Two-plane steering capability available for simultaneous variation of both the refracted angle and skew angle of the ultrasonic beam

The main elements of the 2-D matrix probe are listed in Figure 3-40.

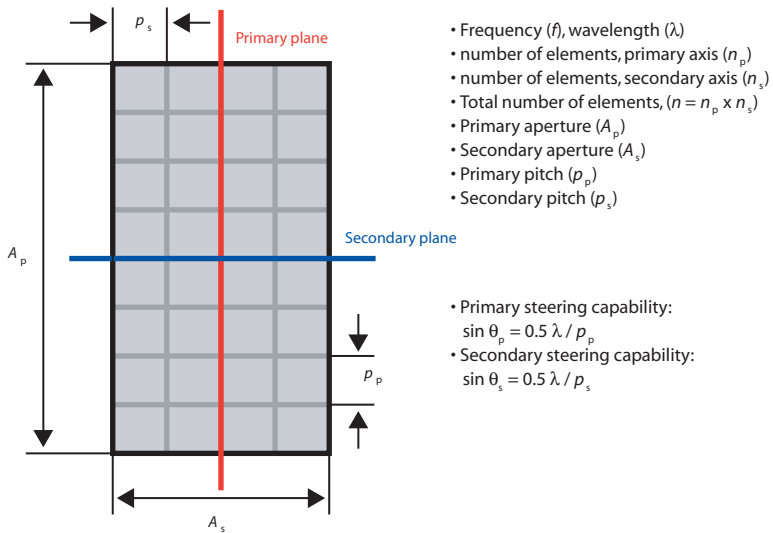


**Figure 3-40** 2-D matrix phased array probe and its main features.

Simulation of a 2-D matrix phased array probe beam focusing on a cylindrical part is presented in Figure 3-41.

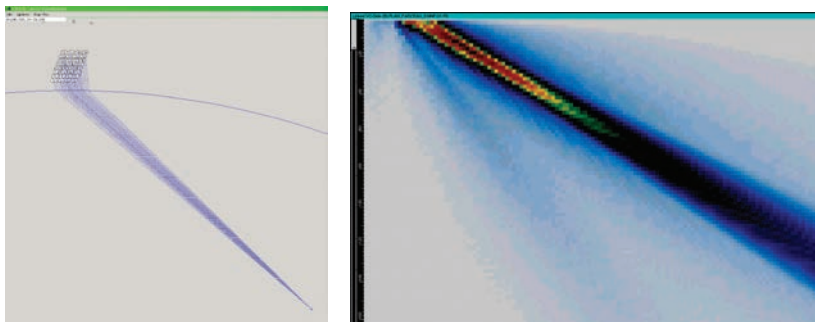


**Figure 3-41** Beam simulation for 2-D matrix probe on cylindrical part; *left*, ray tracing; *right*, beam profile.

An example of delay values for a 2-D matrix phased array probe of 32 elements ( $4 \times 8$ ) for a skew of  $-15^\circ$  and a refracted angle of  $45^\circ$  LW in steel,  $F = 50$  mm, is presented in Figure 3-42.

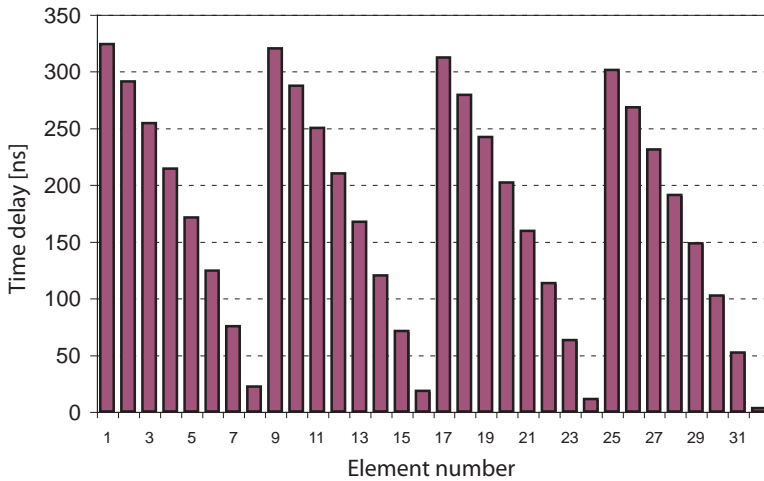


**Figure 3-42** Delay values for a 2-D matrix phased array probe of  $8 \times 4$  elements in pulse-echo configuration.

An example of a pitch-and-catch configuration for a 2-D matrix probe is presented in Figure 3-43. More details about the applications of 2-D probes are presented in chapter 4, “Scanning Patterns and Views.”

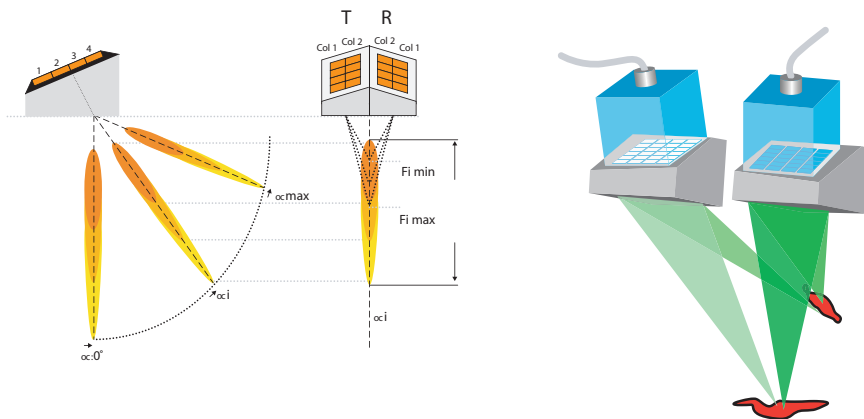
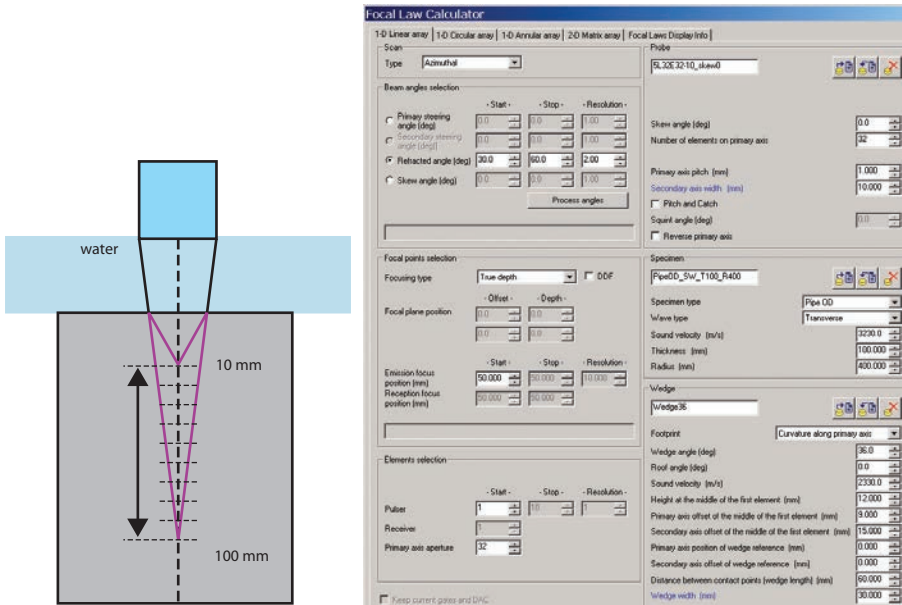


**Figure 3-43** Examples of pitch-and-catch configuration using a 2-D matrix probe on a wedge with a roof:  $4 \times 2$  array (*left*) and  $6 \times 4$  array (*right*).

### 3.9 Focal Law Calculator

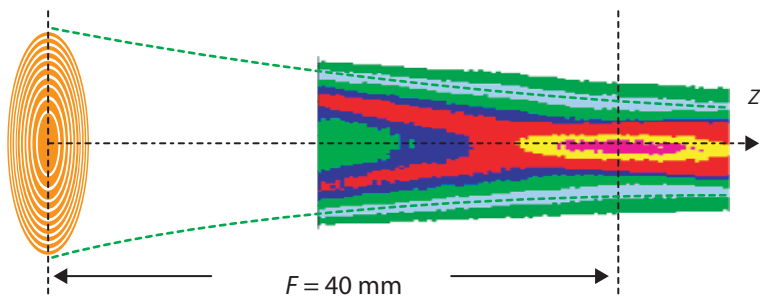
The *focal law calculator* is the vital phased array tool that calculates the specific delays for all active elements in a customized calculation, which includes beam deflection, probe features, wedge characteristics, and test piece properties. Based on these calculated values, the hardware will enable the firing sequence.

Figure 3-44 represents the focal law programming for an annular array probe placed in 20 mm of water and focused on a steel plate at a range of 10 mm to 100 mm.



**Figure 3-44** Inspection scenario (*left*) and focal laws for annular array probe immersed in 20 mm of water (*right*).

The actual beam profile from  $z = 15\text{--}50$  mm is presented in Figure 3-45.



**Figure 3-45** Beam profile of annular array probe from 15 mm to 50 mm in steel ( $F = 40$  mm; beam diameter = 1 mm).

An example of the focal laws calculated for a 2-D matrix probe on a  $28^\circ$  Rexolite wedge with a  $10^\circ$  roof angle is presented in Figure 3-46.

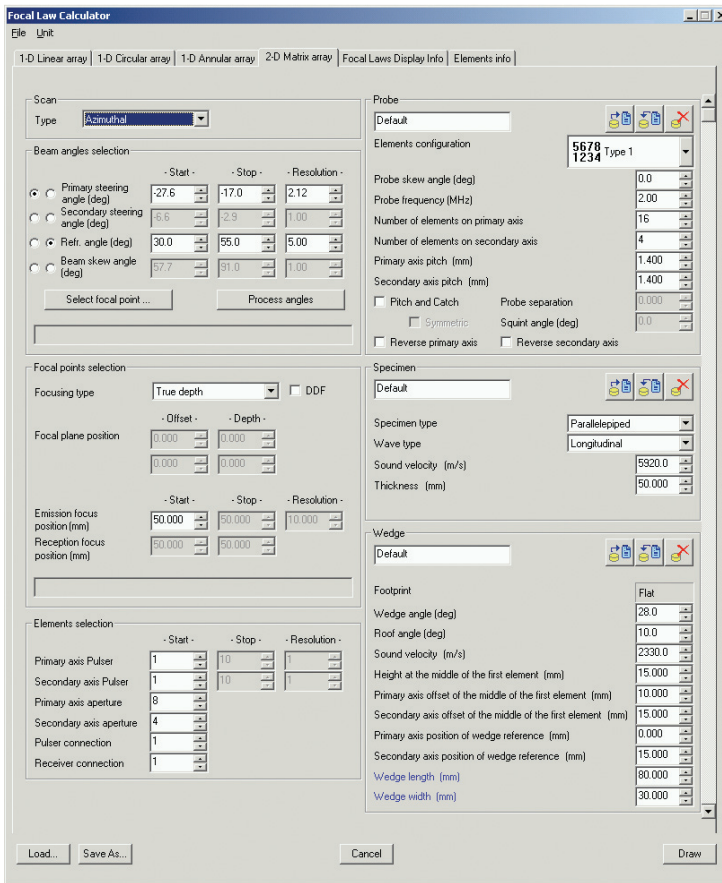


**Figure 3-46** Example of focal law computation for a 2-D matrix probe of  $16 \times 4$  elements.

$f_c = 5 \text{ MHz}$   
 $n = 16$   
 $A = \sim 32 \text{ mm}$   
 $W = 1.4 \text{ mm}$   
 Rexolite wedge (80 mm  $\times$  30 mm);  
 $\omega = 33^\circ$   
 $F = 50 \text{ mm}$

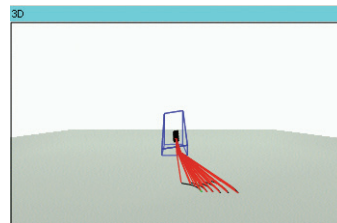


**Figure 3-47** Linear phased array probe characteristics and inspection visualization for a sweep range of  $30^\circ$  to  $60^\circ$ , resolution of  $2^\circ$ , and focusing at 50 mm.

Another example of focal law computation for an annular array on a pipe is

presented in Figure 3-48. Ray tracing visualization of ultrasounds in the component is presented in Figure 3-49.

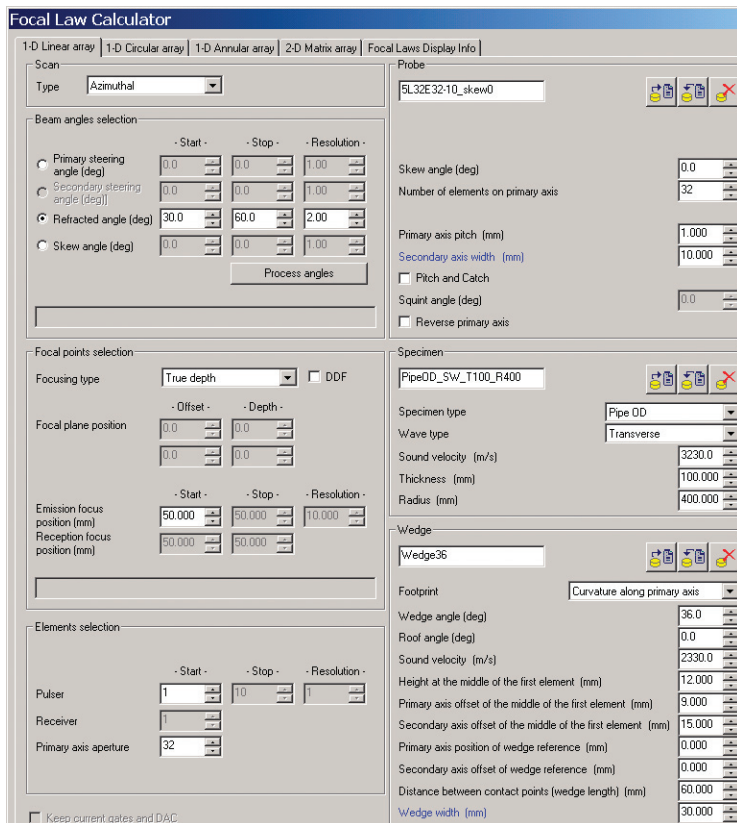


**Figure 3-48** Example of focal law computation for a linear phased array probe on a pipe,  $OD \times t = 400 \text{ mm} \times 100 \text{ mm}$ .

$f_c = 5 \text{ MHz}$   
 $n = 32$   
 $A = -32 \text{ mm}$   
 $W = 10 \text{ mm}$   
 Rexolite wedge (60 mm  $\times$  30 mm);  
 $\omega = 36^\circ$   
 $F = 50 \text{ mm}$

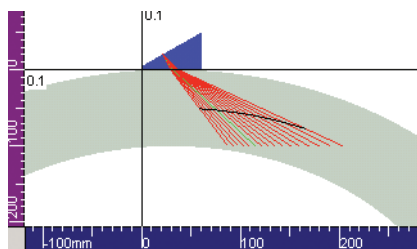


**Figure 3-49** Linear phased array probe characteristics and inspection visualization for a sweep range of  $30^\circ$  to  $60^\circ$ , resolution of  $2^\circ$ , and focusing at 50 mm.

Figure 3-50 shows another visualization tool, ray tracing, to inspect a weld with a counterbore.

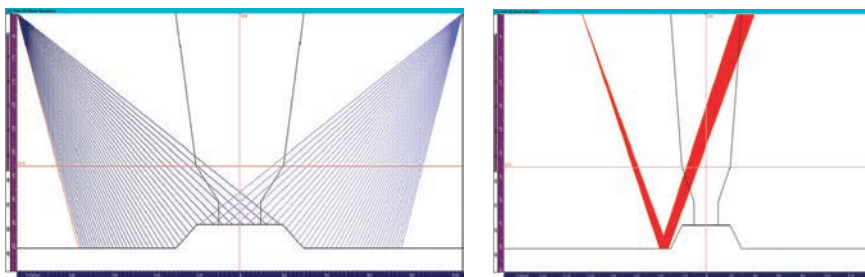


**Figure 3-50** Simulation of pipe weld inspection using ray tracing and S-scans.

### 3.10 Standard Array Probes

An overview of phased array probes is presented in Table 3-4.

**Table 3-4** Probe classification overview.

Probe type	Beam steering*	Beam shape	Remarks
Plan linear	A, L, DDF	Cylindrical	Most commonly used
Plan circular	A, L, DDF	Cylindrical, elliptical	For tubes and cylindrical parts; mirror reflection
Annular	D, DDF	Spherical	Normal beams for forging inspections
2-D matrix	A, L, DDF	Elliptical	Weld inspections
Rho-theta	A, DDF	Spherical/elliptical	Special applications in aeronautics; complex design, complex setup

\*A = azimuthal or sectorial; L = linear; DDF = dynamic depth focusing; D = depth

## 3.11 Other Array Features

Other phased array probe features include sensitivity, electrical impedance, and cross-talk amplitude.

### 3.11.1 Sensitivity

*Sensitivity* ( $S_e$ ): the ratio between the output and input voltages for a specific setup.

$$S_e = 20\log_{10}(V_{\text{out}}/V_{\text{in}})[\text{dB}]$$

### 3.11.2 Impedance

*Impedance* ( $Z_{fc}$ ): the impedance measured at the center frequency (resonant value). Impedance may be evaluated by the KLM model.

### 3.11.3 Cross Talk

*Cross talk between elements*: the dB value of the signal between two elements, which may be adjacent or spaced apart. The acceptable value of cross talk is around  $-30$  dB to  $-40$  dB.

## 3.12 Phased Array Simulation Software (PASS)

Software program developed by the Laboratory of Acoustics at the University of Paris. It is used to visualize the probe design, generate focal laws and beam features, and solve complex probe setups and/or inspection scenarios. The ultrasonic field results (.mnp files) can be analyzed in Olympus TomoView software.

An example of focal point visualizing for an annular probe beam simulation is presented in Figure 3-51.

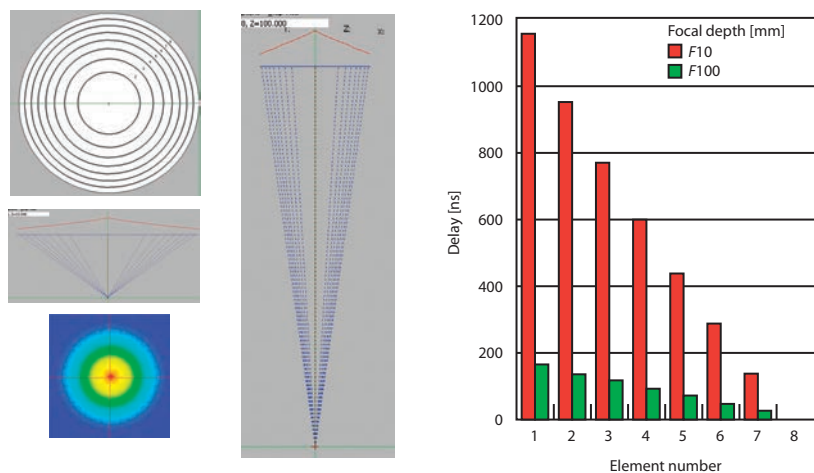


**Figure 3-51** Example of PASS simulation for an annular array probe made out of 8 rings—Fresnel zones—that focus from 10 mm to 100 mm (*left*); delay values for two focus depths (*right*).

### 3.13 Probe Design

For each specific task, probe design should take into account the following principles:

- Compact design, high-quality case, good shock absorbance, good protection from the elements
- Capability of steering the beam through the appropriate sweep range generating no grating lobes with longitudinal waves using direct contact
- Possibility of steering the beam from  $0^\circ$  to  $70^\circ$  for linear arrays in longitudinal wave mode and from  $28^\circ$  to  $85^\circ$  in shear waves mode with the probe on a wedge, or through the appropriate sweep range
- High bandwidth ( $BW > 75\%$ ), that is, pulse duration as short as possible (see Figure 3-52 as a guideline for a  $1.5 \lambda$  probe)
- Possibility of using mode-converted and tandem techniques
- Small sensitivity variation (less than  $\pm 2$  dB in manufacturing conditions) between probe elements
- Small variation of reference gain (less than  $\pm 3$  dB) between different probes from the same family
- Watertight case and cable
- Radiation-resistant ( $10^6$  R/h) for nuclear applications

- Easy to label and identify
- Flexibility for using the phased array probe on multiple projects, and not only in shear wave or longitudinal wave modes

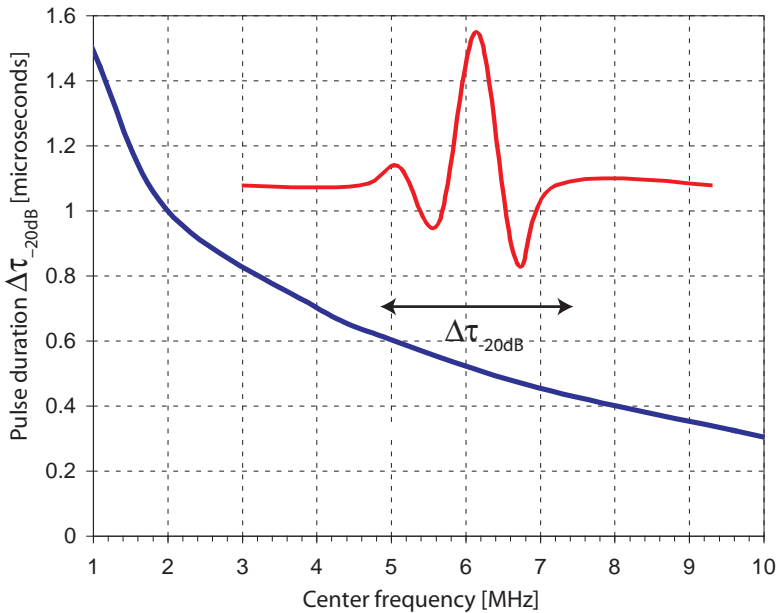


**Figure 3-52** Recommended value for pulse duration of  $1.5 \lambda$  probe.

### 3.13.1 Physics Guidelines

This section presents some considerations and a possible line of reasoning when designing a probe. It is not intended as a universal recipe for probe design.

1. If the test piece is isotropic, check if  $f_{\max} = v_{\text{test piece}}/6D_{\text{grain}}$  (where  $D_{\text{grain}}$  is the grain diameter); this will avoid excessive attenuation and structure noise due to a higher frequency.
2. Find out the maximum sweep range: include a wedge with a refracted angle in the middle of the sweep range; this determines the maximum pitch size.
3. Calculate the angle for grating lobes and avoid the grating lobes by setting  $p < \lambda/2$ .
4. Check if unavoidable grating lobes can generate spurious indications.

5. Check if the pitch exceeds the value of the wavelength when it is used with a wedge, a high frequency ( $f > 6$  MHz), and a high bandwidth ( $BW_{\text{rel}} > 85\%$ ).
6. Find out the optimal focal depth for the maximum refracted angle (minimum effective aperture); this determines the real aperture of the probe.
7. Find out the near-field length.
8. Check if  $F_{\text{max}} < N_0$ .
9. Find out the minimum and maximum focal depths; this determines the passive aperture size.
10. Check if  $A > W_{\text{passive}}$  and  $W_{\text{passive}} > 8p$ .
11. Find out the number of elements:  $n = A/p$ .
12. Specify the  $BW$  and  $\Delta\tau_{-20\text{ dB}}$  values, the cable length, the cross-talk value, or specific elements for the probe as a single entity.
13. Evaluate other factors from the KLM model: cable length influence, electrical impedance, and sensitivity.
14. Evaluate the gain losses from the contact surface (see Figure 3-53) and inner surface roughnesses (see Figure 3-54).
15. Evaluate the gain loss due to attenuation in the wedge and in the test piece (use the graphs from section 2.12, p. 66).
16. Evaluate the useful gain in reserve and the SNR for your reflector (worst-case scenario).
17. Draw the detectability curves for the start and finish angles.
18. If the SNR is less than 10 dB, you may consider one of the following options: increasing or decreasing the frequency, increasing the aperture size, and prefocusing the probe.
19. Perform steps 1 through 16 once more. If the SNR is greater than 10 dB, then find the beam dimensions.
20. Evaluate the axial and lateral resolutions.
21. Run a simulation to confirm the results.

**Note:** Optimization of probe design may be affected by geometric constraints and environmental conditions (radiation, underwater, pressure, temperature, moisture).

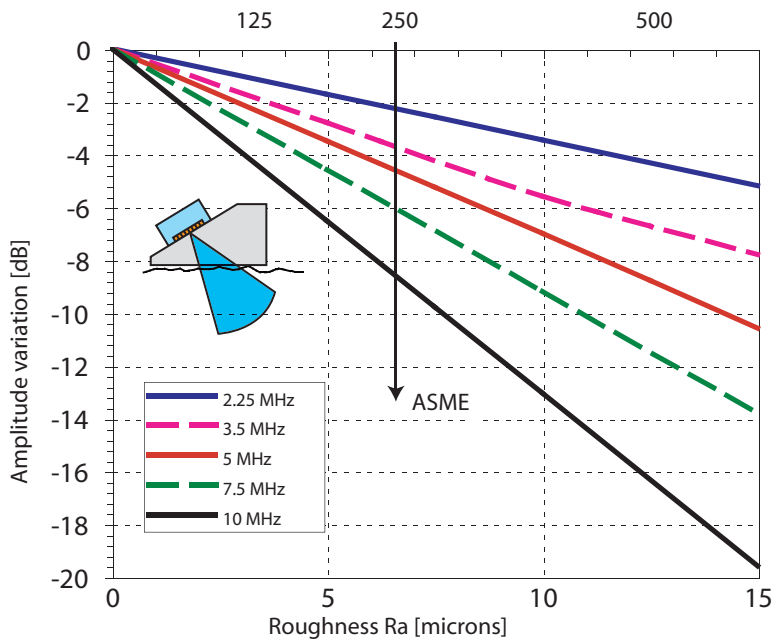


**Figure 3-53** Sensitivity drop due to contact surface roughness. Couplant: glycerine; reference reflector: SDH with a 2-mm diameter.

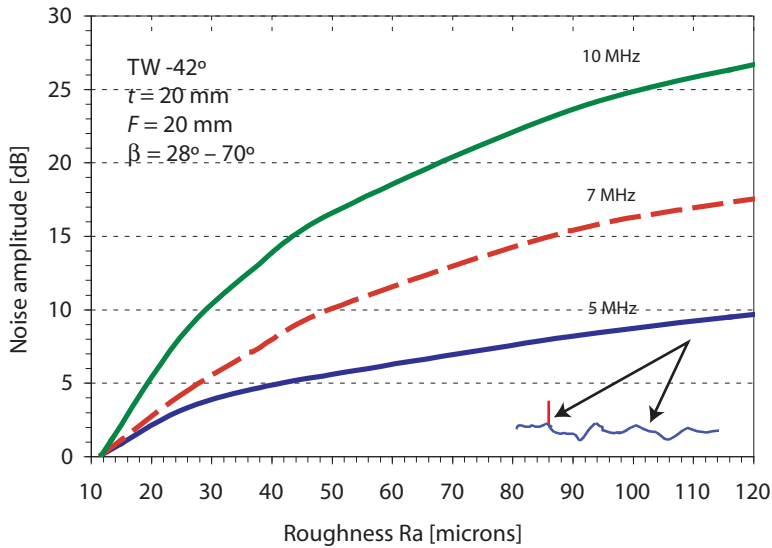


**Figure 3-54** Noise increase due to inner surface roughness. Couplant: glycerine. Reference reflector: EDM notch of 12 mm × 1.5 mm.

### 3.13.2 Practical Guidelines

Besides the above design based on physics, the phased array probe design should include the following functional features:

- Case dimensions
- Cable orientation (top, side, back, front)
- Engraving of the position of specific elements (first element, middle, last)
- Engraving of the probe ID, serial number (see Figure 3-60)
- Connector type and wiring matrix
- Wedge ID, height of the first element, wedge refracted (and roof) angle
- Working temperature range
- Acoustic impedance matching (material, velocity, density)
- Tolerances on main features (center frequency,  $BW$ ,  $\Delta\tau_{-20\text{ dB}}$ , impedance, sensitivity, cross talk) for all elements and for probe as a part
- Check frequency of individual elements
- Experimental setup and QA standards and procedures

Designing a phased array probe is more complicated than it may seem; expert advice is recommended for any unusual applications.

### 3.14 Ultrasonic Setup Details

Ultrasonic parameter adjustment and optimization of the acquisition sequence are performed at different stages:

- Setup mode
- Acquisition mode
- Analysis mode

Examples of adjustable ultrasonic parameters in TomoView 2.2 are presented in Table 3-5.

**Table 3-5** Generic ultrasonic settings for a phased array instrument.

<b>Pulser</b>	<ul style="list-style-type: none"> <li>• Voltage</li> <li>• Pulse width</li> <li>• Rectification</li> <li>• Band-pass filters</li> <li>• Smoothing</li> </ul>
<b>General</b>	<ul style="list-style-type: none"> <li>• Gain/channel</li> <li>• Gain/focal law</li> <li>• Booster gain</li> <li>• Ultrasonic start</li> <li>• Ultrasonic range</li> <li>• Gate start and range</li> <li>• Units (half-path, time, depth, full-path)</li> </ul>
<b>Digitizer</b>	<ul style="list-style-type: none"> <li>• Digitizing frequency</li> <li>• Averaging</li> <li>• Acquisition rate</li> <li>• PRF</li> <li>• Compression</li> </ul>

Some hints on optimizing the ultrasonic settings are given in the following sections.

### 3.14.1 Pulse Width

*Pulse width* refers to the time duration of the high-voltage square pulse used to excite the transducer element. The pulse width should be adjusted according to formula (3.15), where  $f_c$  = center frequency:

$$PW_{\text{pulser}} \times f_c = 500 \quad (3.15)$$

The software may have the optimization function activated; otherwise use the value from Figure 3-55.

Generally, determine the actual ultrasound center frequency in the test piece in close-to-real conditions. Use the FFT function or calibrate in time ( $\mu\text{s}$ ) and count the number of cycles in the zoomed TOF (time-of-flight) window:  $F_c = \text{TOF}/N$  (see chapter 2 for details).

### 3.14.2 Band-Pass Filters

As a general rule, the *band-pass filters* should be chosen according to the probe center frequency. This operation can be performed, for example, by the OmniScan unit. Actual choice of filters depends on beam spread, attenuation (that is, grain structure), and ultrasonic beam path. The best solution is to try different filters to optimize the image.

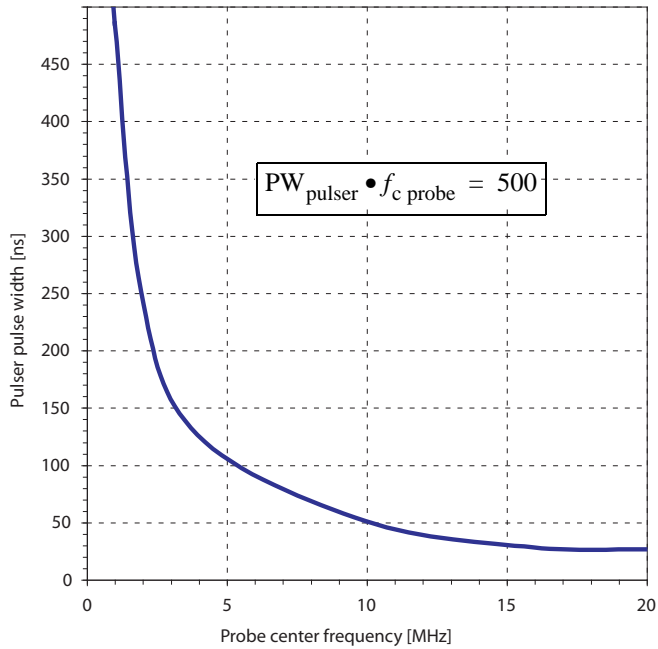


**Figure 3-55** Pulser pulse width dependence on probe center frequency.

### 3.14.3 Smoothing

*Smoothing* is an electronic feature to create an envelope over the rectified signal for reducing the amplitude error; it provides a better display for crack tip detection, reduces the digitizing frequency, and keeps the vertical linearity errors at low values, normally less than 2% to 5% (see Figure 3-56). Smoothing also improves the readability of the display.

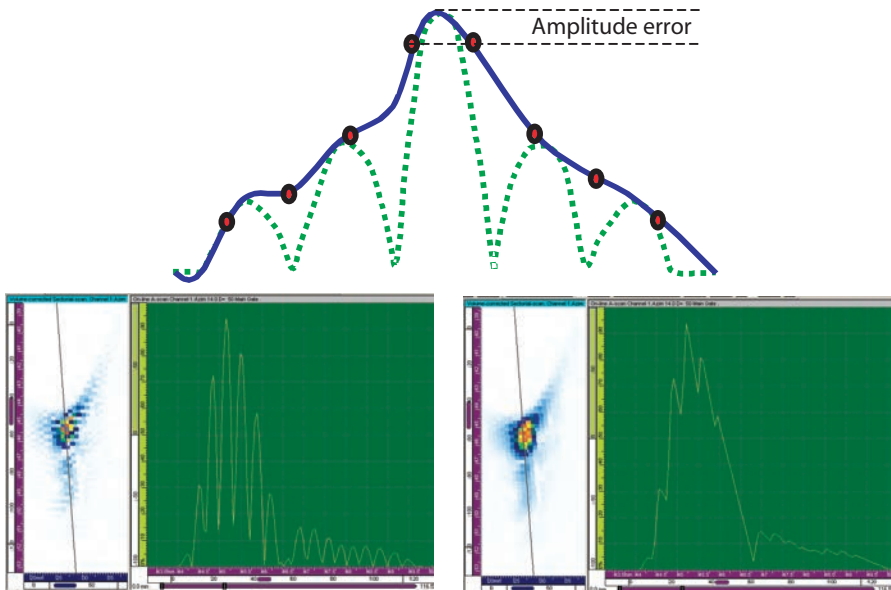
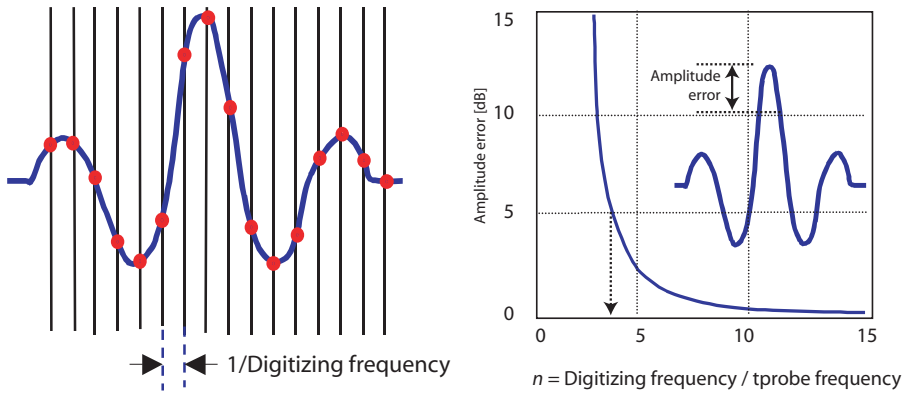


Figure 3-56 Smoothing over the envelope of rectified signal increases the view resolution.

### 3.14.4 Digitizing Frequency

The *digitizing frequency* is the number of A-scan samples in a specific TOF window (see Figure 3-57); it should be greater than three times the probe center frequency; to reduce amplitude errors to less than 1%, the digitizer frequency should be greater than, or equal to, 10 times the probe center frequency.



**Figure 3-57** Digitizing frequency: principle (*left*) and the effect of digitizing frequency ratio on amplitude error (*right*).

### 3.14.5 Averaging

The *averaging* is the number of samples (A-scans) summed for each acquisition step on each A-scan displayed; averaging increases the SNR by reducing random noise:

$$\text{SNR}_{\text{after averaging}} = n^{0.5} \text{SNR}_{\text{before averaging}}$$

The averaging function reduces the acquisition speed.

### 3.14.6 Compression

The *compression* is the reduction in the number of sampled data points based on position and maximum amplitude (see Figure 3-58). Compression reduces the file size without compromising on defect detection.

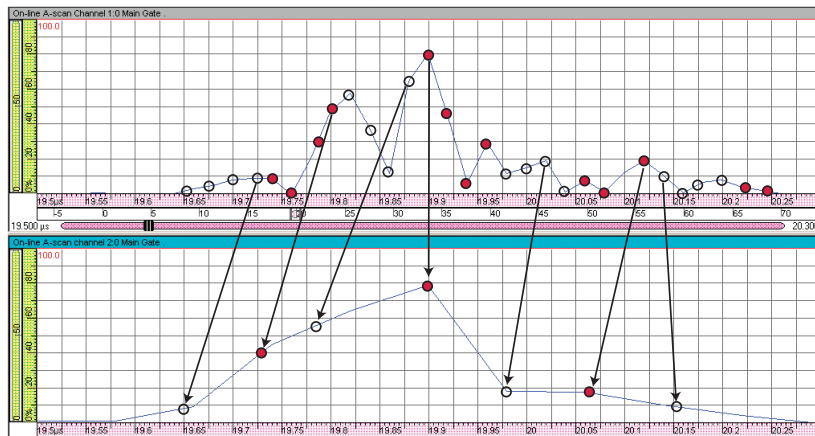


Figure 3-58 Compression by a factor of 4:1 of an A-scan.

### 3.14.7 Repetition Rate (PRF, or Pulse Repetition Frequency)

The *repetition rate* (PRF, or *pulse repetition frequency*) is the firing frequency of the ultrasonic signal; PRF depends on averaging, acquisition time, delay before acquisition, gate length, processing time, and the update rate of the parameters. In general, set the PRF as high as possible, ensuring that any ghost echoes are out of the acquisition range.

### 3.14.8 Acquisition Rate

The *acquisition rate* is the number of complete acquisition sequences (A-scans) per second.

The maximum acquisition rate depends on:

- Ultrasound range
- Digitizing frequency
- Data compression, if used
- Pulse repetition rate (PRF)
- Averaging, if used
- Ultrasonic wrap-around

A higher PRF and acquisition rate will lead to a shorter inspection time.

**Note:** The acquisition rate must be lower than the transfer rate / total number of samples.

### 3.14.9 12-Bit Data Versus 8-Bit Data

Digitalization is part of the signal processing chain and influences the raw data file size and the SNR. Twelve-bit data provides better resolution and SNR than 8-bit data. However, the file size is increased.

### 3.14.10 Setup File

The setup file must include the inspection sequence and the focal laws (multichannel). Generic parameters are presented in Table 3-6 and Table 3-7.

**Table 3-6** Inspection sequence features (example).

<b>Sequence</b>	<ul style="list-style-type: none"> <li>• Type</li> <li>• Start</li> <li>• End</li> <li>• Resolution*</li> <li>• Fire on (encoder, internal clock, external signal)</li> <li>• Scanning speed*</li> <li>• Units</li> <li>• Preset value</li> </ul>
<b>Encoders</b>	<ul style="list-style-type: none"> <li>• Name</li> <li>• Type</li> <li>• Resolution</li> <li>• Invert [option]</li> <li>• Calibration</li> </ul>

**Note:**  $\frac{\text{Inspection speed [mm/s]}}{\text{Scan axis resolution [mm]}} < \text{Acquisition rate [A-scans/s]}$

**Table 3-7** Focal laws and probe parameters (example).

<b>Focal laws (channels)</b>	<ul style="list-style-type: none"> <li>• Steering type (sectorial, electronic, static, depth)</li> <li>• Active element groups (active aperture)</li> <li>• Focal depth</li> <li>• Start angle</li> <li>• Finish angle</li> <li>• Angle resolution</li> <li>• DDF feature activation</li> <li>• Probe type</li> <li>• Skew angle</li> <li>• Number of elements (active)</li> <li>• Pitch</li> <li>• Specimen</li> <li>• Wave type</li> <li>• Sound velocity in test piece</li> <li>• Wedge angle</li> <li>• Roof angle</li> <li>• Sound velocity in wedge</li> <li>• Height of the first element</li> <li>• Active axis offset</li> <li>• Passive axis offset</li> <li>• Number of channels</li> </ul>
<b>Probe</b>	<ul style="list-style-type: none"> <li>• Wave type</li> <li>• Sound velocity</li> <li>• Probe delay (show total, modify probe, modify law)</li> <li>• Offset (active/passive axis)</li> <li>• Beam orientation (refracted and skew angle)</li> </ul>

### 3.14.11 Data File Size

The *raw data file size* is given by the formula:

$$\text{File size} = \sum_{n \text{ channels}} \left( K_S \times D_{SS} \times \text{FL} \times \frac{\text{Scan length}}{\text{Scan resolution}} \times \frac{\text{Index length}}{\text{Index resolution}} \right)$$

where:

$K_S$  = number of samples (A-scan length)

$D_{SS}$  = data sample size (1 for 8-bit, and 2 for 12-bit)

FL = number of focal laws/channel

You can achieve inspection optimization in many ways, such as using a multihead scanner that uses a splitter cable or custom-made breakout boxes (see Figure 3-59).



*Courtesy of Ontario Power Generation Inc., Canada*

**Figure 3-59** 4:1 breakout box used with multihead inspection.

### 3.15 Probe Identification

The minimum features for probe identification (ID) [see Figure 3-60] are:

- Frequency
- Probe type (linear, annular, matrix, rho-theta)
- Number of elements
- Active aperture size
- Passive aperture size
- Pitch size
- Serial number

Other features to be labeled optional:

- First element height
- Wedge angle
- Wedge velocity (material)
- Roof angle (if any)

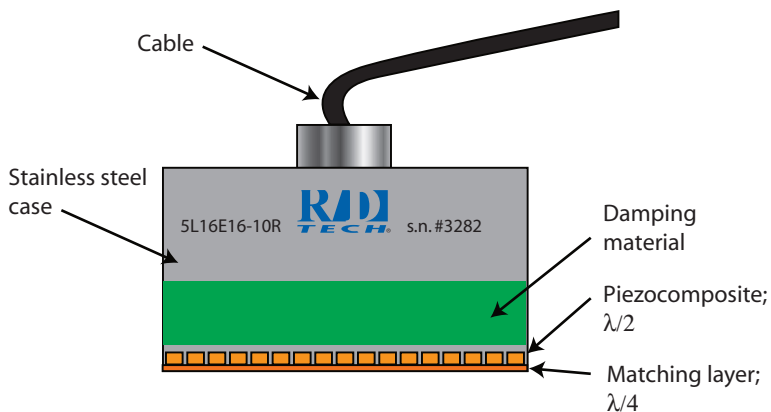


**Figure 3-60** Example of phased array probe identification.

Different types of phased array probes are presented in Figure 3-61.



**Figure 3-61** Different types of phased array probes provided by Olympus.

### 3.16 Probe Characterization and Periodic Checking

In order to assure the repeatability of phased array technology and to allow equipment substitution (probe replacement with a spare), a linear phased array probe must be checked and certified for its main features.

#### 3.16.1 Probe Characterization

*Probe characterization* is a QA evaluation of specific features in a phased array

probe in order to establish the probe's actual value(s) for the inspection sequence/procedure qualification.

Features to be checked:

- Refracted angle/directivity ( $^{\circ}$ )
- Index (mm)
- Wedge/probe delay (s)
- SNR (dB)
- Focal depth (mm)
- Focal length (depth-of-field) [mm]
- Beam divergence (dimensions) [ $^{\circ}$ ]
- Dead zone (mm)
- Far-field resolution (mm)
- Lateral resolution (mm)
- Axial resolution (mm)
- Center frequency (MHz)
- Pulse duration ( $\mu\text{s}$ )
- Bandwidth (%)
- Side lobes location / amplitude ( $^{\circ}$ /dB)
- Grating lobes location / amplitude ( $^{\circ}$ /dB)
- Actual velocity in test piece (mm/ $\mu\text{s}$ , m/s)
- Cross-talk amplitude between elements (dB)
- Number of dead elements
- Electric wiring (linear scanning) [connectivity between pulser number and element number]
- Probe mechanical aspects (cable housing, probe wear, acoustic block misalignment, face damage)
- Electric connection, pin matrix status
- Element reproducibility (sensitivity variation)
- Electric impedance ( $\Omega$ )

The evaluation method and the tolerance/acceptance values may vary based on the specific application.

Additional information regarding probe characterization can be found in references 25, 39–41, 44, 45, 47–49, 51, 53, 54, and 57.

### 3.16.2 Tolerances

Table 3-8 lists the tolerances that are generally acceptable by most standards and practitioners.

**Table 3-8** Practical tolerances on phased array probe features.

Feature	Tolerance	Remarks
Center frequency	$\pm 10\%$	Different evaluation methods
Bandwidth	$\pm 20\%$	Depends on setup
Pulse duration	$\pm 20\%$	Depends on setup
Refracted angle	$\pm 2\%$	
Focal depth	$\pm 30\%$	Depends on measurement method
Impedance	$\pm 30\%$	Depends on setup
Element sensitivity	$\pm 2$ dB	Edge elements may have larger value
Cross-talk amplitude	$< -40$ dB $\pm 10$ dB	Depends on element position and refracted angle

The variation of sensitivity based on these tolerances is approximately  $\pm 5$  dB.

Remember that phased array inspection technology is based on imaging, identifying patterns, tip-echo diffraction techniques, redundancy in refracted angles and/or combinations between shear waves and longitudinal waves, or a combination between pulse-echo techniques and TOFD. Once the phased array probe and system are calibrated for a specific task (reflector type, ultrasonic path range, amplitude threshold, SNR level, reporting level, sizing method), the reproducibility of results must be evaluated versus the defect parameters, not against the reference gain from probe to probe or from inspection to inspection. Random and systematic factors may influence the reference gain value by more than  $\pm 6$  dB.

Tighter tolerances on probe main features may drive the probe price too high without a significant improvement in defect detection and sizing capability.

### 3.16.3 Curved Wedges

This section details some aspects of probe checking in combination with curved wedges for axial and circumferential detection.

Directivity and exit point (wedge index) may be measured on semi-cylinders (see Figure 3-62). The SNR, angle, velocity, and index may also be measured on similar curved blocks with SDH.

The total delay used for calibration comes from:

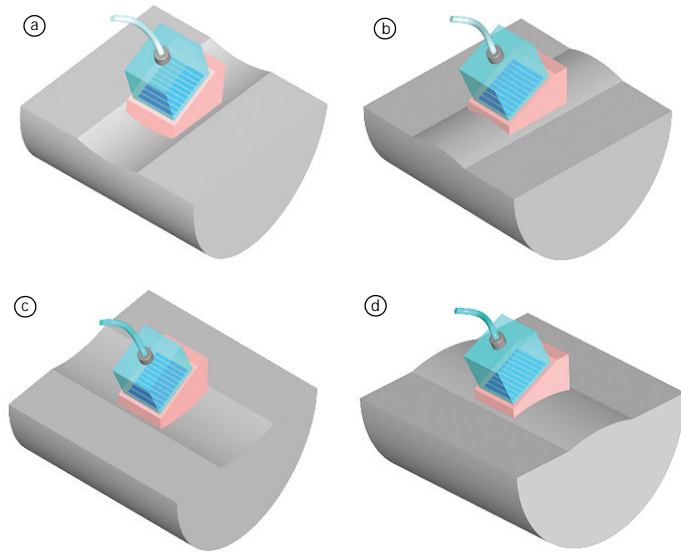
- Electronic delay (generally 1.6  $\mu\text{s}$  to 2.0  $\mu\text{s}$ )
- Law delay—specific to each angle
- Wedge delay (evaluated on SDH)
- Acquisition delay (TOF—time of flight—in the test piece; for pulse-echo, TOF is doubled)

Table 3-9 presents the distance equivalent for various TOF values in different materials.

**Table 3-9** Equivalent half-path distance for TOF (probe/wedge delay).

Material	TOF delay ( $\mu\text{s}$ )						
	0.2	0.3	0.4	0.5	1.0	2.0	3.0
	Ultrasound half path (mm)						
Water	0.15	0.2	0.3	0.4	0.74	1.5	2.2
Plexiglas	0.3	0.4	0.6	0.7	1.36	2.7	4
Rexolite	0.23	0.4	0.5	0.6	1.15	2.3	3.5
Steel—LW	0.6	0.9	1.2	1.5	3.0	6.0	9.0
Steel—TW	0.3	0.5	0.6	0.8	1.6	3.2	4.8
Zircaloy—TW	0.23	0.4	0.5	0.6	1.2	2.4	3.6
Inconel—LW	0.6	0.9	1.2	1.5	2.9	5.8	8.7
Inconel—TW	0.3	0.5	0.6	0.8	1.5	3.0	4.5
Aluminum—LW	0.6	0.9	1.2	1.6	3.1	6.2	9.3
Aluminum—TW	0.3	0.5	0.6	0.8	1.6	3.2	4.8

These values are useful for a correct calibration. Calibration of the phased array system is enabled through the software. Gain compensation with the refracted angle is also included in sensitivity adjustment. See chapters 4 and 5 for specific prerequisite operations before starting an inspection.



**Figure 3-62** Directivity (refracted angle) and index point measurement with a curved wedge adapted to the specimen: (a) concave-transverse; (b) convex-transverse (c) concave-longitudinal; (d) convex-longitudinal.

### 3.17 Olympus Probes for the OmniScan

Olympus manufactures in-house 1-D linear array probes for the OmniScan according to the technical specifications listed in the *Ultrasound Phased Array Transducer Catalog* (available from Olympus).

These probes have a proprietary connector (see Figure 3-63).



**Figure 3-63** Olympus connector for the OmniScan.

The advantages of the Olympus connector are:

- Transducer recognition (the main transducer characteristics are sent to the OmniScan phased array instrument for faster and error-free setups).
- No bending or breaking of pins
- Splashproof casing
- Improved shielding
- Compact design
- Improved signal-to-noise ratio

The probes and associated wedges (see Figure 3-64) can be identified by the OmniScan software.

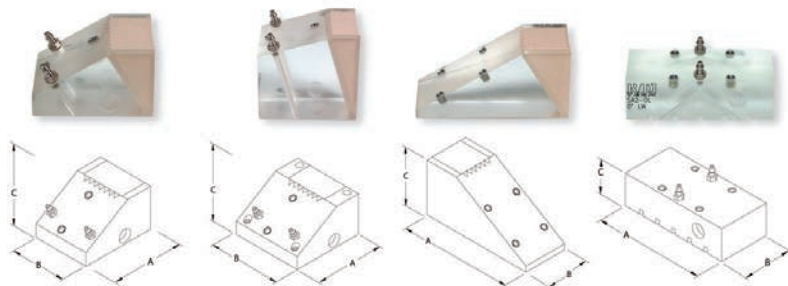


**Figure 3-64** Wedges associated with angle-beam probes.

### *Advantages*

- Availability in standard refracted angles of 0°, 45°, and 60° in steel for angle-beam inspection from 30° to 70°, SW or LW
- New damping material for elimination of parasite echoes
- Stainless steel screw receptacles for a firm anchoring of the wedge to the transducer
- Wedge options available for the improvement of the quality of the inspection, such as mounting holes for the wedge holder to work with any Olympus scanner and carbide pins.
- Wedge design for manual or automated scans
- Wedges can be customized to create different refracted angles with all kind of shapes.
- Irrigation kit available

Some types of probes are presented in Figure 3-65:

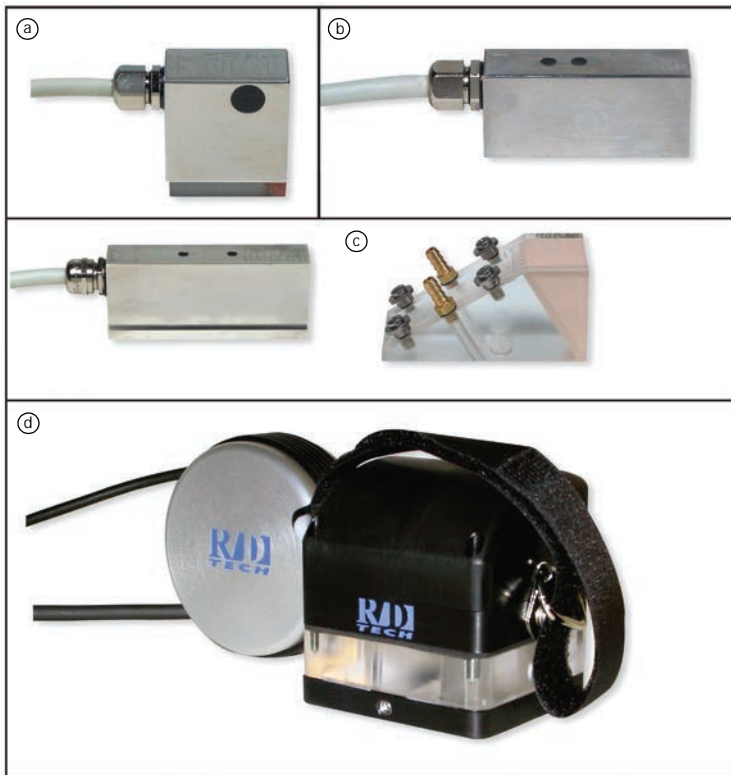


**Figure 3-65** Different Olympus 1-D linear-array probes: (a) encapsulated wedge angle beam; (b) hard-face direct contact longitudinal waves; (c) immersion (longitudinal waves) and wedge (angle beam); (d) water wedge probe with encoder.

## References to Chapter 3

1. Gururaja, T. T. "Piezoelectric composite materials for ultrasonic transducer applications." Ph.D. thesis, The Pennsylvania State University, University Park, PA, May 1984.
2. Hayward, G., and J. Hossack. "Computer models for analysis and design of 1-3 composite transducers." *Ultrasonic International 89 Conference Proceedings*, pp. 532–535, 1989.
3. Smiths, W. A. "The role of piezocomposites in ultrasonic transducers." *1989 IEEE Ultrasonics Symposium Proceedings*, pp. 755–766, 1989.
4. Hashimoto, K. Y., and M. Yamaguchi. "Elastic, piezoelectric and dielectric properties of composite materials." *1986 IEEE Ultrasonic Symposium Proceedings*, pp. 697–702, 1986.
5. Oakley, C. G. "Analysis and development of piezoelectric composites for medical ultrasound transducer applications." Ph.D. thesis, The Pennsylvania State University, University Park, PA, May 1991.
6. Krimholtz, R., D. Leedom, and G. Matthaei. "New equivalent circuits for elementary piezoelectric transducers." *Electronics Letters*, vol. 6 (June 1970): pp. 398–399.
7. ANSI/IEEE Std. 176-1978: IEEE Standard on Piezoelectricity.
8. Dubé, N., A. Lamarre, and F. Mainguy. "Dynamic Depth Focusing Board for Nondestructive Testing: Characterization and Applications."

# Chapter Contents

4.1	Scanning Patterns .....	163
4.2	Ultrasonic Views (Scans) .....	172
	References to Chapter 4.....	190

---

## 4. Scanning Patterns and Views

---

This chapter describes automated ultrasonic inspection (or scan) patterns and typical views currently used by Olympus systems.

### 4.1 Scanning Patterns

Reliable defect detection and sizing is based on scan patterns and specific functional combinations between the scanner and the phased array beam.

The inspection may be:

- *automated*: the probe carrier is moved by a motor-controlled drive unit;
- *semiautomated*: the probe carrier is moved by hand, but the movement is encoded; or
- *manual (or free running)*: the phased array probe is moved by hand and data are saved based on acquisition time(s).

The acquisition may be triggered by the encoder position, the internal clock, or an external signal.

Olympus systems can provide the following inspection types:

- Tomoscan III, Tomoscan FOCUS: automated, semiautomated, manual
- OmniScan PA: automated, semiautomated, manual
- QuickScan PA, PipeWIZARD: automated (semiautomated for calibration/mechanical settings)

The probe carrier may be moved in any of the inspection sequences presented in Table 4-1.

**Table 4-1** Scanning patterns for automated and semiautomated inspections.

Scanning pattern	Number of axes	Remarks
Bidirectional	2	Acquisition is performed in both scanning directions (see Figure 4-1).
Unidirectional	2	Acquisition is performed only in one scanning direction; scanner is moved back and forth on each scanning length (see Figure 4-1).
Linear	1	All data is recorded in a single axial pass (see Figure 4-2).
Skewed	2	Similar to bidirectional, unidirectional, or linear with the main axes skewed against the mechanical axes (see Figure 4-3).
Helical	1	Acquisition is performed along a helicoidal path along and around the cylinder (see Figure 4-4).
Spiral	1	Acquisition is performed along a spiral path on a circular surface (see Figure 4-5).
Custom	1–6	Customized for multiaxis or component profile.

### 4.1.1 Bidirectional Scan

In a *bidirectional sequence*, data acquisition is carried out in both the forward and backward directions along the scan axis (see Figure 4-1).

### 4.1.2 Unidirectional Scan

In a *unidirectional sequence*, data acquisition is carried out in one direction only along the scan axis (see Figure 4-1). The scanner is then stepped for another pass.

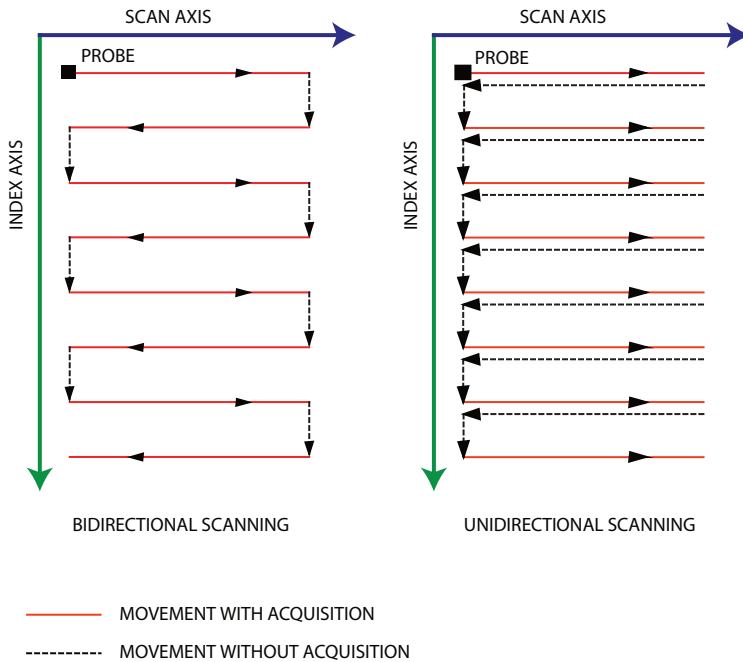


**Figure 4-1** Bidirectional (*left*) and unidirectional (*right*) raster scanning. The red line represents the acquisition path.

### 4.1.3 Linear Scan

A *linear scan* is a one-axis scanning sequence using only one position encoder (either scan or index) to determine the position of the acquisition.

The linear scan is unidimensional and proceeds along a linear path. The only settings that must be provided are the speed, the limits along the scan axis, and the spacing between acquisitions (which may depend on the encoder resolution). Linear scans are frequently used for such applications as weld inspections and corrosion mapping. Linear scans with electronic scanning are typically an order of magnitude faster than equivalent conventional ultrasonic raster scans.

Linear scans are very useful for probe characterization over a reference block with side-drilled holes (see Figure 4-2).

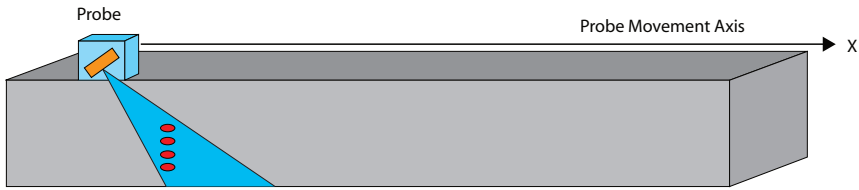


**Figure 4-2** Linear scan pattern for probe characterization.

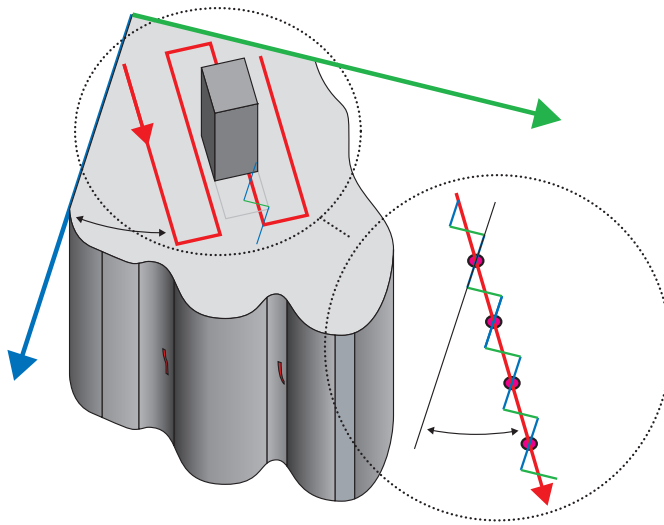
#### 4.1.4 Skewed Scan

The *skewed scan sequence* (also called *angular scan* under the TomoView 2.2 software) is a form of the normal bidirectional scan sequence. This sequence allows the scan and index probe path to be skewed by a software-selectable angle generated by small increments (closer to encoder resolution) on scan and index axis. This angle is different from the mechanical axes. The detail of Figure 4-3 shows the actual probe movement with average line trajectory to approximate this angled scan path.

This sequence is useful when the scanners axes and the inspected part cannot be placed in the best scan path relative to each other, and/or the defect location and orientation requires a specific scan pattern (line) for optimum detection and sizing. Selecting a specific scan path angle that best suits the inspected part or defect orientation can thus eliminate expensive scanner modifications, drastically reducing the file size and speeding up the defect analysis time.

The skewed scan sequence has the following features:

1. The skewed scan is used to inspect complex geometry components with defect orientation at an angle versus orthogonal axis.
2. The skewed scan allows you to adopt the linear array probe to a particular *specimen geometry*.
3. File size is reduced by a factor of 2–3.
4. Defect amplitude increases by 6–8 dB.
5. You may increase the scanning speed by a factor of 2–4.



Courtesy of Ontario Power Generation Inc., Canada

**Figure 4-3** Example of skewed (angular) bidirectional scanning. *Left:* probe scanning pattern versus the mechanical axes on a complex part; *right:* probe trajectory (red line) is skewed versus mechanical rectangular axes for an optimum angle to detect cracks in stress area.

### 4.1.5 Helical Scan

The *helical sequence* is used to inspect *cylindrical surfaces*. The scanner performs a helicoidal movement around the cylinder.

Two independent encoders control the sequence. The *scan-axis* encoder controls the continuous rotation around the cylinder, while the *index-axis* encoder controls the continuous movement along the length of the cylinder. A synchronization signal can be used to reset the scan-axis encoder to position zero after every rotation around the cylinder.

The combinations of these two movements will create a helicoidal scan pattern (see Figure 4-4).

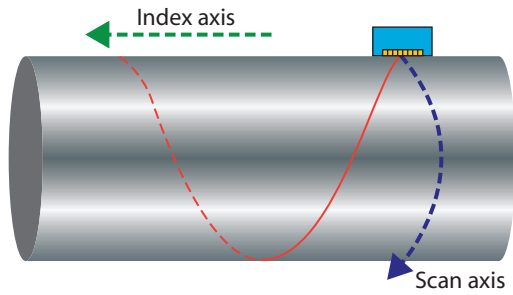


**Figure 4-4** Helical surface scan on cylindrical parts. The red line is the acquisition path.

### 4.1.6 Spiral Scan

The *spiral sequence* is designed to inspect *circular surfaces* such as disc surfaces. The inspection mechanism performs a spiral movement on the circular surface (see Figure 4-5). Two independent encoders control the sequence. The *scan-axis* encoder controls the theta angle ( $\theta$ ) in the continuous rotation around the surface center; while the *index-axis* encoder controls the rho position ( $\rho$ ) in the continuous movement along the radius. A signal can be used to reset the scan-axis encoder to position zero after every rotation.

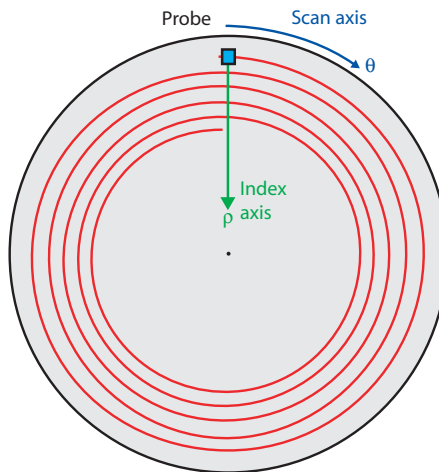


**Figure 4-5** Spiral surface scan pattern. The red line is the acquisition path.

## 4.1.7 Beam Directions

The beam direction of the phased array probe may have the directions showing in Figure 4-6 compared with the scan and index axes. These directions are defined by the *probe skew angle*.

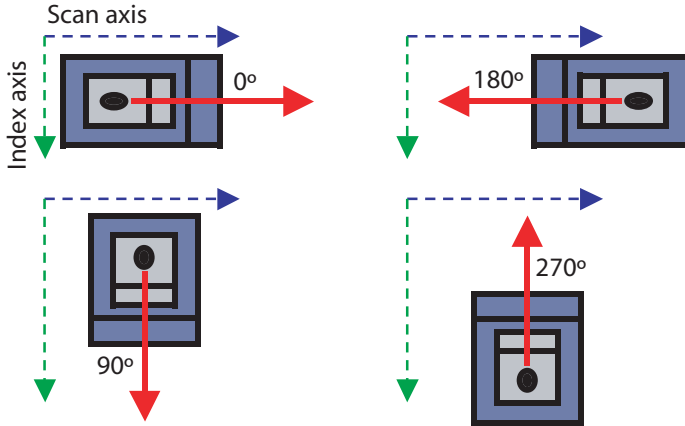


**Figure 4-6** Probe position and beam direction related to scan and index axis. Skew angle must be input in the focal law calculator.

The limits of the inspection surface, as well as the spacing between acquisitions (resolution on each axis), will determine the scanning surface and pixel size of the ultrasonic data.

An example of setting up a scanning sequence using TomoView 2.2R9 is presented in Figure 4-7.

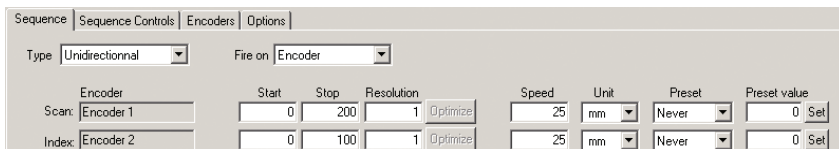


**Figure 4-7** Unidirectional sequence of a 200-mm by 200-mm area. Pixel size of the C-scan is of 1 mm by 1 mm. Scanning speed on both axes is 25 mm/s.

### 4.1.8 Other Scanning Patterns

The part, the probe movement, and the beam direction may generate scanning patterns for any of the following combinations (see Table 4-2 and Figure 4-8 to Figure 4-10).

**Table 4-2** Inspection sequence dependence on part, scanner, and beam.

Part	Scanner	Beam	Sequence
Fixed	Fixed	Linear (translation)	Linear scan
Fixed	Index axis	Linear (rotation)	Helicoidal
Translation	Fixed	Linear (rotation)	Helicoidal
Fixed	Scan axis	Linear (90° skew)	Unidimensional

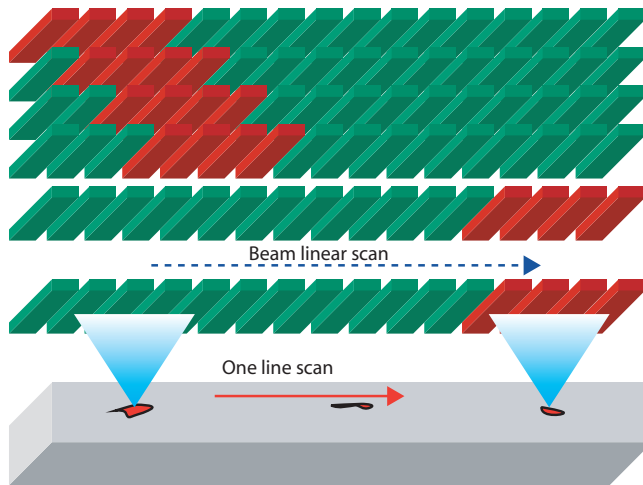


**Figure 4-8** Beam electronic scan generating a linear scan pattern. Part and probe are not moving.

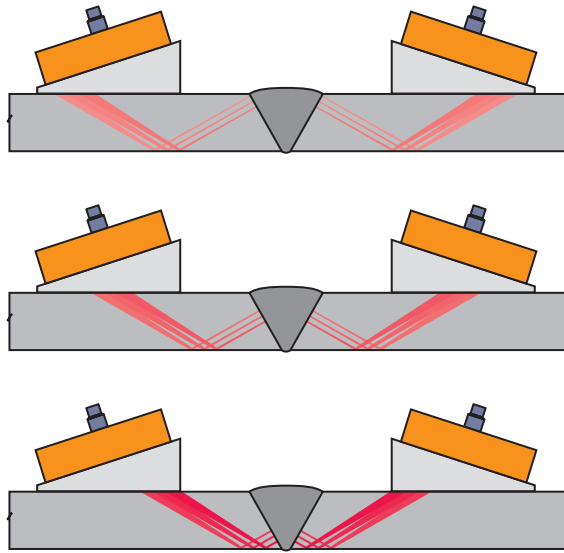


**Figure 4-9** Electronic and linear scan of a weld (principle). Index axis (raster scan in conventional UT) is eliminated through electronic scan from the probe arrays, which increases speed and reliability. Note that wedges are usually used.

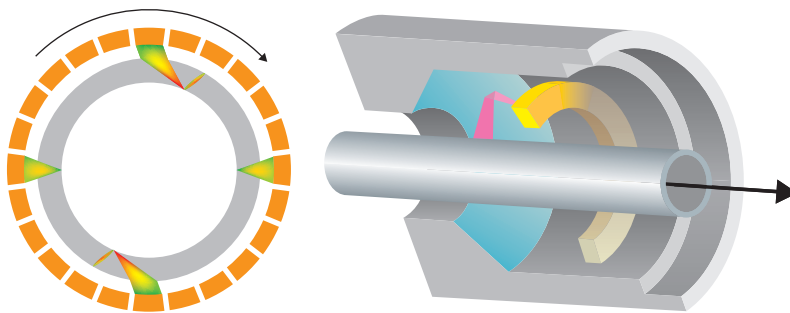


**Figure 4-10** Generation of a helical scan by a combination of part translation and beam rotation.

#### 4.1.9 Time-Base Scanning

If the encoder is set on time (clock), then the acquisition is based on scanning time (seconds) [see Figure 4-11].

The acquisition time for a time-base sequence is calculated by the total number of acquisitions, divided by the acquisition rate:

$$T_{\text{time-base}} = \frac{N_{\text{acquisitions}}}{N_{\text{A-scans/s}}} \quad (4.1)$$

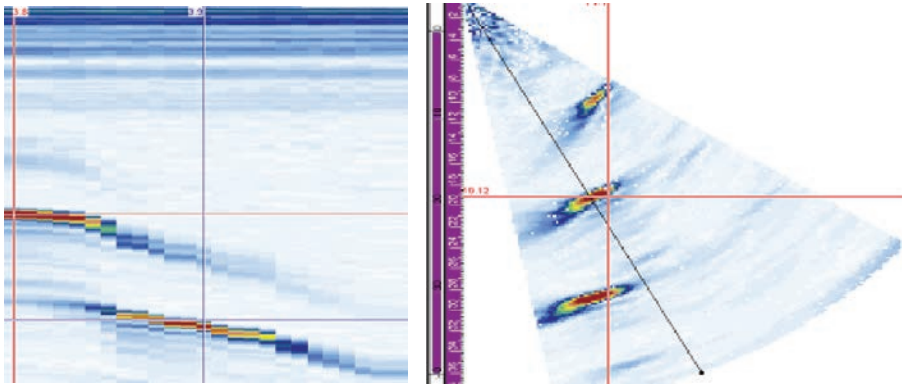


**Figure 4-11** Time-base sequence examples: B-scan (*left*) and S-scan (*right*).

## 4.2 Ultrasonic Views (Scans)

*Ultrasonic views* are images defined by different plane views between the ultrasonic path (U-sound) and scanning parameters (scan or index axis). The most important views, similar to 2-D projections of a technical drawing, are presented in Figure 4-12. These projection views are a plan or cumulated plans coming from C-scan, B-scan, and D-scan; the projection views are also called *top*, *side*, and *end* views.

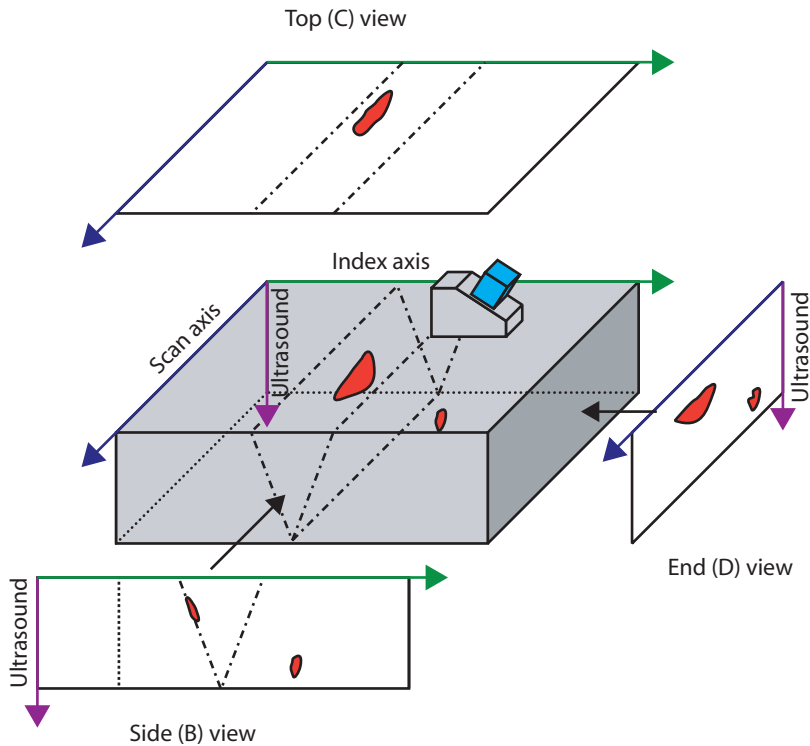


**Figure 4-12** Ultrasonic views (B-scan, C-scan, and D-scan). Probe skew angle is  $270^\circ$ . Red indicates the ultrasound axis; blue, the mechanical index axis; and green, the electronic scan axis for a linear scan.

If the probe skew angle is  $0^\circ$  (or  $180^\circ$ ), the side view (B-scan) will become the end view (D-scan), and vice versa. The B-scan is defined by the depth and probe movement axes. The D-scan is defined by the depth and the electronic scan axis.

The basic ultrasonic views (scans) are:

- A-scan
- B-scan
- C-scan
- D-scan
- S-scan
- Polar view
- Strip chart (amplitude and/or position)

- TOFD view (special gray-scale application of a B-scan)

There are also combined views, such as “top, side, end” or “top, side, TOFD” views.

## 4.2.1 A-Scan

An *A-scan* is a representation (view) of the received ultrasonic pulse amplitude versus time of flight (ultrasonic path), or a waveform. An A-scan can be displayed as an RF (radio-frequency) or bipolar-rectified signal (see Figure 4-13).

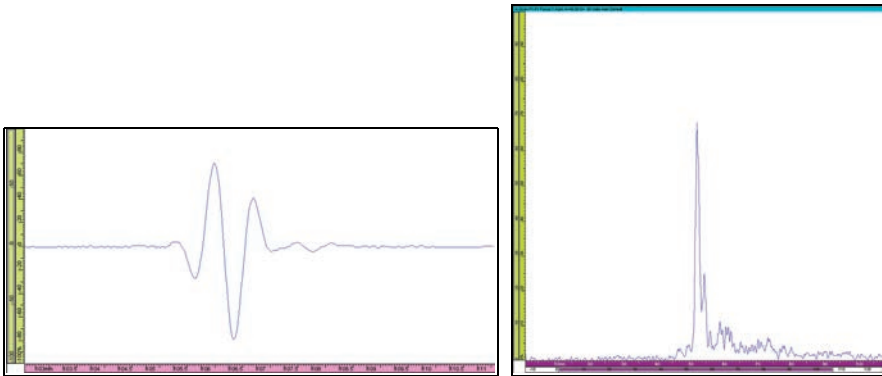


**Figure 4-13** A-scan representation: RF signal (*left*); rectified (*right*).

*Color encoding* of the rectified A-scan signal amplitude (see Figure 4-14) adds another dimension and makes it possible to link the probe movement coordinates (or the acquisition time) with the ultrasonic data as color-encoded amplitude (see Figure 4-14).

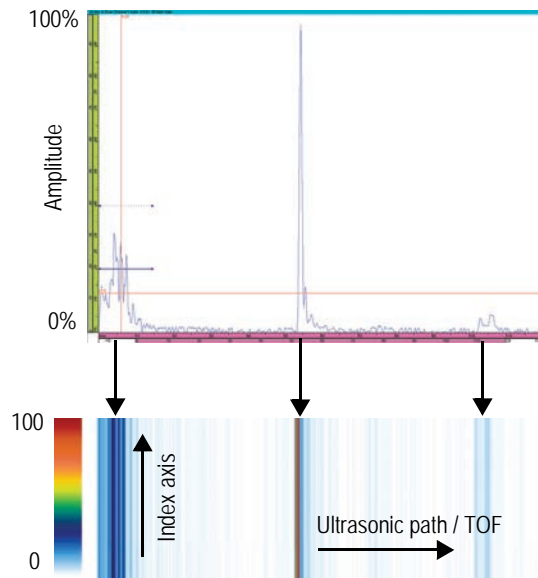


**Figure 4-14** Example of a color-encoded rectified A-scan signal used to create a color-coded B-scan.

Ultrasonic data with an RF display is usually encoded as gray-scale pixels, with black and white limits from  $-100\%$  to  $100\%$  (see Figure 4-15) to preserve the phase information. Gray-scale amplitude encoding is used in TOFD setups and data analysis, as shown in Figure 4-15.

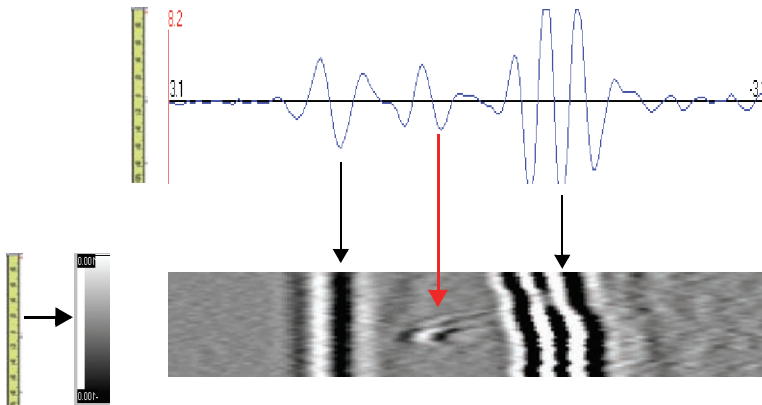


**Figure 4-15** Encoding of RF signal amplitude in gray-scale levels.

The most important 2-D views are presented below.

## 4.2.2 B-Scan

The *B-scan* is a 2-D view of recorded ultrasound data. Usually, the horizontal axis is the scan position and the vertical axis is the ultrasound (USound) path or time (see Figure 4-16); the axes can be reversed, depending on the required display. The position of the displayed data is related to the encoder positions at the moment of the acquisition. Essentially, a B-scan is a series of stacked A-scans or waveforms. Each A-scan is represented by an encoder/time-base sampling position. The A-scan is amplitude color-coded (palette).

Stacked A-scans, or a B-scan, is effectively the echo-dynamic envelope in the axis of mechanical or electronic beam movement. As such, this display elongates the defect image, and distorts the defect size due to beam spread and other factors. Some experience is required with cursor sizing to understand and compensate for this.

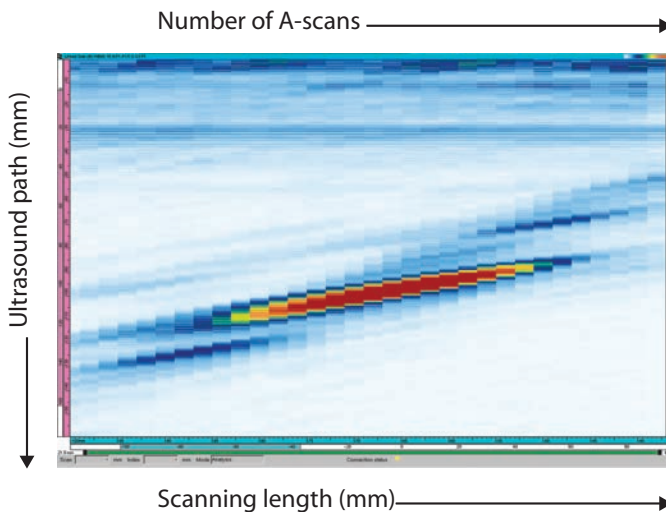


**Figure 4-16** Uncorrected B-scan (side view) of component, showing reflector.

If the ultrasonic path is corrected for the refracted angle and delay, the B-scan will represent the volume-corrected side view of the inspected part, with scan length on the horizontal axis and depth on the vertical axis (see Figure 4-17).

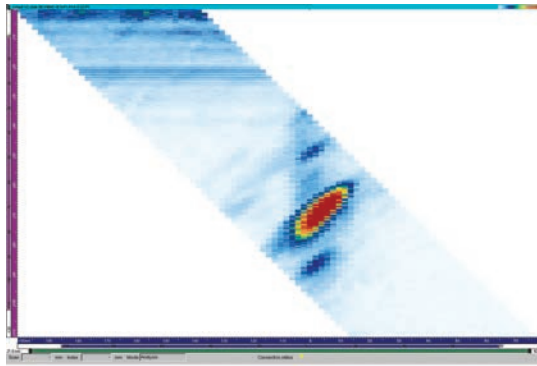


**Figure 4-17** Side (B-scan) view corrected for refracted angle.

### 4.2.3 C-Scan

A *C-scan* is a 2-D view of ultrasonic data displayed as a top or plan view of the test specimen. One of the axes is the scan axis; the other is the index axis. With conventional ultrasonic systems, both axes are mechanical; with linear phased arrays, one axis is mechanical, the other is electronic. The position of the displayed data is related to the encoder positions during acquisition. Only the maximum amplitude for each point (pixel) is projected on this “scan-index” plan view, technically known as a C-scan (see Figure 4-18).

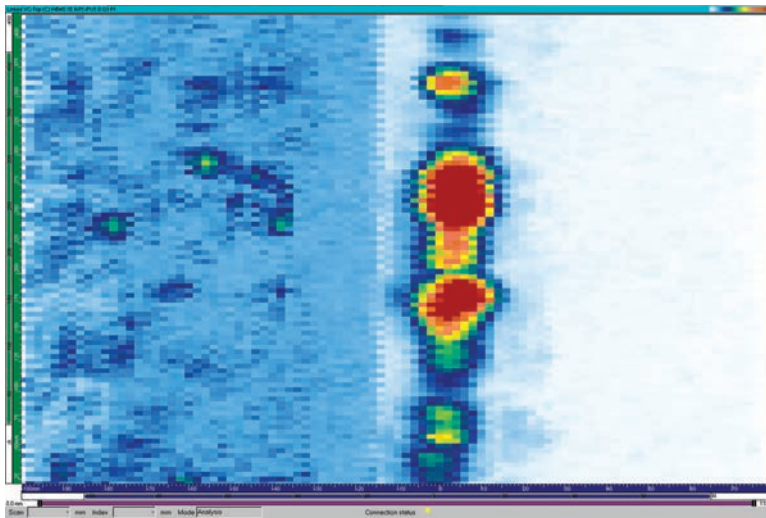


**Figure 4-18** Example of top (C-scan) view.

## 4.2.4 D-Scan

A *D-scan* is a two-dimensional graphical presentation of the data. It is similar to the B-scan, but the view is at the right-angle of the B-scan. If the B-scan is a side view, then the D-scan is an end view. Both D-scans and B-scans are gated to only show data over a predefined depth. One of the axes is defined as the index axis; the other is the ultrasonic path (USound) [see Figure 4-19]. The B-scan displays scan axis versus time, whereas the D-scan displays index axis versus time.

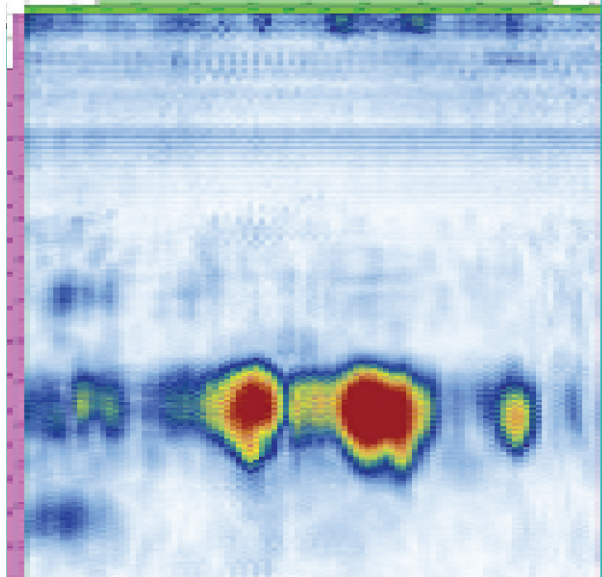


**Figure 4-19** Example of end (D) view.

If the ultrasonic path is corrected for angle and delay, the vertical axis represents the depth. The end (D-scan) view is very useful for data analysis using the 2-D overlay (specimen) drawing, particularly for welds.

## 4.2.5 S-Scan

An *S-scan* (sectorial or azimuthal scan) represents a 2-D view of all A-scans from a specific channel corrected for *delay* and *refracted angle*. A typical S-scan sweeps through a range of angles using the same focal distance and elements. The horizontal axis corresponds to the projected distance (test piece width) from the exit point for a corrected image and the vertical axis corresponds to the depth (see Figure 4-20).

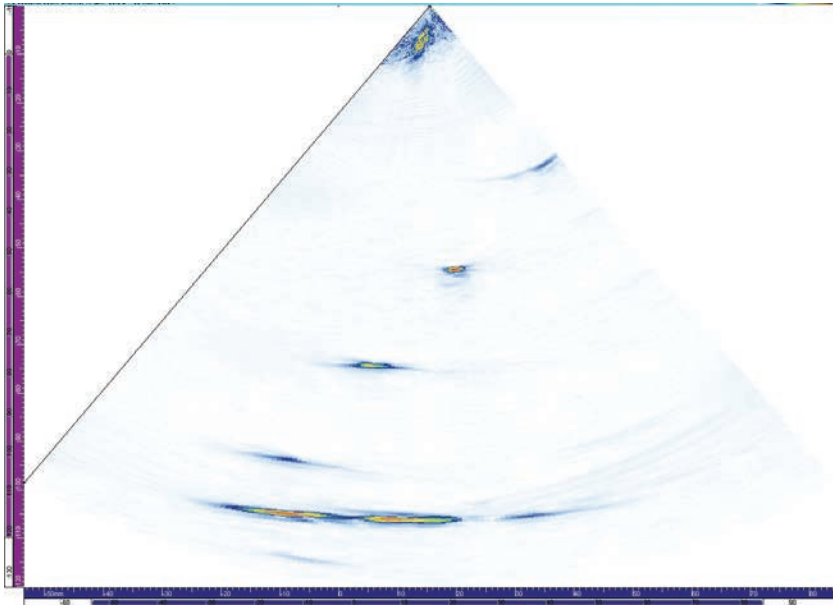


**Figure 4-20** Example of S-scan.

S-scans are unique to phased arrays, and can be longitudinal wave or shear wave, contact, immersion, or mounted on a wedge. S-scans can also be displayed as uncorrected or corrected; corrected S-scans show the actual reflector positions, and are useful for visualization and image comparisons.

## 4.2.6 Polar Views

A *polar view* (see Figure 4-21) is a two-dimensional view, useful for plotting data from boresonic inspections or inspections of cylindrical parts. Used in conjunction with the 2-D specimen layout, it provides the defect location (ID/OD depth and angle).

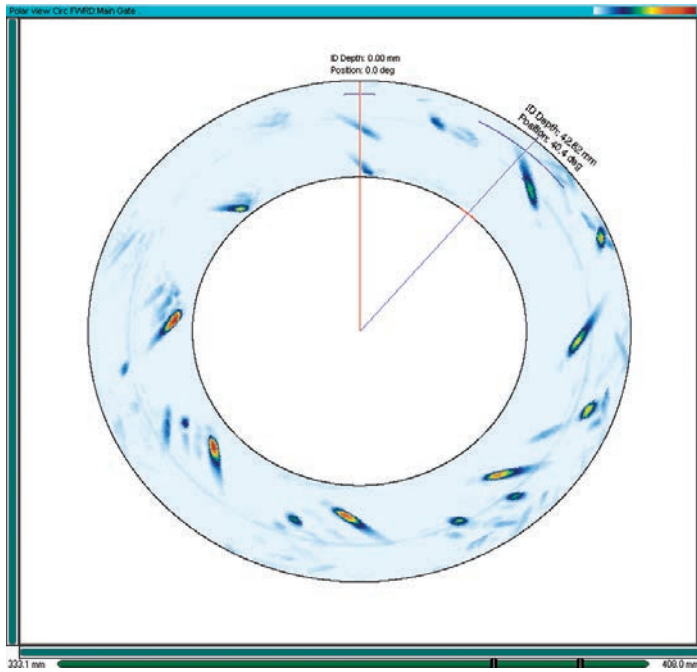
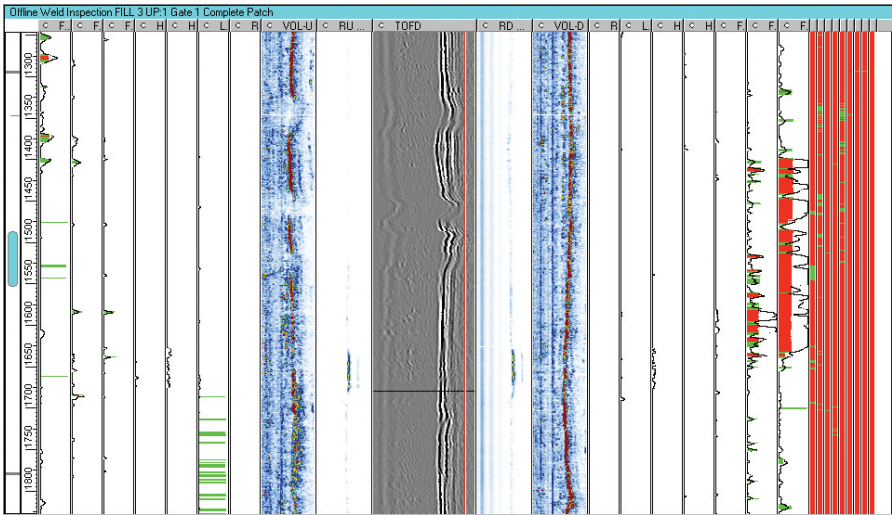


Figure 4-21 Example of polar view.

## 4.2.7 Strip Charts

A *strip chart* is a display of peak signal amplitude in the gate as a function of time, usually for a single channel. In some strip charts, other data such as time-of-flight (or position) is included. Typically, digital strip charts use multiple channels, each displaying the data from specific regions of a weld or other components (see Figure 4-22).



**Figure 4-22** Multichannel strip chart display from pipeline AUT (ASTM E-1961-98 code). Display uses both amplitude and TOF data, plus couplant checks, TOFD, and B-scans.

## 4.2.8 Multiple Views and Layouts

*Multiple views* may be displayed on the screen in *layouts* (see Figure 4-23). These types of displays require full waveform capture (unlike the strip charts shown in Figure 4-22, which only require peak amplitude and time in the gate). Specific properties and group information are associated with each view.

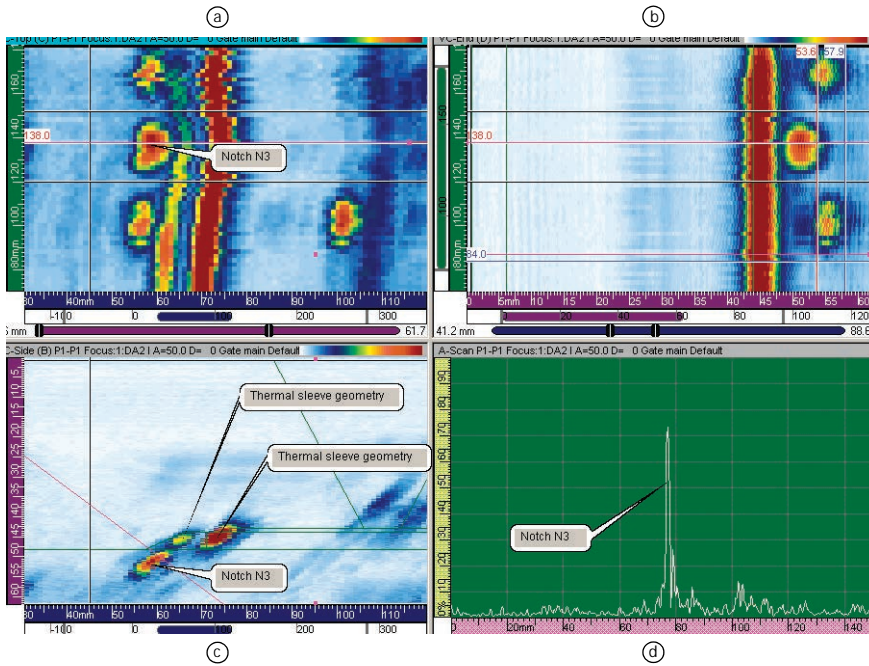


**Figure 4-23** Analysis layout with four views for dissimilar metal weld inspection with low-frequency phased array probes: (a) C-scan; (b) D-scan; (c) B-scan; (d) A-scan.

The views may be displayed as a single plane or as volume projection using the gate selection (see Figure 4-24 and Figure 4-25).

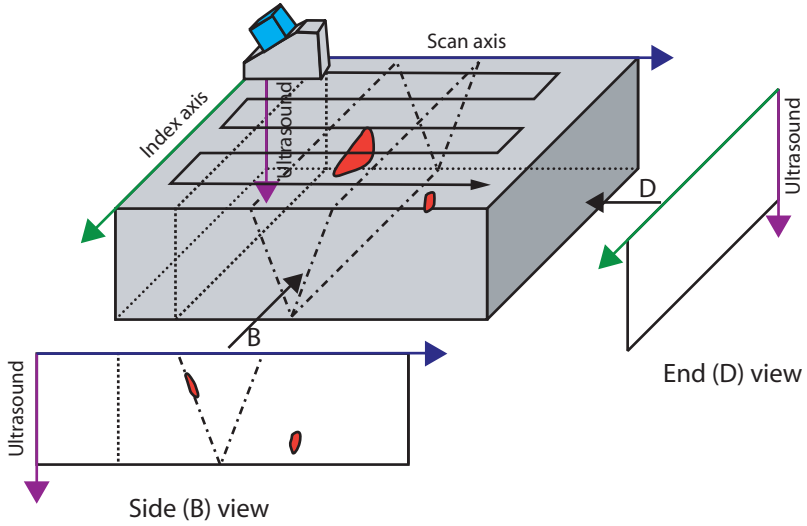


**Figure 4-24** Single plane projection of end (D) and side (B) views.

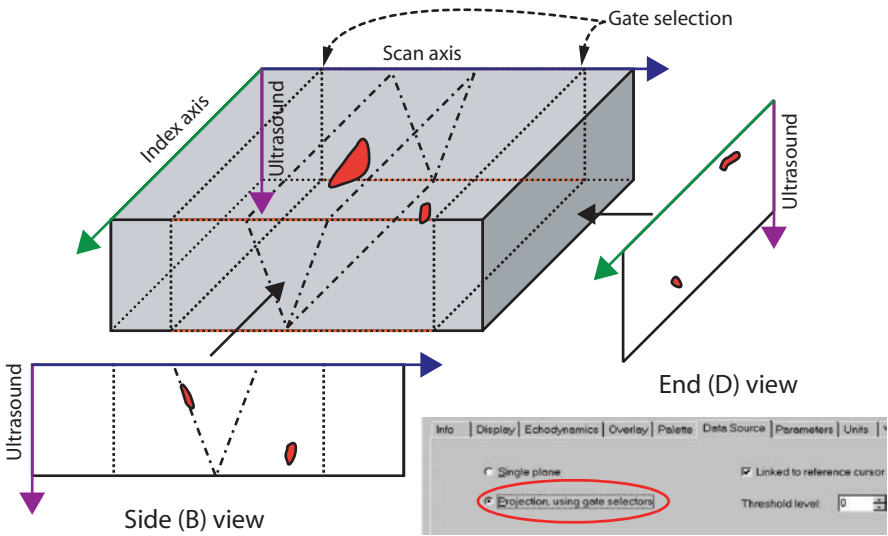


**Figure 4-25** Volume projection with linked reference cursors on end (D) and side (B) views. All defects within the gate range are displayed.



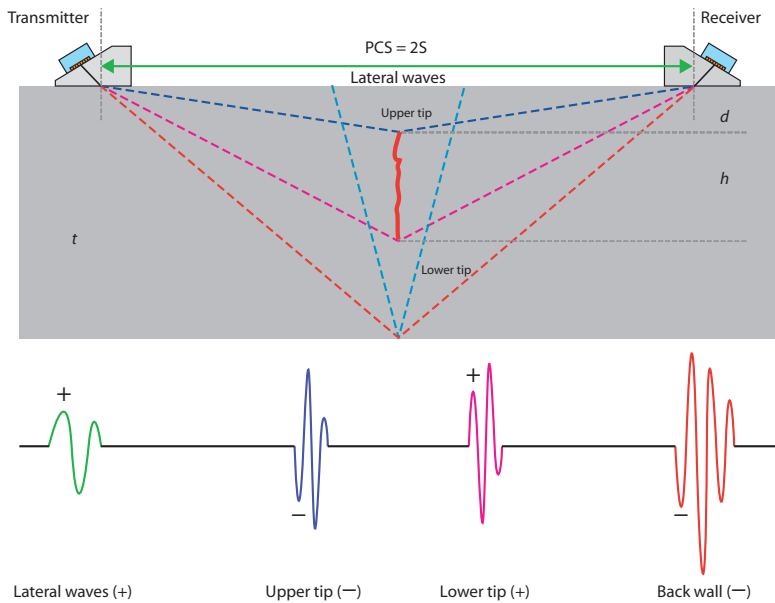


**Figure 4-27** General view of TOFD setup for linear weld inspections showing lateral wave, backwall echo, and diffracted signals on the A-scan.

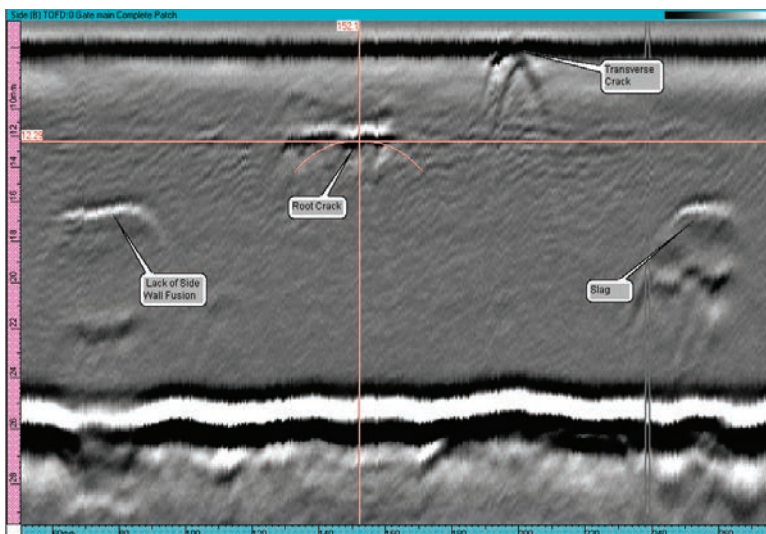


**Figure 4-28** Standard TOFD display, using gray-scale B-scan gated from lateral wave to longitudinal wave backwall.

TOFD is a very powerful technique, and allows the accurate sizing of defects. Sizing is based on the time of arrival of defects, not the amplitude; time of arrival of signals can be measured very accurately.

TOFD also offers a good PoD of defects, including badly oriented defects. TOFD coverage can be around 90% of the through-wall thickness. About 10% is lost in the two dead zones (ID and OD), but the actual figure depends on the TOFD configuration, frequency, and damping. These two dead zones are located near the lateral wave and the backwall reflection.

To get full coverage, TOFD should be combined with the pulse-echo technique, as seen in section 4.2.10. Conveniently, TOFD and PE are complementary; the strong features of pulse-echo (for example, surface defect detection) are the weak points of TOFD, and vice versa.

#### **4.2.10 Combined TOFD and Pulse-Echo (PE)**

The *Rapid Detection TECHnique (RDTECH)* combines TOFD with pulse echo (PE) to give a full coverage of welds, etc. (see Figure 4-29). To simplify the acquisition and the analysis, the *RDTECH* requires an ultrasonic inspection system allowing simultaneous multichannel acquisitions and analysis like the  $\mu$ Tomoscan conventional ultrasonic system or the Tomoscan FOCUS phased array system.

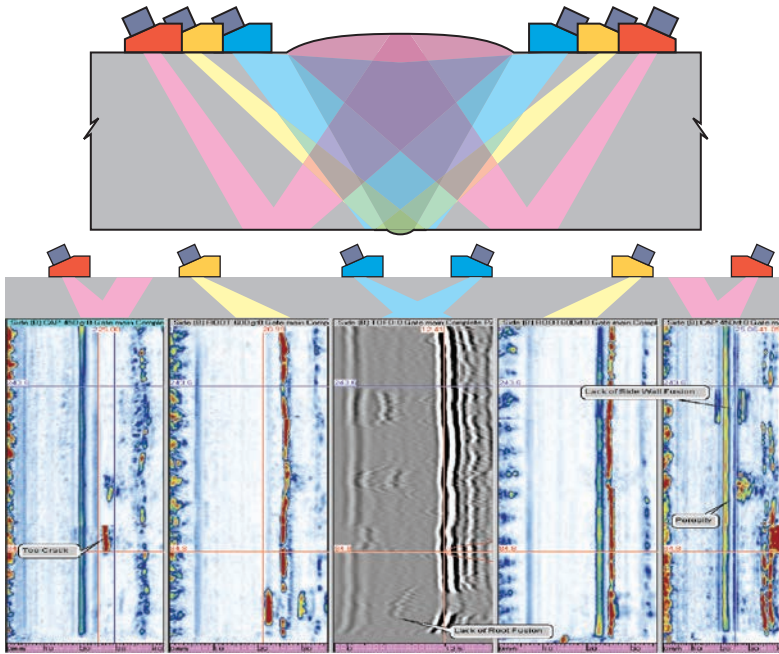


**Figure 4-29** Recommended combined TOFD and pulse-echo technique to optimize detection from each technique.

#### 4.2.11 Combined Strip Charts

A combination of TOFD and phased-array pulse-echo UT data is used for pipelines and pressure vessel AUT. The full weld inspection results can be displayed in a single layout (see Figure 4-30).

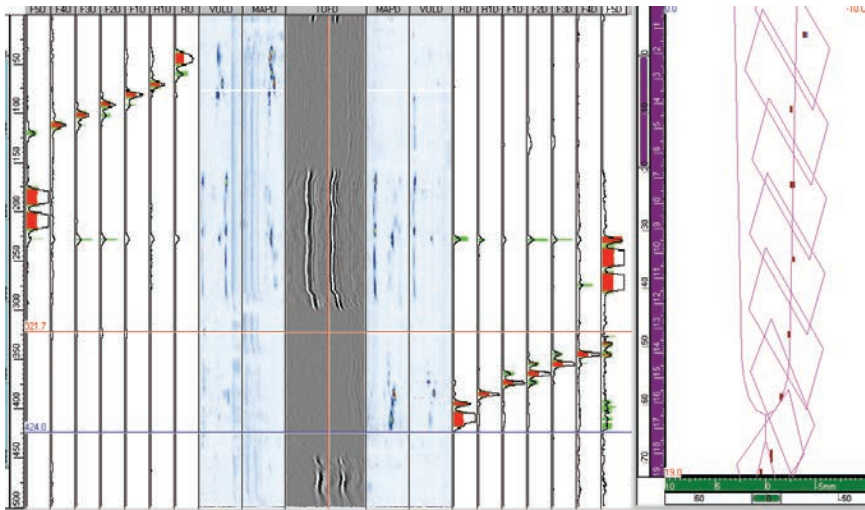


**Figure 4-30** Customized layout for TOFD and phased-array pulse-echo inspection of pipeline and pressure vessel welds. Data is plotted on a specific weld profile.

#### 4.2.12 Olympus TomoView Cube Views

Olympus has developed the *TomoView Cube*, a 3-D display of ultrasonic views (see Figure 4-31). Scanning patterns, linear array passive and active apertures, as well as 2-D volume-corrected top (C-scan), side (B-scan), and end (D-scan) views are presented on five faces of this cube.



**Figure 4-31** Olympus TomoView Cube (*left*), and showing all faces (*right*).

More details regarding the scanning patterns and views may be found in Olympus specific manuals (see references 1–10).

## References to Chapter 4

1. Olympus. *TomoView: User's Manual — Software Version 2.20*. Olympus document number DMTA-20077-01EN. Québec: Olympus, Jan. 2015.
2. Olympus. *TomoView: Advanced User's Manual — Software Version 2.20*. Olympus document number DMTA-20078-01EN. Québec: Olympus, Jan. 2015.
3. R/D Tech. "Technical Documentation Guidelines for TomoView 1.4R9." R/D Tech, Jan. 2001.
4. R/D Tech. "Advanced Training in TomoView 2.2R9." R/D Tech, May 2003.
5. Olympus. *Tomoscan FOCUS: User's Manual*. Olympus document number DUMG004C. Québec, Olympus, November 2002.
6. R/D Tech. *Tomoscan III PA: User's Manual*. R/D Tech document number DUMG049A. Québec: R/D Tech, Aug. 2002.
7. R/D Tech. *TomoView 2: Reference Manual*. Vol. 1, *General Features — Setup and Data Acquisition*. R/D Tech document number DUML039A. Québec: R/D Tech, July 2003.
8. R/D Tech. *TomoView 2: Reference Manual*. Vol. 2, *Analysis and Reporting*. R/D Tech document number DUML040A. Québec: R/D Tech, July 2003.
9. R/D Tech. "TomoView 2.2 — Technical Documentation — Technician Training." Slide presentation, rev. A. R/D Tech, May 2002.
10. Olympus. *OmniScan MX and MX2: User's Manual*. Olympus document number DMTA-20015-01EN. Québec: Olympus, September 2015.
11. R/D Tech. *TechDocE\_Features\_TomoView2\_revA*. R/D Tech, July 2003.
12. R/D Tech. *TechDocE\_TomoView22R9\_Guidelines\_revA*. R/D Tech, July 2003.



## Chapter Contents

5.1	Olympus Instruments.....	194
5.2	On-Site Equipment Checking.....	198
5.3	Active Element Integrity Checking.....	199
5.4	Ray Tracing.....	200
5.5	Aerospace .....	201
5.6	Energy .....	213
5.7	Pressure Vessel Construction Weld Inspection.....	230
5.8	Pipeline Phased Arrays .....	243
5.9	Miscellaneous Applications.....	254
5.10	Mills and Manufacturing .....	258
5.11	Railroad Transportation .....	272
5.12	Portable Phased Array Applications .....	277
	References to Chapter 5.....	297

---

## 5. Applications

---

A reliable phased array inspection is based on the following requirements:

- Well-defined technical specifications:
  - inspection scope
  - reporting/recording criteria
  - special conditions
- An issued ultrasonic engineering design
- Relevant available information about the component—drawings, access, material
- Information regarding the failure/degradation mechanism
- Information about the nature of expected defects: shape, size, location
- Information about the surface scanning conditions: roughness, temperature, curvature (convex or concave)
- Manufactured and certified representative reference blocks and targets for procedure validation, technician training, and field calibration
- Optimized ultrasonic parameters
- Assessment of essential and influential variables for phased array instruments, scanners, phased array probes, and acquisition/analysis software
- Validated procedure for specific setup and hardware configuration
- Personnel trained and certified under realistic inspection conditions
- Assessment of environmental influences on personnel/equipment performance and results (radiation, noise, temperature, humidity, height, depth underwater, etc.)
- Assessment of overall system and personnel performance within an allotted inspection window, without compromising on safety and quality, and based on previous inspections and crew experience.

The procedure development and validation (performance demonstration) should be based on redundancy concepts (defect detection and sizing with

multiple angles and probes) and on diversity (defect confirmation by another complementary technique, or by different type of waves).

In many cases, phased array technology is used to perform a very reliable inspection to detect small linear defects/volumetric inclusions at high speed. Optimizing hardware/software ultrasonic parameters is critical. Section 5.1 will detail some aspects regarding the hardware optimization.

## 5.1 Olympus Instruments

Phased array instruments manufactured by Olympus are<sup>1</sup>: OmniScan, QuickScan PA, Tomoscan FOCUS, and Tomoscan III PA (see Figure 5-1 to Figure 5-4). These instruments can be custom-built, and may be used in different configurations with a wide variety of scanners (see Figure 5-5).

- The OmniScan is a low-cost, battery-operated, self-contained phased array unit that can perform manual, semiautomated, and automated inspections. Normally, the OmniScan is used for applications like corrosion mapping, flaw detection, prove-up, and special portable applications.
- The QuickScan PA is a relatively low-cost, rack-mounted system with high PRF, specifically aimed at pipe mills and other high production rate applications.
- The Tomoscan FOCUS was the first commercial Olympus phased array system, and has been used in high-end laboratories, power generation, petrochemical, aerospace, and many other applications. Hundreds of units are in service.
- The Tomoscan III PA is our high-end phased array system, similar to the Tomoscan FOCUS, but offers much higher data transfer rates and better resolution. Originally developed for power generation applications, the Tomoscan III unit offers advantages for any application which requires collecting lots of data, or needs higher signal-to-noise ratio.

A comparison of technical performances for the main phased array instruments is presented in Table 5-1. QuickScan and Tomoscan III phased array options are presented in Figure 5-2 to Figure 5-4. Figure 5-6 shows the Tomoscan III and QuickScan units in typical industrial configurations.

---

1. Editor's note at fourth printing: Instruments listed here were available at the time of first printing. For an up-to-date list of available instruments and features, please contact Olympus.



**Figure 5-1** OmniScan PA portable instrument.



**Figure 5-2** Tomoscan FOCUS instrument.

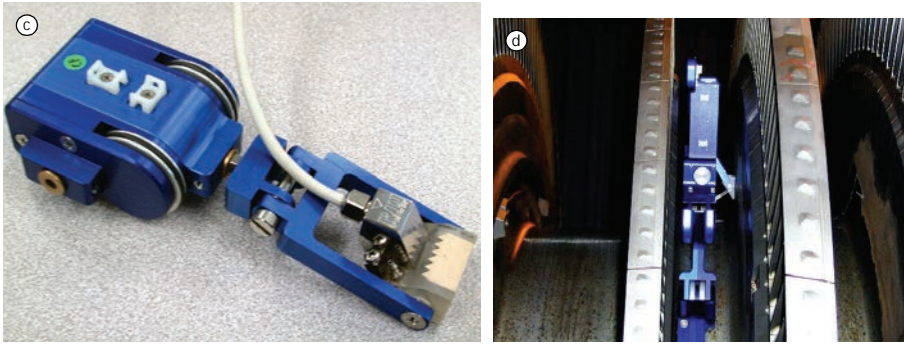


Figure 5-3 Tomoscan III PA instrument.



Figure 5-4 QuickScan PA instrument.





Courtesy of Boeing and GE, USA

**Figure 5-5** Examples of different types of scanners manufactured by Olympus: (a) ROVER for pressure vessels; (b) PS 12-X pipe scanner; (c) "beetle" scanner; (d) rotor disc scanner.

**Table 5-1** Technical performance of Olympus phased array instruments.

Tomoscan III PA	QuickScan PA	OmniScan PA
Main product features		
<ul style="list-style-type: none"> <li>• Large data file</li> <li>• Advanced data analysis</li> <li>• Highly skilled operator</li> <li>• High data transfer and storage &gt; 3 Mb/s</li> <li>• Level-2 and Level-3 operators</li> </ul>	<ul style="list-style-type: none"> <li>• Parallel firing</li> <li>• High PRF</li> <li>• Data storage (TOF, amplitude)</li> <li>• Alarm Go/No Go</li> <li>• Real-time data processing and alarm</li> <li>• Regular operators (no level of skill required)</li> </ul>	<ul style="list-style-type: none"> <li>• Manual/semiautomated</li> <li>• Limited data storage</li> <li>• Flaw detection</li> <li>• Limited data analysis</li> <li>• Level-1 and Level-2 operators</li> </ul>
Main applications		
<ul style="list-style-type: none"> <li>• Power generation</li> <li>• Reactor components</li> <li>• Turbines</li> <li>• Steam generators</li> <li>• Research laboratories</li> <li>• Pressure vessels</li> </ul>	<ul style="list-style-type: none"> <li>• Industrial in-line and manufacture</li> <li>• Aerospace</li> </ul>	<ul style="list-style-type: none"> <li>• Aircraft and military</li> <li>• Civil engineering and structure</li> <li>• Petrochemical and BOP</li> <li>• Corrosion mapping</li> <li>• Fastener inspection</li> <li>• Crack detection/sizing</li> </ul>
Technical data		
Integrated motor control: yes	Not applicable	No
Data storage: >1 GB	C-scan + Indication log	<256 MB
Number of ultrasonic channels: 32 / sequential	Custom-built: up to 64 / parallel	16 / sequential / parallel
Resolution: 12 bits	8 bits	10 bits (8 bits stored)
Digitizer A/D: 100 MHz	100 MHz	100 MHz
Axis support: 2 automatic	2 automatic	2 semiautomatic

**Table 5-1** Technical performance of Olympus phased array instruments. (Cont.)

Tomoscan III PA	QuickScan PA	OmniScan PA
Data file format: RDTIFF	RDTIFF	Special RDTIFF; data can be analyzed in TomoView
Weight: <20 kg (44.1 lbs)	Custom <20.5 kg (45.2 lbs)	<4 kg (8.82 lbs)
Portability: yes	no	yes
Power supply: mains	mains	Battery: 15 V or mains
Price: \$\$\$	\$\$	\$



**Figure 5-6** Olympus Tomoscan III PA (*left*) and QuickScan PA (*right*). These show the instruments in a typical configuration and installation.

## 5.2 On-Site Equipment Checking

Phased array pulser-receiver boards can be checked using an arrow-point generator with a Hypertronics BQUS002 connector (see Figure 5-7), for example.



**Figure 5-7** Hypertronics BQUS002 connector for pulse-echo setups (*left*) and BQUS009 connector for pitch-and-catch setups (*right*).

The normal operation of the pulser/receivers is displayed by a double arrow pattern with no white discontinuities (see Figure 5-8, *left*).

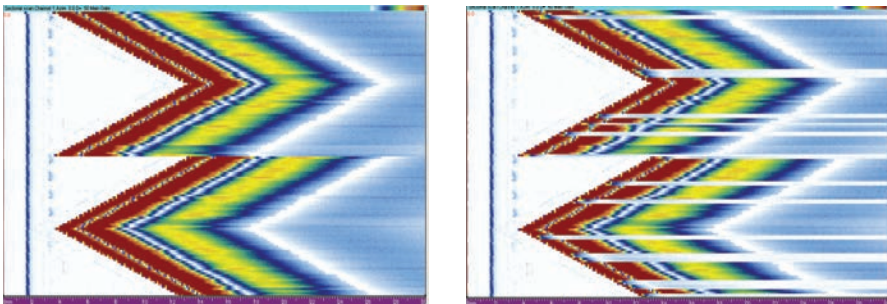


**Figure 5-8** S-scan display for checking the pulser/receivers functionality: normal (*left*); malfunctioning pulsers and receivers (white strips, *right*). (Standard Olympus array acceptance procedure.)

### 5.3 Active Element Integrity Checking

Individual elements active in a specific group of focal laws are checked using a linear scan. Depending on probe pitch and probe type, the operator may use a small screwdriver with a 0.5 mm to 0.8 mm diameter or a 0.5 mm mechanical pencil lead refill. Slowly move the screwdriver/lead refill in front of each element and watch for ultrasonic signals. Each active element should produce a reflection when the screwdriver is placed in front of it. Depending on the application, a phased array probe may work properly even if 10% to 25% of its active elements are damaged (see Figure 5-9).<sup>16</sup>

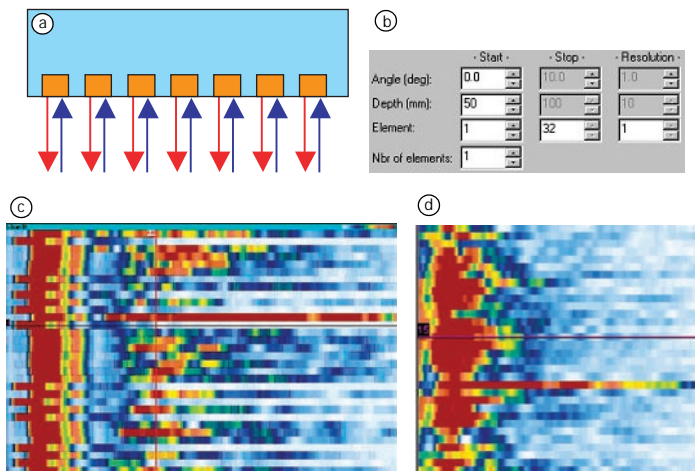


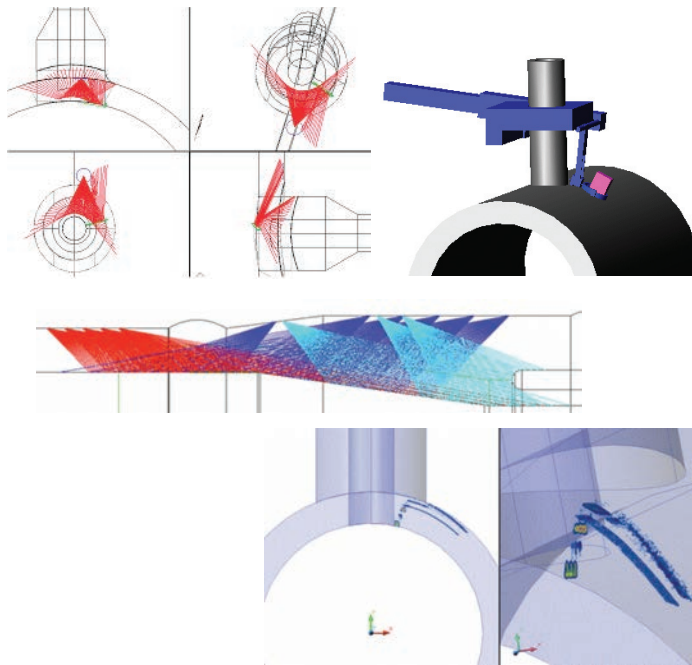
**Figure 5-9** Linear scanning for element/electrical connection integrity: (a) principle; (b) focal laws for a 32-element probe; (c) S-scan display of a linear phased array probe with 10 “dead” elements; (d) uncorrected S-scan using linear array.

## 5.4 Ray Tracing

Ray tracing and data plotting on component geometries (see Figure 5-10) are very useful tools for:

- Assessing the coverage area
- Setting up the focal laws and ultrasound range
- Optimizing the scanning parameters (scan axis, index axis, orientation, and resolution)
- Evaluating the mode-converted zones and the wedge skew angle
- Achieving advanced imaging (merged data, multiple scan displays, pattern recognition)
- Locating defects relative to important features, such as weld fusion lines
- Reporting

Ray tracing may be part of the technical justification for procedure qualification. Ray tracing packages are now commercially available in low-cost or high-end versions. Often, such packages “solve” inspection problems with minimal cost and effort, and can be highly beneficial.



Courtesy of NDT Soft, UK

**Figure 5-10** Example of ray tracing and data plotting of phased array inspection on nozzle weld.

## 5.5 Aerospace

This section covers various types of inspections used in the aerospace industry. More information can be found in references 10 and 17.

### 5.5.1 Inspection of Titanium Billets

More information about the inspection of titanium billets can be found in references 12 and 17.

#### a) *NDT problem*

- Detecting and sizing hard-alpha and ceramic inclusions in titanium billets with diameters from 7.5 cm to 35 cm (3 in. to 14 in.)

#### b) *Other requirements*

- Coupling check

- Fully automated system
- Fine mechanical adjustment
- Customized user interface

c) *Ultrasonic challenge*

- Coarse-grain microstructure
- Small defects (0.4 mm to 0.8 mm)

d) *Phased array solution*

- Use a 12-ring annular array probe using Fresnel zones, with a total aperture of 80 mm and the DDF feature in immersion and/or a 113-element rho-theta probe (see Figure 5-11).

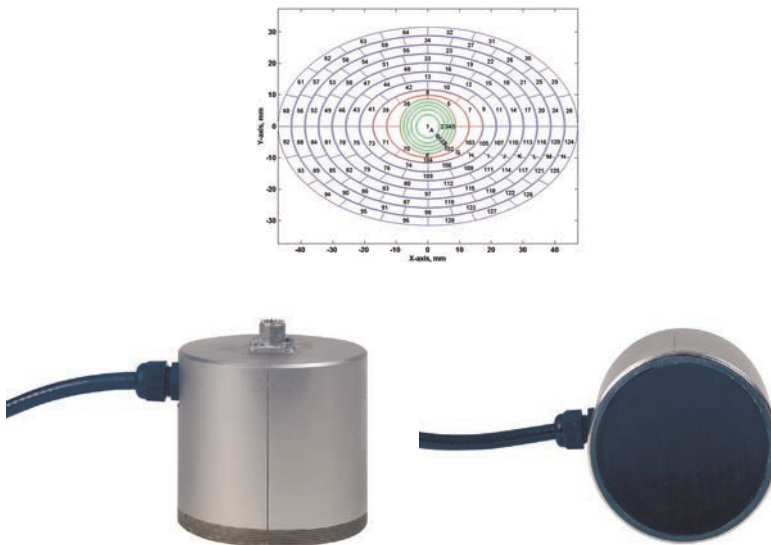


**Figure 5-11** Five-MHz annular array (*top*) and rho-theta probe (*bottom*) used for titanium billet inspection.

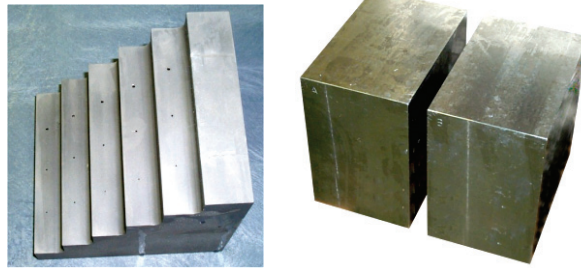
e) *Description of the solution*

- Use a single-segmented elliptical-annular phased array probe to cover a large range of diameters.
- DDF keeps the beam very narrow (5 mm to 125 mm depth).
- The same phased array probe can generate two beams for large diameter billets.

- Alignment of the phased array probe is performed ultrasonically using four elements of the probe.
- Detection capability on FBH: 0.4 mm (0.016 in.) up to 7.5 cm (3 in.) depth, and 0.8 mm (0.032 in.) up to 12 cm (5 in.) depth.
- Detection capability on hard-alpha particles: 0.5 mm (0.020 in.) up to 5 cm depth (2 in.), and 1.0 mm (0.040 in.) up to 12 cm (5 in.) depth.
- Automatic defect detection is performed by software for easy analysis.

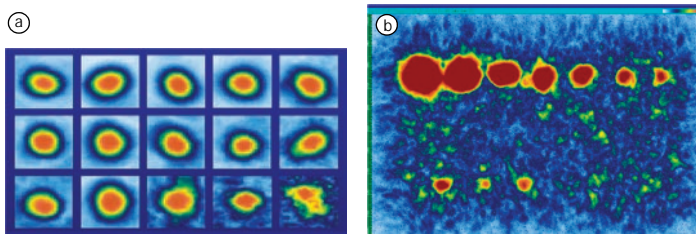
*f) Details*

- Use reference blocks with FBH and hard-alpha inclusions (see Figure 5-12).



**Figure 5-12** Reference blocks from titanium billets with FBH (*left*) and hard-alpha inclusions (*right*).

- Phased array results on reference blocks are presented in Figure 5-13.



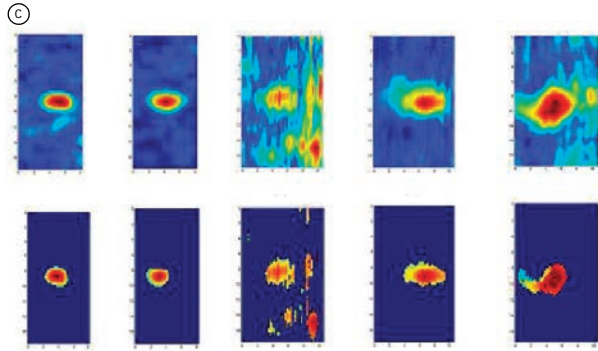


**Figure 5-13** Unprocessed phased array results on titanium reference blocks on: (a) FBH and (b) hard-alpha. (c) Data processing using cut spectrum processing algorithm.

- The industrial application of phased arrays using the rho-theta array is presented in Figure 5-14.



**Figure 5-14** Immersion testing with a rho-theta probe on titanium billets.

## 5.5.2 Inspection of Friction Stir Welds

More information about the inspection of friction stir welds (FSW) can be found in reference 1, 2, and 10. Inspection of friction stir welds is an ongoing development. This inspection was primarily for conventional defects.

### a) *Typical NDT inspection requirements*

- Weld length: up to 12 m (~40 ft)
- Wall thickness: 3 mm to 15 mm or more (0.012 in. to 0.60 in.)
- Diameter range: 2.5 m to 5 m (8 ft to 17 ft)
- Material: normally aluminum, although this technology can be used on any material welded by friction stir welding
- Vertical or horizontal weld configuration
- Inspect irregular weld shape and lips, which hinder raster scanning
- Problem due to limited access space
- Coupling check
- Fully automated inspection
- Rapid inspection

### b) *Defects to be detected*

- Lack of penetration
- Kissing bonds (entrapped oxide defects)
- Wormholes
- Root toe defects
- Axial and transverse defects
- Porosity

### c) *Description of the phased array solution*

- One phased array probe on each side of the weld for axial detection, plus a third phased array probe for transverse defect detection if specified
- Inspection with 65° SW and 35° SW angles for axial defects in this application
- Inspection with a 45° SW refraction angle and skew angles of -30°, 0°, and 30° for transverse defects
- Electronic scanning of the beam for all configurations
- Full weld inspection performed in a linear scan (up to 20 meters)
- Coupling performed with local immersion wedges

*d) Phased array industrial system components*

- Tomoscan FOCUS 32:128
- Scanner: ROVER with special adapter
- Motor driver: MCDU-02 with joystick
- Probes: three linear phased array probes (10 MHz, 64 elements)
- Coupling: local immersion
- Water recirculation system
- Umbilical cable with air, 110 VAC, scanner control, and ultrasonic signal
- Portable track for autonomous work
- Computer cabinet (air-conditioned)

*e) Examples (see Figure 5-15 to Figure 5-20)*

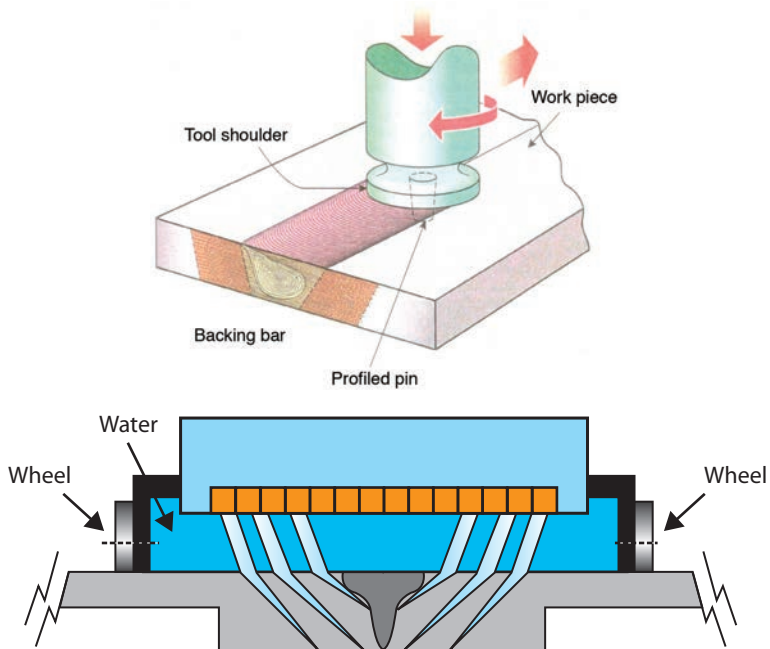


**Figure 5-15** Electronic scanning of aluminum friction stir weld: welding principle (*top*); focused beams for scanning the weld (*bottom*).

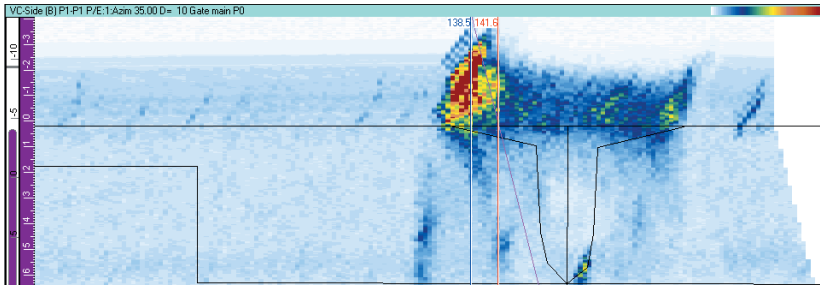
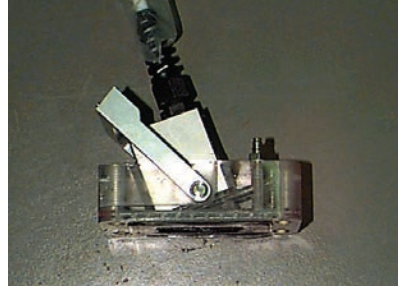
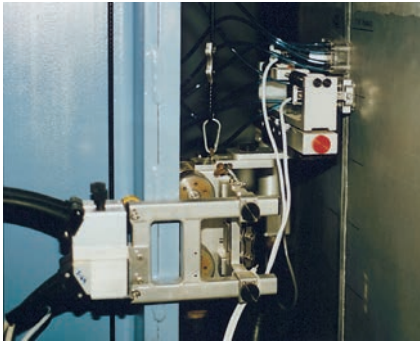


**Figure 5-16** Crack image detected in the weld root with a 2-D weld overlay for imaging.



*Courtesy of Boeing, USA*

**Figure 5-17** Tomoscan FOCUS 32:128, MCDU-02 driver, and computer enclosed in an air-conditioned cabinet (*left*); water recirculation system (*right*).



Courtesy of Boeing, USA

**Figure 5-18** Special adapter (*left*) and linear phased array probe with a local immersion fixture (*right*).

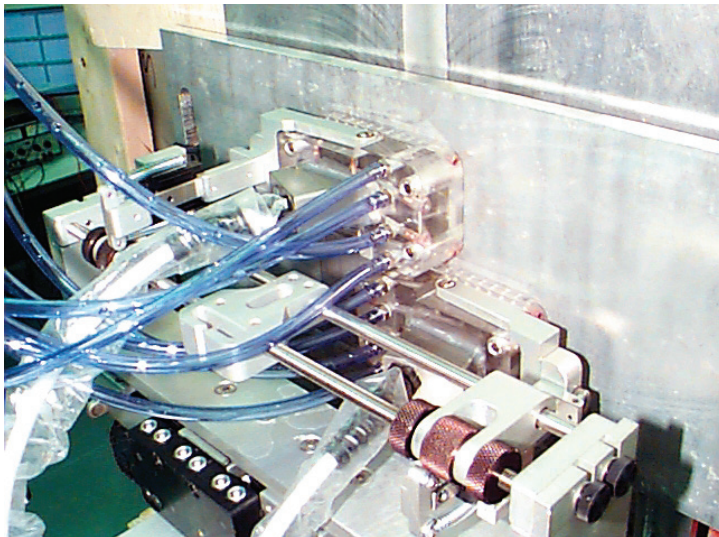


**Figure 5-19** Phased array system in production inspecting FSW.

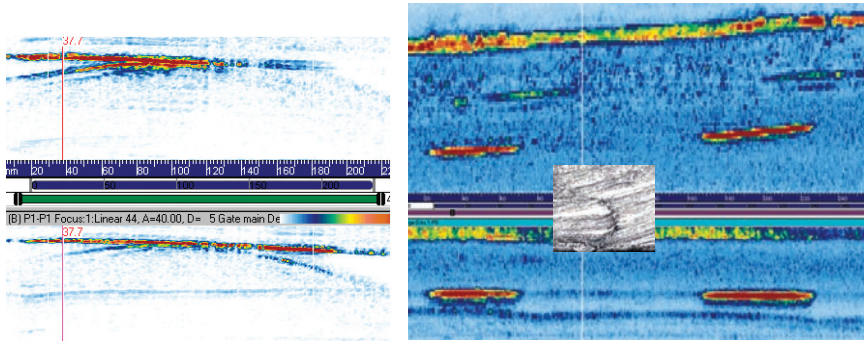


**Figure 5-20** Detection of faying surface defect (*left*) and kissing bond (*right*).

### 5.5.3 Inspection of Fastener Holes

#### a) NDT problem

- Detection of fatigue cracks of 0.75 mm (0.030 in.) in length around faying surface fastener holes
- Wide variety of skin thicknesses and fastener hole diameters (see Figure 5-21)
- Scanning time of less than 1 minute per fastener
- Handheld phased array head
- Validated system

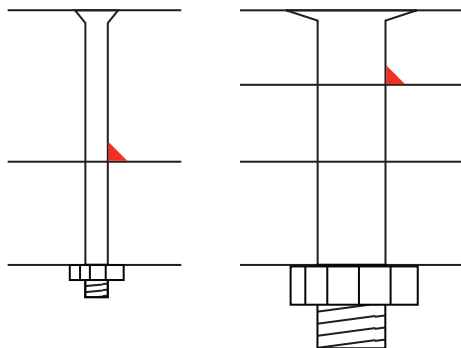
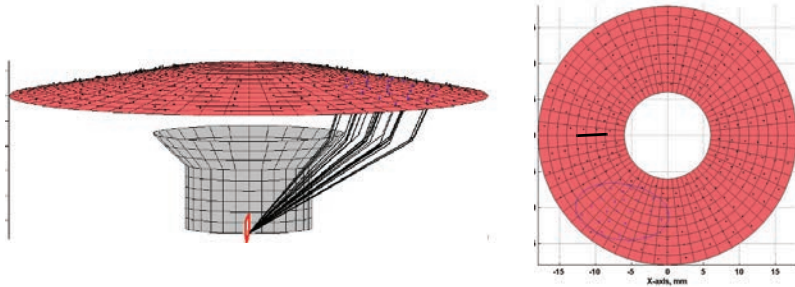


**Figure 5-21** Faying surface corner cracks in fastener of two sizes: small head / thick skin (*left*); large head / thin skin (*right*).

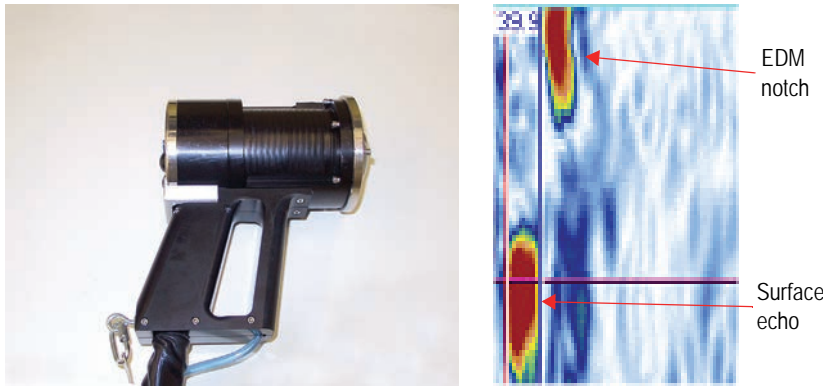
**b) Phased array solution**

- Use a conical matrix phased array probe with a large number of elements (504, for example).
- Perform an electronic scanning 360° around the fastener hole (see Figure 5-22).
- Randomize the elements in each subgroup to reduce the amplitude of grating lobes.
- Reduce probe head weight to under 2 kg (4.41 lbs) [see Figure 5-23].
- Adjust gains so that all elements have the same sensitivity.
- Perform multiangle, multiposition scanning to maximize PoD.
- Automatic centering of the probe around the fastener hole.
- Phased array system must fire up to 64 elements simultaneously (see Figure 5-24). FastFOCUS system uses two QuickScan PA 32:256 units.



*Courtesy of USAF and Lockheed Martin AS, USA*

**Figure 5-22** Conical matrix phased array probe design: isometric beam (*left*); tangential detection of the crack in the fastener hole (*right*).



Courtesy of USAF and Lockheed Martin AS, USA

**Figure 5-23** Photo of conical matrix array probe, also known as “hair dryer” (left); ultrasonic data from 0.75 mm EDM notch (right).



**Figure 5-24** Phased array system including two QuickScan PA units.

## 5.5.4 Inspection of Landing Gear Using Manual Phased Arrays

### a) NDE problem

Landing gears are subject to intense stress upon takeoff and landing. The section that must be inspected is a cylinder possessing three different

diameters in the zone of interest. The best way to inspect that zone is to use a phased array technique with steering capabilities to simultaneously fire  $40^\circ$  to  $65^\circ$  shear-wave refracted angles in the part.

The adapted wedge and the combination of angles provided by the phased array system allow the complete inspection of the zone of interest in a single pass.

Some of the advantages of this technique, compared to conventional techniques, are simplicity (performing a single linear scan instead of a raster scan) and the ability to cover a complete volume using multiple angles at the same time. Using this system, an inspector can perform the inspection faster and with better reliability.

**b) Typical inspection requirements**

- Adaptation of probe and wedge to the curved surface
- A-scan, B-scan, and sectorial scan (S-scan) displays
- Storage of a linear scan for subsequent analysis
- Landing gear diameter from 12.5 cm to 20 cm (5 in. to 8 in.)
- Part thickness from 12 mm to 38 mm (0.5 in. to 1.5 in.)
- User-friendly operating system
- Portable system, such as OmniScan PA (see Figure 5-25)



*Courtesy of Northwest Airlines, USA*

**Figure 5-25** Portable OmniScan PA system used for inspection of landing gears.

## 5.5.5 Corrosion Mapping of Aircraft Fuselage

### a) *NDT problem*

Corrosion degradation is a major source of concern for the aircraft industry. As aircrafts are flying longer than expected from their design life, the development of a fast and reliable inspection technique is necessary.

Corrosion mapping of lap joints is a challenge because fastener heads protrude, making the use of a conventional contact ultrasound probe impossible. Also, aircraft surfaces are rarely flat.

### b) *NDT solution*

This phased array system uses a special probe holder with a water column and a flexible motorized scanner. The system allows accurate corrosion sizing, as well as fast inspections (see Figure 5-26).

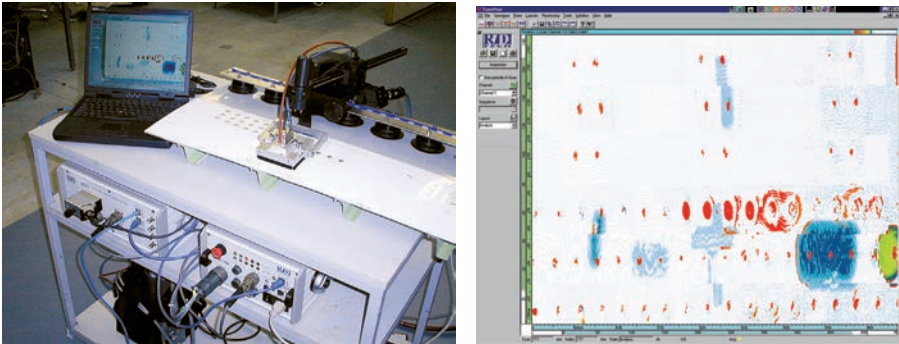


**Figure 5-26** Phased array system for corrosion mapping of lap joints (*left*) and C-scan display of different degrees of corrosion (*right*).

## 5.6 Energy

This section covers various types of inspections that are used in the energy generation industry. More information can be found in references 4, 6, 7, 9, 11, and 15.

## 5.6.1 Dissimilar Welds Inspection of BWR Core Shroud

### a) NDT problems and challenges

- Different materials with different expansion coefficients welded together can lead to cracking.
- Strong attenuation and velocity variation in austenitic material
- Beam skewing and distortion
- Noisy microstructure
- Limited probe access because of geometry and weld configuration
- Qualification and endorsement of the procedure by a regulator

### b) Phased array solution

- Develop a TRL (transmitter-receiver L-waves) phased array probe with a 1.5-D configuration.
- Optimize the roof angle.
- Use the skew angle to increase the SNR.
- Increase the probe bandwidth (>100%).
- Decrease the probe frequency (between 0.8 MHz and 2 MHz).
- Use merged images and 2-D weld overlays.
- Qualify the TRL phased array probe on representative mock-ups (see Figure 5-27 to Figure 5-31).
- Use 0° for profile and coupling checking; sweep angle of 30° to 80°, resolution of 1°; multiple focal depths (5–50 mm range); one line scan with 20 mm/s.

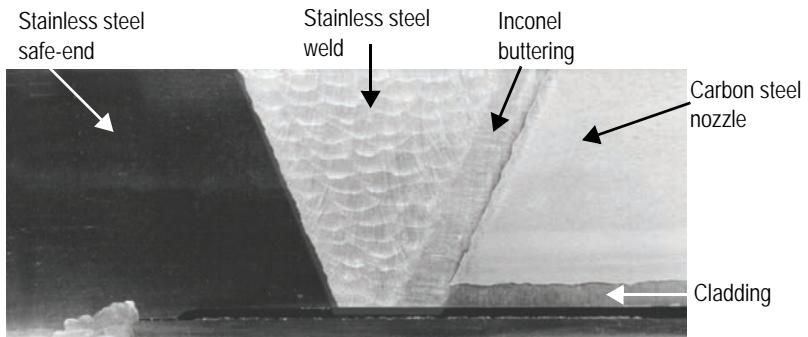


**Figure 5-27** Macrostructure of a dissimilar metal weld.

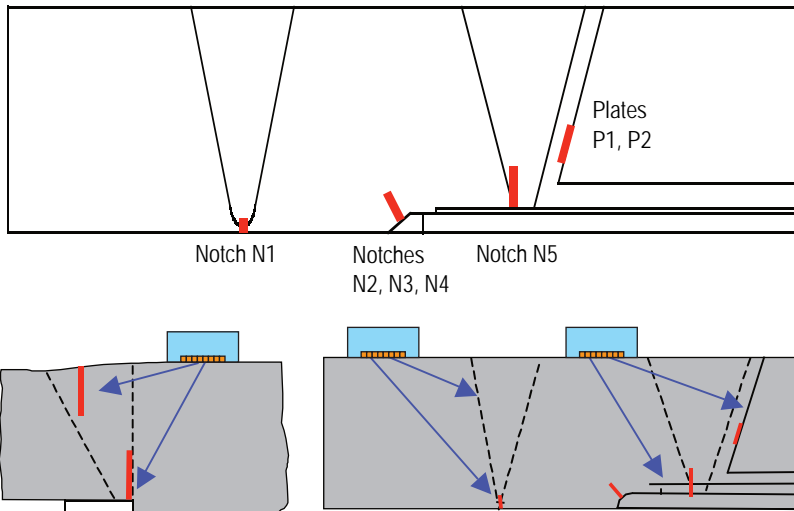


**Figure 5-28** Location of EDM notches in reference block (*top*) and scanning modes (*bottom*).

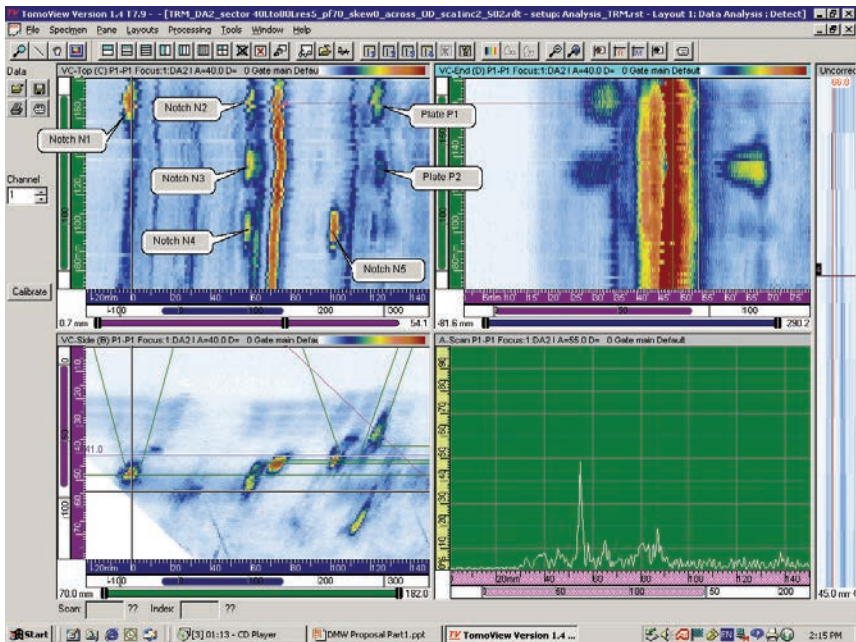


**Figure 5-29** Detection capability of all notches (merged view).

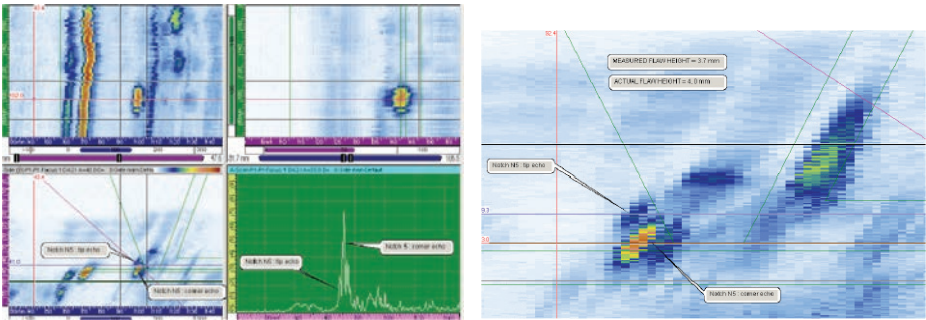


**Figure 5-30** Detection and notch sizing in dissimilar metal welds. Length accuracy is  $\pm 3$  mm. Height accuracy is  $\pm 0.3$  mm.

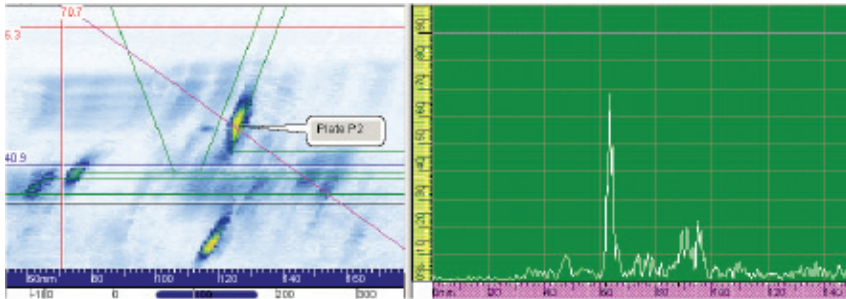


**Figure 5-31** Notch detection in the buttering; SNR = 18 dB.

## 5.6.2 High-Speed Inspection of Stainless Steel and Carbon Steel Pipe Welds

### a) NDT problem and challenges

- Detecting and sizing weld defects in the inner part of weld and HAZ (heat-affected zone)
- Setting up in minimal time
- Scanning in minimal time
- Acquiring reproducible data
- Operating in high-radiation fields

### b) Phased array solution

- Manufacture a “simple to set up” pipe scanner (see Figure 5-32).
- Use laser-beam centering device.

- Perform linear scanning to minimize inspection time (resolution = 1 mm, speed = 38 mm/s) with two phased array probes on each side of the weld.
- Merge data images (see Figure 5-33).
- Perform pipe inspection in less than 5 minutes per weld.
- Measure the length using the -12-dB drop technique.
- Use tip-echo diffraction for height sizing (see Figure 5-34).

*c) Phased array system*

- Tomoscan III PA
- Phased array probes: linear 5 MHz/32 elements: 5L32E32-10 for a 12-in. pipe
- Phased array probes: 1.5-D, frequency of 1 MHz for 36-in. SS narrow gap weld
- Scanner: PS 12X + MPSU-01 power supply

*d) Advantages*

- Dose reduction of 10:1
- Scanning time: less than one minute/weld

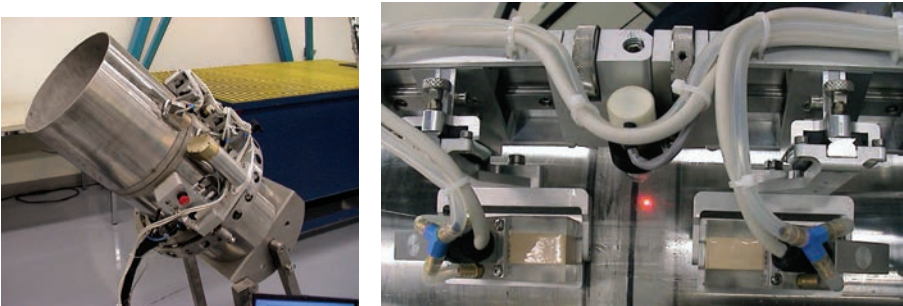


**Figure 5-32** Pipe scanner (*left*) with two phased array probes and laser centering device (*right*).

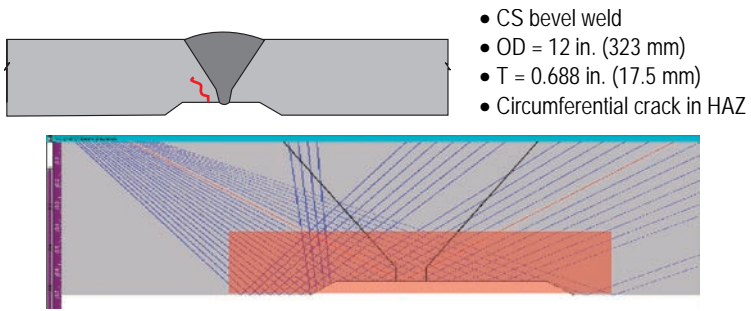


**Figure 5-33** Carbon steel weld profile (*top*) and beam simulation for phased array ultrasonics (*bottom*).

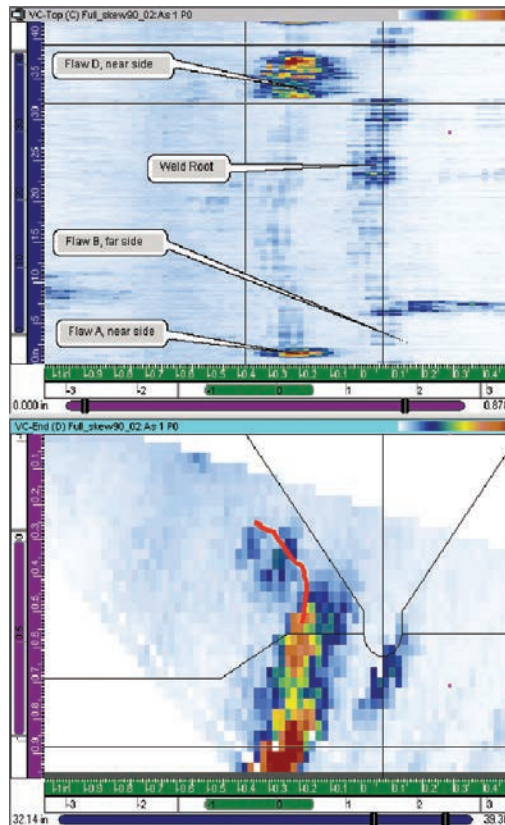


**Figure 5-34** Example of defect detection, imaging and sizing in a 30-cm (12-inch) diameter pipe.

Defect sizing capability is presented in Table 5-2.

**Table 5-2** Phased array sizing capability\* on 30-cm (12-inch) carbon steel pipe weld.

Flaw ID	Location	Phased array	Actual	Error
<b>Length in mm (in.) using the -12 dB drop method</b>				
A	Up	27 (1.06)	21 (0.83)	+8 (+0.23)
B	Down	30 (1.18)	30 (1.18)	0.00
D	Up	131 (5.16)	115 (4.51)	+16 (+0.65)
<b>Height in mm (in.)</b>				
A	Up	8.3 (0.328)	8.7 (0.344)	0.4 (-0.016)
B	Down	13.8 (0.544)	13.6 (0.537)	0.2 (+0.007)
D	Up	7.3 (0.288)	7.2 (0.282)	0.1 (+0.006)

\*ASME XI tolerances for performance demonstration are:  $\pm 19$  mm (0.75 in.) for length and  $\pm 3$  mm (0.12 in.) for defect height.

### 5.6.3 Inspection of PWR Main Coolant Piping Weld Made of Wrought Stainless Steel Using Phased Arrays

*a) NDT parameters*

- Dimensions: OD  $\times$  t = 36 in.  $\times$  3 in. (900 mm  $\times$  75 mm)
- Weld prep: narrow gap
- Reference reflector: sharp EDM notches PISC type A with height = 10 mm

*b) Phased array system and ultrasonic settings*

- Tomoscan III PA
- PS 12 scanner [adapted to 914-mm (36-in.) OD]
- 1.5-D dual phased array probe: 1 MHz, 2  $\times$  (2  $\times$  11) elements, pitch: 4.5 mm
- Sector scan (30° to 60° LW; resolution: 1°) for ID region coverage
- Linear and sectorial scanning; resolution: 1 mm (0.04 in.); speed: 40 mm/s (1.6 in./s)

- Fast and efficient analysis using volumetric merge feature

The details of this inspection are presented in Figure 5-35 and Figure 5-36.

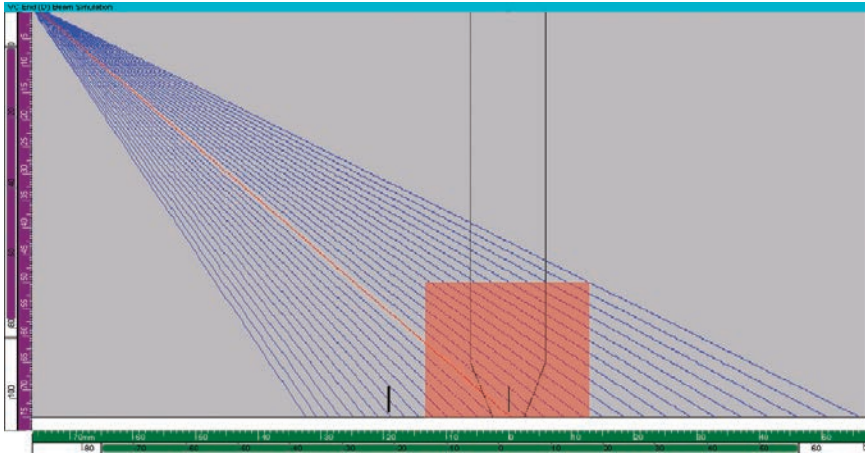


**Figure 5-35** Beam simulation for phased array inspection of narrow gap-weld.

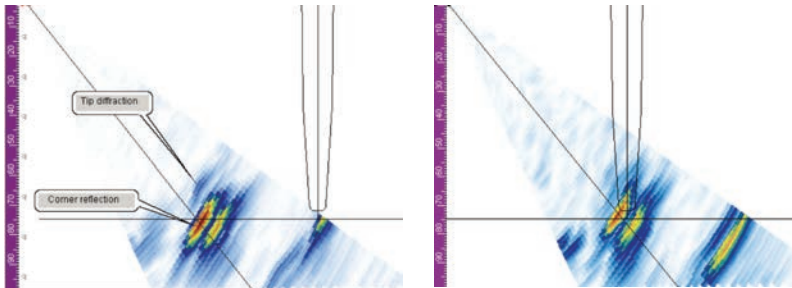


**Figure 5-36** Detection and height sizing of reference reflectors.

## 5.6.4 Reactor Vessel Nozzle-to-Shell Weld

### a) NDT problem

- Performing a reliable inspection on the nozzle inner radius and weld (see Figure 5-37)
- Demonstrating that the ultrasonic beams cover the full 360° circumference, with variable wall thickness and geometry
- Detecting and sizing planar defects with a vertical extent of 3 mm and length greater than 20 mm

- Reporting, visualization, and data displays with easy interpretation

b) *Phased array solution*

- Use a waterproof 1.5-D/2-D phased array probe (see Figure 5-38).
- Use a ray-tracing to validate the angles and focal laws.
- Use a 2-D/3-D specimen to plot phased array data (see Figure 5-39).
- Use a DDF capability.
- Use a 12-bit digitizer.
- Use a cylindrically corrected view to detect under-cladding defects.
- Use customer-owned, dedicated manipulator.

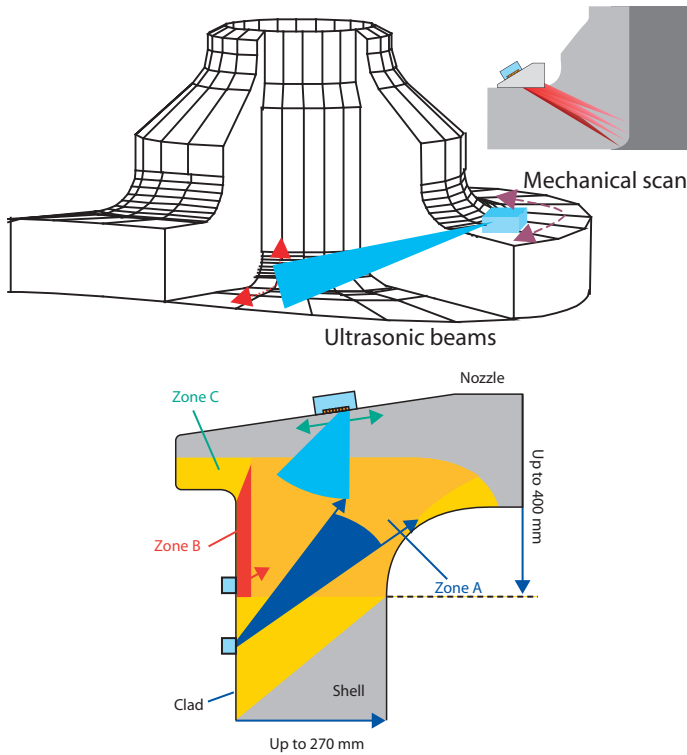


**Figure 5-37** Inspection principle of inner radius and weld of pressure vessel nozzle.



**Figure 5-38** Waterproof TRL phased array probes for pressure vessel nozzle.

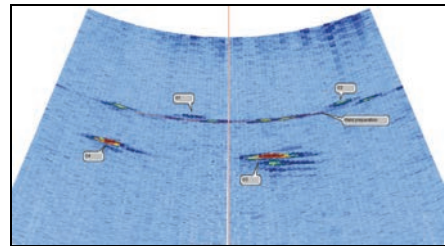
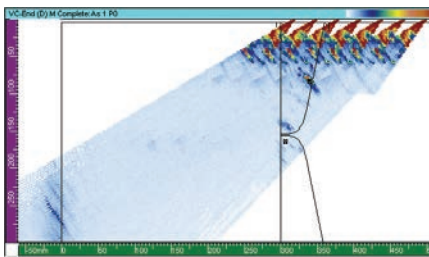


**Figure 5-39** Phased array data of EDM notches in the mock-up: merged scans (*left*) and cylindrical corrected view (*right*).

*c) Benefits*

- Reliable inspection
- Faster by a factor of 5 to 10
- Easy reporting for the regulator

## 5.6.5 CANDU Feeder Tube Cracking

*a) NDT problem and challenges*

- Detecting and sizing fatigue cracks in the feeder pipe
- Very limited access
- Crack height of less than 1 mm
- High-radiation area

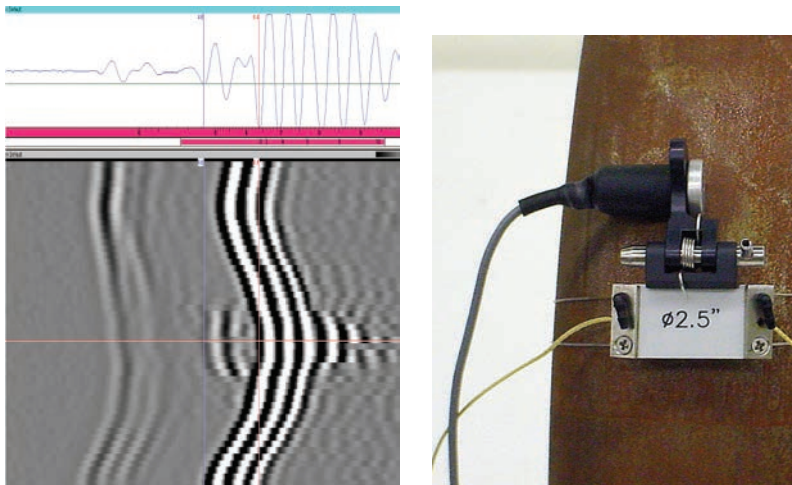
*b) Phased array solution*

- Use a wheel encoder attached to the array (see Figure 5-40).

- Use a 10 MHz, 16-element linear phased array probe.
- Use the Tomoscan FOCUS or OmniScan phased array instruments.
- Combine phased array and pulse-echo techniques for detection with time-of-flight diffraction (TOFD) for sizing (see Figure 5-41).
- Simplify the analysis layout (see Figure 5-40).



**Figure 5-40** Phased array detection of fatigue cracks in CANDU feeder tubes: scanning setup (left) and crack detection (right).



*Courtesy of Embalse NGS, Argentina*

**Figure 5-41** Feeder crack sizing with TOFD technique.

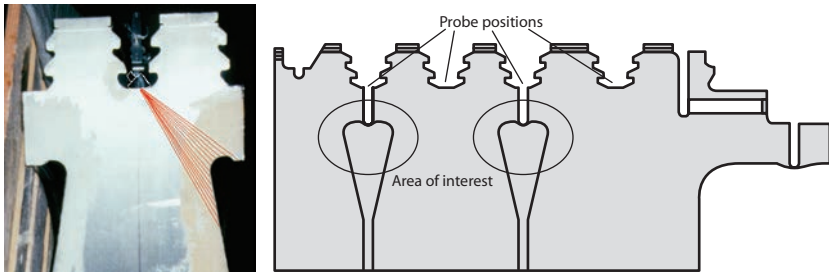
## 5.6.6 Detection of Stress Corrosion Cracking in Welded Rotor or Single Block Rotor

### a) NDT problem and challenges

- Detecting small stress corrosion cracking (SCC) at long ultrasonic paths [150 mm to 400 mm (6 in. to 16 in.)] in the different stages of the welded rotor (see Figure 5-42)
- Limited probe access

### b) Phased array solution

- Use sectorial scan of 30° to 60° shear waves, resolution of 1°.
- Use a linear phased array probe (5 MHz, 16 elements).
- Calibrate on EDM notches 2 mm × 0.5 mm (length × height).
- Build a custom probe manipulator.
- Perform a 360° scan with fixed probes and rotate the rotor on the power stands.



Courtesy of Alstom/ABB, Switzerland

Figure 5-42 Phased array inspection of welded rotor.

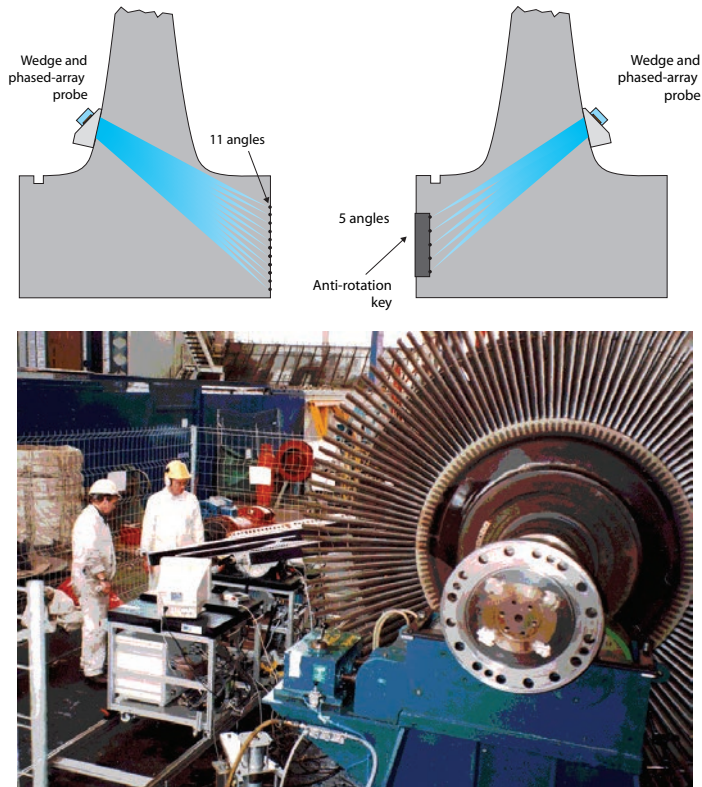
## 5.6.7 Detection of SCC in Disc Keyway and Anti-Rotation Key in Low-Pressure Turbine Rotor

### a) NDT problem and challenges

- Small SCC (defect height between 1 mm to 3 mm)
- Long ultrasonic path (300 mm to 600 mm)
- Variable SCC location
- Inspection window: 2 days/rotor (each rotor generally has 6 to 10 discs)

**b) Phased array solution**

- Use a linear phased array probe of 4 MHz to 6 MHz, 32 elements, and active aperture of 30 mm to 60 mm.
- Use a dedicated manipulator with a fixed linear phased array probe.
- Create scanning zones depending on key/disc geometry.
- Rotate the LP rotor on power stands (see Figure 5-43).



*Courtesy of SGS and EDF, France*

**Figure 5-43** Phased array inspection of bore and anti-rotation key of low-pressure turbine rotor: phased array principle (*top*) and field scanning (*bottom*).

## 5.6.8 Boresonic Inspection: Detect and Size SCC in the Rotor Body

**a) NDT problem and challenges**

- Limited access: the bore hole is used for access

b) *Phased array solution*

- Design and use a Fermat-surface phased array probe.
- Rotate the rotor and push the phased array probe down the bore hole (see Figure 5-44).
- Plot data in polar coordinates (see Figure 4-13, p. 174).

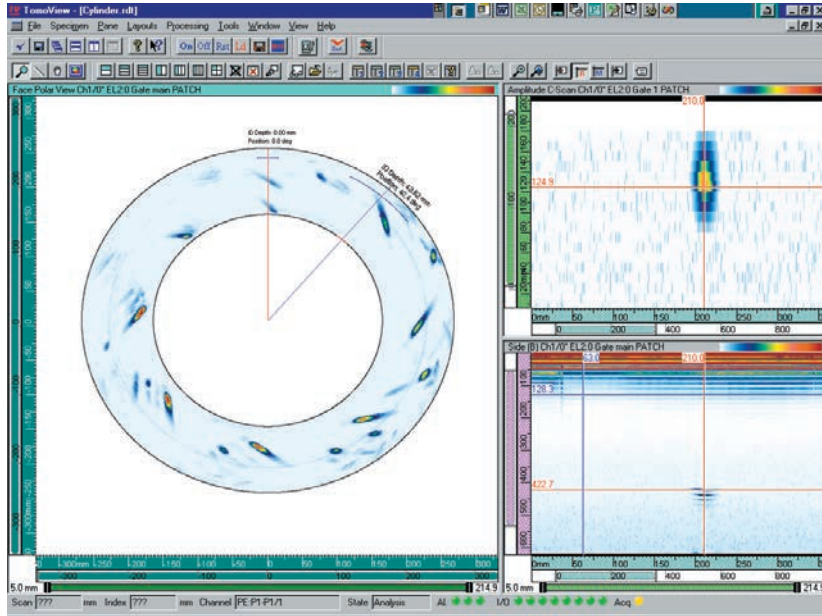


Figure 5-44 Phased array boresonic inspection (*top*) and ultrasonic data presentation in polar view (*bottom*).

## 5.6.9 Detection and Sizing of SCC in Low-Pressure Turbine Components

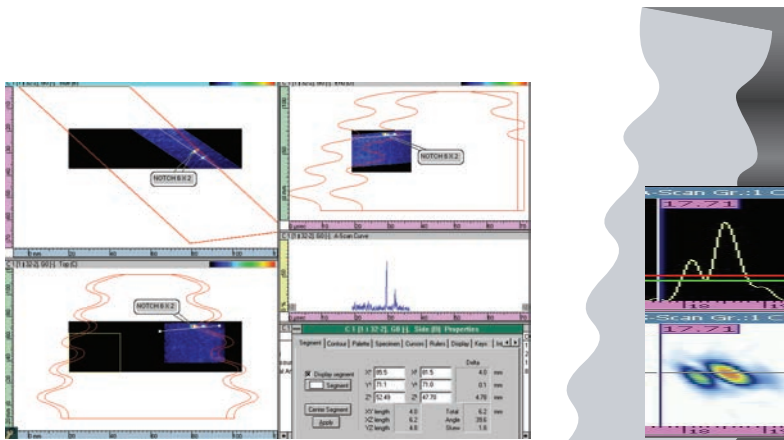
a) *NDT problem and challenges*

- Detecting and sizing SCC in rotor steeple and blade roots (rows 0 and 1)
- High productivity (7,500 inspection locations over 5 days)
- High reliability (must avoid false calls and de-blading)
- Small defect sizes ( $3 \times 1$  mm,  $5 \times 1$  mm,  $4 \times 1.5$  mm,  $9 \times 0.5$  mm,  $9 \times 2$  mm)
- Limited probe movement

- Variable ultrasonic range (12–130 mm, 10–90 mm, 60–100 mm, 2–45 mm)

**b) Phased array solution**

- Use PASS to optimize the probe design.
- Use high-frequency linear arrays (6 MHz to 12 MHz).
- Use ray tracing to optimize the focal laws.
- Use multiplexed box to pulse four phased array probes on four L-1 steeples and three phased array probes on five hooks of L-0 steeples.
- Manufacture custom probes and scanners for each component.
- Use multiple phased array systems and network data transfer for real-time analysis.
- Combine automated and manual phased arrays (Tomoscan III, Tomoscan FOCUS, OmniScan).
- Plot ultrasonic data on 2-D specimen overlay (see Figure 5-45 and Figure 5-46).



Courtesy of Ontario Power Generation, Canada, and GEC ALSTOM

**Figure 5-45** Plotting phased array data in L-0 blade 2-D layout (*left*) and OmniScan detection and sizing of 9 mm × 0.5 mm EDM notch on hook 1 L-0 steeple (*right*).



Courtesy of Ontario Power Generation, Canada

**Figure 5-46** Detection and sizing principle for L-1 steeples: hook 1 (a) and (b); typical display (c); inspection with multiple phased array systems: Tomoscan FOCUS (d), OmniScan (e), and Tomoscan III (f).

### 5.6.10 Detection and Sizing of SCC in Disc Rim-Blade Attachment—GE Style

#### a) NDT problem and challenges

- Detecting and sizing small SCC in low-pressure turbine rotor disc rims (see Figure 5-47)
- Developing image recognition for SCC versus corrosion pits
- Inspecting 6 to 10 discs (one LP rotor) in 1 to 2 days
- Using phased array results as a reliable life-assessment tool

#### b) Phased array solution

- Single- or double-arm phased array probe

- High frequency: 6 MHz to 10 MHz, longitudinal waves
- Scanning pattern using volume-corrected S-scan with shadowing and skip (see Figure 5-48)
- Amplitude-based analysis tool for assistance
- Use Tomoscan III with compression and high acquisition rate.
- Use an angular resolution of  $0.3^\circ$  to  $0.5^\circ$ .
- Scroll  $3^\circ$  to  $4^\circ$  upward/downward from the best detection and use advanced imaging.

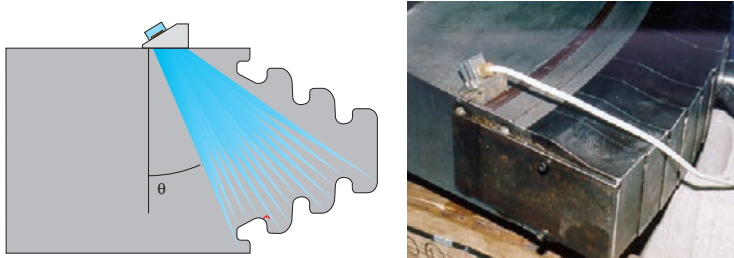


**Figure 5-47** Phased array scanning pattern (*left*) and 10-MHz phased array probe of 32 elements on mock-up (*right*).

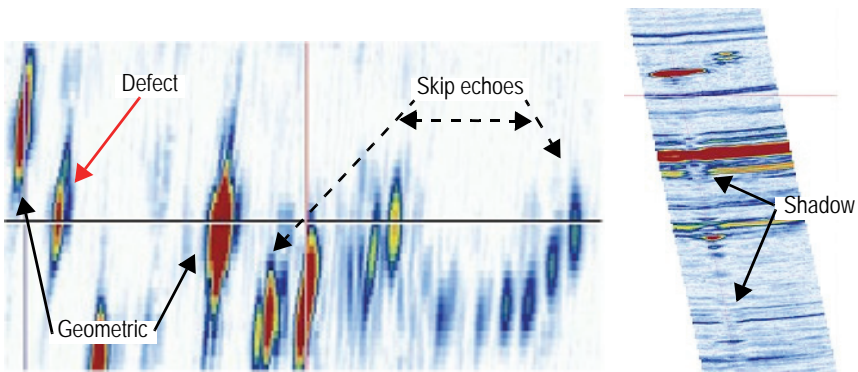


**Figure 5-48** Skip crack signals (*left*) and shadowing effect on geometric signals (*right*).

### 5.6.11 Detection and Sizing of Fatigue Cracks in Blade Roots—Axial Entry Style

#### a) NDT problem and challenges

- Detecting and sizing small fatigue/SCC cracks in blade roots

- Complex geometry with limited access
- High reliability
- High productivity
- Adjusting the scanner to different curvatures and blade sizes

**b) Phased array solution**

- Use ray tracing to validate the focal laws and optimize the S-scan approach.
- Use high frequency linear/matrix phased array probes (7 MHz to 10 MHz).
- Plot data onto 2-D blade specimen overlay (see Figure 5-49).
- Develop and commission a custom scanner.

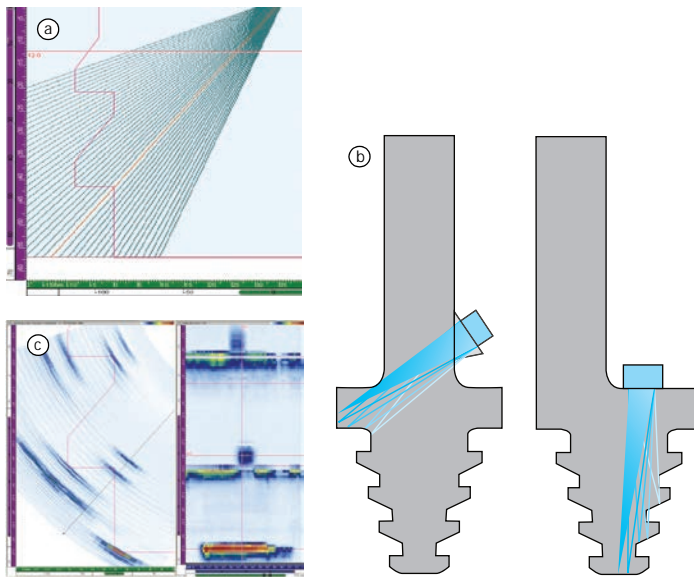


**Figure 5-49** Phased array inspection of blade root (axial entry): (a) ray tracing; (b) ultrasonic techniques; and (c) ultrasonic data plotted on 2-D specimen overlay.

## 5.7 Pressure Vessel Construction Weld Inspection

This section describes some of the pressure vessel inspections that can be performed using phased arrays, starting with relevant codes.

## 5.7.1 Inspection Codes for Pressure Vessels

Typically, pressure vessels are inspected using the ASME or a related code. The precise code depends on the application.

1. The **ASME code** family provides the basic scanning pattern for most inspections. This approach uses one or two fixed angle transducers scanned over the weld, the heat-affected zone, and the nearby parent plate. Typically, two angles are used. One is often a 45° shear wave, which is optimal for detecting surface-breaking defects through corner reflections. The other angle must differ by at least 10°. The angles should be selected as appropriate for the component and weld to be inspected. The beams are “rastered” over the weld and adjacent area, and then stepped along the weld to repeat. Beam coverage requirements are dictated by codes.
2. **ASME TOFD:** ASME Code Case 2235 is a unique code that permits the use of automated time-of-flight diffraction (and pulse echo) for welds greater than 12.7 mm (½ in.). TOFD is a very useful technique that has good detection capabilities in the mid-wall region and it offers the best sizing readily available. However, TOFD is somewhat difficult to interpret, and has significant dead zones on the OD and ID. There is presently no North American code regulating the application of TOFD. The European Union and United Kingdom have two codes (BS7706:1993 and ENV 583-6), and the ASME and ASTM are working on draft versions. The ASME has made a “generic” acceptance criterion based on information obtained from TOFD (Code Case 2235). ASME 2235 requires a performance demonstration.
3. **Line Scanning Codes:** These include API 5L and similar codes for line pipe. The most relevant linear scanning code is ASTM E-1961 for pipeline girth welds. This is essentially the only ultrasonic code written for automated ultrasonics, and uses a novel technique called “zone discrimination” for narrow-gap pipeline welds. Zone discrimination divides the weld into vertical zones, each inspected by a focused, angled beam. The inspection head then runs round along the weld in a linear path. Either phased arrays or conventional ultrasonics can be used. ASTM E-1961 is compatible with ASME codes.

Phased array technology permits major changes in the inspection approach for pressure vessels. Instead of back-and-forth raster scanning (which is slow and restricted), phased arrays allow linear scanning at selected angles to optimize PoD and minimize time. The linear scanning philosophy is shown in Figure 5-50.

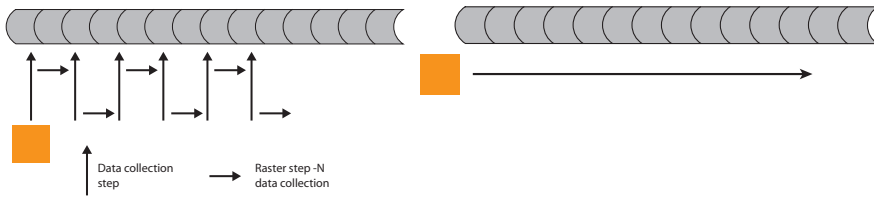


**Figure 5-50** Schematic showing conventional raster scanning (*left*), and phased array linear scanning (*right*). The array on the right uses electronic scanning (or electronic rastering) and linear scanning to give full weld coverage and code compliance.

The advantage of phased arrays is that multiple angle scans can be performed, or tailored angles can be used as appropriate. Figure 5-51 shows a phased array electronic scan using 45° and 60° ASME-type rasters from a single linear phased array probe using a linear scan and electronic rastering.

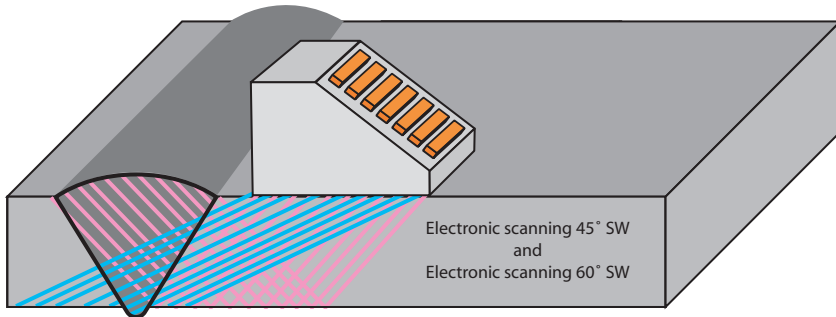


**Figure 5-51** Schematic showing two different angle inspections using phased arrays and electronic scanning. The same array also performs TOFD.

There are many different approaches for inspecting pressure vessels to code compliance. The inspection techniques and procedures will depend on the component, costs, wall thickness and diameter of the part, expected duty cycle, and particularly any fitness-for-service requirements.

The various approaches include:

- TOFD (in conjunction with pulse echo for the surfaces and near-surface regions) [see section 5.7.2];
- ASME raster pulse-echo, also with TOFD (see section 5.7.3);
- Advanced inspection systems with multiple and redundant NDT systems (see section 5.7.4);

- Zone discrimination, as used in pipelines (see section 5.8).

The general challenges facing pressure vessel inspections are listed below. For each technical solution, the specific challenges and advantages are listed separately in each section.

*a) General NDT problems and challenges*

- Reliably detect construction welding defects of characteristic orientation
- Perform rapid inspections
- Display data in a meaningful manner
- Perform cost-effective inspections
- Provide data for engineering critical assessment (ECA) or fitness-for-purpose analyses
- Replace radiography and X-rays for safety reasons

*b) Phased array solutions*

- Use phased arrays to perform two or more angle beam inspections, plus TOFD.
- Use linear scanning to greatly increase inspection speed.
- Use “top, side, end” views or “top, side, TOFD” views for display.
- Use cursors to measure defect sizes for ASME.
- Use an appropriate delivery system:
  - magnetic wheel scanner
  - welding band for smaller diameters
  - rotating vessel
  - external robot
  - hand scanner
  - manual encoder

## **5.7.2 PV-100: Linear Scanning Using TOFD and PE**

*a) NDT challenges*

- Low-cost system required
- Portable system desirable
- Code compatibility essential
- Automation not essential

**b) Phased array solution**

- Use linear scanning with a hand scanner (see Figure 5-52 and Figure 5-53).
- Use low-cost phased array instrumentation, such as the OmniScan.
- Use low-cost labor; no automation to minimize cost.
- Adapt setup to compensate for delivery system inaccuracies.

**c) Limitations**

- Portable systems have limited capability compared to automated systems based on the Tomoscan FOCUS or Tomoscan III.
- Manual operators are not as accurate as automated delivery systems.
- Output displays are typically more restricted.
- Coverage is more limited than with full phased array systems (see section 5.7.3).

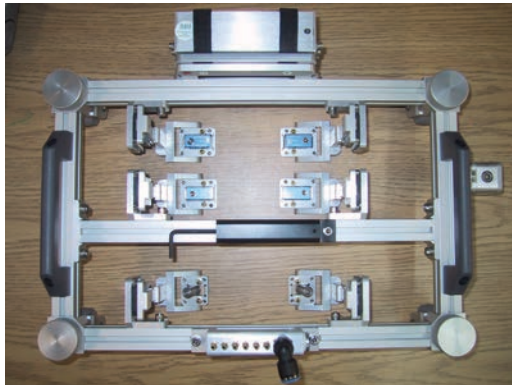


**Figure 5-52** Photo of an HST-X03 scanner. This unit contains conventional and TOFD transducers, but can also use phased arrays.

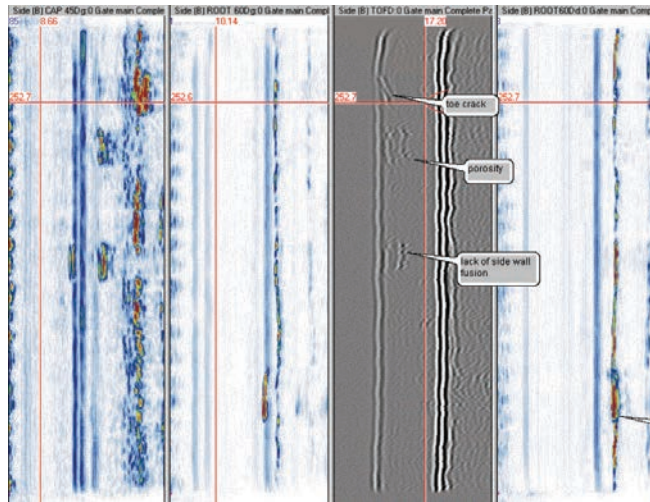


**Figure 5-53** Pressure vessel weld inspection by a combination of pulse echo and TOFD.

**Note:** There are advantages to having multiple inspection techniques. For example (in Figure 5-53), TOFD missed the lack of root fusion, but it was detected using PE.

### 5.7.3 PV-200: Versatile Phased Array and TOFD System

#### a) NDT challenges

- Versatile system for the inspection of a wide range of pressure vessel wall thicknesses and geometries to many codes
- Automated, semiautomated, and manual system
- Capable of many different inspection procedures: pulse echo, TOFD, zone discrimination, multiple NDE techniques
- Can utilize many different scanners
- High-speed scanning and data collection
- Software capable of detailed defect analysis

#### b) Phased array solution

- Use Tomoscan III for high data collection rates (see Figure 5-54).
- Perform electronic scanning, linear scanning, zone discrimination, and TOFD as required (see Figure 5-55).

- Interface with appropriate scanner, such as TRAKER (see section 5.7.5).
- Use TomoView 2 software for detailed data analysis: for example, “top, side, end” view, “top, side, TOFD” view, and 3-D cursors (see Figure 5-56 and Figure 5-57).
- Very flexible solution



**Figure 5-54** Tomoscan III inspection system for major pressure vessel inspections.

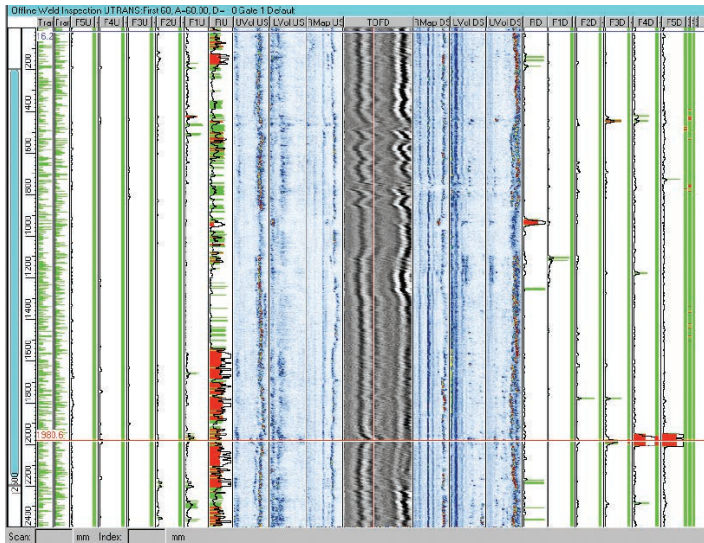


**Figure 5-55** Display of zone discrimination weld inspection using TomoView (see section 5.8).

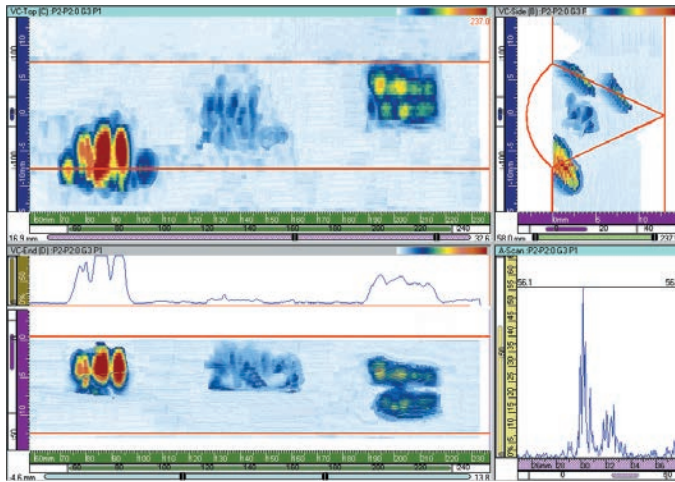


**Figure 5-56** Typical “top, side, end” view of weld with weld overlay showing precise location of defects.

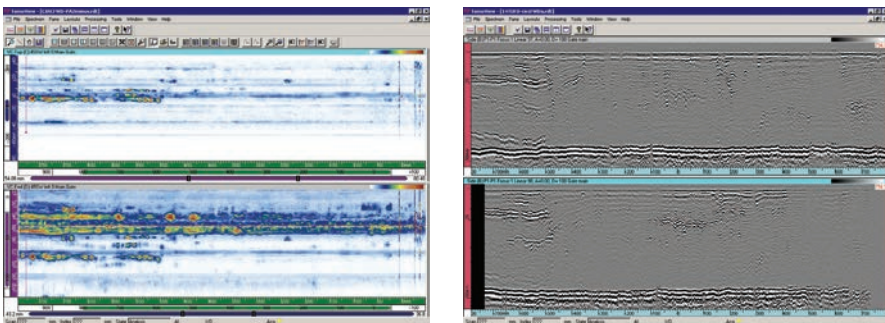


**Figure 5-57** “Top, side, TOFD” view of weld. This example uses merged data in the C-scan and B-scan, and twin TOFD pairs for improved defect detection and sizing.

## 5.7.4 PV-300: Premium Inspection System Using Ultrasonics, Phased Arrays, and Eddy Current Arrays

### a) NDT challenges

- Provide an NDT system with maximum PoD capability for critical fitness-for-service components
- Provide 200% NDE capability, that is, two NDE systems for each region (surfaces, near surfaces, mid-wall) [see Figure 5-58]

- System must have flexibility for many different scan types, weld profiles, and inspection requirements.
- Detect both axial and transverse defects
- Provide automated surface inspection system
- Provide good reporting for regulator and fitness-for-purpose applications

***b) Phased array solution***

- Use multiple phased array instruments for axial scans to improve beam forming.
- Use additional phased array instrument at 45° and 70° for transverse defects.
- Use pulse echo, zone discrimination, tandem, and TOFD to maximize PoD.
- Use double dedicated TOFD units to further increase PoD.
- Use improved beam forming for back diffraction and TOFD for sizing.
- Use eddy current (EC) arrays for surface and near-surface defect detection.
- Customize the inspection head to the application; automated inspection only possible due to size and weight.

***c) Advantages of PV-300 system (see Figure 5-59)***

- Double (redundant) NDT for all regions:
  - Pulse echo and EC arrays for surfaces
  - Tandem, TOFD for mid-wall regions
  - Double TOFD pairs for better mid-wall PoD and sizing
  - Dual shear waves for transverse defects
- Increased number of elements permitting detailed inspections of thicker walled vessels
- Highest possible PoD for critical components
- Optimum and redundant defect sizing for fitness for purpose

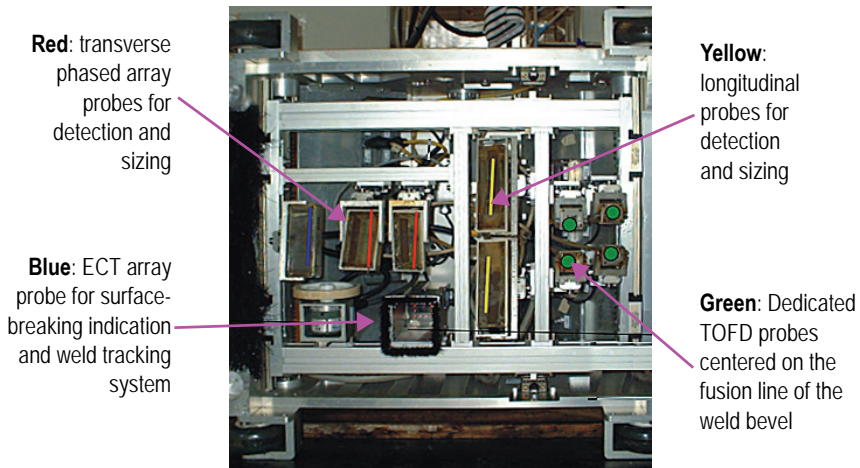


**Figure 5-58** Schematic showing layout of arrays for PV-300 premium pressure vessel inspection system.



**Figure 5-59** Photos of PV-300 probe pan (*left*), and cabinet containing three Tomoscan FOCUS or Tomoscan III systems, EC array instrumentation, and coupling system (*right*).

### 5.7.5 Typical Pressure Vessel Mechanics

Figure 5-60 to Figure 5-65 show examples of various mechanical delivery systems. The choice of delivery system depends on the application, budget, etc.

*a) Rotating vessel*



**Figure 5-60** Example of rotating vessel for phased array inspection of pressure vessels under construction using a fixed head containing two linear arrays with linear and electronic scanning.

*b) Welding band for pipes of less than ~2 meters (~64 in.) diameter*



*Courtesy of Canspec, Canada*

**Figure 5-61** Pipeline welding band and probe pan. This pan contains two well-protected linear phased array probes and can significantly outperform competing multiprobe technologies.

c) *Magnetic wheel scanners*

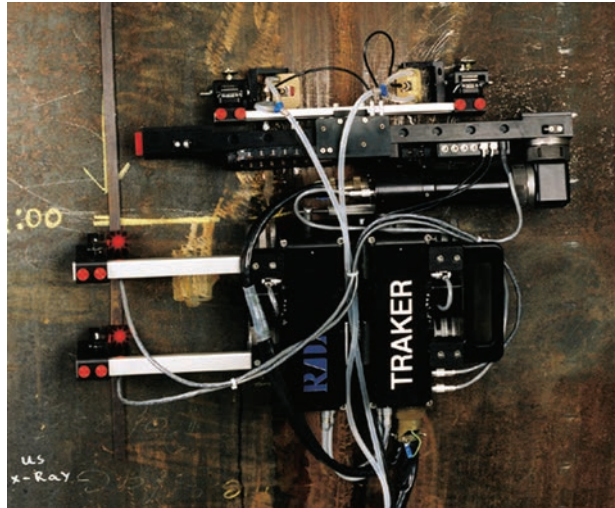


**Figure 5-62** Magnetic wheel scanner performing a linear weld scan using two arrays in pulse echo and TOFD. This scanner (TRAKER) follows a magnetic strip, and can inspect nozzles and complex components as well.

d) *Hand scanner*



**Figure 5-63** Hand scanner for weld inspections. This version contains either phased arrays or multiple conventional transducers (see "Rapid Detection TECHnique" in section 4.2.10, p. 186, and "PV-100" in section 5.7.2, p. 233).

e) *Robotic scanner*

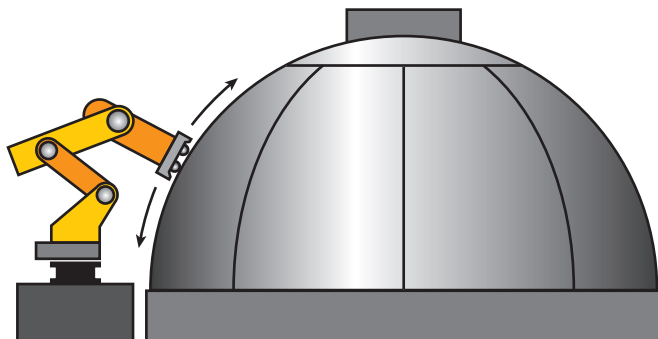


**Figure 5-64** Schematic showing robot inspecting complex curved vessel. Probe pan holds two arrays for pulse echo and TOFD.

*f) Manual encoder for scans performed by hand*

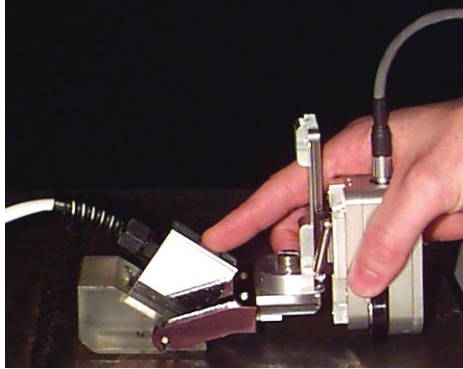


**Figure 5-65** Single (or double) array with encoder, the semiautomated solution. This is the simplest and cheapest solution for linear scanning using phased arrays.

## 5.8 Pipeline Phased Arrays

This section covers various types of inspections used in the pipeline AUT (automated ultrasonic testing) market. Phased arrays offer significant advantages over the competing multiprobe technology.

### 5.8.1 Standard Pipeline Zone Discrimination

More information about standard pipeline zone discrimination can be found in references 3, 5, and 14.

*a) NDT problems and challenges*

- Rapidly and reliably inspect narrow-gap gas pipeline welds with ultrasonic zone discrimination (see Figure 5-66 and Figure 5-67)
- Reliably detect defects of a few percent of wall thickness
- Detect defects that have a distinctive orientation, specifically near-vertical LoF
- Size to within  $\pm 1$  mm or so (depending on application)
- Accept or reject weld in near real time (see Figure 5-68 and Figure 5-69)

**b) Phased array solution**

- Use two linear phased arrays on either side of weld to perform pulse-echo, tandem, and TOFD inspections, plus any “special” techniques (see Figure 5-70 and Figure 5-71).
- Use highly focused beams to optimize PoD and sizing.
- Perform zone discrimination, as per code ASTM E-1961-98.
- Scan at 100 mm/s and display strip charts.
- Show both amplitude and TOF in gate to locate defects.
- Use colored threshold to observe recordable defects in real time.
- Display results on screen and save to disk in real time.
- Use lookup table to accept or reject defects very quickly.

**c) Phased array advantages vs. conventional multiprobe ultrasonics**

- Automated setup procedures (see Figure 5-72)
- Linear scanning with increased number of zones (see Figure 5-73)
- Better beam shaping and imaging (see Figure 5-74)
- Flexibility for a wide range of pipe dimensions (wall, diameter, weld profile)
- Cost-effective operation due to faster setups
- Reduced operating costs due to lower equipment inventory (“One size fits all”)
- Great for specials, such as seamless pipe, cladding, thick-walled pipe, small-diameter pipes, quality inspections
- Telemaintenance: phased arrays can be operated from Olympus via the Internet anywhere in the world for setups and repairs.

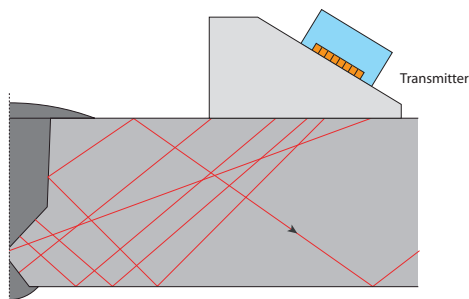


**Figure 5-66** Schematic of zone discrimination concept showing slicing of CRC-Evans weld into zones with correctly angled and focused beams to detect LoF and other defects.



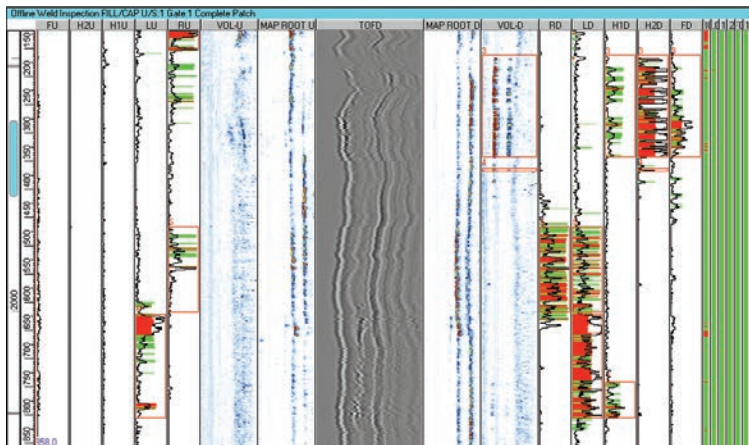


**Figure 5-69** Zone discrimination display from pipelines. Above-threshold defects are in red, while coupling and low-level signals are in green. Real-time readout provides defect location, position, and length.



**Figure 5-70** PipeWIZARD phased array system showing instrumentation box (computer, Tomoscan FOCUS, driver box), 21-in. monitor, and keyboard.



**Figure 5-71** Phased array probe pan containing two well-protected linear arrays. Umbilical contains the 128 micro-coaxial cables, power, encoder, and water line for coupling.

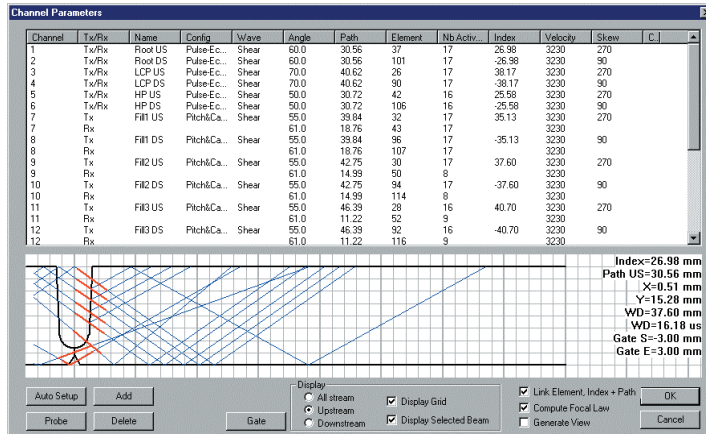


**Figure 5-72** Automated setup procedure for pipeline or general weld phased arrays. Operator inputs weld profile via AutoCAD or drawing, and phased array system calculates focal laws and setup.

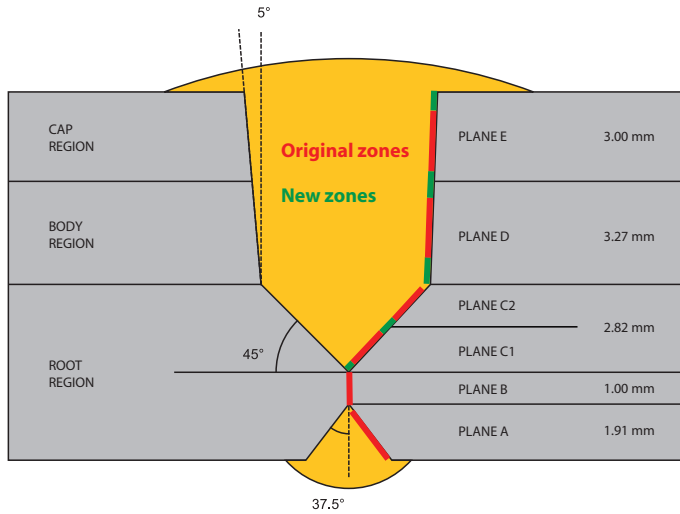


**Figure 5-73** Beam-splitting. Additional zones can be added using phased arrays to improve coverage and sizing. This advantage is unique to phased arrays, as the number of available channels limits multiple probes. (PipeWIZARD can use up to 128 individual channels.)

POD comparison for five qualification welds

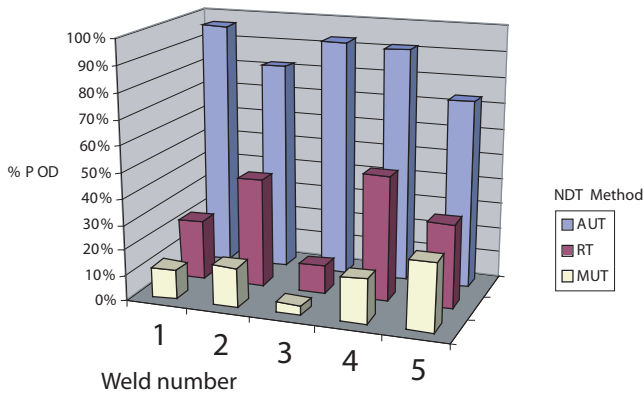


**Figure 5-74** Results comparing AUT, radiography, and manual ultrasonics from one pipeline study. Detection by AUT is much better than either radiography or manual ultrasonics due to focused beams and appropriately oriented inspection angles.

## 5.8.2 Seamless Pipe Girth Welds

### a) NDT problems and challenges

- Seamless pipe is often used offshore.
- Wall thickness can vary by as much as  $\pm 12\%$ .
- Big thickness variations will seriously impair AUT zone discrimination approach (see Figure 5-75).
- Conventional raster scanning is too slow.

### b) Phased array solution

- Use multiple setups to cover all wall thickness variations.
- Run setups simultaneously.
- Operator measures wall thickness from TOFD channel and selects appropriate display to evaluate accordingly (see Figure 5-76).

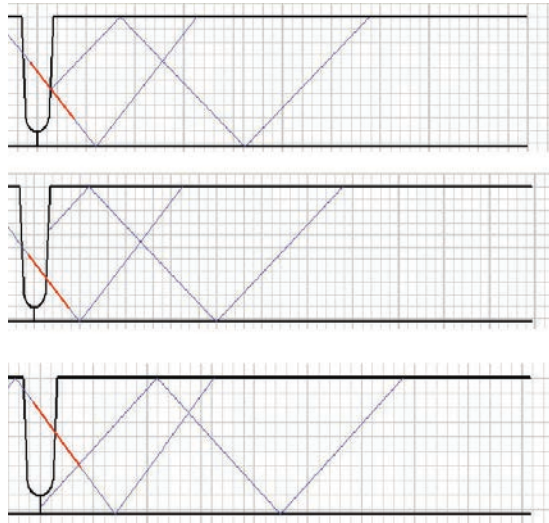
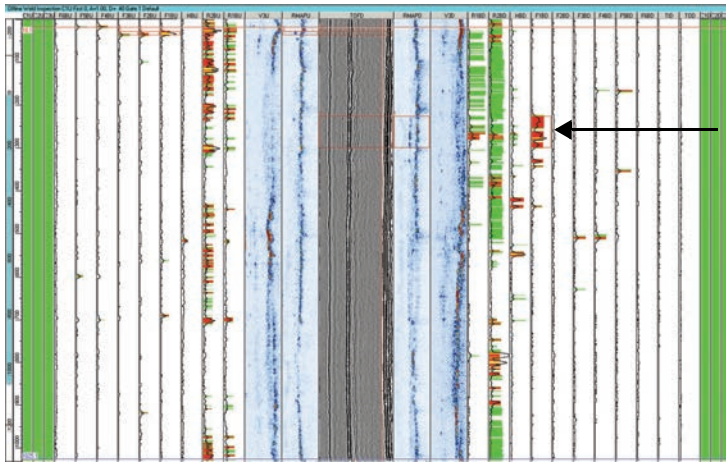


**Figure 5-75** Ray tracing beam paths for nominal, maximum, and minimum walls. Note that predicted beams will miss defects if the wrong wall thickness view is analyzed.



Courtesy of Total, and Oceaneering International

**Figure 5-76** Phased array display from nominal wall setup showing defect (arrow). This was an unacceptable defect. Note that TOFD detected the defect in all three views, but only this view found the defect in pulse echo.

### 5.8.3 Risers and Tendons

#### a) *NDT problems and challenges*

- Very high reliability inspection is required.
- Pipe walls are thick, up to 50 mm.
- Optimum inspection angles vary according to location in weld.
- Probability of detection required is very high.
- Sizing requirements are extremely demanding.
- Relatively high inspection speed is required.
- Full documentation is needed.

#### b) *Phased array solution*

- Use modified version of zone discrimination with many extra channels.
- Appropriate angles are used to detect defects in different parts of weld.
- Many extra beams used in selected areas (root and cap, for example) to ensure good PoD (see Figure 5-77, Figure 5-78, and Figure 5-79).

- Special sizing techniques used to improve accuracy, especially back diffraction. Also includes standard TOFD and zone discrimination sizing.

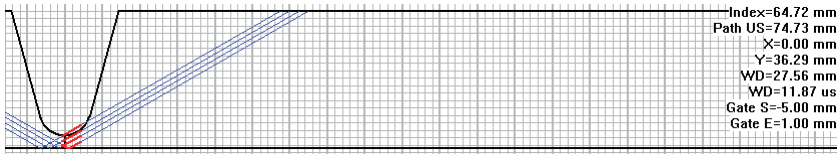


**Figure 5-77** Ray tracing showing extra beams in root to improve detection and sizing.

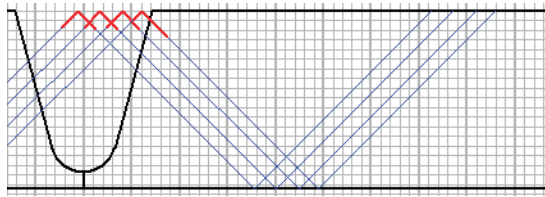


**Figure 5-78** Ray tracing showing extra beams in cap area.

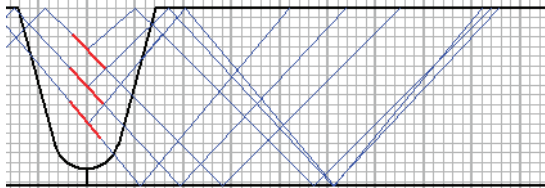


**Figure 5-79** Ray tracing showing additional beams in mid-wall region to detect any shrinkage cracking.

**c) Advantages of phased arrays over multiple probes**

- Phased arrays can use many more beams: 84 vs. 26 in this application.
- Standard phased array technology can work on thicker walls, with relative ease.
- Phased arrays allow many more hits in root and cap, the critical areas.
- Phased arrays can use a variety of angles in one area (root, for example) in order to ensure better PoD.

- Phased arrays are better suited to new sizing techniques, like back diffraction.

## 5.8.4 Small Diameter Piping

### a) *NDT problems and challenges*

- Single-angle inspection not enough for quality weld inspection
- Major geometric constraints often present (for example, other piping nearby)
- A go-no-go acceptance system required
- Need for portable, cost-effective delivery system
- High inspection speed essential

### b) *Phased array solution 1*

- Use a special scanner for PipeWIZARD system (or Tomoscan FOCUS or Tomoscan III) [see Figure 5-80].
- Use small arrays if geometry dictates it.
- Use special probe pans.
- Generate multiple angles in appropriate locations.
- Program for a go-no-go acceptance.

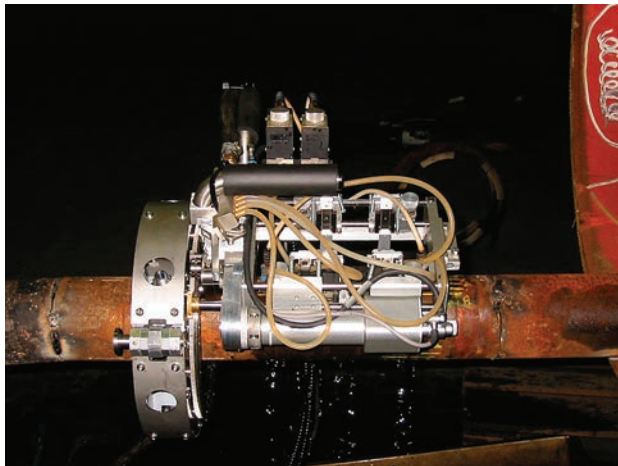


**Figure 5-80** Photo of ring-type scanner for pipes 2.5 in. to 16 in. (63 mm to 400 mm) in diameter.

*c) Advantages of solution 1*

- Convenient if you already own a PipeWIZARD, Tomoscan FOCUS, or Tomoscan III
- Provide very high quality inspections
- Fast
- Excellent displays, data analysis, scanning options, and reporting

*d) Phased array solution 2*

- Use a custom orbital scanner for delivery system (see Figure 5-81 and Figure 5-82).
- Use an OmniScan for fully portable solution.
- Low cost
- Better inspection than conventional ultrasonics, but less capability than phased array solution 1 above

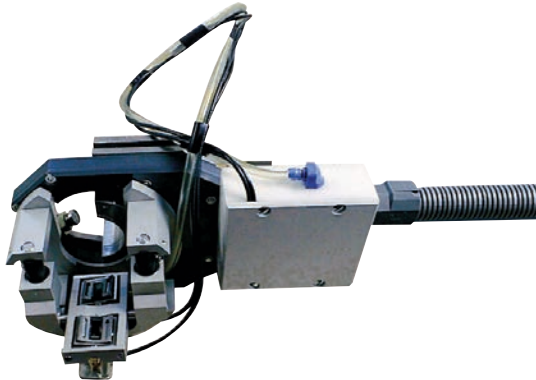


**Figure 5-81** Photo of typical orbital scanner head with two gimbal arrays visible. Scanner clamps on pipe and arrays rotate around them.



**Figure 5-82** Photo of scanner clamped onto boiler tubes during construction inspection.

## **5.9 Miscellaneous Applications**

This section describes a variety of applications that occur in a number of industries, yet are unique. Stress corrosion cracking (a specific type of failure mechanism) is an example.

### **5.9.1 In-Service Inspection of Pipe for Stress Corrosion Cracking**

The OmniScan is used for pipe weld inspection to detect stress corrosion cracking (SCC) in heat-affected zones (see Figure 5-83).



**Figure 5-83** Inspection of pipe welds in a refinery with an OmniScan: on site (*left*); OmniScan with S-scan display (*right*).

For this application, S-scans are normally used since SCC reflects at multiple angles.

## 5.9.2 Seam Weld Inspections of Coiled Tubing for Offshore Petrochemical Applications

More information about seam weld inspections of coiled tubing for offshore petrochemical applications can be found in reference 8.

### *a) NDT problems and challenges*

- Reliable detection required for high-speed testing of seam welds in coiled tubing
- Variable thickness and tube OD dimensions (ovality)
- Need to satisfy ASTM 273 and API 5LCP code requirements
- Weld geometry echoes from internal flash
- Quick identification of weld defect zone required

### *b) Phased array solution*

- Use two linear phased array probes for weld inspection and four for conventional thickness measurements (see Figure 5-84).
- Use custom algorithm to subtract the weld geometric echo (see Figure 5-85).
- Preshape the probe aperture to accommodate the tube average diameter.

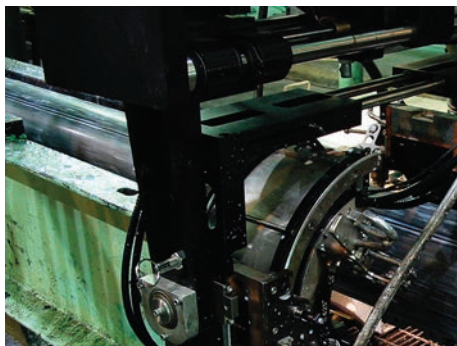
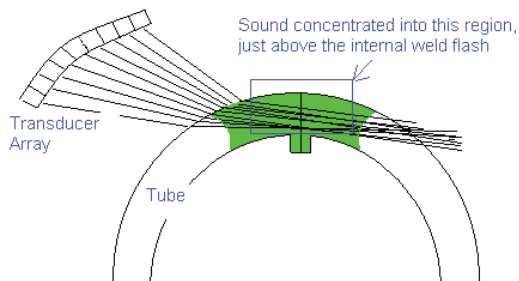


**Figure 5-84** Phased array inspection of coiled tube seam weld: principle (*top*) and industrial system (*bottom*).

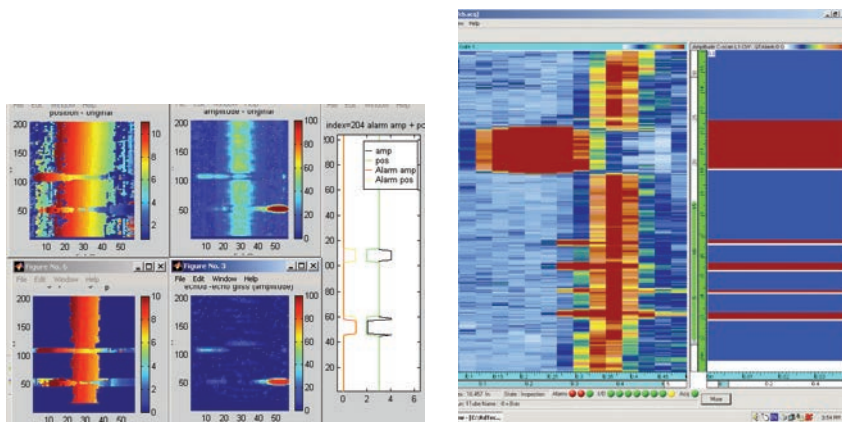


**Figure 5-85** Phased array data display with software algorithm for internal geometry weld echo removal (*left*); online ultrasonic display (*right*).

### 5.9.3 T-Weld Inspection of Bridge Structure

#### a) *NDT problems and challenges*

- Weld thickness between 10 mm and 16 mm
- Reliable detection of linear defects (cracks, LoF, LOP) essential
- Multiple angles required
- Limited probe movement (within 37 mm or 1.5 inch)
- Cost-effective solution required

#### b) *Phased array solution*

- Use an OmniScan and manually encoded array (see Figure 5-86).
- Use a linear phased array probe (5 MHz, 16 elements).
- Perform linear scan with a S-scan  $40^\circ$  to  $70^\circ$  on each side of the weld.
- Use real-time display of A-scans and S-scans.

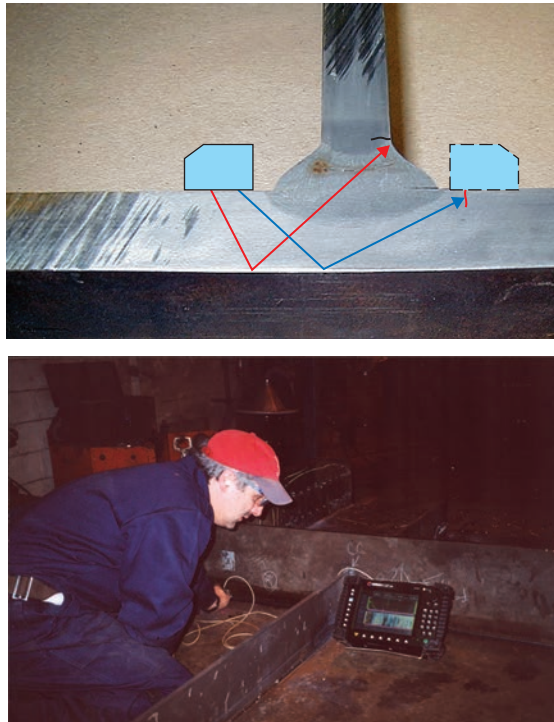


**Figure 5-86** Inspecting T-welds using an OmniScan and a manually encoded array. Inspection procedure (*top*); field inspection (*bottom*).

## 5.10 Mills and Manufacturing

This section describes applications specific to the pipe mills and manufacturing industries, which are typically interested in high production and functional convenience.

### 5.10.1 ERW Pipes Using Phased Arrays

#### a) *NDT problems and challenges*

- ERW (electric-resistance-welded) piping is used for a large variety of pipes with OD varying from 25 mm to 175 mm (1 in. to 7 in.), and wall thicknesses varying from 1 mm to 6 mm (0.040 in. to 0.250 in.).
- High-speed testing: 2 m/s (400 ft./min)
- Weld line wander:  $\pm 30^\circ$
- Weld geometric constraints: OD bead-scarfed, ID bead-scarfed or unscarfed
- High reliability of detection specified: ID/OD notches 5%  $t$ , 1/8-in. and 1/16-in. drill hole
- Code requirements: API 5LX, CSA 662
- Defects to be detected: hook crack, penetrator, lack of fusion, and cold weld
- Inspection angles: 45° and/or 70° shear wave
- Reports about weld quality and weld profile control

#### b) *Phased array solution*

- Acoustic approach for weld quality inspection:
  - One phased array probe on each side of the weld for CW and CCW inspection
  - Beam deflection to select the appropriate inspection angle
  - Electronic scanning for the full length of each probe
  - Inspection angle from 35° SW to 70° SW
  - 0° LW for coupling check
  - Phased array probes of 128 elements each
- Acoustic approach for weld profilometry:
  - One phased array probe on top of the weld to cover the weld-line wander
  - Electronic scanning for the full length of each probe

- Mechanical requirements:
  - Cover diameters ranging from 15 mm to 170 mm
  - Water cell for local immersion
  - Allow continuous inspection while the 1/8-in. butt weld crosses the UT water cell
  - Allow continuous inspection while the “window” crosses the UT water cell (only in some cases)
  - Include four degrees of freedom to adapt to tube movement
  - Water cell with unique auto-centering capability
  - Positioning table to adapt to all diameters

c) *Phased array system requirements*

- Software:
  - Dedicated software with tube wizard, plus operator and supervisor levels
  - Load setup for complete system configuration
  - Tube wizard for new tube diameters and wall thicknesses
  - Function for electronic detection of the optimum inspection angle
  - Function for electronic adjustment of the sensitivity
  - Alarm data available on Microsoft Access data table
  - A-scan display and strip chart
- System performance:
  - Defect detection: hook crack, ID/OD 5% notch, penetrator
  - Weld profilometry: accuracy; 0.0254 mm (0.001 in.)
  - Inspection speed: detection of the 1/8 in. drill hole at 2 m/s
- List of items:
  - 2 QuickScan PA 16:128 units
  - 1 industrial computer (including a monitor) with remote maintenance
  - 1 dedicated tube wizard software
  - 4 phased array probes for weld quality to cover diameter ranges from 25 mm to 125 mm in three ranges
  - 1 UT head assembly
  - 1 positioning table
  - 1 guiding and protection mechanism
  - 1 water coupling system
  - 1 console and industrial housing

- 1 basic PLC
- 1 integration, setup, test on sample
- Options:
  - One extra UT head
  - Profilometry function; one extra QuickScan PA 16:128 with one UT probe
  - Extra PA probes

*d) In-line applications (see Figure 5-87 and Figure 5-88)*



*Courtesy of IPSCO, Canada*

**Figure 5-87** Phased array inspection of ERW pipes: principle, probe, and weld wander.

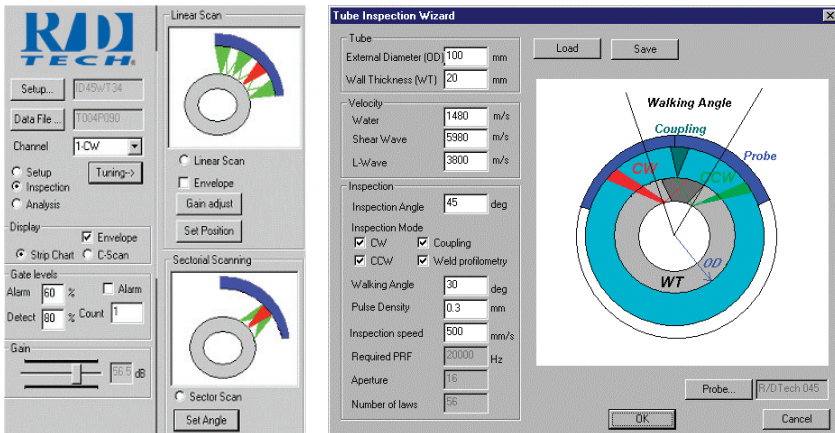
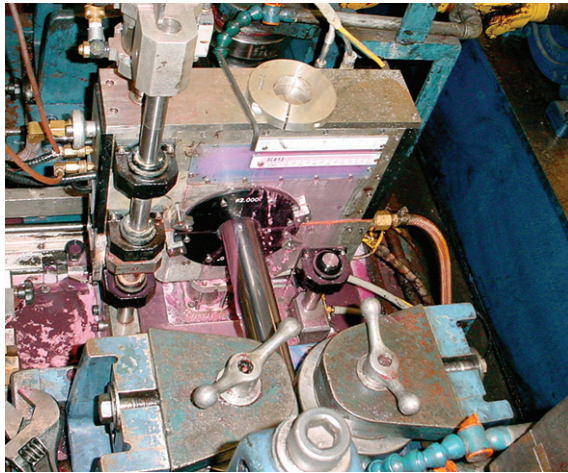


**Figure 5-88** Phased array industrial system for ERW pipe (top) and parameter adjustment (bottom).

## 5.10.2 Volumetric Phased Array Inspection of Bars

### a) NDT problems and challenges

- Typical inspection requirements:
  - Type of material: carbon steel, bearing steel, spring steel, nickel-based steel
  - Line speed: 1 m/s
  - Diameter range: 15 mm to 75 mm (0.55 in. to 3 in.)
  - Code requirement: application program interface (API)

- Bar length: 2 m to 10 m
- Straightness of bar: up to 4 mm/m (precentering device to reject bent bars)
- Volumetric inspection: longitudinal waves at 0° and angled
- Surface inspection: shear waves at optimized angle to detect surface defects.
- Distance between bars: 1.2 m to 1.5 m
- Length of ends not inspected: <50 mm
- Defects to be detected
  - Calibration: FBH 0.7 mm or equivalent SDH
  - Detection of calibration defect: 0.35 mm × 5 mm
  - Defect: volume defects caused by the manufacturing process.

***b) Phased array solution***

- Acoustic approach for the inspection of bars:
  - Four phased array probes covering 90° each
  - High-accuracy centering during inspection
  - Beam focus at different depths according to the bar diameter
  - Electronic beam rotation through 360°
  - One set of four phased array probes to cover a diameter variation of 25 mm.
- Mechanical requirements:
  - Cover diameters ranging from 10 mm to 100 mm
  - Water cell for local immersion
  - Continuous inspection with minimum untested bar end
  - Four degrees of freedom to adapt to tube movement
  - Water cell with unique autocentering capability
  - Positioning table to adapt to all diameters
  - Pinch roller and automation with PLC to close and open powerful roller

***c) Phased array system capabilities***

- Software:
  - Dedicated software with bar wizard, plus operator and supervisor levels
  - Setup loading for complete system configuration
  - Bar wizard for new bar diameter and wall thickness

- Electronic scanning function for sensitivity adjustment of each probe
- Automatic calibration sequence
- Data available on Microsoft Access data table
- A-scan display and strip chart
- Performance of the system—defect detection:
  - Defect FBH 0.7 mm with SNR >15 dB
  - Defect 0.35 mm × 5 mm with SNR >12 dB
  - Inspection speed: 1.2 m/s
  - Length of ends not inspected: <10 mm
  - Setup loading for each diameter
  - Focusing at different depths according to the diameter of the bar to control
  - Volume inspection with a focused ultrasound beam adapted to each diameter
  - Inspection for surface defects using angle beam ultrasonics from 0.2 mm to 5 mm in depth

d) *In-line application (see Figure 5-89, Figure 5-90, and Figure 5-91)*

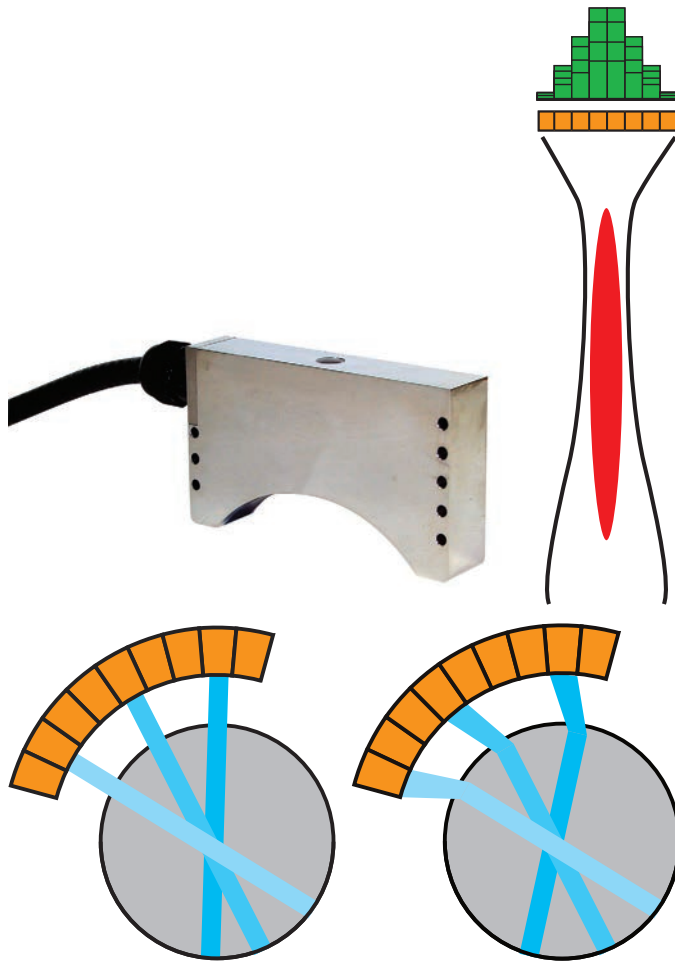


**Figure 5-89** Phased array solution for in-line rod inspection ( $0^\circ$  LW and SW angle beam inspection).

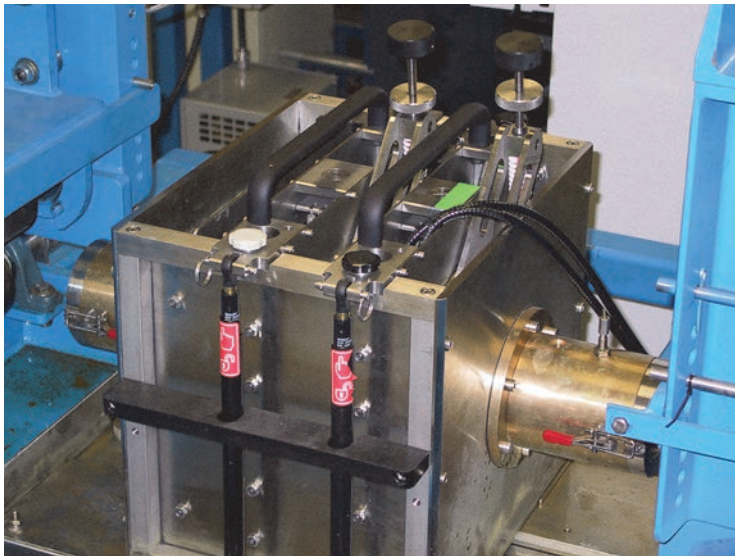
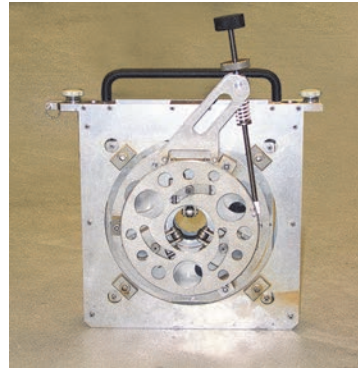
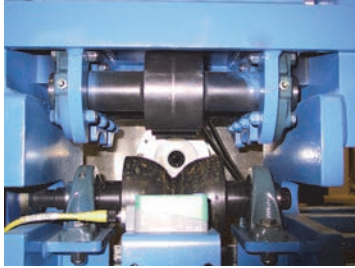
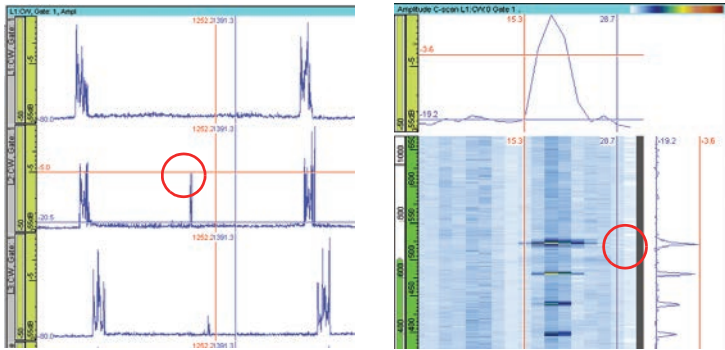


**Figure 5-90** Phased array system for in-line bar inspection.



Strip chart showing FBH defect at 0.35 mm.

For the supervisor level, A-scan, C-scan, and strip chart display. FBH 0.7 mm at different depths; 2 mm to 15.5 mm with SNR from 10 dB to 15 dB.

**Figure 5-91** Examples of phased array inspection results for in-line bar inspection.

### 5.10.3 Phased Array Inspection of Full-Body Pipe (In-line)

#### a) NDT problems and challenges

- Inspect a large variety of tubes (OD = 15 mm to 45 mm;  $t = 0.8$  mm to 5 mm)
- Inspect a large variety of pipes (OD = 50 mm to 500 mm;  $t = 2$  mm to 25 mm)
- Reliably detect small defects regardless of their orientation: defect height < 0.5 mm; length < 6 mm in tube/pipe body
- Reliably monitor the wall thickness and tube or pipe ovality
- High productivity: 0.5 m/s
- High reliability: 24 hours a day, 7 days a week
- Uninspectable tube or pipe ends must be less than 75 mm long.
- Setup time for another batch with different OD and thickness must be less than 30 minutes.

#### b) Phased array solution

- Longitudinal defects
  - Full coverage with 4 or 6 cylindrical phased array probes (128 elements):
    - 4 probes (diameters from 15 mm to 45 mm)

- 6 probes (diameters from 45 mm to 90 mm)
- Electronic scanning of up to 16-element apertures
- Electronic beam focusing on ID and OD (using water and metal path compensation)
- Interlaced clockwise and counterclockwise inspections
- Simultaneous firing of ultrasonic beams (see Figure 5-92)

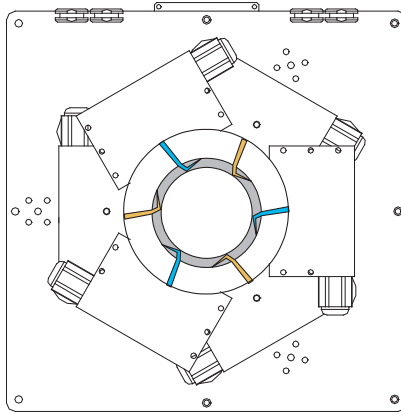


**Figure 5-92** Phased array inspection of tubes with six linear phased array probes for longitudinal defects.

- Transverse defects
  - Full coverage with four conical phased array probes (64 elements)
  - Mechanical beam deflection to generate SW
  - Electronic scanning of a 6-element aperture for virtual beam rotation
  - Electronic beam focusing on ID and OD (by water and metal path compensation)
  - Forward and backward axial inspections
  - Simultaneous firing of ultrasonic beams (see Figure 5-93)

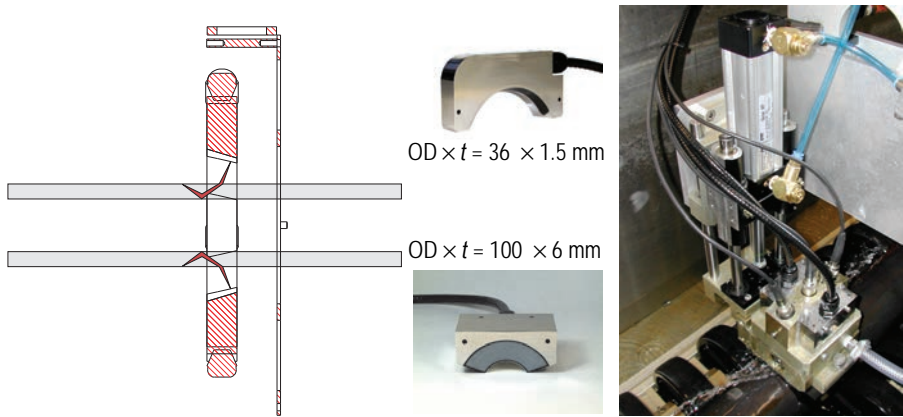


**Figure 5-93** Phased array principle for detecting transverse defects (*left*), two types of cluster probes (*middle*), and multihead assembly for pipe inspection (*right*).

- Dimensional gauging
  - Eight conventional probes (see Figure 5-94)
  - Dimensional measurements:
    - Inside and outside diameter
    - Wall thickness
  - Advanced dimensional measurements (optional):
    - Inside and outside diameter ovality
    - Wall thickness eccentricity
  - High resolution (up to 5  $\mu\text{m}$ )

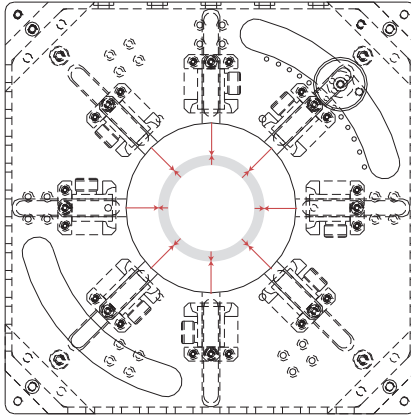


**Figure 5-94** Dimensional gauging with eight conventional probes.

*c) Phased array performance in industrial environment (see Figure 5-95)*

- Flaw type
  - Longitudinal flaws: 25 mm long, 0.2 mm deep
  - Transverse flaws: 10 mm long, 0.2 mm deep
- Flaw repeatability
  - Static test:
    - 2.0 dB ( $\pm 1.0$  dB) in longitudinal mode
    - 3.0 dB ( $\pm 1.5$  dB) in transverse mode
  - Dynamic test:
    - 3.0 dB ( $\pm 1.5$  dB) in longitudinal mode
    - 4.0 dB ( $\pm 2.0$  dB) in transverse mode
- SNR higher than 12 dB for all studied tubes (15 mm to 90 mm)
- Uninspectable beginning and end portions limited to 50 mm
- Inspection speed (advanced hardware configuration)
  - Up to 1.5 m/s in longitudinal mode only
  - Up to 1 m/s in mixed longitudinal and transverse mode
- Batch transfer time of less than 10 minutes

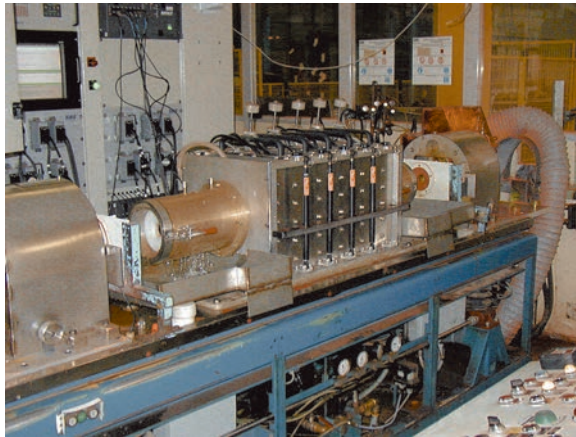


**Figure 5-95** Phased array inspection of tubes (pass-through, *top*) and pipes (rotating, *bottom*).

#### **5.10.4 Phased Array Inspection of Copper Canister Weld for Nuclear Waste Fuel**

More information about the phased array inspection of copper canister electron beam welds for nuclear waste fuel can be found in reference 11.

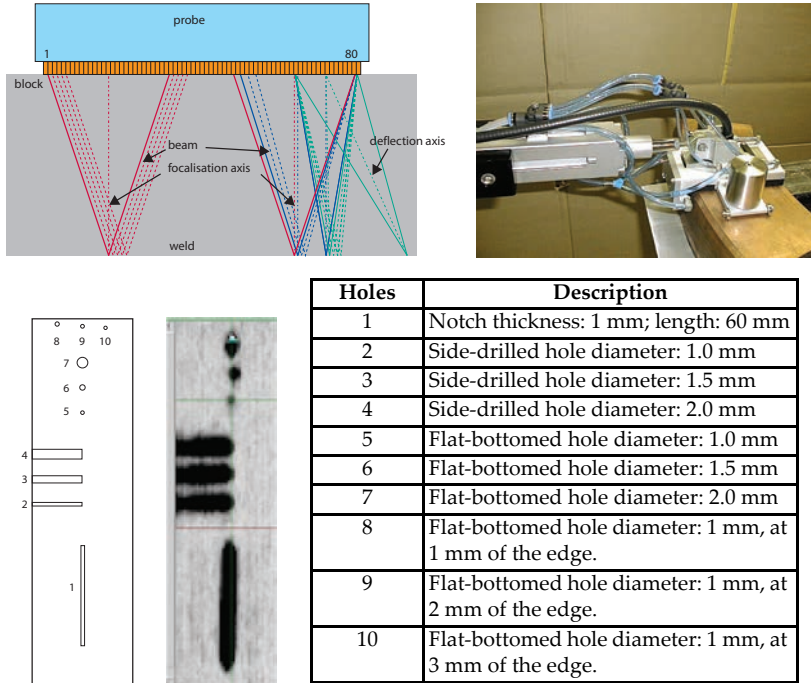
##### *a) NDT problems and challenges*

- Reliable inspection of electron beam weld between the canister and the lid, at a depth of 60 mm depth
- Coarse-grained material
- Must be remote-controlled and automated.
- High-speed inspection required

- All results must be validated on real mock-ups.

**b) Phased array solution**

- Use electronic and linear scanning.
- Use a 3-MHz linear phased array probe; pitch: 1 mm.
- Optimize the active aperture on reference block (see Figure 5-96).
- Scan 360° around the canister.



Courtesy of SKB, Sweden

**Figure 5-96** Phased array inspection of electron beam weld between the copper canister and the lid: principle and the probe (top), results on reference block (bottom).

Material: copper (ultrasound velocity: 4700 m/s)

Detection of FBH numbers 8 to 10 is achieved with another setup: active aperture of up to 16-element probe firing at 10°.

## 5.10.5 Phased Array Inspection of Heavy Forgings

### a) *NDT problems and challenges*

- High-quality inspection required
- Large volume to cover
- Documented results needed

### b) *Phased array solution*

- Use phased arrays to increase coverage and speed (see Figure 5-97).
- Collect and display results as appropriate.



**Figure 5-97** Photo of circular forging being inspected by phased arrays.

## 5.11 Railroad Transportation

This section describes phased array applications for the railway industry, which has specific aspects such as high volume and difficult defects and geometry.

### 5.11.1 Axle (with or without Wheel)

#### a) *NDT problems and challenges*

- *In-situ* inspection with wheels on axle

- Limited access for probe
- Very small fatigue cracks in five major areas
- Continuous inspection (system reliability)
- Minimize costs of system

**b) Phased array solution**

- Multiple phased array probes using shear waves with an angle range from 30° to 70° (see Figure 5-98)
- Merged images
- Single phased array probe with a large active aperture and multiple sectors (when access is possible only from outside)

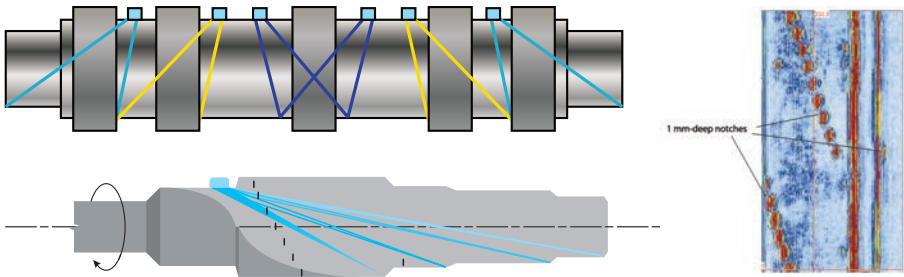


**Figure 5-98** Axle inspection with wheels on using multiple phased array probes (*top*); with restricted access, single phased array probe (*bottom*).

## 5.11.2 Rail Inspection

**a) NDT problems and challenges**

- Detect small cracks oriented in different planes and located within the rail body
- Perform online scanning with a test speed of 50 km/h
- Easy analysis and reporting

**b) Phased array solution**

- Use a phased array probe to scan the main body of the rail (see Figure 5-99).
- Use multiple S-scans.
- Plot data on a 2-D specimen overlay.

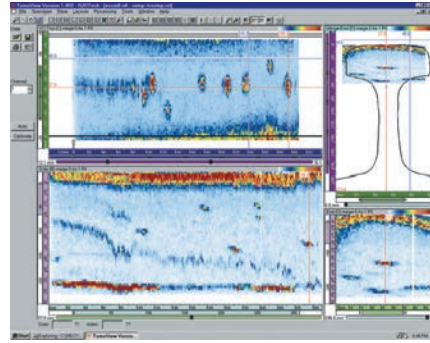
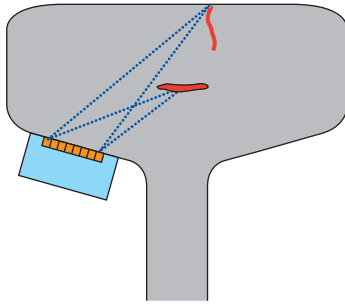
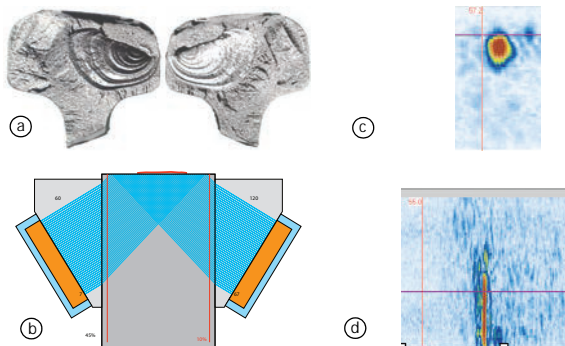


**Figure 5-99** Rail inspection with phased array probe: principle (*left*); data plotted on overlay (*right*).

Transverse cracks can be detected and sized with a pitch-and-catch configuration (see Figure 5-100).



*Courtesy of Transportation Technology Center, USA*

**Figure 5-100** Phased array detection of transverse cracks (a) with pitch-and-catch linear scanning – 8 elements (b) over a 60-element probe; beam width = 1.2 mm. Sizing is possible using different displays [see (c) and (d)].

### 5.11.3 Wheel Inspection

#### *a) NDT problems and challenges*

- Need to detect defects in specific regions of the wheel (see Figure 5-101)
- Near-surface detection required
- High-speed inspections necessary

- Low-cost solution preferred
- Wheels may be worn or corroded.
- User-friendly software required

**b) *Phased array solution***

- Based on the QuickScan PA ultrasonic system (see Figure 5-102)
- User-friendly software (see Figure 5-103)
- Inspection done at 200 mm/s (maximum rotation speed)
- Arrays designed to inspect all kinds of wheels
- No mechanical adjustment
- Calibration done on FBH of 1.6 mm
- Conventional or phased arrays can be added to inspect any part of the wheel.
- Dynamic depth focusing (DDF) is used to increase the detectability of defects.
- User-friendly operator software interface
- Strip chart display
- Alarm for each zone
- Automatic calibration (no human intervention)
- Aperture calibration
- $\pm 1.5$  dB of repeatability in static mode
- Systems can be supplied to meet AAR and/or customer's specifications.
- All data is stored in a Microsoft Access database enabling manipulations.
- The wheel is divided into inspection zones, and one strip chart is used for each zone. The exact position ( $x, y, z$ ) of each FBH is entered in the software, and then the calibration is performed automatically.
- The sensitivity of each aperture is calibrated. There is a 0.3-dB difference on the envelope between the apertures.
- Probes
  - Probe fixtures were designed to ensure a constant probe position.
  - The probes are designed to fit any kind of wheel. To optimize the sensitivity and signal-to-noise ratio, 5-MHz array probes with 128 elements are used.

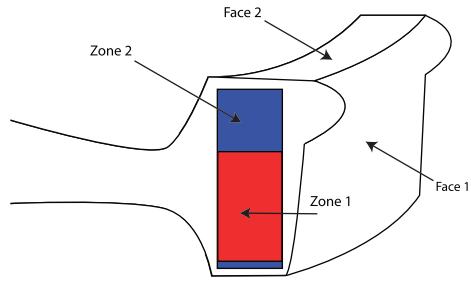


**Figure 5-101** Phased array zones for automated wheel inspection.



**Figure 5-102** Phased array automated inspection of train wheel for *in-situ* or shop-floor maintenance.

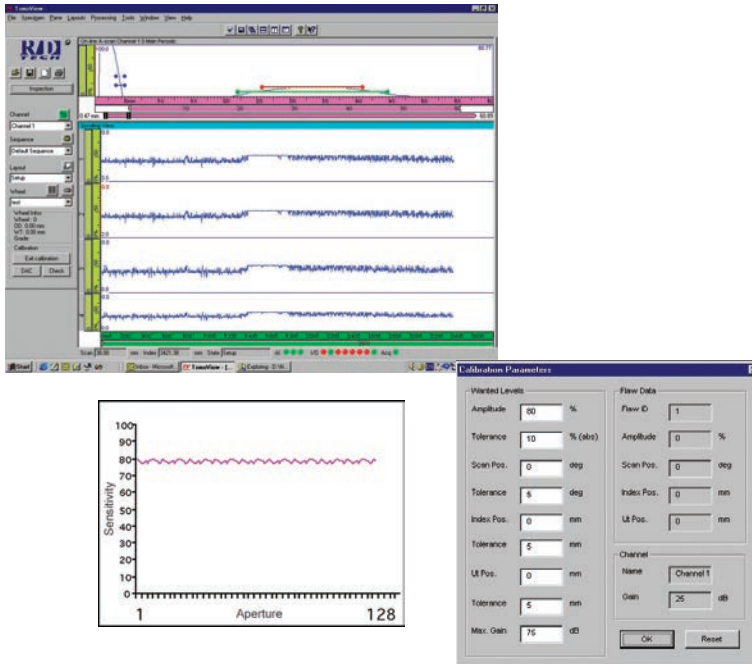


Figure 5-103 Automated calibration example.

## 5.12 Portable Phased Array Applications

Some portable phased array applications have already been covered in specific sections. See:

- “CANDU Feeder Tube Cracking” (section 5.6.5, p. 222)
- “Detection and Sizing of SCC in Low-Pressure Turbine Components” (section 5.6.9, p. 226)
- “Typical Pressure Vessel Mechanics” (section 5.7.5, p. 239, and Figure 5-60, p. 240)
- “Small Diameter Piping” (section 5.8.4, p. 252)
- “In-Service Inspection of Pipe for Stress Corrosion Cracking” (section 5.9.1, p. 254)
- “T-Weld Inspection of Bridge Structure” (section 5.9.3, p. 257)

Other OmniScan inspections are listed below. Further applications are being developed, such as the code-acceptable inspection of welds using electronic and linear scanning.

## 5.12.1 Construction Welding: T-Joints

### a) NDE challenges

- Difficult geometry
- Relatively thick material
- Rapid and reliable inspection required
- High volume requires cost-effective inspection.
- Imaging is important due to difficult geometry (see Figure 5-104).

### b) Phased array solution

- Use S-scans from 25° to 60°, with 0.5° increments.
- Use the A-scan display to optimize signal on crack and size.
- Use shear waves and S-scan display for visualization (see Figure 5-105).

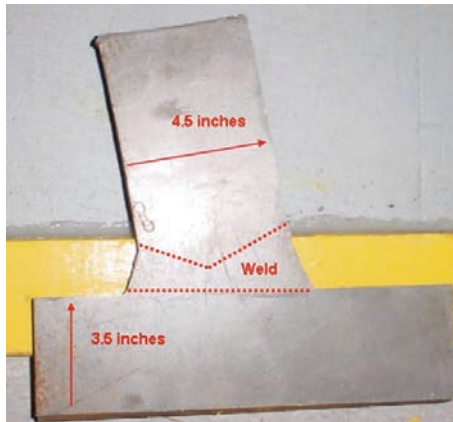


**Figure 5-104** Cross section of T-weld showing geometry and weld.

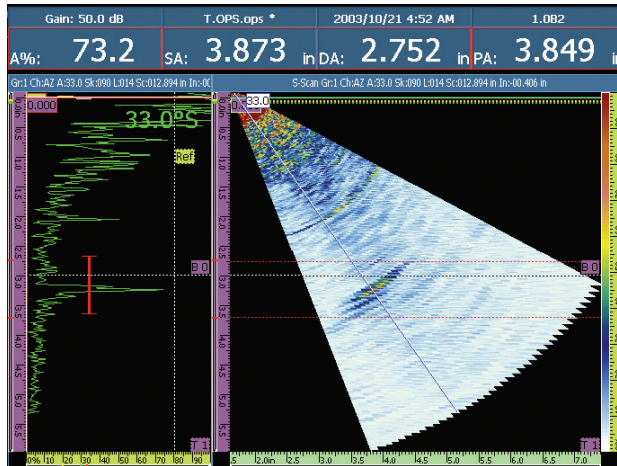


**Figure 5-105** S-scan display of T-weld showing crack with peaked A-scan (the blue line in the S-scan corresponds to the A-scan and signal in red gate).

## 5.12.2 Construction Welding: Butt Weld Inspections

### a) NDE challenges

- Perform rapid and reliable inspections of butt welds in plates or tubes
- Store data for reference
- Image defect for optimum sizing

### b) OmniScan solution

- Use array on wedge to generate shear waves.
- Perform S-scans in linear scan along weld (round tube or along weld).
- Store and display data as S-scans or “top, side, end” views (see Figure 5-106).

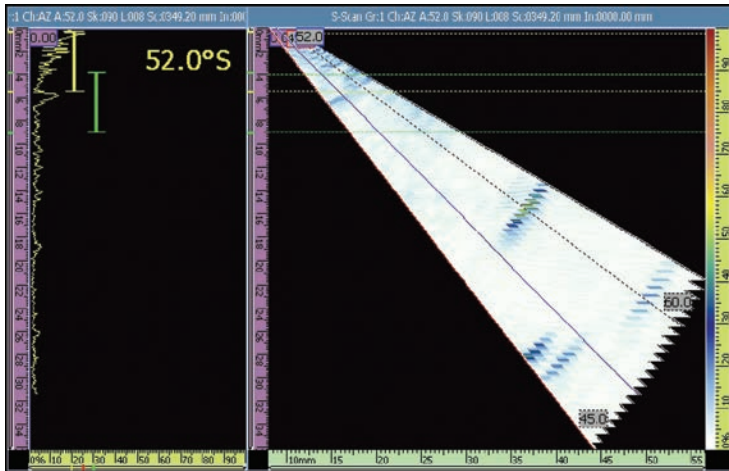


**Figure 5-106** Typical S-scan of butt weld, showing lack of fusion defects.

### 5.12.3 Small Diameter Austenitic Welds

#### a) NDE challenges

- Rapid inspection of difficult stainless steel welds (beam skewing and attenuation)
- Reliable inspection required
- Save all data

#### b) OmniScan solution

- Use twin shear-wave arrays on wedges, one on either side of the weld.
- Calibration is performed by creating a two-point TCG (DAC), using 10% ID and OD notches.
- Use a 4-mm electronic raster that can resolve the 10% ID and OD notches at a fixed distance from the weld centerline.
- Use a splitter umbilical to pulse both arrays.
- Use a mechanized scanner for reliability.
- Scan using a low-profile scanner (see Figure 5-107).
- Use a MiniME mini encoder for data positioning.
- Use S-scans for thin walls, with C-scans to display data.
- Use cursors to display key waveforms with defects for analysis (see Figure 5-108).

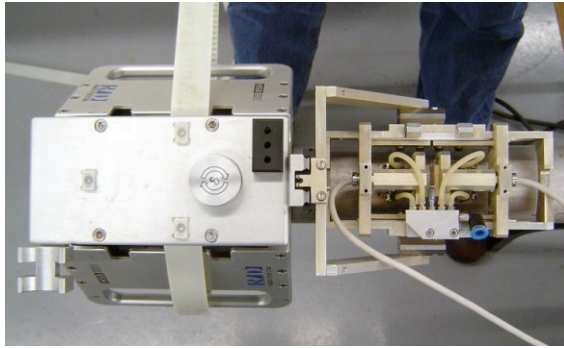


**Figure 5-107** Twin SW wedges with low-profile scanner for weld inspections.

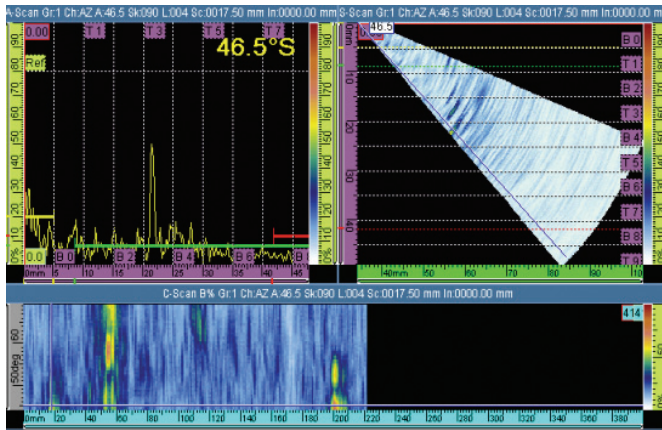


**Figure 5-108** Typical A-scan, S-scan, and C-scan display showing 1.5 mm calibration hole.

## 5.12.4 Hydrogen-Induced Cracking (HIC)

### a) NDE challenges

- HIC is easily detected, but SOHIC (stress-oriented hydrogen-induced cracking or stepwise cracking) is more difficult to characterize.
- HIC forms lamellar reflectors parallel to the surface; SOHIC forms cracking between HIC, at an angle to the surface.
- The objective is to reliably determine if SOHIC exists amongst HIC.
- Inspection must be rapid and comparatively low-cost.
- Data storage is desirable.

b) *OmniScan solution*

- Perform S-scans using  $\pm 30^\circ$  S-scans.
- Use AutoTrack mode to display the A-scan angle with the highest amplitude waveform.
- Typically focus at mid-wall since most HIC and SOHIC occur at 1/3 to 2/3 of depth.
- Calibrate only at  $0^\circ$  for convenience, but refocus if necessary.
- Skew the array back and forth to optimize the signal.
- Look for additional signals between HIC reflections to identify SOHIC (see Figure 5-109 and Figure 5-110).

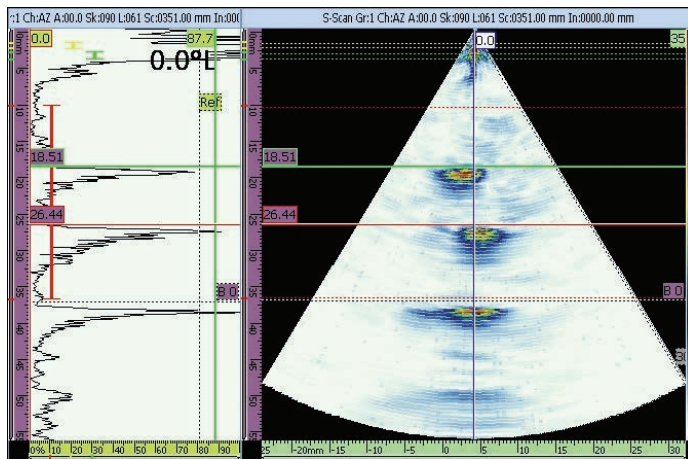


Figure 5-109 HIC with no visible stepwise cracking (no SOHIC).

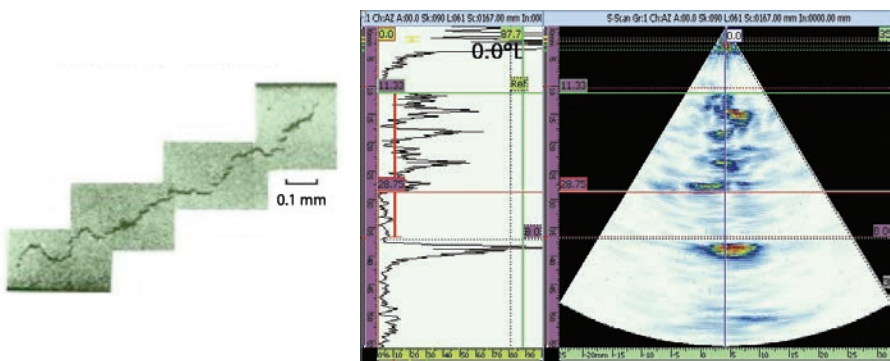


Figure 5-110 HIC with visible SOHIC.

## 5.12.5 Tie-Ins for Pipeline Welds

### a) *NDE problems*

- Pipeline tie-ins are often manual welds that are inspectable to, for example, API 1104.
- Conventional pipeline AUT equipment is too valuable and large to use for tie-ins.
- Tie-ins can take time to manufacture, so equipment delays can be significant.

### b) *OmniScan solution*

- Use an OmniScan with multiple passes.
- Perform linear scans with a manual scanning rig.
- Perform 45°, 60°, and 70° electronic scans and TOFD multiple scans to qualify for code.
- Minimizes cost and inconvenience.

## 5.12.6 Flange Corrosion Under Gasket

### a) *NDE challenges*

- Detect corrosion under gasket seat
- Difficult angles for ultrasonic inspection (see Figure 5-111)
- Scanning needed, but area limited
- Inspection possible only from pipe
- No bolt removal

### b) *OmniScan solution*

- Use a 16-element phased array probe with a 45° fixed angle performing an S-scan from 30° to 85°.
- Use a 16.5 cm (6.5 in) diameter guide placed at the end of the weld (neck of the flange). This ensures maximum coverage with the bolts in place.

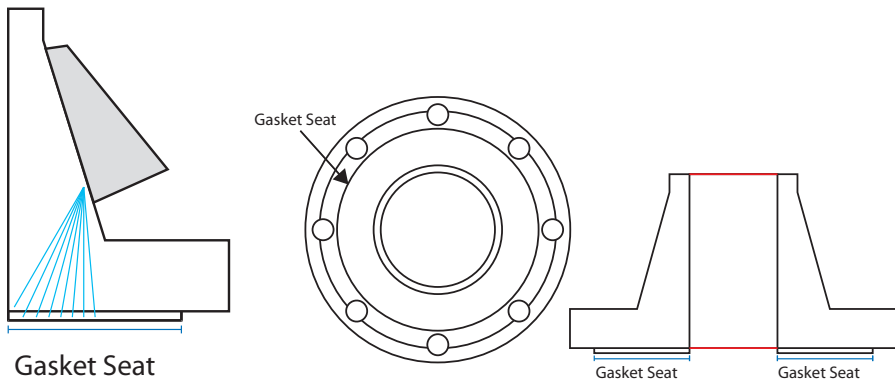


**Figure 5-111** Schematic showing flange gasket with area to be scanned (*left*), and bolt locations and limited access (*right*).

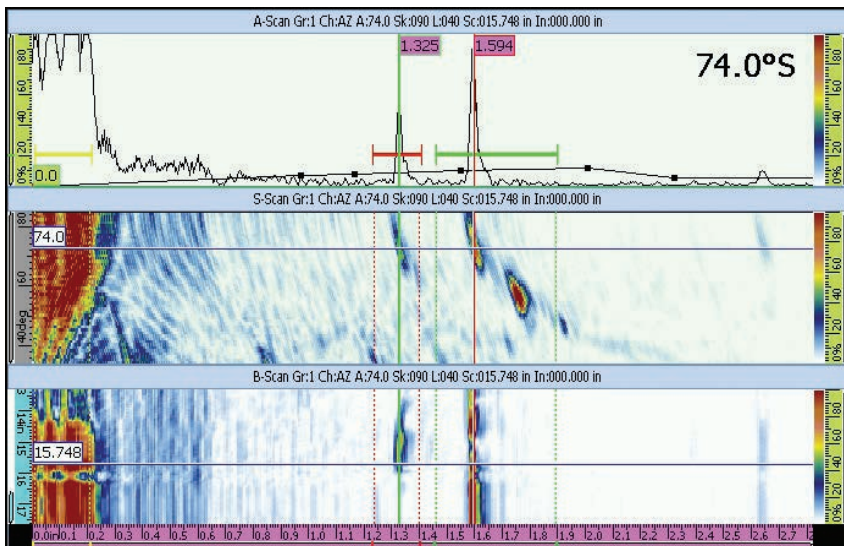


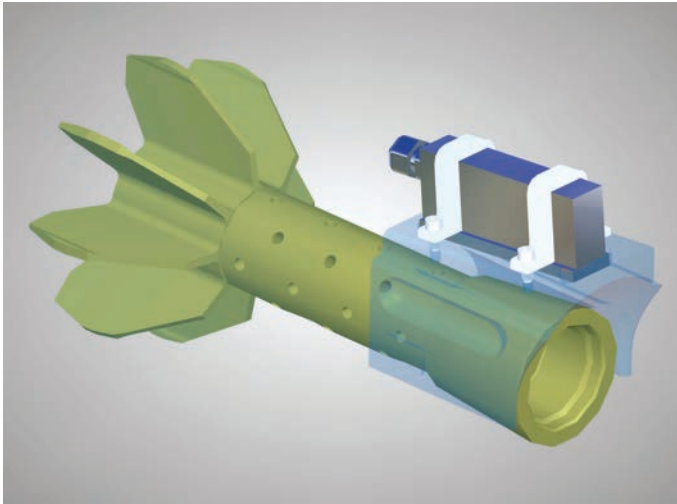
**Figure 5-112** A-scan, B-scan, and corrected B-scan displays of corrosion mapping.

## 5.12.7 Component Testing: Thread Inspection

### a) NDE challenges

- Reliably inspect threads on munition shafts to determine if they are correctly threaded or double-threaded (see Figure 5-113 and Figure 5-114).

- Requires an easy-to-interpret display.
- Rapid inspection is required.
- Data must be stored.



*Courtesy of USAF, USA*

**Figure 5-113** Drawing showing munition tail and mock-up of probe on custom wedge.

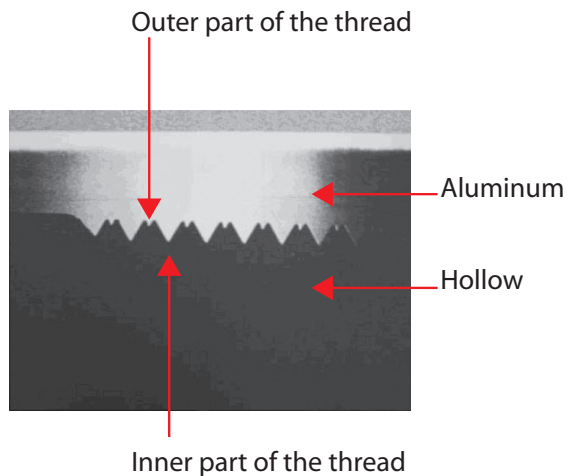


**Figure 5-114** Cross section through shaft showing double threading.

**b) OmniScan solution**

- Use an OmniScan with custom wedge to fit the shaft.
- Use a linear scan with focused beams.
- Use a B-scan display to show correct or bad threading (see Figure 5-115).

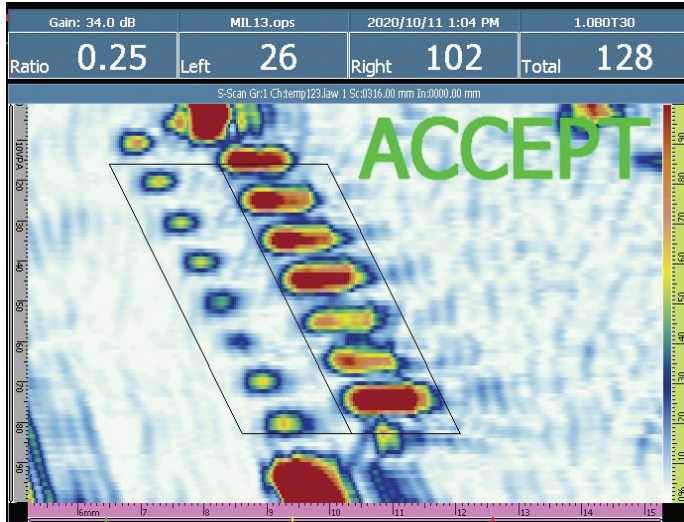


**Figure 5-115** B-scan of threads showing correct threading.

## 5.12.8 Component Testing: Spindle Inspection

**a) NDE challenges**

- Inspect long spindles axially for cracking (see Figure 5-115).
- Rapid and reliable inspection is required.
- Data interpretation can be difficult due to multiple reflections.
- Detect and size defects.

**b) OmniScan solution**

- Use single-array rotating probe on top of spindle (see Figure 5-116).
- Perform a narrow-angle S-scan to sweep from the centerline to the edge of the spindle.
- Display results as corrected S-scan.
- Use known features (example: lands) to determine locations.
- Calibrate using machined notches.

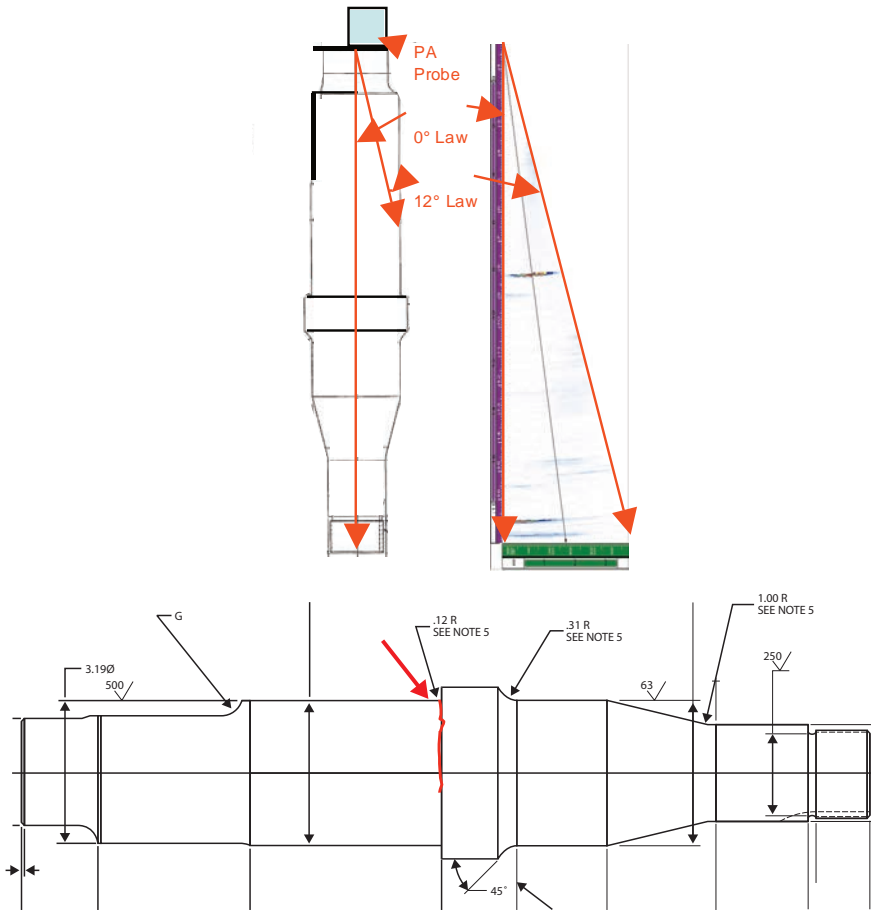


**Figure 5-116** Spindle and true depth (or volume-corrected) S-scan display with known reflectors (*top*) and cracking location (*bottom*).

## 5.12.9 Aerospace: Laser Weld Inspection

### a) NDE challenge

- Construction inspection of laser welds
- Complex component geometry
- Rapid inspection required
- Data storage needed

### b) OmniScan solution

- Use water box for coupling.

- Perform manual inspections using encoders.
- 10-metre linear scan at 25 mm/s
- Normal beam raster inspection (electronic scan)
- Real-time C-scan display
- All data stored



**Figure 5-117** Normal beam scan of aluminum laser weld with water box.

### 5.12.10 Aerospace: Composite Inspection

#### a) *NDE challenges*

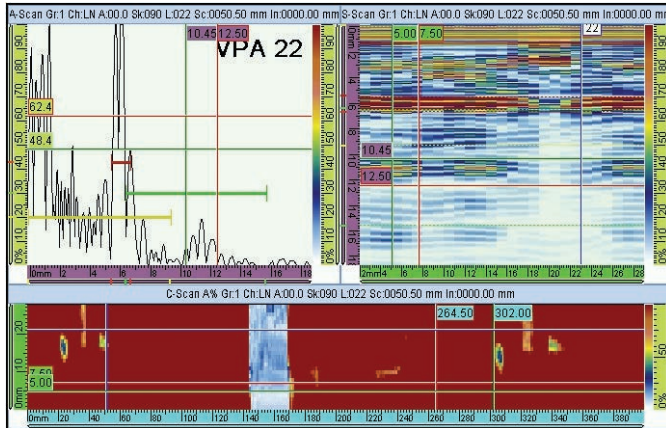
- 6-mm thick carbon composite examination
- Sample simulating lay-up tape commonly found during the manufacturing process (see Figure 5-118)
- Reliably detect and size defects
- Store data

#### b) *OmniScan solutions*

- Linear scan with electronic scanning
- 5-MHz, 32-element probe with a 1-mm pitch programmed to perform a linear electronic scan.
- Element grouping set to five (a 64-element probe with a 0.6 mm pitch is recommended for greater resolution)
- Use loss-of-backwall for defect detection.
- C-scan and A-scan displays
- Data stored



**Figure 5-118** Photo of composite specimen for inspection.



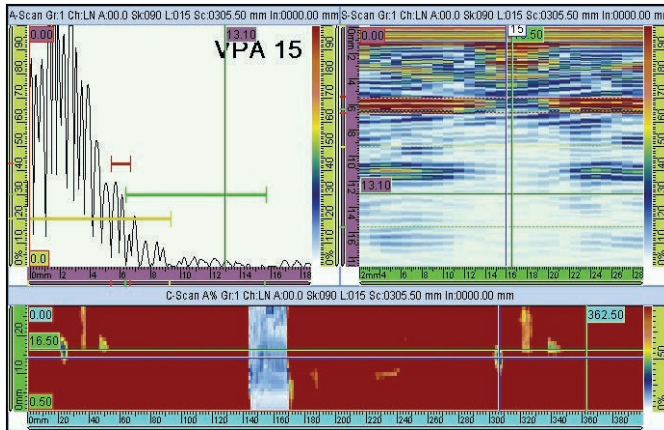


**Figure 5-119** Scan results from composite specimen. Good sample showing backwall (*top*); near-surface defect obscures backwall (*bottom*). Visible on C-scan.

## 5.12.11 Aerospace: T-Joint Composite

### a) NDE challenges

- Reliably inspect specific areas of T-composites (see Figure 5-120)
- Perform rapid and cost-effective inspections

### b) OmniScan solution

- Perform rapid linear scan using a linear array probe (see Figure 5-121).
- Perform electronic scans for coverage.
- Use contact probe.
- Confirm notch detection (see Figure 5-122).

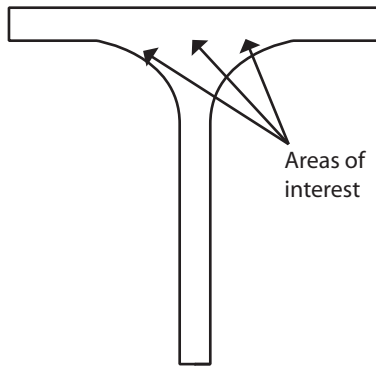


**Figure 5-120** Schematic of composite T-joint, showing areas of interest.

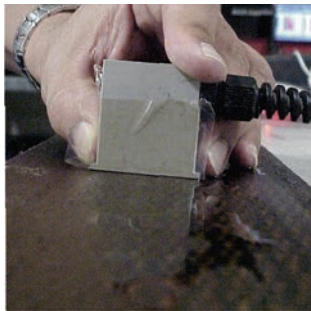


**Figure 5-121** Photo of linear array used for T-joint inspection.

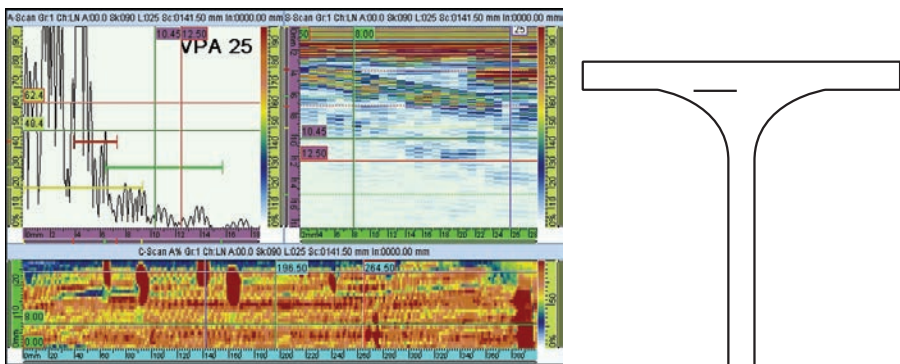


**Figure 5-122** A-scan, B-scan, and C-scan of T-joint inspection (*left*), and reference defect in T-joint (*right*).

## 5.12.12 Power Generation: Turbine Blade Root Inspection

### a) NDE challenges

- Detect cracking in turbine blade roots
- Rapid and cost-effective inspection of noncritical areas

### b) OmniScan solution

- Perform sectorial scan and tip diffraction for crack height sizing (see Figure 5-123).
- Use manual UT with phased arrays to replace AUT, except for critical areas.

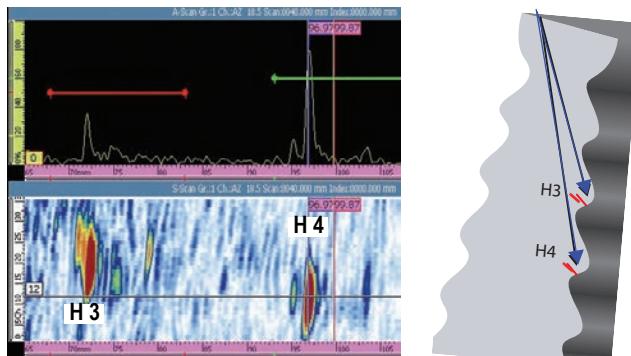


**Figure 5-123** Schematic showing typical defects in blade root area (*right*) and B-scan results (*left*).

## 5.12.13 Petrochemical Industry: Nozzle Inspection

### a) NDE challenges

- Detect and measure erosion-corrosion on the inside surface of a 17.5 cm (7 in.) nozzle
- Rapidly perform in-service inspection
- Cost-effective inspection required

### b) OmniScan solution

- Use a 32-element, 10-MHz PA probe (see Figure 5-124).
- Perform an S-scan using L-waves from 0° to 70°.
- Display as volume-corrected (true depth) S-scan for imaging.
- Measure erosion-corrosion (see Figure 5-125).

- Zoom if needed.

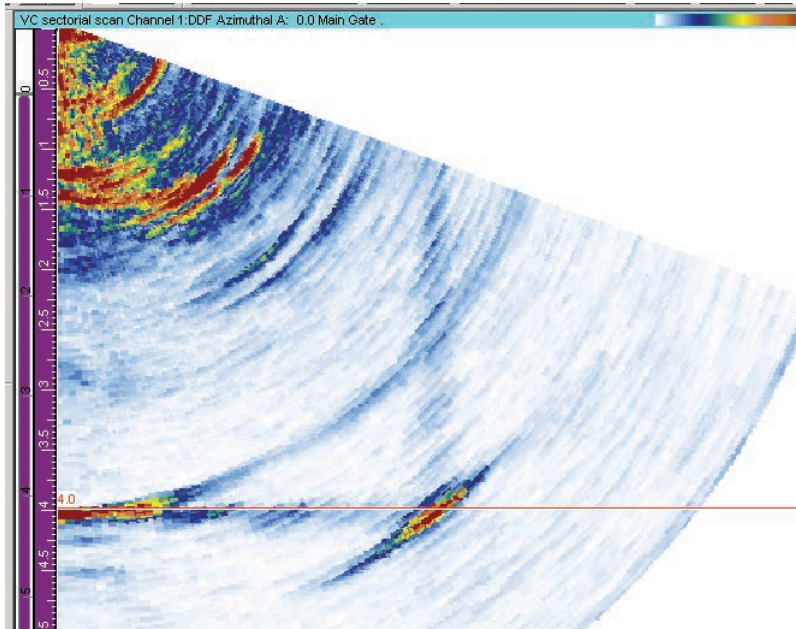


**Figure 5-124** S-scan of nozzle, showing bottom surface, corner, and smooth end surface.

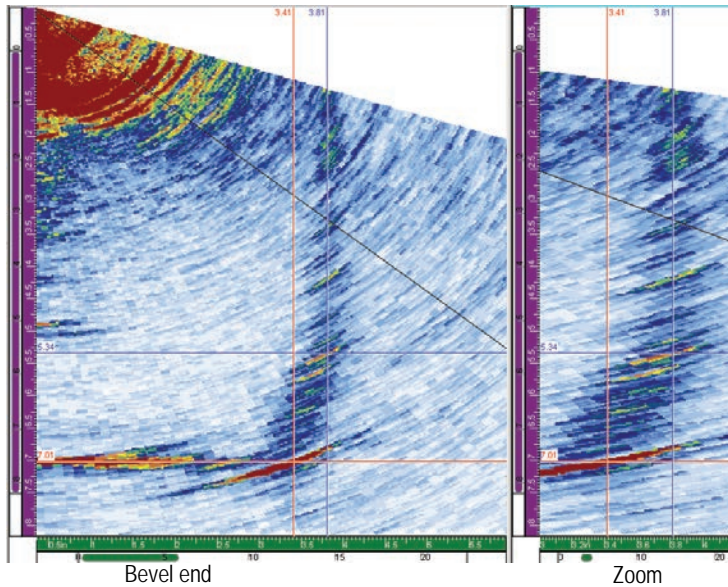


**Figure 5-125** S-scans showing eroded corner. The image on the right is a zoomed image.

### 5.12.14 Compressor Blade

#### a) *NDE challenges*

- Multiple angle inspection required (see Figure 5-126)
- Difficult imaging of defects
- Rapid and cost-effective inspection needed

#### b) *OmniScan solution*

- Use a 10 MHz array.
- Sectorial scan from  $-25^{\circ}$  to  $+25^{\circ}$  (see Figure 5-127)
- Volume-corrected image

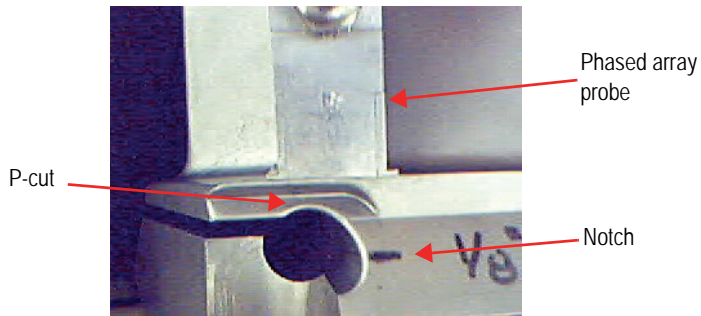


**Figure 5-126** Photo of array scanning compressor blade and reference notch.

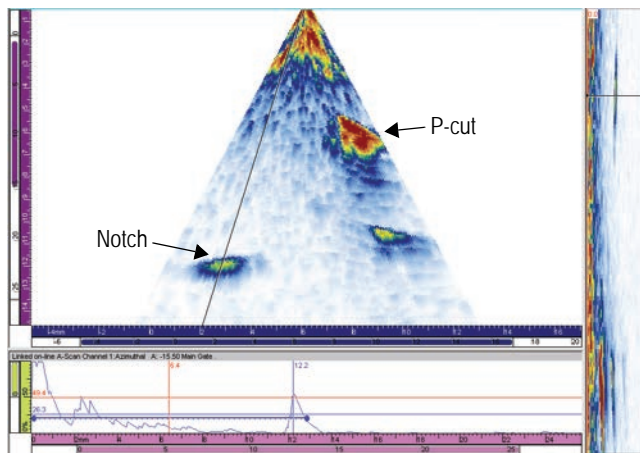


**Figure 5-127** +25° S-scan of compressor blade showing P-cut and notch.

### 5.12.15 Austenitic Welds

#### a) NDE challenges

- Rapid weld inspections required
- Significant problems using standard S-wave inspections in austenitic materials (see Figure 5-128)
- Portable equipment desirable
- Need to detect and size defects

#### b) OmniScan solution

- Use L-waves to minimize beam redirection.

- For example: for 20 mm (0.8 in.) stainless steel, use a 16-element array (5 MHz; pitch: 1 mm).
- Perform sectorial scan (S-scan) from 35° to 65°. The array and angles used depend on conditions (see Figure 5-129).
- Use linear scan for rapid coverage.

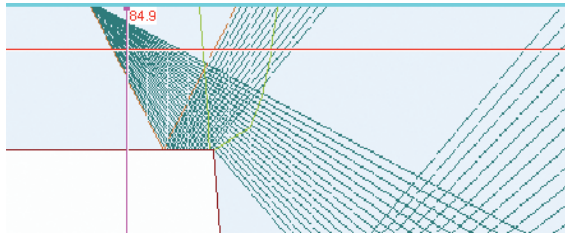


**Figure 5-128** Ray tracing of austenitic weld at 45° and 75°.

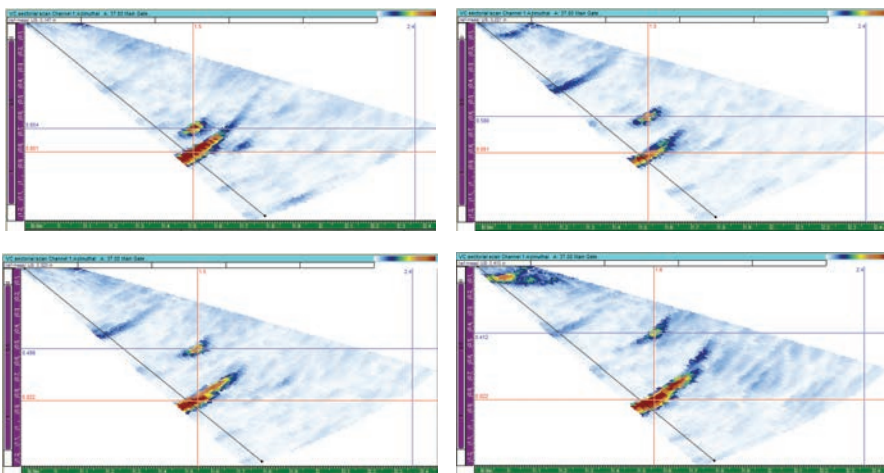


**Figure 5-129** S-scan images of notches in 20-mm stainless steel, showing corner trap signal (red cursor) and notch tip (blue cursor). The notches are 20% (a), 30% (b), 40% (c), and 50% (d).

## References to Chapter 5

1. Bird, C. R. "Ultrasonic phased array inspection technology for the evaluation of friction stir welds." *Insight*, vol. 46, no. 1 (January 2004): pp. 31–36.
2. Kleiner, D., and C. R. Bird. "Signal processing for quality assurance in friction stir welds." *Insight*, vol. 46, no. 2, (February 2004): pp. 85–87.
3. Moles, M., F. Jacques, and N. Dubé. "Linear Weld Inspections Using Ultrasonic Phased Arrays."
4. Lamarre, A., N. Dubé, P. Ciorau, and B. Bevins. "Feasibility study of ultrasonic inspection using phased array of ABB L-0 blade root."
5. Moles, M., N. Dubé, and E. Ginzel. "Ultrasonic Phased Arrays for Pipeline Girth Weld Inspections."
6. Maes, G., and M. Delaide. "Improved UT Inspection Capability on Austenitic Materials Using Low-Frequency TRL Phased Array Transducers."
7. Lafontaine, G., and F. Cancre. "Potential of UT Phased Arrays for Faster, Better, and Lower Cost Inspections."
8. Dubé, N., F. Moriera, and R. Stanley. "Phased Arrays for Improved Inspection of Coiled Tubing."
9. Delaide, M., G. Maes, and D. Verspeelt. "Design and Application of Low-Frequency Twin Side-by-Side Phased Array Transducers for Improved UT Capability on Cast Stainless Steel Components."
10. Lamarre, A., M. Moles, and F. Cancre. "Use of state-of-the art phased-array ultrasound for the inspection of Friction Stir Welds (FSW)."
11. Pasquer, V., and T. Stepinski. "Ultrasonic Array Technique for Inspection of Copper Canisters for Nuclear Waste Fuel."
12. Banchet, J., R. Sicard, D. E. Zellouf, and A. Chahbaz. "Phased Array Techniques and Split Spectrum Processing for Inspection of Thick Titanium Casting Components."
13. Langlois, P., P. Ciorau, and D. Macgillivray. "Technical Assessment and Field Application of Portable 16-pulser Phased Array Instrument."
14. Moles, M., F. Cancre, and N. Dubé. "Alternative Sizing Technique Using Ultrasonic Phased Arrays and Zone Discrimination."
15. Maes, G. "High Performance Pipe Weld Inspection Using State-of-the-Art Phased Array UT Equipment and Methodology."
16. Cancre, F., and M. Dennis. "Effect of the Number of Damaged Elements on the Performance of an Array Probe."
17. Lamarre, A., J. Gauthier, M. A. Zaidi, and A. Agarwal. "New Developments of the Ultrasonic Phased-Array for the Inspection of Thick Titanium Casting Structural Parts." Aeromat 2002, Orlando.

## Chapter Contents

6.1	Advantages of Phased Arrays .....	299
6.2	General Phased Array Solutions to Inspection Problems .....	300
6.3	Implementing Phased Array Technology .....	302

---

## 6. Conclusions and Recommendations

---

Our journey into phased array technology for industrial applications is near the end. As presented in “Introduction,” this guide is the first Olympus book dealing with the new industrial phased array technology. This book is an introduction to phased array applications, a way to better acquaint you with basic principles, probe types, scan patterns, specific views, and detailed applications. A basic ultrasonics chapter was added to help with graphs, tables, and formulas.

### 6.1 Advantages of Phased Arrays

The main advantages of phased arrays can be summarized below:

1. *Speed.* Phased array inspections with linear scanning typically have a faster magnitude order than conventional single probe raster scanning. This provides significant savings terms of plant downtime and operator costs.
2. *Flexibility.* Using electronic setup files, a single array can inspect many different components and inspection patterns.
3. *Complex inspections.* Phased arrays can be programmed to inspect geometrically complex components, such as automated welds or nozzles, with relative ease. Phased arrays can also be programmed to perform special scans, such as tandem, multiangle, multimode, and zone discrimination.
4. *Small array size.* Steerable probes permit the use of a single probe where multiple probes were previously required, much simplifying some inspections.
5. *Mechanical reliability.* Fewer moving parts make for a more reliable inspection system. Replacing mechanics with electronics reduces wear and tear, as well as significantly increases system reliability.
6. *Defect sizing* without probe movement.
7. *A focused beam* where it is required without multiple probes.

## 6.2 General Phased Array Solutions to Inspection Problems

The main phased array approaches to solving general inspection problems are summarized in Table 6-1.

**Table 6-1** Overview of phased array solutions.

Feature	Phased array solution
High-speed inspections	<ul style="list-style-type: none"> <li>• QuickScan PA for pipe mills</li> <li>• Tomoscan III PA for high-end applications</li> <li>• Reduced gating and data collection to maximize PRF</li> <li>• Combined multiple phased array probe setups</li> </ul>
Limited scanning access due to difficult geometry	<ul style="list-style-type: none"> <li>• Miniature arrays</li> <li>• S-scan with multiple angles</li> <li>• Multiple channels with different wave types</li> <li>• Single probe (1-D, 2-D) scanning all parameter sets</li> <li>• Ray tracing and 2-D data plotting</li> </ul>
Inspection flexibility	<ul style="list-style-type: none"> <li>• Scan by simply loading the setup file</li> <li>• Great flexibility for inspecting different parameter sets simply by modifying setup files</li> </ul>
High inspection reliability	<ul style="list-style-type: none"> <li>• Many test angles and procedures</li> <li>• S-scans, composite B-scans, multiple setups (channels) with PE, TOFD, SW, and LW—all ensure redundancy</li> <li>• Defect characterization based on results from multiple analysts</li> </ul>
High dose rate for nuclear	<ul style="list-style-type: none"> <li>• Rapid setup time (load file and calibrate)</li> <li>• Faster scanning (linear scans versus raster)</li> <li>• Relevant S-scan information acquired within a few minutes</li> </ul>
Equipment reliability	<ul style="list-style-type: none"> <li>• Fewer probes, simplified design</li> <li>• Less moving parts means greater mechanical reliability.</li> <li>• More electronics, less mechanics means improved reliability.</li> <li>• Easy maintenance and repair</li> <li>• Telemaintenance</li> </ul>
High productivity	<ul style="list-style-type: none"> <li>• Maximize electronic scanning for speed.</li> <li>• Combine multiple phased array probe setups.</li> <li>• Use data compression, smoothing, digitalization, high PRF, and DDF.</li> </ul>
Maximize defect detection (PoD)	<ul style="list-style-type: none"> <li>• Optimize inspection procedures.</li> <li>• High-frequency focused beams</li> <li>• Smaller beam dimensions, higher SNR</li> <li>• Use DDF.</li> <li>• Include tip-echo diffraction techniques.</li> <li>• Averaging and data processing</li> </ul>

**Table 6-1** Overview of phased array solutions. (Cont.)

Feature	Phased array solution
Imaging	<ul style="list-style-type: none"> <li>• S-scan and linked views (volume-corrected)</li> <li>• Multiple angles, different defect displays</li> <li>• Merged displays</li> <li>• Signal processing</li> </ul>
Real-time analysis	<ul style="list-style-type: none"> <li>• Networking</li> <li>• High data transfer rate</li> <li>• Multiple workstations</li> <li>• One file may be analyzed by several analysts at the same time.</li> </ul>
Underwater applications	<ul style="list-style-type: none"> <li>• Watertight phased array probes, pressure-resistant</li> </ul>
Data reproducibility	<ul style="list-style-type: none"> <li>• Tight encoder tolerances (&lt;0.25 mm)</li> <li>• Automatic sensitivity calibration</li> <li>• Data plotting in 2-D specimens</li> <li>• Qualified procedure, equipment, and personnel</li> </ul>
Coarse-grained material inspections (for example, stainless steel and cladding)	<ul style="list-style-type: none"> <li>• Use TRL phased array probe with high bandwidth, lower frequency.</li> <li>• Use longitudinal waves.</li> <li>• Use cut-spectrum processing (CSP).</li> <li>• Increased averaging</li> <li>• Smaller beam dimensions</li> </ul>
In-line reliability	<ul style="list-style-type: none"> <li>• Use a QuickScan dedicated setup and software for speed and cost.</li> <li>• Optimized ultrasonic head, multiple probes</li> <li>• Linear scanning</li> <li>• DDF, optimized PRF</li> <li>• Rugged equipment, designed for 24/7 jobs.</li> </ul>
Data analysis and reporting	<ul style="list-style-type: none"> <li>• Customized layout</li> <li>• Use TomoView data analysis capability for OmniScan scanning data.</li> <li>• Use defect tables for convenience.</li> <li>• Use Microsoft Excel or Access, or MATLAB.</li> <li>• Customized reports</li> </ul>
Performance demonstration	<ul style="list-style-type: none"> <li>• EPRI qualified the phased array procedure for dissimilar weld inspections according to ASME XI-Appendix VIII</li> <li>• OmniScan PDI qualification underway</li> <li>• Petrochemical industry approvals for phased array technology for pipelines and pressure vessels</li> </ul>
Fitness-for-purpose inspection	<ul style="list-style-type: none"> <li>• High accuracy and small errors in length and height sizing</li> <li>• Accurate defect plotting (coordinates and orientation)</li> <li>• Increased axial and lateral resolution provides possibility of defect discrimination/interaction.</li> <li>• Defect classification based on advanced imaging.</li> </ul>

**Table 6-1** Overview of phased array solutions. (Cont.)

Feature	Phased array solution
Personnel training and certification	<ul style="list-style-type: none"> <li>• Olympus Training Center, Canada, offers an official training program on phased arrays since 2004.</li> <li>• The Welding Institute (TWI), UK, offers a phased array training program.</li> <li>• EPRI NDE Center offers a phased array training program.</li> <li>• NDE Professionals offers an official phased array training course.</li> </ul>
Investment cost	<ul style="list-style-type: none"> <li>• Initial cost is within the normal range for off-the-shelf automated systems.</li> <li>• Full life-cycle cost supports phased array technology as operating costs are lower than conventional systems.</li> <li>• Cost-effective base on technical capability</li> <li>• OmniScan offers low-cost solutions.</li> <li>• OmniScan may include additional modules (conventional probes, TOFD, as well as phased arrays).</li> <li>• Phased array probes will be standardized (weld kit, corrosion kit, pipe kit), and the price is dropping for standard products.</li> </ul>

Phased arrays are a mature technology, and solutions to many problems are already available. Costs are decreasing, as is normal with electronics. For example, the battery-powered OmniScan is closing the price gap between advanced phased array systems and conventional ultrasonic single-channel instruments.

### 6.3 Implementing Phased Array Technology

Follow the recommendations listed below to implement the phased array technology in your organization:

- Be familiar with the specific applications of phased array technology for your project.
- Determine the advantages of phased array technology.
- Read the relevant operating manuals.
- Determine what defects must be detected, that is, define the problem precisely.
- Take into account the component and defect characteristics (thickness, curvature, defect size, orientation, location, attenuation, beam skewing etc.).
- Develop an ultrasonic problem-solving approach for the inspection procedure: sweep angle, effective aperture, ultrasound range (half-path,

TOF), phased array probe, inspection scenarios (immersion, wedge-contact, direct contact, wave mode, pitch-and-catch, etc.).

- Call an Olympus office to discuss your phased array application. You can also contact Olympus to get additional technical information and recommendations from our specialists.
- “Web Site Forum”<sup>1</sup> presents the web-hosted discussion forum where you can browse to find or post added information about phased array problems.

---

1. Editor’s note at fourth printing: *Web Site Forum* existed at the time of first printing, but has since been removed. For information on current online discussions, please contact Olympus.



---

## Appendix: Unit Conversion

---

This appendix provides the metric-English conversions for units used in this book.

**Table A-1** Conversion from metric to English units.

Measure	Metric unit	English unit
Length	1 mm	= 39.37 mils = 0.03937 in.
	1 cm	= 0.3937 in.
	1 m	= 39.37 in. = 3.28 ft
Area	1 cm <sup>2</sup>	= 0.155 in. <sup>2</sup>
	1 m <sup>2</sup>	= 10.7639 ft <sup>2</sup>
Velocity	1 mm/ $\mu$ s	= 0.03937 in./ $\mu$ s
	1 m/s	= 3.28 ft/s = 196.85 ft/min
Mass	1 g	= 0.03527 oz
	1 kg	= 35.2739 oz = 2.20462 lbs
Mass density	1 kg/m <sup>3</sup>	= 0.062428 lb/ft <sup>3</sup>
Acoustic impedance	1 kg/m <sup>2</sup> s	= 0.001423 lb/in. <sup>2</sup> s = 0.204816 lb/ft <sup>2</sup> s
Temperature	°C	= (5/9) × (°F – 32)
	(°C × 1.8) + 32	= °F



---

# Glossary

---

This section presents a glossary of abbreviations, acronyms, and symbols that are used in this book.

Term	Unit	Designation
$a$	mm	Crack tip radius
$A$	%, mV	Amplitude height
$A$	mm	Active aperture
$A_{\text{eff}}$	mm	Effective active aperture
$A_{\text{min}}$	mm	Minimum active aperture
AATT	-	Absolute arrival time technique
A-scan	-	Ultrasonic view of a single pulse or waveform
ATTN	-	Attenuation curve
AUT	-	Automated ultrasonic testing; terminology used in pipelines
B-scan	-	Ultrasonic view of a vertical slice through the component
BW	-	Backwall curve
$BW_{\text{abs}}$	MHz	Absolute bandwidth
$BW_{\text{rel}}$	%	Relative bandwidth
BWR	-	Boiling water reactor
CBH	-	Conical bored hole
CBW	-	Cylindrical backwall
CE 1	-	Collateral echo 1; 30-70-70; mode-converted echo T-L-L
CE 2	-	Collateral echo 2; creeping wave echo
CN	-	Number of cycles
Cr-EDM-N	-	Crack-like electrical discharged machining notch
$\text{CRT}_{\text{TW}}$		Shear wave time of arrival from the screen
C-scan	-	Ultrasonic view, plan view of component
$d_{33}$	$10^{-12}$ m/V	Piezoelectric modulus for thickness oscillations in the 33 crystal direction
$d_A$	-	Damping factor
$D_{\text{eff}}$	mm	Probe effective diameter
$D_{\text{FBH}}$	mm	Flat-bottomed hole diameter

Term	Unit	Designation
$D_{\text{probe}}$	mm	Probe diameter
$D_{\text{SDH}}$	mm	Side-drilled hole diameter
$D_{\text{sphere}}$	mm	Sphere diameter
$D_{\text{void}}$	mm	Void diameter
$D_{\text{wedge}}$	$\mu\text{s}$	Wedge delay
$D(\eta)$	-	Diffraction coefficient
dB	dB	Decibel
DDF	-	Dynamic depth focusing
DGS	-	German system for sizing defects using gain and distance.
D-scan	-	Ultrasonic view of vertical slice through component, at right angle to a B-scan (see the "B-scan" entry)
$e$	mm	Element size
$E$	$\text{N/m}^2$	Modulus of elasticity (Young's modulus)
ECA	-	Engineering critical assessment (see FFP and FFS)
EDM-N	-	Electrical discharged machining notch
EDM-N <sub>hor</sub>	-	Electrical discharged machining notch parallel to the beam axis
EPRI	-	Electric Power Research Institute, USA
$f_c$	MHz	Center frequency
$f_L$ (-3 dB)	MHz	Lower frequency for free field at -3 dB point
$f_L$ (-6 dB)	MHz	Lower frequency for echo at -6 dB point
$f_n$	MHz	Nominal frequency
$f_{\text{peak}}$	MHz	Peak frequency
$f_U$ (-3 dB)	MHz	Upper frequency for free field at -3 dB point
$f_U$ (-6 dB)	MHz	Upper frequency for echo at -6 dB point
$F$	mm	Focal depth for the maximum refracted angle
$F_{\text{ac}}$	mm	Actual focal depth
$F_D$	mm	Depth-of-field (normally -6dB drop-off)
$F_{\text{DDF}}$	mm	DDF focal depth
$F_L$	mm	Focal length (distance)
FBH	-	Flat-bottomed hole
FFP	-	Fitness for purpose
FFS	-	Fitness for service
FFT	-	Fast Fourier transform
FL	-	Number of focal laws
FSW	-	Friction stir welds
$g$	mm	Gap between adjacent elements
$g_{33}$	$10^{-3} \text{ Vm/N}$	Piezoelectric pressure constant in the 33 crystal direction
$G$	$\text{N/m}^2$	Shear modulus
G	dB	Gain

Term	Unit	Designation
$G_{\text{reserve}}$	dB	Gain in reserve
$G_{\text{useful}}$	dB	Useful gain, or “gain in hand” after calibration
$h_{33}$	$10^9$ V/m	Piezoelectric deformation constant
$H_1$	mm	First element height
$H_{\text{crack}}$	mm	Crack height
$H_{\text{notch}}$	mm	Notch height
$H_w$	mm	Wedge height
$I_i$	mm	Wedge index for incident angle
ID	mm	Inside diameter
$I$	$\text{W/m}^2$	Intensity of acoustic power
$J_1(X)$	-	Bessel’s function of first degree
$k$	-	Wavelength factor
$k_{\square}$	-	Near-field correction factor (rectangular probe)
$k_{33}$	-	$= \sqrt{d_{33} \times h_{33}}$ , a-dimensional
$k_{\text{height}}$	-	Height factor (RAT)
$k_t$	-	Thickness-mode electromechanical coupling
$L_{-6 \text{ dB}}$	mm	Depth-of-field at –6 dB drop
$L_{\text{crystal}}$	mm	Length of the crystal
$L_{\text{probe}}$	mm	Length of the probe
$L_{\text{wedge}}$	mm	Length of the wedge
LoF	-	Lack of fusion, a welding defect
L-L-T	-	Mode-converted echo from L-waves to L-waves and T(S)-waves
L-T-L	-	Mode-converted echo from L-waves to T-waves and L-waves
L-T-T	-	Mode-converted echo from L-waves to T-waves and T-waves
LW	-	Longitudinal waves
M		Figure of merit
MC	-	Mode-converted
MUT	-	Manual ultrasonic testing
$n$	-	Number of elements
$N_0$	mm	Near-field length
$N_{\text{acquisition}}$	-	Number of acquisitions
$N_{\text{A-scans/s}}$	-	Acquisition rate
N-Cr	-	Reflectivity curve symbol from an EDM notch for creeping waves
NDE	-	Nondestructive evaluation
NDI	-	Nondestructive inspection

Term	Unit	Designation
NDT	-	Nondestructive testing
N-LW	-	Reflectivity curve symbol from an EDM notch for L-waves
NOISE	-	Noise curve
NSR	-	Near-surface resolution curve
N-SW	-	Reflectivity curve symbol from an EDM notch for S-waves
OD	mm	Outside diameter
$p$	mm	Element pitch
$P$	Pa = N/m <sup>2</sup>	Sound pressure
$P_{FBH}$	dB	Sound pressure reflected by the flat-bottomed hole
$P_{wedge}$	mm	Ultrasonic path in the wedge – mean value
$P(z)$	dB	Sound pressure on acoustic axis at z-mm distance
PASS	-	Phased array simulation software
PCS	-	Probe center separation
PipeWIZARD	-	Pipeline girth weld phased array inspection system
PN	-	Number of peaks
PoD	-	Probability of detection (of defects)
PRF	s <sup>-1</sup>	Pulse repetition frequency
$PW_{pulsar}$	10 <sup>-9</sup> s (ns)	Pulsar pulse width
PWR	-	Pressurized water reactor
Q	-	Quality factor
QuickScan PA	-	Industrial phased array instrument
R	mm	Radius of the lens curvature
R	-	Reflection coefficient
RATT	-	Relative arrival time technique
RF	-	Radio frequency
$S_{ac}$	-	Acoustic focusing factor
$S_e$	dB	Electric sensitivity
$S_F$	-	Normalized focal depth
$S_{opt}$	-	Optical focusing factor
$S_{probe}$	mm <sup>2</sup>	Probe surface
SCC	-	Stress corrosion cracking
SDH	-	Side-drilled hole
SDH <sub>hor</sub>	-	Side-drilled hole – horizontally drilled
SDH <sub>spherical</sub>	-	Side-drilled hole – spherical bottom
SDH <sub>vert</sub>	-	Side-drilled hole – vertically drilled
SDH-SW	-	Reflectivity curve symbol from SDH for S-waves
SNR	dB	Signal-to-noise ratio
S-scan	-	Sectorial scan; phased array inspection which sweeps through a range of angles

Term	Unit	Designation
SW	-	Shear waves (S-waves), also called transverse waves or T-waves or TW
$t$	mm	Thickness
$t/D$	-	Thickness / outside diameter ratio
$T$	-	Transmission coefficient $T_{\text{lat. wave}} = \frac{\text{PCS}}{v_L} = \frac{2S}{v_L}$ $T_{\text{upper tip}} = \frac{2(S^2 + d^2)^{0.5}}{v_L}$ $T_{\text{lower tip}} = \frac{2[S^2 + (d + h)^2]^{0.5}}{v_L}$ $T_{\text{backwall}} = \frac{2(S^2 + t^2)^{0.5}}{v_L}$
$T_{\text{time-base}}$	-	Time-base acquisition duration
TCG	-	Time-of-flight correction gain
T-L-L	-	Mode-converted echo from T-waves to L-waves and L-waves
T-L-T	-	Mode-converted echo from T-waves to L-waves and T(S)-waves
TOF	$\mu\text{s}$	Time of flight
TOFD	-	Time-of-flight diffraction
T-S-T	-	T-wave reflection from defect including satellite pulse
T-T	-	Direct T-wave reflection from defect
T-T-L	-	Mode-converted echo from T-waves to T-waves and L-waves
TW	-	Transverse waves (T-waves), also called shear waves or S-waves or SW
UT	-	Ultrasonic testing
$UT_{\text{path}}$	mm	Half ultrasonic path
$v_1$	mm/s	Ultrasound velocity in the first medium
$v_L$	mm/s	Ultrasound velocity in test piece for longitudinal waves
$v_R$	mm/s	Ultrasound velocity in test piece
$v_S$	mm/s	Ultrasound velocity in test piece for surface waves (Rayleigh)
$v_T$	mm/s	Ultrasound velocity in test piece for transverse waves
$v_w$	mm/s	Ultrasound velocity in wedge
$V_{\text{in}}$	V	Peak-to-peak input, or excitation
$V_{\text{out}}$	V	Peak-to-peak output

Term	Unit	Designation
$V_{pp}$	%, mV	Peak-to-peak amplitude
VPA	-	Virtual probe aperture
$W$	mm	Passive aperture
$W_{crystal}$	mm	Width of the crystal
$W_{min}$	mm	Minimum passive aperture
$W_{probe}$	mm	Width of the probe
$X$	-	Bessel's function argument: $\pi(D/\lambda) \sin \gamma$
$z$	mm	Axial distance
$Z$	$\Omega$ (ohm)	Electrical impedance
$Z_{ac}$	kg/m <sup>2</sup> s	Acoustic impedance
$\alpha$	°	Incident angle
$\beta$	°	Refracted angle
$\beta_{couplant}$	°	Refracted angle in the couplant
$\beta_{grating}$	°	Grating lobe location angle
$\beta_R$		Refracted angle in the test piece
$\delta$	°	Squint angle
$\Delta A$	dB	Amplitude variation
$\Delta \beta$	°	Angular sweep range
$\Delta d$	mm	Lateral resolution
$\Delta G_{attenuation}$	dB	Gain loss due to attenuation
$\Delta G_{reflection}$	dB	Reflection loss
$\Delta G_{transmission}$	dB	Transmission loss
$\Delta t_{void}$	$\mu$ s	Time-of-flight difference between TT and TST signals
$\Delta \tau_{-20 \text{ dB}}$	$\mu$ s	Pulse width
$\Delta UT$	mm	Ultrasonic half-path variation
$\Delta UT_{RATT}$	mm	Ultrasonic half-path difference between crack leg and crack tip
$\Delta X_{-6 \text{ dB}}$	mm	-6 dB beam width in $x$ direction (incident plane)
$\Delta Y_{-6 \text{ dB}}$	mm	-6 dB beam width in $y$ direction (perpendicular plane on beam)
$\Delta z_{axial}$	mm	Axial resolution
$\epsilon$	°	Impingement angle
$\Phi_{-3 \text{ dB}}$	mm	Beam diameter at -3 dB drop
$\Phi_{-6 \text{ dB}}$	mm	Beam diameter at -6 dB drop
$\Phi_{-12 \text{ dB}}$	mm	Beam diameter at -12 dB drop
$\Phi_{-20 \text{ dB}}$	mm	Beam diameter at -20 dB drop
$\Phi_{zero}$	mm	Beam diameter at zero crossing
$\gamma$	°	Wedge skew angle
$\gamma(\Delta \text{dB})$	°	Half-angle beam divergence
$\eta$	°	Angle between crack plane and beam axis
$\varphi$	°	Radial angle

Term	Unit	Designation
$\Phi_{\text{defect}}$	$^{\circ}$	Radial angle for a defect located in a pipe
$\Phi_{\text{skip}}$	$^{\circ}$	Radial angle for reflection on a pipe inner wall
$\lambda$	mm	Wavelength
$\mu$	-	Poisson's ratio
$\theta$	$^{\circ}$	Divergent angle
$\theta_p$	$^{\circ}$	Primary steering angle (2-D matrix probe)
$\theta_s$	$^{\circ}$	Secondary steering angle (2-D matrix probe)
$\rho$	$\text{kg/m}^3$	Mass density
$\omega$	$^{\circ}$	Wedge angle



---

## References

---

1. Somer, J. C. "Electronic Sector Scanning for Ultrasonic Diagnosis," *Ultrasonics*, vol. 6 (1968): p. 153.
2. Gebhardt, W., F. Bonitz, and H. Woll. "Defect Reconstruction and Classification by Phased Arrays." *Materials Evaluation*, vol. 40, no. 1 (1982): pp. 90–95.
3. Von Ramm, O. T., and S. W. Smith. "Beam Steering with Linear Arrays." *Transactions on Biomedical Engineering*, vol. 30, no. 8 (August 1983): pp. 438–452.
4. Erhards, A., H. Wüstenberg, G. Schenk, and W. Möhrle. "Calculation and Construction of Phased Array-UT Probes." *Proceedings 3rd German-Japanese Joint Seminar on Research of Structural Strength and NDE Problems in Nuclear Engineering*, Stuttgart, Germany, August 1985.
5. Hosseini, S., S. O. Harrold, and J. M. Reeves. "Resolutions Studies on an Electronically Focused Ultrasonic Array." *British Journal of Non-Destructive Testing*, vol. 27, no. 4 (July 1985): pp. 234–238.
6. Gururaja, T. T. "Piezoelectric composite materials for ultrasonic transducer applications." Ph.D. thesis, The Pennsylvania State University, University Park, PA, May 1984.
7. McNab, A., and I. Stumpf. "Monolithic Phased Array for the Transmission of Ultrasound in NDT Ultrasonics." *Ultrasonics*, vol. 24 (May 1984): pp. 148–155.
8. McNab, A., and M. J. Campbell. "Ultrasonic Phased Array for Nondestructive Testing." *NDT International*, vol. 51, no. 5: pp. 333–337.
9. Hayward, G., and J. Hossack. "Computer models for analysis and design of 1-3 composite transducers." *Ultrasonic International 89 Conference Proceedings*, pp. 532–535, 1989.
10. Poon, W., B. W. Drinkwater, and P. D. Wilcox. "Modelling ultrasonic array performance in simple structures." *Insight*, vol. 46, no. 2 (February 2004): pp. 80–84.
11. Smiths, W. A. "The role of piezocomposites in ultrasonic transducers." *1989 IEEE Ultrasonics Symposium Proceedings*, pp. 755–766, 1989.
12. Hashimoto, K. Y., and M. Yamaguchi. "Elastic, piezoelectric and dielectric properties of composite materials." *1986 IEEE Ultrasonic Symposium Proceedings*, pp. 697–702, 1986.
13. Oakley, C. G. "Analysis and development of piezoelectric composites for medical ultrasound transducer applications." Ph.D. thesis, The Pennsylvania State University, University Park, PA, May 1991.

14. American Society for Nondestructive Testing. *Nondestructive Testing Handbook*. 2nd edition. Vol. 7, *Ultrasonic Testing*, pp. 284–297. Columbus, OH: American Society for Nondestructive Testing, 1991.
15. Krautkramer, J., and H. Krautkramer. *Ultrasonic Testing of Materials*. 4th fully rev. ed., pp. 194–195, 201, and 493. Berlin; New York: Springer-Verlag, c1990.
16. DGZfP [German Society for Non-Destructive Testing]. *Ultrasonic Inspection Training Manual Level III-Engineers*. 1992. <http://www.dgzfp.de/en>.
17. EPRI. *Ultrasonic advanced sizing course*. 1987.
18. M. Davis. *Ultrasonic advanced sizing course*. 1994.
19. Harumi, K., M. Uchida, and H. Okada. *Ultrasonic Defect Sizing - Japanese Tip Echo Handbook*. 2nd version. Edited by K. Harumi, Y. Ogura, and M. Uchida. Translated by D. C. Moles and N. Miura. JSNDI (Japanese Society for Non-Destructive Inspection), 1989.
20. Schelengermann, U. "Sound field structure of plane ultrasonic sources with focusing lenses." *Acustica*, vol. 30, no. 6 (1974): pp. 291–300.
21. Schelengermann, U. "The characterization of focusing ultrasonic transducers by means of single frequency analysis." *Materials Evaluation*, vol. 38, no. 12 (Dec. 1980): pp. 73–79.
22. Wüstenberg, H., E. Schenk, W. Möhrle, and E. Neumann. "Comparison of the performances of probes with different focusing techniques and experiences." *10<sup>th</sup>-WCNDT Proceedings*, vol. 7, pp 563–567.
23. Wüstenberg, H., J. Kutzner, and W. Möhrle. "Focusing probes for the improvement of flaw size in thick-walled reactor components." [In German.] *Materialprüfung*, vol. 18, no. 5 (May 1976): pp. 152–161.
24. Singh, G. P., and J. L. Rose. "A simple model for computing ultrasonic beam behavior of broad-band transducers." *Materials Evaluation*, vol. 40, no. 7 (1982): pp. 880–885.
25. Fowler, K. A., H. C. Hotchkiss, and T. V. Yamartino. "Important characteristics of ultrasonic transducers and their factors related to their applications." Panametrics, USA, 1993.
26. Hotchkiss, F. H., D. R. Patch, and M. E. Stanton. "Examples of ways to evaluate tolerances on transducer manufacturing specifications." *Materials Evaluation*, vol. 45, no. 10 (1987): pp. 1195–1202.
27. Murphy, R. V. "Focussed Ultrasonic Probes for Contact Inspection." *Materials Evaluation*, vol. 38, no. 9 (1980): pp. 53–58.
28. Onozawa, M., and Y. Ishii. "The industrial application of improved narrow-beam probes for ultrasonic inspection." *British Journal of Non-Destructive Testing*, vol. 28, no. 1 (1986): pp. 23–26.
29. Beck, K. H. "Ultrasonic transducers focusing for inspection of cylindrical material." *Materials Evaluation*, vol. 49, no. 7 (July 1991): pp. 875–882.
30. Silk, M. G. "Ultrasonic Transducers for Nondestructive Testing." Adam Hilger Ltd., UK, 1984.
31. Fleury, G., and C. Gondard. "Improvements of Ultrasonic Inspections through the Use of Piezo Composite Transducers." *6th Eur. Conference on Non Destructive Testing*, Nice, 1994.

32. Ritter, J. "Ultrasonic Phased Array Probes for Non-Destructive Examinations Using Composite Crystal Technology." DGZfP, 1996.
33. Spies, M., W. Gebhardt, and M. Kröning (IZFP Saarbrücken). "Recent Developments in Phased Array Technology." [In German.] *NDT of Welds Conference*, Bamberg, Sept. 7–9, 1998.
34. Wüstenberg, H., A. Erhard, and G. Schenk. "Some Characteristic Parameters of Ultrasonic Phased Array Probes and Equipments." *The e-Journal of Nondestructive Testing*, vol. 4, no. 4 (April 1999). NDTnet, <http://www.ndt.net/v04n04.htm>.
35. Wüstenberg, H., A. Erhard, and G. Schenk. "Scanning Modes at the Application of Ultrasonic Phased Array Inspection Systems." *WCNDT*, paper idn 193, Rome, Oct. 2000.
36. Gros, X. E, N. B. Cameron, and M. King. "Current Applications and Future Trends in Phased Array Technology." *Insight*, vol. 44, no. 11 (Nov. 2002).
37. Pogue, J., J. Marguet, F. Pichonnat, and Laurent Chupin. "Phased Array Technology." *The e-Journal of Nondestructive Testing*, vol. 7, no. 5 (May 2004). NDTnet, <http://www.ndt.net/v07n05.htm>.
38. Wooh, Shi-Chang, and Shi, Yijun. "Influence of phased array element size on beam steering behavior." *Ultrasonics* 36 (1998): pp. 737–749.
39. Garcia, A., and J. Vazquez. "Applications of the phased array technique in the ultrasonic inspection of electric power plant." *Insight*, vol. 43, no. 3 (March 2001): pp. 183–187.
40. Bird, C. R. "Ultrasonic phased array inspection technology for the evaluation of friction stir welds." *Insight*, vol. 46, no. 1 (January 2004): pp. 31–36.
41. Kleiner, D., and C. R. Bird. "Signal processing for quality assurance in friction stir welds." *Insight*, vol. 46, no. 2, (February 2004): pp. 85–87.
42. EPRI. Proceedings, 1st Phased Array Inspection Seminar, Portland, USA, September 1998.
43. EPRI. Proceedings, 2nd Phased Array Inspection Seminar, Montreal, Canada, August 2001.
44. EPRI. Proceedings, 3rd Phased Array Ultrasound Seminar, Seattle, USA, June 2003.
45. Krimholtz, R., D. Leedom, and G. Matthaei. "New equivalent circuits for elementary piezoelectric transducers." *Electronics Letters*, vol. 6 (June 1970): pp. 398–399.
46. American Society for Testing and Materials. E1324-00 Standard Guide for Measuring Some Electronic Characteristics of Ultrasonic Examination Instruments. ASTM International, 2003.
47. American Society for Testing and Materials. E1065-99 Standard Guide for Evaluating Characteristics of Ultrasonic Search Units. ASTM International, 2003.
48. American Society of Mechanical Engineers. ASME XI-Article VIII-4000: Essential Variables Tolerances. ASME, 2003.
49. EU 12 668-1-2000: Characterization and verification of ultrasonic examination equipment. Instruments.
50. EU 12 668-2-2001: Characterization and verification of ultrasonic examination equipment. Probes.

51. EU 12 668-3-2000: Characterization and verification of ultrasonic examination equipment. Combined equipment.
52. ISO 10375:1997: Non-Destructive Testing—Ultrasonic Inspection—Characterization of Search Unit and Sound Field.
53. ISO 12710:2002: Non-Destructive Testing—Ultrasonic Inspection-Evaluating Electronic Characteristics of Ultrasonic Test Instruments.
54. ISO 12715:1999: Ultrasonic Non-Destructive Testing—Reference Blocks and Test Procedures for the Characterization of Contact Search Unit Beam Profiles.
55. NF-A 09-325:1987: Non-Destructive Testing—Ultrasonic Beams—Generalities. [In French.]
56. DIN 54 127 part 1: Calibration of ultrasonic flaw detection equipment and echo height evaluation. [In German.]
57. JIS Z 2350:2002: Method for measurement of performance characteristics of ultrasonic probes.
58. JIS Z 2351:1992: Method for assessing the electrical characteristics of ultrasonic testing instrument using pulse echo technique.
59. JIS Z 2352:1992: Method for assessing the overall performance characteristics of ultrasonic pulse echo testing instrument.
60. Kwun, H., W. D. Jolly, G. M. Light, and E. Wheeler. "Effects of variations in design parameters of ultrasonic transducers on performance characteristics." *Ultrasonics*, vol. 26, no. 2 (March 1988): pp. 65–72.
61. ANSI/IEEE Std. 176-1978: IEEE Standard on Piezoelectricity.
62. Coffey, J. M., and R. K. Chapman. "Description and application of elastic scattering theory for smooth flat cracks to the quantitative prediction of ultrasonic defect detection and sizing." CEGB-UK, Report SSD83-0056-R, May 1983.
63. McGrath, B. A., R. K. Chapman, and I. Einav. "A study of changes in ultrasonic probe performance due to the thickness of the couplant layer." *12th WCNDT*, Amsterdam, 1988.
64. Gruber, J. G. "Defect identification and sizing by the ultrasonic satellite pulse technique." SwRI, USA, 1979.
65. Chapman, R. K. "Code of practice on the assessment of defect measurement errors in the ultrasonic NDT of welds." CEGB, UK, Report STN-87-2013-R, July 1987.
66. DGZfP [German Society for Non-Destructive Testing]. "Ultrasonic testing of clad, dissimilar and austenitic welds." [In German.] 1995.
67. EUR 15786 EN: IIW Handbook on the Ultrasonic Examination of Austenitic Clad Steel Components. Joint Research Centre, 1994.
68. Gardner, W. E., ed. *Improving the Effectiveness and Reliability of Non-Destructive Testing*. Chapters 4 and 8. Oxford; New York: Pergamon Press, 1992.
69. Silk, M. G., A. M. Stoneham, and J. A. G. Temple. *The reliability of non-destructive inspection: assessing the assessment of structures under stress*. Bristol, UK: Adam Hilger, 1987.

## Olympus and R/D Tech<sup>1</sup> Manuals and Technical Documents

70. Olympus. *TomoView: User's Manual — Software Version 2.20*. Olympus document number DMTA-20077-01EN. Québec: Olympus, Jan. 2015.
71. Olympus. *TomoView: Advanced User's Manual — Software Version 2.20*. Olympus document number DMTA-20078-01EN. Québec: Olympus, Jan. 2015.
72. R/D Tech. "Technical Documentation Guidelines for TomoView 1.4R9." R/D Tech, Jan. 2001.
73. R/D Tech. "Advanced Training in TomoView 2.2R9." R/D Tech, May 2003.
74. Olympus. *Tomoscan FOCUS: User's Manual*. Olympus document number DUMG004C. Québec, Olympus, November 2002.
75. R/D Tech. *Tomoscan III PA: User's Manual*. R/D Tech document number DUMG049A. Québec: R/D Tech, Aug. 2002.
76. R/D Tech. *TomoView 2: Reference Manual*. Vol. 1, *General Features — Setup and Data Acquisition*. R/D Tech document number DUML039A. Québec: R/D Tech, July 2003.
77. R/D Tech. *TomoView 2: Reference Manual*. Vol. 2, *Analysis and Reporting*. R/D Tech document number DUML040A. Québec: R/D Tech, July 2003.
78. RD Tech. *MPSU-01: User's Manual*. R/D Tech document number DUMG065A. Québec: R/D Tech, Aug. 2003.
79. R/D Tech. "TomoView 2.2 — Technical Documentation — Technician Training." Slide presentation, rev. A. R/D Tech, May 2002.
80. Olympus. *MCDU-02: User's Manual*. Olympus document number DUMG017B. Québec: Olympus, July 2008.
81. R/D Tech. "Phased Array Simulation Software—PASS v. 2.3." R/D Tech, 1998.
82. Olympus. *OmniScan MX and MX2: User's Manual*. Olympus document number DMTA-20015-01EN. Québec: Olympus, September 2015.
83. R/D Tech. TechDocE\_Features\_TomoView2\_revA. R/D Tech, July 2003.
84. R/D Tech. TechDocE\_TomoView22R9\_Guidelines\_revA. R/D Tech, July 2003.

## R/D Tech Technical Papers [Single or Co-author and Presented to Conferences, Workshops, and Seminars]

85. Moles, M., F. Jacques, and N. Dubé. "Linear Weld Inspections Using Ultrasonic Phased Arrays."
86. Selman, J. J., J. T. Miller, M. Moles, O. Dupuis, and P. Herzog. "A Novel Fastener Hole Inspection Method Using an Ultrasonic Phased Array Probe."
87. Dubé, N., A. Lamarre, and F. Mainguy. "Dynamic Depth Focusing Board for Nondestructive Testing: Characterization and Applications."
88. Lamarre, A., N. Dubé, P. Ciorau, and B. Bevins. "Feasibility study of ultrasonic inspection using phased array of ABB L-0 blade root."

---

1. Editor's note at fourth printing: R/D Tech operated at the time of first printing; it was later acquired by Olympus and now operates under the new name.

89. Moles, M., N. Dubé, and E. Ginzel. "Ultrasonic Phased Arrays for Pipeline Girth Weld Inspections."
90. Maes, G., and M. Delaide. "Improved UT Inspection Capability on Austenitic Materials Using Low-Frequency TRL Phased Array Transducers."
91. Lafontaine, G., and F. Cancre. "Potential of UT Phased Arrays for Faster, Better, and Lower Cost Inspections."
92. Moles, M., N. Dubé, and F. Jacques. "Ultrasonic Phased Arrays for Thick Section Weld Inspections."
93. Moles, M. "Phased Arrays for Linear Weld Inspections."
94. Dubé, N., F. Moriera, and R. Stanley. "Phased Arrays for Improved Inspection of Coiled Tubing."
95. Delaide, M., G. Maes, and D. Verspeelt. "Design and Application of Low-Frequency Twin Side-by-Side Phased Array Transducers for Improved UT Capability on Cast Stainless Steel Components."
96. Lamarre, A., M. Moles, and F. Cancre. "Use of state-of-the art phased-array ultrasound for the inspection of Friction Stir Welds (FSW)."
97. Pasquer, V., and T. Stepinski. "Ultrasonic Array Technique for Inspection of Copper Canisters for Nuclear Waste Fuel."
98. R/D Tech. "Ultrasound Phased Array." *The e-Journal of Nondestructive Testing*, vol. 7, no. 5 (May 2004). NDTnet, <http://www.ndt.net/v07n05.htm>.
99. Banchet, J., R. Sicard, D. E. Zellouf, and A. Chahbaz. "Phased Array Techniques and Split Spectrum Processing for Inspection of Thick Titanium Casting Components."
100. Langlois, P., P. Ciorau, and D. Macgillivray. "Technical Assessment and Field Application of Portable 16-pulser Phased Array Instrument."
101. Moles, M., F. Cancre, and N. Dubé. "Alternative Sizing Technique Using Ultrasonic Phased Arrays and Zone Discrimination."
102. Cancre, F., and M. Moles. "New Generation of Multi-dimensional Arrays and Their Applications."
103. Moles, M., F. Cancre, and N. Dubé. "Ultrasonic Phased Arrays for Weld Inspections."
104. Rager, K. "Repeatable Characterization for Industrial Phased Array Transducers."
105. Ciorau, P., D. Macgillivray, D. Jansen, N. Dubé, and A. Lamarre. "Reference Blocks and Reflectors Used in Ultrasonic Examination of Steel Components." Part 1 and part 2.
106. Maes, G. "High Performance Pipe Weld Inspection Using State-of-the-Art Phased Array UT Equipment and Methodology."
107. Cancre, F., and M. Dennis. "Effect of the Number of Damaged Elements on the Performance of an Array Probe."
108. Jacques, F., F. Moreau, and E. Ginzel. "Ultrasonic backscatter sizing using phased array-developments in tip diffraction flaw sizing." *Insight*, vol. 45, no. 11 (Nov. 2003): pp. 724–728.
109. Batra, N. K., and F. Cancre. "Measurement of Depth of Oriented Corrosion Pitting Holes in Steel Plates through Ultrasonic Phased Array Imaging."

110. Lamarre, A., J. Gauthier, M. A. Zaidi, and A. Agarwal. "New Developments of the Ultrasonic Phased-Array for the Inspection of Thick Titanium Casting Structural Parts." Aeromat 2002, Orlando.

## **EPRI Turbine Workshops**

111. EPRI. Proceedings, 5th EPRI Steam Turbine/Generator Workshop, Florida, USA, August 1997.
112. EPRI. Proceedings, 6th EPRI Steam Turbine/Generator Workshop, St. Luis, USA, August, 1999.
113. EPRI. Proceedings, 7th EPRI Steam Turbine/Generator Workshop, Baltimore, USA, August 2001.
114. EPRI. Proceedings, 8th EPRI Steam Turbine/Generator Workshop, Nashville, USA, August 2003.

## **EPRI International NDE Conferences**

115. EPRI. Proceedings, 1st Int. NDE Conf., Amsterdam, Netherland, Oct. 1998.
116. EPRI. Proceedings, 2nd Int. NDE Conf., New Orleans, USA, May 2000.
117. EPRI. Proceedings, 3rd Int. NDE Conf., Seville, Spain, Nov. 2001.

## **European and World Conferences**

118. ECNDT. Proceedings, 6th European Conference on Nondestructive Testing, Nice, France, 1994.
119. ECNDT. Proceedings, 7th European Conference on Nondestructive Testing, Copenhagen, Denmark, 1998.
120. ECNDT Proceedings 8th European Conference on Nondestructive Testing, Barcelona, Spain, 2002.
121. ICNDT. Proceedings, 14th World Conference on Nondestructive Testing, New Delphi, India, 1996.
122. ICNDT. Proceedings, 15th World Conference on Nondestructive Testing, Rome, Italy, 2000.



---

# List of Figures

---

## 1. Basic Concepts of Phased Array Ultrasonic Technology

Figure 1-1	Detection of misoriented cracks by monocrystal ( <i>left</i> ) and multielement probes ( <i>right</i> ). The beam is divergent and unidirectional for the monocrystal probe, while it is focused and multiangled for the phased array probe. Cracks of most orientations can be detected by the phased array probe. ....	10
Figure 1-2	Beam forming and time delay for pulsing and receiving multiple beams (same phase and amplitude). ....	11
Figure 1-3	Beam focusing principle for (a) normal and (b) angled incidences. ....	11
Figure 1-4	Electronic scanning with normal beam (virtual probe aperture = 16 elements). ....	12
Figure 1-5	Delay values ( <i>left</i> ) and depth scanning principles ( <i>right</i> ) for a 32-element linear array probe focusing at 15-mm, 30-mm, and 60-mm longitudinal waves. Direct contact, no angled wedge. ....	13
Figure 1-6	Delay dependence on pitch size for the same focal depth. ....	14
Figure 1-7	Example of delay dependence on refracted angle and element position for a phased array probe on a 37° Plexiglas wedge ( $H_1 = 5$ mm). ....	14
Figure 1-8	Example of delay dependence on generated angle, and element position and focal depth for a probe with no wedge (longitudinal waves, refracted angle in steel: 15–60°). ....	15
Figure 1-9	Basic components of a phased array system and their interconnectivity. ....	16
Figure 1-10	Detection of four side-drilled holes (SDH): (a) sectorial scanning principle; (b) S-scan view using $\pm 30^\circ$ . ....	17
Figure 1-11	Advanced imaging of artificial defects using merged data: defects and scanning pattern ( <i>top</i> ); merged B-scan display ( <i>bottom</i> ). ....	17
Figure 1-12	Detection and sizing of misoriented defects by a combination of longitudinal wave (1) and shear wave sectorial scans (2). ....	18
Figure 1-13	Discrimination (resolution) of cluster holes: (a) top view (C-scan); (b) side view (B-scan). ....	18
Figure 1-14	Multiple scan patterns and merged data to show potential imaging	

	techniques for defects. ....	19
Figure 1-15	Multiple scan patterns and merged data to show potential imaging techniques for defects. ....	20

## 2. Main Formulas and Ultrasonic Reference Data

Figure 2-1	Examples of propagation for spherical (point source) and cylindrical (line source) waves. ....	29
Figure 2-2	Possible events from longitudinal and shear wave reflection/refraction in steel, with different interfaces (2nd medium) [red line is LW; blue line is SW]: (1) LW at normal incidence steel-air; (2) LW at 29° steel-air; (3) LW at 61° steel-air; (4) LW on the wedge-steel; (5) LW from steel to the wedge; (6) LW at first critical angle 1; (7) LW at second critical angle 2; (8) LW generating creeping waves; (9) SW at normal incidence (honey/viscose resin as couplant) steel-air; (10) SW at 29° steel-air; (11) SW at 61° steel-air. ....	31
Figure 2-3	Reflection and transmission coefficients for immersion ( <i>left</i> ) and direct contact (wedge) [ <i>right</i> ], taking the couplant layer into account. ....	32
Figure 2-4	Relationship between the amplitudes of two signals. ....	33
Figure 2-5	Graph representation between amplitude ratio and dB value. Example for 40% of FSH vs. 100% of FSH; $\Delta G = -8$ dB. ....	33
Figure 2-6	Snell's law for a Rexolite wedge on mild steel. ....	34
Figure 2-7	Snell's law for a Plexiglas wedge on mild steel. ....	35
Figure 2-8	Snell's law for immersion–mild steel. ....	35
Figure 2-9	Snell's law for water-aluminum. ....	36
Figure 2-10	Velocity variation in a Plexiglas wedge in relation to temperature. ....	37
Figure 2-11	Velocity variation in water and heavy water in relation to temperature. ....	37
Figure 2-12	Velocity variation of longitudinal waves in steel in relation to temperature. ....	38
Figure 2-13	Velocity variation of shear waves in steel in relation to temperature. ....	38
Figure 2-14	Sound region definition in xz plane for a circular probe ( <i>top</i> ) and the pressure variation on the acoustic axis with distance ( <i>bottom</i> ) [disc-shaped transducer under continuous and constant excitation]. Note that this figure is for a theoretical monofrequency crystal with a sinusoidal pulse. ....	40
Figure 2-15	Sound pressure dependence on pulse shape (duration) excitation for plane disc-shaped crystal. <sup>3</sup> ....	41
Figure 2-16	Effective probe diameter and effective near-field length given by refraction law on planar and curved surfaces. ....	42
Figure 2-17	Dependence of effective near-field length on refracted angle;	

	longitudinal waves refracted from a $0^\circ$ to $60^\circ$ range. ....	43
Figure 2-18	Isometric ( <i>top</i> ), top view isobars display ( <i>middle</i> ), and cross section of sound pressure in the near field ( <i>bottom</i> ) from a circular probe. ....	45
Figure 2-19	Normalized amplitude dependence on divergence angle ( <i>top</i> ) and beam diameter dependence on distance and dB drop of normalized amplitude for a circular probe ( <i>bottom</i> ). ....	47
Figure 2-20	6 dB half-angle beam spread for longitudinal waves in carbon steel. ....	48
Figure 2-21	Beam divergence and shape for a rectangular probe. ....	49
Figure 2-22	Near-field length correction factor for a rectangular probe. <sup>9</sup> ....	51
Figure 2-23	Lateral resolution discrimination of two adjacent defects: (a) probe movement; (b) echo dynamics of two defects; (c) ultrasonic data to resolve volumetric defects (same depth and same angle of detection) spaced apart by a distance of less than 1 mm. ....	52
Figure 2-24	Examples of focusing the ultrasonic beam: (a) concave lens ( $v_1 > v_2$ ); (b) concave mirror in water; (c) with a wedge and a concave lens for angled beam; (d) convex lens ( $v_1 < v_2$ ); (e) concave crystal; (f) conical lens. <sup>7,8</sup> Note that axion lenses do not make a point focal spot. ....	52
Figure 2-25	Dependence of $S_{opt}$ on $S_{ac}$ for $0.2 \leq F_{ac} / N_0 \leq 0.8$ . ....	55
Figure 2-26	Definition of focal depth and depth of field (focal length). ....	55
Figure 2-27	Dependence of depth of field on acoustic focusing factor. ....	56
Figure 2-28	Increased sensitivity for an annular array probe (spherical focused) with $D_{probe} / \lambda = 15$ in detecting small inclusions with diameter of less than 1 mm in titanium billets. ....	57
Figure 2-29	RF signal characteristics: (a) $V_{pp} = 700$ mV; (b) $\Sigma\tau_{-20\text{ dB}} = 3.25$ $\mu\text{s}$ ; (c) peak number PN = 10; (d) cycle number CN = 5; (e) damping factor $k_A = 1.4$ . ....	58
Figure 2-30	FFT response of a 5-MHz phased array probe; $f_c = (2.539 + 7.813)$ MHz / 2 = 5.2 MHz; $BW_{rel} = (7.813 - 2.539)$ MHz / 5.2 MHz $\times$ 100% = 54%. ....	59
Figure 2-31	Probe classification based on relative bandwidth. ....	60
Figure 2-32	Axial resolution: principle ( <i>left</i> ); poor and good resolution ( <i>right</i> ). ....	61
Figure 2-33	Definition of the detectability region. ....	63
Figure 2-34	SNR evaluation for TCG feature. SNR typically should be greater than 3:1 (10 dB). ....	64
Figure 2-35	The most commonly used reflectors for sensitivity setting. ....	64
Figure 2-36	Amplitude dependence on normalized defect size for: sphere; FBH; SDH-SW; N-LW; N-SW; N-Cr. ....	66
Figure 2-37	Attenuation dependence on frequency for glycerin/Hamikleer and Rexolite. ....	67

Figure 2-38	Attenuation in 2.25 Cr-Mo steel for longitudinal waves. ....	67
Figure 2-39	Attenuation in steel for shear waves. ....	68
Figure 2-40	Principle of TOFD and the phase sign of four major signals. The defect is assumed to be symmetrically located between the probes. The phase of each RF signal is marked with “+” and “-”. ....	71
Figure 2-41	Detection and sizing of a lack of fusion by TOFD D-scan. Phase reversal of upper and lower defect edges is displayed in gray levels. ....	72
Figure 2-42	TOFD dead zones due to lateral waves and backwall. Dead zone size depends on frequency, pulse length, probe center separation, material thickness, and velocity. Errors can occur with TOFD if the defect is not symmetrically placed between the two probes. ....	73
Figure 2-43	TOFD errors in lateral location and upper ligament caused by the TOF locus of L-waves. ....	74
Figure 2-44	TOFD imaging of defects in weld. ....	77
Figure 2-45	RATT crack height evaluation based on relative measurement of ultrasound path between crack tip and crack corner trap signals. ....	78
Figure 2-46	RF display of the crack tip by direct and skip beam. ....	79
Figure 2-47	Crack height factor for RATT and a sizing example. ....	79
Figure 2-48	Crack height measurement principle using AATT. ....	80
Figure 2-49	Example of AATT sizing of a fatigue crack with phased array probe in static position and beam sweeping over the crack: (a) principle; (b) sizing a 7.1 mm crack with the skip tip; (c) sizing a $H_{\text{crack}} = 10.2$ mm crack; $H_{\text{AATT}} = 9.9$ mm. ....	81
Figure 2-50	Detection of inner surface-breaking cracks using MC techniques. ....	82
Figure 2-51	Techniques for detection of outside and inner surface-breaking cracks using mode conversion. ....	82
Figure 2-52	Detection of embedded linear defects using MC techniques. ....	83
Figure 2-53	Type of waves generated by “creeper” probe. ....	84
Figure 2-54	Ultrasound path dependence on thickness for CE 1 (30°-70°-70°) and for CE 2 (creeping waves). ....	84
Figure 2-55	Detection, confirmation, and sizing of a fatigue crack by LL doublet and CE 1 (30°-70°-70°) for a 60° LW probe; <i>left</i> = crack signals; <i>right</i> = EDM notch signals; ligament = 5 mm; height = 11 mm. ....	85
Figure 2-56	Principle of $\Delta 60^\circ$ technique and an example of ID-connected crack sizing; note the crack tip detection by skip. ....	86
Figure 2-57	Detection of four vertical FBH with a phased array pitch-and-catch mode-converted setup in a 100-mm test piece. Blue lines show shear waves, and red lines show longitudinal waves. ....	86
Figure 2-58	Detection of side lack of fusion in a narrow gap weld by MC techniques with a single ( <i>left</i> ) and double (pitch-and-catch) probe ( <i>right</i> ). ....	87

Figure 2-59	Mode-converted detection and sizing of cylindrical voids; principle ( <i>left</i> ); ultrasonic B-scan display of SDH of $D_{SDH} = 0.6$ mm ( <i>right</i> ). Blue lines show shear waves, and red lines show longitudinal waves. ....	88
Figure 2-60	The relationship between wedge length and part radius. ....	89
Figure 2-61	Ultrasonic examination of an axial weld pipe. ....	89
Figure 2-62	Length sizing of a 2-mm diameter $SDH_{spherical}$ using different dB amplitude drops from echo-dynamic single-peak curves. ....	92

### 3. Probes and Ultrasonic Field Formula

Figure 3-1	The 1-3 composite coordinates according to Smith's theory. <sup>3,5</sup> ..	100
Figure 3-2	Dependence of longitudinal velocity on ceramic concentration. ....	101
Figure 3-3	Acoustic impedance dependence on volume fraction of PZT. ...	102
Figure 3-4	Figure of merit M and quality factor Q dependence on PZT volume for a 1-3 piezocomposite rod of 0.45-mm diameter. ....	102
Figure 3-5	Annular phased array probes of equal Fresnel surfaces. ....	103
Figure 3-6	1-D linear phased array probe. ....	103
Figure 3-7	2-D matrix phased array probe. ....	104
Figure 3-8	1.5-D matrix phased array probe. ....	104
Figure 3-9	Rho-theta (segmented annular) phased array probe. ....	104
Figure 3-10	1-D circular phased array probes ("daisy probes"). ....	105
Figure 3-11	Cluster phased array probe for small diameter pipe/tube inspection showing typical beam angles (R/D Tech U.S. patent 2004/0016299AL). ....	105
Figure 3-12	2-D matrix conical phased array probe (R/D Tech U.S. patent 10-209,298). ....	105
Figure 3-13	Mechanically focused phased array probes: (a) toroidal convex prefocused; (b) annular concave; (c) linear concave; (d) linear convex. ....	106
Figure 3-14	Spherical focusing (1-D depth) pattern and simulation of the beam profile for an annular phased array probe. ....	106
Figure 3-15	Cylindrical focusing pattern (2-D; depth and angle) of linear phased array probe for detecting a SCC at the inner surface and a fatigue crack at mid-wall; simulation of beam profile for both depths. ....	107
Figure 3-16	Spherical/elliptical focusing pattern (3-D solid angle) of segmented annular phased array probe and beam simulation at two depths and two angles. Note the noise increase due to the grating lobes. ....	107
Figure 3-17	Elliptical focusing pattern (3-D solid angle) of 2-D matrix phased array probe and beam simulation for two depths and two angles. ....	108
Figure 3-18	Active and passive aperture. ....	109
Figure 3-19	Effective aperture definition. ....	110

Figure 3-20	Influence of passive aperture width on beam width and shape: (a) deflection principle and beam dimensions; (b) beam shape for $W = 10$ mm; (c) beam shape for $W = 8$ mm, 5 MHz shear wave, pitch $p = 1$ mm; $n = 32$ ; $F = 50$ mm in steel. ....	111
Figure 3-21	Definition of sweep range for direct contact (longitudinal wave) and wedge (shear/longitudinal wave) inspection. ....	113
Figure 3-22	Steering focus power dependence on refracted angle. ....	113
Figure 3-23	Amplitude dependence on steering angle for longitudinal waves in steel ( $-60^\circ$ to $+60^\circ$ )[ <i>left</i> ], and shear waves with a sweep range: $20^\circ$ to $70^\circ$ with a central ray refracted angle of $45^\circ$ ( <i>right</i> ). ....	114
Figure 3-24	Beam length evaluation on FBH placed on a step block. ....	115
Figure 3-25	Beam width dependence on refracted angle and depth. ....	116
Figure 3-26	Types of focusing for linear phased array probe. ....	117
Figure 3-27	Focal range definition for $-6$ dB cutoff (pulse-echo). ....	117
Figure 3-28	The near-surface and far-surface resolution definitions. ....	118
Figure 3-29	Angular resolution and detection of three 0.5-mm SDHs spaced apart by 0.8 mm and 1.2 mm. SDHs are located at $z = 25.7$ mm. Principle (a); angle-corrected true depth (b); and echo dynamic (c). ....	119
Figure 3-30	Directivity plot for a phased array probe: $M$ = main lobe; $S$ = side lobes; $G$ = grating lobes. $\beta_{\text{grating}}$ is shown in orange; the main lobe, in yellow. ....	120
Figure 3-31	Grating lobe dependence on: (a) frequency; (b) pitch size and number of elements (same aperture of 72 mm). ....	121
Figure 3-32	Influence of damping ( $BW_{\text{rel}}$ ) on grating lobes for a 1-MHz probe focusing at $z = 60$ mm (simulation using PASS). ....	122
Figure 3-33	Dynamic depth focusing (DDF): (a) principle-resulting beam by product; (b) comparison between standard phased array focusing ( <i>top</i> ) and DDF on the depth-of-field ( <i>bottom</i> ). Note the detection of two SDHs in the near-surface zone by DDF that are missed by standard phased array focusing. ....	123
Figure 3-34	Beam divergence: (a) principle; (b) longitudinal waves at $0^\circ$ ; (c) comparison between standard phased arrays (SPAF) and DDF. ....	124
Figure 3-35	Wedge elements for computation of wedge delay and index. ...	126
Figure 3-36	Sample plot of migration of the index point with refraction angle for a linear phased array probe. TomoView software compensates for this migration. ....	127
Figure 3-37	Wedge dimensions: (A) length; (B) width; and (C) height. ....	128
Figure 3-38	Beam deflection on the wedge: (a) sectorial/azimuthal; (b) lateral; (c) sectorial/azimuthal with a roof (skewed). ....	129
Figure 3-39	Active ( <i>left</i> ) and passive ( <i>right</i> ) offset definition. ....	130
Figure 3-40	2-D matrix phased array probe and its main features. ....	131
Figure 3-41	Beam simulation for 2-D matrix probe on cylindrical part; <i>left</i> , ray	

	tracing; <i>right</i> , beam profile. ....	131
Figure 3-42	Delay values for a 2-D matrix phased array probe of $8 \times 4$ elements in pulse-echo configuration. ....	132
Figure 3-43	Examples of pitch-and-catch configuration using a 2-D matrix probe on a wedge with a roof: $4 \times 2$ array ( <i>left</i> ) and $6 \times 4$ array ( <i>right</i> ). ....	132
Figure 3-44	Inspection scenario ( <i>left</i> ) and focal laws for annular array probe immersed in 20 mm of water ( <i>right</i> ). ....	133
Figure 3-45	Beam profile of annular array probe from 15 mm to 50 mm in steel ( $F = 40$ mm; beam diameter = 1 mm). ....	134
Figure 3-46	Example of focal law computation for a 2-D matrix probe of $16 \times 4$ elements. ....	135
Figure 3-47	Linear phased array probe characteristics and inspection visualization for a sweep range of $30^\circ$ to $60^\circ$ , resolution of $2^\circ$ , and focusing at 50 mm. ....	135
Figure 3-48	Example of focal law computation for a linear phased array probe on a pipe, $OD \times t = 400$ mm $\times$ 100 mm. ....	136
Figure 3-49	Linear phased array probe characteristics and inspection visualization for a sweep range of $30^\circ$ to $60^\circ$ , resolution of $2^\circ$ , and focusing at 50 mm. ....	136
Figure 3-50	Simulation of pipe weld inspection using ray tracing and S-scans. ....	137
Figure 3-51	Example of PASS simulation for an annular array probe made out of 8 rings—Fresnel zones—that focus from 10 mm to 100 mm ( <i>left</i> ); delay values for two focus depths ( <i>right</i> ). ....	139
Figure 3-52	Recommended value for pulse duration of $1.5 \lambda$ probe. ....	140
Figure 3-53	Sensitivity drop due to contact surface roughness. Couplant: glycerine; reference reflector: SDH with a 2-mm diameter. ....	142
Figure 3-54	Noise increase due to inner surface roughness. Couplant: glycerine. Reference reflector: EDM notch of 12 mm $\times$ 1.5 mm. ....	143
Figure 3-55	Pulsar pulse width dependence on probe center frequency. ....	146
Figure 3-56	Smoothing over the envelope of rectified signal increases the view resolution. ....	147
Figure 3-57	Digitizing frequency: principle ( <i>left</i> ) and the effect of digitizing frequency ratio on amplitude error ( <i>right</i> ). ....	148
Figure 3-58	Compression by a factor of 4:1 of an A-scan. ....	149
Figure 3-59	4:1 breakout box used with multihead inspection. ....	152
Figure 3-60	Example of phased array probe identification. ....	153
Figure 3-61	Different types of phased array probes provided by Olympus. ....	153
Figure 3-62	Directivity (refracted angle) and index point measurement with a curved wedge adapted to the specimen: (a) concave-transverse; (b) convex-transverse (c) concave-longitudinal; (d) convex-longitudinal. ....	157
Figure 3-63	Olympus connector for the OmniScan. ....	158
Figure 3-64	Wedges associated with angle-beam probes. ....	158

Figure 3-65	Different Olympus 1-D linear-array probes: (a) encapsulated wedge angle beam; (b) hard-face direct contact longitudinal waves; (c) immersion (longitudinal waves) and wedge (angle beam); (d) water wedge probe with encoder. ....	160
-------------	--	-----

#### 4. Scanning Patterns and Views

Figure 4-1	Bidirectional ( <i>left</i> ) and unidirectional ( <i>right</i> ) raster scanning. The red line represents the acquisition path. ....	165
Figure 4-2	Linear scan pattern for probe characterization. ....	166
Figure 4-3	Example of skewed (angular) bidirectional scanning. <i>Left</i> : probe scanning pattern versus the mechanical axes on a complex part; <i>right</i> : probe trajectory (red line) is skewed versus mechanical rectangular axes for an optimum angle to detect cracks in stress area. ....	167
Figure 4-4	Helical surface scan on cylindrical parts. The red line is the acquisition path. ....	168
Figure 4-5	Spiral surface scan pattern. The red line is the acquisition path. ....	168
Figure 4-6	Probe position and beam direction related to scan and index axis. Skew angle must be input in the focal law calculator. ....	169
Figure 4-7	Unidirectional sequence of a 200-mm by 200-mm area. Pixel size of the C-scan is of 1 mm by 1 mm. Scanning speed on both axes is 25 mm/s. ....	169
Figure 4-8	Beam electronic scan generating a linear scan pattern. Part and probe are not moving. ....	170
Figure 4-9	Electronic and linear scan of a weld (principle). Index axis (raster scan in conventional UT) is eliminated through electronic scan from the probe arrays, which increases speed and reliability. Note that wedges are usually used. ....	171
Figure 4-10	Generation of a helical scan by a combination of part translation and beam rotation. ....	171
Figure 4-11	Time-base sequence examples: B-scan ( <i>left</i> ) and S-scan ( <i>right</i> ). ..	172
Figure 4-12	Ultrasonic views (B-scan, C-scan, and D-scan). Probe skew angle is 270°. Red indicates the ultrasound axis; blue, the mechanical index axis; and green, the electronic scan axis for a linear scan. ....	173
Figure 4-13	A-scan representation: RF signal ( <i>left</i> ); rectified ( <i>right</i> ). ....	174
Figure 4-14	Example of a color-encoded rectified A-scan signal used to create a color-coded B-scan. ....	175
Figure 4-15	Encoding of RF signal amplitude in gray-scale levels. ....	175
Figure 4-16	Uncorrected B-scan (side view) of component, showing reflector. ....	176
Figure 4-17	Side (B-scan) view corrected for refracted angle. ....	177
Figure 4-18	Example of top (C-scan) view. ....	177
Figure 4-19	Example of end (D) view. ....	178
Figure 4-20	Example of S-scan. ....	179
Figure 4-21	Example of polar view. ....	180

Figure 4-22	Multichannel strip chart display from pipeline AUT (ASTM E-1961-98 code). Display uses both amplitude and TOF data, plus couplant checks, TOFD, and B-scans. ....	181
Figure 4-23	Analysis layout with four views for dissimilar metal weld inspection with low-frequency phased array probes: (a) C-scan; (b) D-scan; (c) B-scan; (d) A-scan. ....	182
Figure 4-24	Single plane projection of end (D) and side (B) views. ....	183
Figure 4-25	Volume projection with linked reference cursors on end (D) and side (B) views. All defects within the gate range are displayed. ....	183
Figure 4-26	Top (a), side (b), and end (c) views, plus waveform (d) and TOFD (e). Weld overlay included in red and blue lines. ....	184
Figure 4-27	General view of TOFD setup for linear weld inspections showing lateral wave, backwall echo, and diffracted signals on the A-scan. ....	185
Figure 4-28	Standard TOFD display, using gray-scale B-scan gated from lateral wave to longitudinal wave backwall. ....	185
Figure 4-29	Recommended combined TOFD and pulse-echo technique to optimize detection from each technique. ....	187
Figure 4-30	Customized layout for TOFD and phased-array pulse-echo inspection of pipeline and pressure vessel welds. Data is plotted on a specific weld profile. ....	188
Figure 4-31	Olympus TomoView Cube ( <i>left</i> ), and showing all faces ( <i>right</i> ). .	189

## 5. Applications

Figure 5-1	Omniscan PA portable instrument. ....	195
Figure 5-2	Tomoscan FOCUS instrument. ....	195
Figure 5-3	Tomoscan III PA instrument. ....	196
Figure 5-4	QuickScan PA instrument. ....	196
Figure 5-5	Examples of different types of scanners manufactured by Olympus: (a) ROVER for pressure vessels; (b) PS 12-X pipe scanner; (c) "beetle" scanner; (d) rotor disc scanner. ....	197
Figure 5-6	Olympus Tomoscan III PA ( <i>left</i> ) and QuickScan PA ( <i>right</i> ). These show the instruments in a typical configuration and installation. ....	198
Figure 5-7	Hypertronics BQUS002 connector for pulse-echo setups ( <i>left</i> ) and BQUS009 connector for pitch-and-catch setups ( <i>right</i> ). ....	199
Figure 5-8	S-scan display for checking the pulser/receivers functionality: normal ( <i>left</i> ); malfunctioning pulsers and receivers (white strips, <i>right</i> ). (Standard Olympus array acceptance procedure.) ....	199
Figure 5-9	Linear scanning for element/electrical connection integrity: (a) principle; (b) focal laws for a 32-element probe; (c) S-scan display of a linear phased array probe with 10 "dead" elements; (d) uncorrected S-scan using linear array. ....	200
Figure 5-10	Example of ray tracing and data plotting of phased array inspection on nozzle weld. ....	201

Figure 5-11	Five-MHz annular array ( <i>top</i> ) and rho-theta probe ( <i>bottom</i> ) used for titanium billet inspection. ....	202
Figure 5-12	Reference blocks from titanium billets with FBH ( <i>left</i> ) and hard-alpha inclusions ( <i>right</i> ). ....	203
Figure 5-13	Unprocessed phased array results on titanium reference blocks on: (a) FBH and (b) hard-alpha. (c) Data processing using cut spectrum processing algorithm. ....	204
Figure 5-14	Immersion testing with a rho-theta probe on titanium billets. ..	204
Figure 5-15	Electronic scanning of aluminum friction stir weld: welding principle ( <i>top</i> ); focused beams for scanning the weld ( <i>bottom</i> ). ..	206
Figure 5-16	Crack image detected in the weld root with a 2-D weld overlay for imaging. ....	207
Figure 5-17	Tomoscan FOCUS 32:128, MCDU-02 driver, and computer enclosed in an air-conditioned cabinet ( <i>left</i> ); water recirculation system ( <i>right</i> ). ....	207
Figure 5-18	Special adapter ( <i>left</i> ) and linear phased array probe with a local immersion fixture ( <i>right</i> ). ....	208
Figure 5-19	Phased array system in production inspecting FSW. ....	208
Figure 5-20	Detection of faying surface defect ( <i>left</i> ) and kissing bond ( <i>right</i> ). ....	209
Figure 5-21	Faying surface corner cracks in fastener of two sizes: small head / thick skin ( <i>left</i> ); large head / thin skin ( <i>right</i> ). ....	209
Figure 5-22	Conical matrix phased array probe design: isometric beam ( <i>left</i> ); tangential detection of the crack in the fastener hole ( <i>right</i> ). ....	210
Figure 5-23	Photo of conical matrix array probe, also known as “hair dryer” ( <i>left</i> ); ultrasonic data from 0.75 mm EDM notch ( <i>right</i> ). ....	211
Figure 5-24	Phased array system including two QuickScan PA units. ....	211
Figure 5-25	Portable OmniScan PA system used for inspection of landing gears. ....	212
Figure 5-26	Phased array system for corrosion mapping of lap joints ( <i>left</i> ) and C-scan display of different degrees of corrosion ( <i>right</i> ). ....	213
Figure 5-27	Macrostructure of a dissimilar metal weld. ....	214
Figure 5-28	Location of EDM notches in reference block ( <i>top</i> ) and scanning modes ( <i>bottom</i> ). ....	215
Figure 5-29	Detection capability of all notches (merged view). ....	215
Figure 5-30	Detection and notch sizing in dissimilar metal welds. Length accuracy is $\pm 3$ mm. Height accuracy is $\pm 0.3$ mm. ....	216
Figure 5-31	Notch detection in the buttering; SNR = 18 dB. ....	216
Figure 5-32	Pipe scanner ( <i>left</i> ) with two phased array probes and laser centering device ( <i>right</i> ). ....	217
Figure 5-33	Carbon steel weld profile ( <i>top</i> ) and beam simulation for phased array ultrasonics ( <i>bottom</i> ). ....	218
Figure 5-34	Example of defect detection, imaging and sizing in a 30-cm (12-inch) diameter pipe. ....	218
Figure 5-35	Beam simulation for phased array inspection of narrow	

	gap-weld. ....	220
Figure 5-36	Detection and height sizing of reference reflectors. ....	220
Figure 5-37	Inspection principle of inner radius and weld of pressure vessel nozzle. ....	221
Figure 5-38	Waterproof TRL phased array probes for pressure vessel nozzle. ....	222
Figure 5-39	Phased array data of EDM notches in the mock-up: merged scans ( <i>left</i> ) and cylindrical corrected view ( <i>right</i> ). ....	222
Figure 5-40	Phased array detection of fatigue cracks in CANDU feeder tubes: scanning setup ( <i>left</i> ) and crack detection ( <i>right</i> ). ....	223
Figure 5-41	Feeder crack sizing with TOFD technique. ....	223
Figure 5-42	Phased array inspection of welded rotor. ....	224
Figure 5-43	Phased array inspection of bore and anti-rotation key of low-pressure turbine rotor: phased array principle ( <i>top</i> ) and field scanning ( <i>bottom</i> ). ....	225
Figure 5-44	Phased array boresonic inspection ( <i>top</i> ) and ultrasonic data presentation in polar view ( <i>bottom</i> ). ....	226
Figure 5-45	Plotting phased array data in L-0 blade 2-D layout ( <i>left</i> ) and OmniScan detection and sizing of 9 mm × 0.5 mm EDM notch on hook 1 L-0 steeple ( <i>right</i> ). ....	227
Figure 5-46	Detection and sizing principle for L-1 steeple: hook 1 (a) and (b); typical display (c); inspection with multiple phased array systems: Tomoscan FOCUS (d), OmniScan (e), and Tomoscan III (f). ....	228
Figure 5-47	Phased array scanning pattern ( <i>left</i> ) and 10-MHz phased array probe of 32 elements on mock-up ( <i>right</i> ). ....	229
Figure 5-48	Skip crack signals ( <i>left</i> ) and shadowing effect on geometric signals ( <i>right</i> ). ....	229
Figure 5-49	Phased array inspection of blade root (axial entry): (a) ray tracing; (b) ultrasonic techniques; and (c) ultrasonic data plotted on 2-D specimen overlay. ....	230
Figure 5-50	Schematic showing conventional raster scanning ( <i>left</i> ), and phased array linear scanning ( <i>right</i> ). The array on the right uses electronic scanning (or electronic rastering) and linear scanning to give full weld coverage and code compliance. ....	232
Figure 5-51	Schematic showing two different angle inspections using phased arrays and electronic scanning. The same array also performs TOFD. ....	232
Figure 5-52	Photo of an HST-X03 scanner. This unit contains conventional and TOFD transducers, but can also use phased arrays. ....	234
Figure 5-53	Pressure vessel weld inspection by a combination of pulse echo and TOFD. ....	235
Figure 5-54	Tomoscan III inspection system for major pressure vessel inspections. ....	236
Figure 5-55	Display of zone discrimination weld inspection using TomoView (see section 5.8). ....	236

Figure 5-56	Typical “top, side, end” view of weld with weld overlay showing precise location of defects. ....	237
Figure 5-57	“Top, side, TOFD” view of weld. This example uses merged data in the C-scan and B-scan, and twin TOFD pairs for improved defect detection and sizing. ....	237
Figure 5-58	Schematic showing layout of arrays for PV-300 premium pressure vessel inspection system. ....	239
Figure 5-59	Photos of PV-300 probe pan ( <i>left</i> ), and cabinet containing three Tomoscan FOCUS or Tomoscan III systems, EC array instrumentation, and coupling system ( <i>right</i> ). ....	239
Figure 5-60	Example of rotating vessel for phased array inspection of pressure vessels under construction using a fixed head containing two linear arrays with linear and electronic scanning. ....	240
Figure 5-61	Pipeline welding band and probe pan. This pan contains two well-protected linear phased array probes and can significantly outperform competing multiprobe technologies. ....	240
Figure 5-62	Magnetic wheel scanner performing a linear weld scan using two arrays in pulse echo and TOFD. This scanner (TRAKER) follows a magnetic strip, and can inspect nozzles and complex components as well. ....	241
Figure 5-63	Hand scanner for weld inspections. This version contains either phased arrays or multiple conventional transducers (see “Rapid Detection TECHnique” in section 4.2.10, p. 186, and “PV-100” in section 5.7.2, p. 233). ....	242
Figure 5-64	Schematic showing robot inspecting complex curved vessel. Probe pan holds two arrays for pulse echo and TOFD. ....	242
Figure 5-65	Single (or double) array with encoder, the semiautomated solution. This is the simplest and cheapest solution for linear scanning using phased arrays. ....	243
Figure 5-66	Schematic of zone discrimination concept showing slicing of CRC-Evans weld into zones with correctly angled and focused beams to detect LoF and other defects. ....	244
Figure 5-67	Typical pipeline AUT calibration block, with flat-bottomed holes for each zone, upstream and downstream. ....	245
Figure 5-68	Calibration display from FBHs. Each strip displays one zone, upstream and downstream, so the weld is essentially “opened out.” The gray B-scan is the TOFD; the blue channels are volumetric B-scans to detect porosity. ....	245
Figure 5-69	Zone discrimination display from pipelines. Above-threshold defects are in red, while coupling and low-level signals are in green. Real-time readout provides defect location, position, and length. ....	246
Figure 5-70	PipeWIZARD phased array system showing instrumentation box (computer, Tomoscan FOCUS, driver box), 21-in. monitor, and keyboard. ....	246

Figure 5-71	Phased array probe pan containing two well-protected linear arrays. Umbilical contains the 128 micro-coaxial cables, power, encoder, and water line for coupling. ....	247
Figure 5-72	Automated setup procedure for pipeline or general weld phased arrays. Operator inputs weld profile via AutoCAD or drawing, and phased array system calculates focal laws and setup. ....	247
Figure 5-73	Beam-splitting. Additional zones can be added using phased arrays to improve coverage and sizing. This advantage is unique to phased arrays, as the number of available channels limits multiple probes. (PipeWIZARD can use up to 128 individual channels.)	248
Figure 5-74	Results comparing AUT, radiography, and manual ultrasonics from one pipeline study. Detection by AUT is much better than either radiography or manual ultrasonics due to focused beams and appropriately oriented inspection angles. ....	248
Figure 5-75	Ray tracing beam paths for nominal, maximum, and minimum walls. Note that predicted beams will miss defects if the wrong wall thickness view is analyzed. ....	249
Figure 5-76	Phased array display from nominal wall setup showing defect (arrow). This was an unacceptable defect. Note that TOFD detected the defect in all three views, but only this view found the defect in pulse echo. ....	250
Figure 5-77	Ray tracing showing extra beams in root to improve detection and sizing. ....	251
Figure 5-78	Ray tracing showing extra beams in cap area. ....	251
Figure 5-79	Ray tracing showing additional beams in mid-wall region to detect any shrinkage cracking. ....	251
Figure 5-80	Photo of ring-type scanner for pipes 2.5 in. to 16 in. (63 mm to 400 mm) in diameter. ....	252
Figure 5-81	Photo of typical orbital scanner head with two gimbal arrays visible. Scanner clamps on pipe and arrays rotate around them. ....	253
Figure 5-82	Photo of scanner clamped onto boiler tubes during construction inspection. ....	254
Figure 5-83	Inspection of pipe welds in a refinery with an OmniScan: on site ( <i>left</i> ); OmniScan with S-scan display ( <i>right</i> ). ....	255
Figure 5-84	Phased array inspection of coiled tube seam weld: principle ( <i>top</i> ) and industrial system ( <i>bottom</i> ). ....	256
Figure 5-85	Phased array data display with software algorithm for internal geometry weld echo removal ( <i>left</i> ); online ultrasonic display ( <i>right</i> ). ....	256
Figure 5-86	Inspecting T-welds using an OmniScan and a manually encoded array. Inspection procedure ( <i>top</i> ); field inspection ( <i>bottom</i> ). ....	257
Figure 5-87	Phased array inspection of ERW pipes: principle, probe, and weld wander. ....	260
Figure 5-88	Phased array industrial system for ERW pipe ( <i>top</i> ) and parameter	

	adjustment ( <i>bottom</i> ). .....	261
Figure 5-89	Phased array solution for in-line rod inspection (0° LW and SW angle beam inspection). .....	264
Figure 5-90	Phased array system for in-line bar inspection. ....	265
Figure 5-91	Examples of phased array inspection results for in-line bar inspection. ....	266
Figure 5-92	Phased array inspection of tubes with six linear phased array probes for longitudinal defects. ....	267
Figure 5-93	Phased array principle for detecting transverse defects ( <i>left</i> ), two types of cluster probes ( <i>middle</i> ), and multihead assembly for pipe inspection ( <i>right</i> ). ....	268
Figure 5-94	Dimensional gauging with eight conventional probes. ....	269
Figure 5-95	Phased array inspection of tubes (pass-through, <i>top</i> ) and pipes (rotating, <i>bottom</i> ). ....	270
Figure 5-96	Phased array inspection of electron beam weld between the copper canister and the lid: principle and the probe ( <i>top</i> ), results on reference block ( <i>bottom</i> ). ....	271
Figure 5-97	Photo of circular forging being inspected by phased arrays. ....	272
Figure 5-98	Axle inspection with wheels on using multiple phased array probes ( <i>top</i> ); with restricted access, single phased array probe ( <i>bottom</i> ). ....	273
Figure 5-99	Rail inspection with phased array probe: principle ( <i>left</i> ); data plotted on overlay ( <i>right</i> ). ....	274
Figure 5-100	Phased array detection of transverse cracks (a) with pitch-and-catch linear scanning – 8 elements (b) over a 60-element probe; beam width = 1.2 mm. Sizing is possible using different displays [see (c) and (d)]. ....	274
Figure 5-101	Phased array zones for automated wheel inspection. ....	276
Figure 5-102	Phased array automated inspection of train wheel for <i>in-situ</i> or shop-floor maintenance. ....	276
Figure 5-103	Automated calibration example. ....	277
Figure 5-104	Cross section of T-weld showing geometry and weld. ....	278
Figure 5-105	S-scan display of T-weld showing crack with peaked A-scan (the blue line in the S-scan corresponds to the A-scan and signal in red gate). ....	279
Figure 5-106	Typical S-scan of butt weld, showing lack of fusion defects. ....	280
Figure 5-107	Twin SW wedges with low-profile scanner for weld inspections. ....	281
Figure 5-108	Typical A-scan, S-scan, and C-scan display showing 1.5 mm calibration hole. ....	281
Figure 5-109	HIC with no visible stepwise cracking (no SOHIC). ....	282
Figure 5-110	HIC with visible SOHIC. ....	282
Figure 5-111	Schematic showing flange gasket with area to be scanned ( <i>left</i> ), and bolt locations and limited access ( <i>right</i> ). ....	284
Figure 5-112	A-scan, B-scan, and corrected B-scan displays of corrosion	

	mapping. ....	284
Figure 5-113	Drawing showing munition tail and mock-up of probe on custom wedge. ....	285
Figure 5-114	Cross section through shaft showing double threading. ....	285
Figure 5-115	B-scan of threads showing correct threading. ....	286
Figure 5-116	Spindle and true depth (or volume-corrected) S-scan display with known reflectors ( <i>top</i> ) and cracking location ( <i>bottom</i> ). ....	287
Figure 5-117	Normal beam scan of aluminum laser weld with water box. ....	288
Figure 5-118	Photo of composite specimen for inspection. ....	289
Figure 5-119	Scan results from composite specimen. Good sample showing backwall ( <i>top</i> ); near-surface defect obscures backwall ( <i>bottom</i> ). Visible on C-scan. ....	290
Figure 5-120	Schematic of composite T-joint, showing areas of interest. ....	291
Figure 5-121	Photo of linear array used for T-joint inspection. ....	291
Figure 5-122	A-scan, B-scan, and C-scan of T-joint inspection ( <i>left</i> ), and reference defect in T-joint ( <i>right</i> ). ....	291
Figure 5-123	Schematic showing typical defects in blade root area ( <i>right</i> ) and B-scan results ( <i>left</i> ). ....	292
Figure 5-124	S-scan of nozzle, showing bottom surface, corner, and smooth end surface. ....	293
Figure 5-125	S-scans showing eroded corner. The image on the right is a zoomed image. ....	294
Figure 5-126	Photo of array scanning compressor blade and reference notch. ....	295
Figure 5-127	+25° S-scan of compressor blade showing P-cut and notch. ....	295
Figure 5-128	Ray tracing of austenitic weld at 45° and 75°. ....	296
Figure 5-129	S-scan images of notches in 20-mm stainless steel, showing corner trap signal (red cursor) and notch tip (blue cursor). The notches are 20% (a), 30% (b), 40% (c), and 50% (d). ....	296

## 6. Conclusions and Recommendations

### Appendix: Unit Conversion



---

# List of Tables

---

## 1. Basic Concepts of Phased Array Ultrasonic Technology

### 2. Main Formulas and Ultrasonic Reference Data

Table 2-1	Velocities and acoustic impedance for frequently used and tested materials at 20°C. ....	25
Table 2-2	Wavelengths for the most commonly used couplants, wedges, and materials in industrial ultrasonic inspection at 20°C. ....	27
Table 2-3	Near-field length for circular crystals (in millimeters). ....	43
Table 2-4	Half-angle beam divergence constant: $\gamma_{-D \text{ dB}} = \arcsin(k\lambda/D_{\text{probe}})$ . .	46
Table 2-5	Beam spread of disc-shaped and rectangular-shaped probes. ....	47
Table 2-6	Reflectivity pattern for small reference reflectors. ....	65
Table 2-7	Example of source of errors; results are from CEGB [UK], after a 6-year experimental program during 1980's. <sup>15,16</sup> .....	93

### 3. Probes and Ultrasonic Field Formula

Table 3-1	Main properties of commonly used piezoelectric materials. <sup>1,7</sup> .....	97
Table 3-2	Values of $d_{33}$ $g_{33}$ for different combinations between PZT and polymer resins. <sup>1</sup> .....	99
Table 3-3	Typical phased array probes widely available. ....	103
Table 3-4	Probe classification overview. ....	137
Table 3-5	Generic ultrasonic settings for a phased array instrument. ....	144
Table 3-6	Inspection sequence features (example). ....	150
Table 3-7	Focal laws and probe parameters (example). ....	151
Table 3-8	Practical tolerances on phased array probe features. ....	155
Table 3-9	Equivalent half-path distance for TOF (probe/wedge delay). ....	156

### 4. Scanning Patterns and Views

Table 4-1	Scanning patterns for automated and semiautomated inspections. ....	164
Table 4-2	Inspection sequence dependence on part, scanner, and beam. ....	170

## **5. Applications**

Table 5-1	Technical performance of Olympus phased array instruments. ....	197
Table 5-2	Phased array sizing capability* on 30-cm (12-inch) carbon steel pipe weld. ....	219

## **6. Conclusions and Recommendations**

Table 6-1	Overview of phased array solutions. ....	300
-----------	--	-----

## **Appendix: Unit Conversion**

Table A-1	Conversion from metric to English units. ....	305
-----------	---	-----

---

# Index

---

## Numerics

2-D matrix phased array probes 130  
8-bit data 150  
1.5-D matrix phased array probe 104  
12-bit data 150  
1-3 structure, piezocomposite 99  
1-D circular phased array probes 105  
1-D linear phased array probe 103  
2-D matrix conical phased array probe 105  
  figure 211  
2-D matrix phased array probe 104  
2-D matrix probe 137

## A

AATT (absolute arrival time technique) 80  
abbreviations 307  
absolute arrival time technique (AATT) 80  
acoustic impedance 25  
acquisition rate 149  
acronyms 307  
active aperture 108, 128  
  effective 109  
  minimum 110  
active axis offset 129  
advantages of DDF 124  
advantages of phased arrays 299  
aerospace 201, 213  
  composite inspection 288  
  inspection of titanium billets 201  
  laser weld inspection 287  
  T-joint composite inspection 290  
aircraft fuselage 213  
amplitude, grating lobe 121  
amplitude, peak-to-peak 58  
angle, skew 169  
angle, theta 168

angular resolution 119  
angular scan sequence 166  
angular scanning 12  
annular concave probe 106  
annular phased array probes 103  
annular probe 137  
  figure 202  
aperture  
  active 108  
  effective active 109  
  minimum active 110  
  passive 110  
aperture, active 128  
aperture, passive 128  
API (application program interface) 261  
API 5LCP code 255  
API 5LX code 258  
API 1104 283  
API 5L code 231  
apodization, beam 121  
appendixes  
  unit conversion 305  
application program interface (API) 261  
applications 193  
applications, miscellaneous 254  
  bridge structure 257  
  in-service inspection of pipe 254  
  offshore petrochemical applications 255  
applications, portable PA 277  
  austenitic weld inspection 280  
  austenitic welds 295  
  butt weld inspection 279  
  composites 288  
  compressor blade 294  
  corrosion under gasket 283  
  hydrogen-induced cracking (HIC) 281

- laser welds 287
- nozzles 292
- spindles 286
- threads 284
- tie-ins for pipeline welds 283
- T-joint composite 290
- T-joint inspection 278
- turbine blade roots 292
- array size, small 299
- arrays, linear 108
- A-scan 174
- ASME code 231
- ASME Code Case 2235 231
- ASME TOFD 231
- ASME XI code 301
- assessment, engineering critical 2
- ASTM 273 code 255
- ASTM E-1961 code 231
- ASTM E-1961-98 code 181, 244
- attenuation 30, 66
- attenuation curve (ATTN) 61
- ATTN (attenuation curve) 61
- austenitic weld inspection 295
- austenitic weld inspection (small diameter) 280
- AUT (automated ultrasonic testing) 243
- automated inspection 163
- automated ultrasonic testing (AUT) 243
- averaging 148
- axial resolution 118
- axion lenses 53
- axis offset
  - active 129
  - passive 129
- axle, inspection of 272
- azimuthal (or sectorial) deflection on the wedge 128
- azimuthal scan (S-scan) 178
- azimuthal scanning 12

**B**

- backing material 98
- backwall (BW) 61
- backwall reflection 69
- band-pass filters 145
- bars, volumetric PA inspection 261
- basic components of phased array system 16
- basic concepts of phased array ultrasonic technology 9
  - basic scanning and imaging 16
  - basic system components 16
  - delay laws, or focal laws 13
  - principles 9
- basic scanning and imaging 16
- beam
  - apodization 121
  - deflection on the wedge 127
    - azimuthal (or sectorial) deflection 128
    - lateral deflection 128
    - skew deflection 128
  - directions 169
  - divergence 46
    - DDF 123
  - focused 299
  - length 114
  - width 115
- beam focusing principle 11
- beam scanning patterns 12
  - DDF (dynamic depth focusing) 12
  - electronic scanning 12
  - sectorial scanning 12
- beetle scanner 197
- Bessel's function 44
- bidirectional sequence 164
- billets, inspection of titanium 201
- blade inspection, compressor 294
- blade root inspection, turbine 292
- blade roots 229
- blade roots, detection and sizing of
  - fatigue/SCC cracks 229
- boiling water reactor 1
- boresonic inspection 225
- bridge structure 257
- BS7706:1993 code 231
- B-scan 176
- B-scan, electronic 16
- butt weld inspection 279
- BW (backwall) 61
- BWR (boiling water reactor) 1
- BWR core shroud 214

**C**

- calculator, focal law 133
- CANDU feeder tube cracking 222
  - inspection 222
- CE (collateral echo)
  - no. 1 84

- no. 2 84
- ceramic inclusions 201
- characteristics of phased array ultrasonic technology 2
- characterization, probe 153
  - curved wedges 156
  - tolerances 155
- chart, strip 180
- checking
  - equipment 198
  - integrity 199
  - periodic 153
- circular phased array probe, 1-D 105
- circular surfaces 168
- circular transducers 39
- classification of phased array probes 137
- classification, probe 59
- cluster phased array probe 105
- CN (cycle number) 58
- codes
  - API 5LCP 255
  - API 5LX 258
  - API 5L 231
  - ASME 231
  - ASME Code Case 2235 74
  - ASME XI 301
  - ASTM 273 255
  - ASTM E-1961 231
  - ASTM E-1961-98 181, 244
  - BS7706:1993 231
  - CSA 662 258
  - ENV 583-6 231
  - line scanning codes 231
  - pressure vessels, inspection codes for 231
- collateral echo
  - no. 1 84
  - no. 2 84
- color encoding 174
- combined strip charts 187
- combined TOFD and pulse-echo technique 186
- compensation, gain 114
- complex inspections 299
- component testing
  - spindle inspection 286
  - thread inspection 284
- components of phased array system 16
- composite inspection 288
- compression 148
- compression (longitudinal) wave type 23
- compressor blade inspection 294
- computer-controlled excitation 9
- concave crystal 53
- concave lens 52
- concave mirror 52
- concave/convex lens 52
- conclusions and recommendations 299
  - advantages of phased arrays 299
  - implementing phased array technology 302
  - phased array solutions to inspection problems 300
- conical lens 53
- conical phased array probe, 2-D 105
  - figure 211
- connector, OmniScan 158
- construction weld, pressure vessel
  - inspection 230
  - inspection codes 231
  - mechanics 239
  - PV-100 system 233
  - PV-200 system 235
  - PV-300 system 237
- construction welding
  - butt weld inspection 279
  - T-joint inspection 278
- conversion, unit 305
- convex lens 52
- co-phasal plane wave 29
- copper canister weld, inspection of 270
- core shroud, BWR 214
- corrosion mapping 213
- corrosion under gasket 283
- cracking, CANDU feeder tube 222
- cracking, hydrogen-induced (HIC) 281
- cracking, stress corrosion (SCC)
  - detection
    - in low-pressure turbine rotor 224
    - in welded or single block rotor 224
  - detection and sizing
    - in blade roots 229
    - in disc rim-blade attachment 228
    - in low-pressure turbine components 226
    - in rotor body 225
- cracks, detection of misoriented 10
- CRC-Evans weld 244

- creeper probe 83
  - creeping (head) wave type 23
  - creeping-wave technique 83
  - critical assessment, engineering 2
  - cross talk, phased array probe 138
  - crystal, piezoelectric 48
  - crystals
    - concave 53
    - curved 52
  - CSA 662 code 258
  - C-scan 177
  - CSP (cut-spectrum processing) 301
  - Cube, TomoView 188
  - curve, attenuation (ATTN) 61
  - curved crystals 52
  - curved wedges 156
  - cut-spectrum processing (CSP) 301
  - cycle number (CN) 58
  - cylindrical surfaces 167
  - cylindrical waves, sound pressure formula 29
- D**
- daisy probes 105
  - damping factor 58
  - data
    - 8-bit 150
    - 12-bit 150
  - data file size 151
  - data plotting 200
  - data, ultrasonic reference 23
  - DDF (dynamic depth focusing) 12, 57, 122
    - advantages 124
    - beam divergence 123
  - dead zone 118
  - defect sizing 68, 299
    - AATT (absolute arrival time technique) 80
    - MC (mode-converted) techniques 81
    - pitch-and-catch technique 86
    - RATT (relative arrival time technique) 78
    - satellite pulse-echo technique 87
    - tandem technique 86
    - TOFD (time-of-flight diffraction) 68
  - defects, measuring the lengths of small 90
  - definitions of ultrasonics 23
  - deflection on the wedge, beam 127
    - azimuthal (or sectorial) deflection 128
    - lateral deflection 128
    - skew deflection 128
  - delay laws 13
  - delay, wedge 125
  - delta technique 85
  - density, mass ( $\rho$ ) 24
  - depth of field 117
  - depth, focal 116
  - design, probe 139
    - physics guidelines 140
    - practical guidelines 143
  - detectability region 61
  - detection and sizing of SCC
    - blade roots 229
    - disc rim-blade attachment 228
    - low-pressure turbine components 226
    - rotor body 225
  - detection of misoriented cracks 10
  - detection of SCC
    - low-pressure turbine rotor 224
    - welded or single block rotor 224
  - DGS 62
  - diffracted (edge) wave type 24
  - diffraction 30
  - diffuse scattering 66
  - digitalization 150
  - digitizing frequency 147
  - dimensions, small probe 2
  - directions, beam 169
  - disc rim-blade attachment, detection and sizing of SCC in 228
  - discrimination, zone 243
  - dispersion 30
  - divergence, beam 46
    - DDF 123
  - doublet, LL 85
  - D-scan 178
  - duration, pulse 58
  - dynamic depth focusing (DDF) 12, 57, 122
    - advantages 124
    - beam divergence 123
- E**
- $E$  (modulus of elasticity) 24
  - EC (eddy current) arrays 238
  - ECA (engineering critical assessment) 233
  - echo, collateral
    - no. 1 84
    - no. 2 84
  - eddy current arrays 238

- edge (diffracted) wave type 24
- EDM (electrical discharged machining) 33
- effective active aperture 109
- 8-bit data 150
- electronic B-scan 16
- electronic setups 2
- element gap 112
- element size, maximum 112
- element width 112
- elementary pitch 111
- encoders
  - index-axis 167, 168
  - scan-axis 167, 168
- encoding, color 174
- end view 172
- energy 213
- engineering critical assessment 2
- engineering critical assessment (ECA) 233
- ENV 583-6 code 231
- equipment checking 198
- ERW (electric-resistance-welded) pipes 258
- example of temperature effects 39
- excitation, computer-controlled 9

## F

- factor, damping 58
- far-field zone 39
- far-surface resolution 118
- fast Fourier transform (FFT) 58
- fastener holes, inspection of 209
- FastFOCUS 210
- FBH (flat-bottomed hole) 62, 64
- features, phased array probe 138
  - cross talk 138
  - impedance 138
  - sensitivity 138
- feeder tube cracking, CANDU 222
- FEM (finite element model) 99
- Fermat's principle 13
- Fermat-surface phased array probe 226
- FFT (fast Fourier transform) 58
- field, depth 117
- fields, focused sound 51
- files
  - .mn 138
  - RDTIFF file format 198
  - setup file 150
- filters
  - band-pass 145

- smoothing 146
- finite element model (FEM) 99
- fitness for purpose 2
- flange corrosion under gasket 283
- flat-bottomed hole (FBH) 62, 64
- flexibility, setup 2, 299
- focal depth 116
- focal laws 13
  - calculator 133
- focal length 117
- focal range 117
- focus power, steering 113
- FOCUS, Tomoscan 194
  - figure 195
- FOCUS, Tomoscan *See* Tomoscan FOCUS
- focused beam 299
- focused sound fields 51
- focusing principle, beam 11
- forgings, inspection of heavy 272
- format, RDTIFF file 198
- formulas 23
  - longitudinal, transverse, and surface waves 24
  - sound pressure 29
    - cylindrical waves 29
    - spherical waves 29
  - ultrasonic field 97
- Fraunhofer region 51
- free running inspection 163
- frequency, digitizing 147
- Fresnel region 51
- Fresnel zones 202
- friction stir welds, inspection of 205
- FSH (full screen height) 33
- FSW (friction stir welds) 205
- full-body pipe, inspection of 266
- function, Bessel's 44
- fuselage, aircraft 213

## G

- gain compensation 114
- gain, useful 62
- gap, element 112
- gasket, corrosion under 283
- gear, landing 211
- girth welds, pipe 249
- glossary 307
- grating lobes 120
  - amplitude 121

guided (Lamb) wave type 24  
guidelines for probe design 139  
  physics 140  
  practical 143

## H

hard-alpha inclusions 201, 203  
hard-alpha particles 203  
HAZ (heat-affected zone) 216  
head (creeping) wave type 23  
heat-affected zone (HAZ) 216  
heavy forgings, inspection of 272  
helical sequence 167  
HIC (hydrogen-induced cracking) 281  
holes  
  flat-bottomed (FBH) 64  
  side-drilled (SDH) 64  
  spherical-bottomed 65  
holes, fastener 209  
HST-X03 scanner 234  
hydrogen-induced cracking (HIC) 281

## I

ID, probe 143, 152  
ID, wedge 143  
identification, probe 152  
imaging, basic scanning and 16  
impedance, acoustic 25  
impedance, phased array probe 138  
implementing phased array technology  
  302  
inclusion, ceramic 201  
inclusions, hard-alpha 201, 203  
index point length 126  
index point migration 127  
index-axis encoder 167, 168  
industrial applications, phased array  
  probes for 103  
in-service inspection of pipe 254  
inspection  
  automated 163  
  blade roots 229  
  boresonic 225  
  bridge structure 257  
  BWR core shroud 214  
  CANDU feeder tube cracking 222  
  coiled tubing 255  
  complex inspections 299  
  disc rim-blade attachment 228

fastener holes 209  
friction stir welds 205  
landing gear 211  
low-pressure turbine components 226  
low-pressure turbine rotor 224  
manual (or free running) 163  
mills and manufacturing 258  
  bars 261  
  copper canister weld 270  
  ERW pipes 258  
  full-body pipe 266  
  heavy forgings 272  
miscellaneous applications 254  
pipe welds 216  
pipeline phased arrays 243  
piping weld 219  
portable PA applications 277  
  austenitic welds 295  
  butt weld 279  
  composites 288  
  compressor blade 294  
  corrosion under gasket 283  
  hydrogen-induced cracking (HIC) 281  
  laser welds 287  
  nozzles 292  
  small diameter austenitic welds 280  
  spindles 286  
  threads 284  
  tie-ins for pipeline welds 283  
  T-joint composite 290  
  T-joints 278  
  turbine blade roots 292  
pressure vessel construction weld 230  
railroad transportation 272  
  rail 273  
  wheel 274  
reactor vessel nozzle-to-shell weld 220  
reliability of ultrasonic ~ 92  
rotor body 225  
semiautomated 163  
titanium billets 201  
turbine rotor 224  
  welded or single block rotor 224  
inspection codes for pressure vessels 231  
instruments, phased array 194  
instruments, R/D Tech 194  
integrity checking 199  
interaction, ultrasonic beam 61  
interference 30

introduction 1

## J

joints, lap 213

## K

kerf 112

KLM model 98, 138

## L

Lamb (guided) wave type 24

landing gear, inspection of 211

lap joints 213

laser weld inspection 287

lateral deflection on the wedge 128

lateral resolution 118

lateral wave (TOFD) 69

law, Snell's 30, 125

laws, delay 13

laws, focal 13

layer and cable requirements, matching 98

layouts 181

top, side, and end views 184

lead zirconate titanate (PZT) 99

length, beam 114

length, focal 117

length, index point 126

length, waveform 58

lens, concave/convex 52

lenses

axion 53

concave 52

conical 53

convex 52

life assessment/disposition-inspection

interval strategy 2

limitations

TOFD 72

line scanning codes 231

linear arrays 108

linear concave probe 106

linear convex probe 106

linear phased array probe, 1-D 103

linear scan sequence 165

linear scanning 69

linear scanning using TOFD and PE 233

linear-array probe 111

LL doublet 85

lobes

grating 120

amplitude 121

main 119

side 119

longitudinal (compression) wave type 23

formula 23

L-waves 24

## M

$\mu$  (Poisson's ratio) 24

main lobe 119

manual inspection 163

manufacture, piezocomposite 99

manufacturing, mills and 258

mapping, corrosion 213

mass density ( $\rho$ ) 24

matching layer and cable requirements 98

material, backing 98

materials, piezocomposite 48, 97

matrix conical phased array probe, 2-D 105

figure 211

matrix phased array probe, 1.5-D 104

matrix phased array probe, 2-D 104

maximum element size 112

MC (mode-converted) techniques 81

MCDU-02 206

measuring the lengths of small defects 90

mechanical reliability 299

mechanically focused phased array probes

106

annular concave 106

linear concave 106

linear convex 106

toroidal convex 106

mechanics, pressure vessel 239

$\mu$ Tomoscan 186

migration, index point 127

mills and manufacturing 258

bar inspection 261

copper canister inspection weld 270

ERW pipe inspection 258

full-body pipe inspection 266

heavy forging inspection 272

minimum active aperture 110

mirrors 52

concave 52

misoriented cracks, detection of 10

.mnp files 138

mode-conversion 30

- mode-converted techniques 81
- model, KLM 98, 138
- modulus of elasticity ( $E$ ) 24
- modulus, Young's ( $E$ ) 24
- motor control drive unit (MCDU-02) 206
- MPSU-01 217
- multiple views 181
  - top, side, and end views 184
- N**
- NDE (nondestructive evaluation) 1
- NDT (nondestructive testing) 1
- near-field zone 39
- near-surface resolution (NSR) 61, 118
- NOISE 62
- noise level 62
- nondestructive evaluation (NDE) 1
- nondestructive testing (NDT) 1
- nozzle inspection 292
- NSR (near-surface resolution) 61, 118
- number, cycle (CN) 58
- number, peak (PN) 58
- O**
- offset
  - active axis 129
  - passive axis 129
- offshore petrochemical applications 255
- OmniScan 3, 145, 163, 194, 212, 223, 227, 234, 253, 257, 283, 286
  - connector 158
  - figure 195
  - probes 157
- P**
- parameters, TomoView ultrasonic 144
- particles, hard-alpha 203
- parts, testing round 88
- PASS (phased array simulation software) 138, 227
- passive aperture 110, 128
- passive axis offset 129
- PATT (pulse arrival time technique) 80
- patterns, beam scanning 12
  - DDF (dynamic depth focusing) 12
  - electronic 12
  - sectorial 12
- patterns, scanning 163
- PCS (probe center separation) 69
- PE (pulse-echo) technique 186
- peak number (PN) 58
- peak-to-peak amplitude 58
- periodic checking 153
- petrochemical applications, offshore 255
- petrochemical industry, nozzle inspection 292
- phased array instruments 194
- phased array probes
  - 1.5-D matrix 104
  - 1-D circular 105
  - 1-D linear 103
  - 2-D matrix 104, 130
  - 2-D matrix conical 105
    - figure 211
  - annular 103
  - classification 137
  - cluster 105
  - daisy 105
  - features 138
  - for industrial applications 103
  - mechanically focused 106
  - rho-theta 104
- phased array simulation software (PASS) 138
- phased array solutions to inspection problems 300
- phased array system
  - basic components 16
- phased array ultrasonic technology
  - basic concepts 9
  - basic scanning and imaging 16
  - basic system components 16
  - characteristics 2
  - delay laws, or focal laws 13
  - implementing 302
  - principles 9
- phased arrays, advantages of 299
- physics guidelines for probe design 140
- physics of ultrasonics, definitions 23
- piezocomposites
  - description 99
  - manufacture 99
  - materials 48, 97
  - PZT (lead zirconate titanate) 99
- piezoelectric crystal 48
- pipe girth welds 249
- pipe welds, inspection of 216
- pipe, full-body 266

- pipeline inspection
  - in-service inspection for SCC 254
  - phased arrays 243
  - pipe girth welds 249
  - risers and tendons 250
  - small diameter piping 252
  - zone discrimination 243
- pipeline welds, tie-ins 283
- pipes, ERW 258
- PipeWIZARD 163, 252
  - figure 246
  - probe design 112
- piping weld, inspection of 219
- piping, small diameter 252
- pitch, elementary 111
- pitch-and-catch mode
  - TOFD 68
- pitch-and-catch technique 86
- pixel 177
- plan circular probe 137
- plan linear probe 137
- plotting, data 200
- PN (peak number) 58
- PoD (probability of detection), TOFD 186
- point length, index 126
- point migration, index 127
- Poisson's ratio ( $\mu$ ) 24
- polar view 179
- polarization 30
- portable PA applications 277
  - austenitic weld inspection 280
  - austenitic welds 295
  - butt weld inspection 279
  - composites 288
  - compressor blade 294
  - corrosion under gasket 283
  - hydrogen-induced cracking (HIC) 281
  - laser welds 287
  - nozzles 292
  - spindles 286
  - threads 284
  - tie-ins for pipeline welds 283
  - T-joint composite 290
  - T-joint inspection 278
  - turbine blade roots 292
- position, rho 168
- power generation
  - inspection problems 1
  - turbine blade root inspection 292
- power supply, MPSU-01 217
- power, steering focus 113
- practical guidelines for probe design 143
- pressure formulas, sound 29
- pressure vessel construction weld
  - inspection 230
  - inspection codes 231
  - mechanics 239
  - PV-100 system 233
  - PV-200 system 235
  - PV-300 system 237
- pressurized water reactor 1
- PRF (pulse repetition frequency) 149
- principle, beam focusing 11
- principle, Fermat's 13
- probe center separation (PCS) 69
- probe design
  - physics guidelines 140
  - practical guidelines 143
- probe dimensions, small 2
- probe on the wedge 125
- probes 97
  - characterization 153
    - curved wedges 156
    - tolerances 155
  - classification 59
  - creeper 83
  - design 139
  - ID 143
  - identification 152
  - linear-array 111
  - OmniScan 157
  - rectangular 48
  - skew angle 169
- probes, phased array
  - 1.5-D matrix 104
  - 1-D circular 105
  - 1-D linear 103
  - 2-D matrix 104, 130, 137
  - 2-D matrix conical 105
    - figure 211
  - annular 103, 137
    - figure 202
  - classification 137
  - cluster 105
  - daisy 105
  - features 138
  - for industrial applications 103
  - mechanically focused 106

- plan circular 137
- plan linear 137
- rho-theta 104, 137
  - figure 202
- properties, ultrasonic wave *See* wave properties, ultrasonic
- PS 12 scanner 219
- PS 12-X scanner 197, 217
- pulse arrival time technique (PATT) 80
- pulse duration 58
- pulse repetition frequency (PRF) 149
- pulse width 145
- pulse-echo (PE) technique 186
- pulse-echo technique, satellite 87
- PV-100 system 233
- PV-200 system 235
- PV-300 system 237
- PWR (pressurized water reactor) 1
- PZT (lead zirconate titanate) 99

## Q

- QuickScan PA 163, 194, 210, 259, 260, 275, 300
  - figure 196

## R

- $\rho$  (mass density) 24
- R/D Tech instruments 194
- radio frequency (RF) 57
- rail inspection 273
- railroad transportation 272
  - axle inspection 272
  - rail inspection 273
  - wheel inspection 274
- range, focal 117
- range, sweep 112
- rapid detection technique (RDTECH) 186
- raster scanning 69
- rate, acquisition 149
- rate, repetition 149
- ratio, Poisson's ( $\mu$ ) 24
- RATT (relative arrival time technique) 78
- ray tracing 200
- Rayleigh (surface) wave type 23
- Rayleigh scattering 66
- RDTECH (rapid detection technique) 186
- RDTIFF file format 198
- reactor vessel nozzle-to-shell weld,
  - inspection of 220

- reactor, boiling water 1
- reactor, pressurized water 1
- recommendations, conclusions and 299
  - advantages of phased arrays 299
  - implementing phased array technology 302
  - phased array solutions to inspection problems 300
- rectangular probes 48
- reference data, ultrasonic 23
- reflected wave (TOFD) 69
- reflection 30
- refraction 30
- region, detectability 61
- region, Fraunhofer 51
- region, Fresnel 51
- relative arrival time technique (RATT) 78
- reliability of ultrasonic inspection 92
- reliability, mechanical 299
- repetition rate 149
- requirements, layer and cable 98
- resolution
  - angular 119
  - axial 118
  - lateral 118
- resolution, far-surface 118
- resolution, near-surface (NSR) 61, 118
- response, time-frequency 57
- RF (radio frequency) 57
- rho position 168
- rho-theta phased array probe 104
- rho-theta probe 137
  - figure 202
- risers 250
- rotor disc scanner 197
- rotor inspection
  - low-pressure turbine rotor 224
  - rotor body 225
  - welded or single block rotor 224
- round parts, testing 88
- ROVER 197, 206

## S

- satellite pulse observation time technique (SPOT) 78
- satellite pulse-echo technique 87
- scan, sectorial (S-scan) 16
- scan-axis encoder 167, 168
- scanners

- HST-X03 234
- PS 12 219
- PS 12-X 197, 217
- ROVER 206
- TRAKER 236
- scanning and imaging, basic 16
- scanning patterns 163
  - angular 166
  - beam directions 169
  - bidirectional 164
  - helical 167
  - linear 69
  - linear scan 165
  - raster 69
  - skewed 166
  - spiral 168
  - time-base 171
  - unidirectional 164
  - others 170
- scanning patterns, beam 12
  - DDF (dynamic depth focusing) 12
  - electronic 12
  - sectorial 12
- scanning speed 2, 299
- scattering
  - diffuse 66
  - Rayleigh 66
  - stochastic 66
- SCC (stress corrosion cracking) 2
  - detection and sizing in blade roots 229
  - detection and sizing in disc rim-blade attachment 228
  - detection and sizing in low-pressure turbine components 226
  - detection and sizing in rotor body 225
  - detection in low-pressure turbine rotor 224
  - detection in welded or single block rotor 224
  - in-service inspection of pipe 254
- SDH (side-drilled hole) 64
- seam weld inspection of coiled tubing 255
- sectorial (or azimuthal) deflection 128
- sectorial scan (S-scan) 16, 178
- semiautomated inspection 163
- sensitivity, phased array probe 138
- sequences
  - angular scan 166
  - bidirectional 164
  - helical 167
  - linear scan 165
  - skewed scan 166
  - spiral 168
  - time-base scanning 171
  - unidirectional 164
  - others 170
- setup file 150
- setup flexibility 2, 299
- setup, ultrasonic 144
  - acquisition rate 149
  - averaging 148
  - band-pass filters 145
  - compression 148
  - data file size 151
  - digitalization 150
  - digitizing frequency 147
  - pulse width 145
  - repetition rate 149
  - setup file 150
  - smoothing 146
- setups, electronic 2
- shear (transverse) wave type 23
- shroud, BWR core 214
- side lobes 119
- side view 172
- side-drilled hole (SDH) 64
- signal-to-noise ratio (SNR)
  - definition 63
  - requirement to improve 1
  - size, data file 151
  - size, maximum element 112
  - size, small array 299
- sizing, defect *See* defect sizing
- skew angle 169
- skew deflection on the wedge 128
- skewed scan sequence 166
- small defects, measuring the lengths of 90
- small diameter piping 252
- Smith's theory 99
- smoothing 146
- Snell's law 30, 125
- SNR (signal-to-noise ratio)
  - requirement to improve 1
- SNR (signal-to-noise ration)
  - definition 63
- software
  - PASS 138
  - TomoView 138, 169, 236

SOHIC (stress-oriented hydrogen-induced cracking) 281  
 solutions, phased array 300  
 sound fields, focused 51  
 sound pressure formulas 29  
   cylindrical waves 29  
   spherical waves 29  
 speed, scanning 2, 299  
 spherical waves, sound pressure formula 29  
 spherical-bottomed hole 65  
 spindle inspection 286  
 spiral sequence 168  
 SPOT (satellite pulse observation time technique) 78  
 S-scan 16, 178  
 steering focus power 113  
 stochastic scattering 66  
 stress corrosion cracking (SCC) 2  
   detection and sizing in blade roots 229  
   detection and sizing in disc rim-blade attachment 228  
   detection and sizing in low-pressure turbine components 226  
   detection and sizing in rotor body 225  
   detection in low-pressure turbine rotor 224  
   detection in welded or single block rotor 224  
   in-service inspection of pipe 254  
 stress-oriented hydrogen-induced cracking (SOHIC) 281  
 strip chart 180  
 strip charts, combined 187  
 structure, bridge 257  
 surface (Rayleigh) wave type 23  
   formula 23  
 surfaces  
   circular 168  
   cylindrical 167  
 S-waves 24  
 sweep range 112  
 symbols 307

**T**  
 tandem technique 86  
 TCG (time-of-flight corrected gain) 63  
 techniques  
   AATT (absolute arrival time technique) 80  
   creeping wave 83  
   delta 85  
   mode-converted (MC) 81  
   PATT (pulse arrival time technique) 80  
   pitch-and-catch 86  
   RATT (relative arrival time technique) 78  
   satellite pulse-echo 87  
   SPOT (satellite pulse observation time technique) 78  
   tandem 86  
   TOFD (time-of-flight diffraction) 68  
 temperature effects, example 39  
 tendons 250  
 testing round parts 88  
 theory, Smith's 99  
 theta angle 168  
 thread inspection 284  
 tie-ins for pipeline welds 283  
 time-base scanning 171  
 time-frequency response 57  
 time-of-flight corrected gain (TCG) 63  
 time-of-flight diffraction *See* TOFD (time-of-flight diffraction)  
 tip diffracted wave 69  
 titanium billets, inspection of 201  
 T-joint composite inspection 290  
 T-joint inspection 278  
 TOFD (time-of-flight diffraction) 68, 184  
   ASME 231  
   limitations 72  
   PoD 186  
   principles 69  
   PV-100 system 233  
   PV-200 system 235  
   PV-300 system 237  
   setup 185  
   standard display 185  
   waves  
     backwall reflection 69  
     lateral 69  
     reflected 69  
     tip diffracted wave 69  
 tolerances 155  
 Tomoscan FOCUS 2, 163, 186, 194, 206, 223, 227, 234, 252  
   beam apodization 121  
   figure 195, 246  
 Tomoscan III 163, 229, 234, 235, 252, 300

- figure 196
- Tomoscan III PA 194, 219, 227
- TomoView 127, 138, 169, 236
  - ultrasonic parameters 144
- TomoView Cube 188
- top view 172
- toroidal convex probe 106
- tracing, ray 200
- TRAKER scanner 236
- transducers, circular 39
- transit-field zone 39
- transmitter-receiver L-waves (TRL) 214
- transportation, railroad 272
  - axle inspection 272, 273
  - wheel inspection 274
- transverse (shear) wave type 23
  - formula 23
- TRL (transmitter-receiver L-waves) 214
- tube cracking, CANDU feeder 222
- turbine blade root inspection 292
- turbine inspection: detection and sizing of SCC 226
- turbine rotor 224
- T-weld inspection of bridge structure 257
- 12-bit data 150
- types of waves *See* wave types

## U

- ultrasonic beam interaction 61
- ultrasonic field formula 97
- ultrasonic inspection, reliability of 92
- ultrasonic parameters, TomoView 144
- ultrasonic reference data 23
- ultrasonic setup *See* setup, ultrasonic
- ultrasonic views *See* views, ultrasonic
- ultrasonic wave properties *See* wave properties, ultrasonic
- ultrasonics, definitions 23
- unidirectional sequence 164
- units 307
  - conversion 305
- useful gain 62

## V

- velocities and wavelengths 25
- vessel, reactor 220
- views 163, 172
  - end 172
  - side 172

- top 172
- views, multiple 181
  - top, side, and end views 184
- views, ultrasonic 172
  - A-scan 174
  - B-scan 176
  - combined strip charts 187
  - combined TOFD and pulse-echo 186
  - C-scan 177
  - D-scan 178
  - multiple views 181
  - polar view 179
  - S-scan 178
  - strip chart 180
  - TOFD 184
  - TomoView Cube 188
- volumetric PA inspection of bars 261

## W

- wave properties, ultrasonic 30
  - attenuation 30
  - diffraction 30
  - dispersion 30
  - interference 30
  - mode-conversion 30
  - polarization 30
  - reflection 30
  - refraction 30
- wave types 23
  - creeping (head) 23
  - edge (diffracted) 24
  - formulas 24
  - guided (Lamb) 24
  - longitudinal (compression) 23
  - surface (Rayleigh) 23
  - transverse (shear) 23
- wave, co-phasal plane 29
- waveform length 58
- wavelengths and velocities 25
- waves, TOFD 69
  - backwall reflection 69
  - lateral 69
  - tip diffracted wave 69
- wedge
  - beam deflection on the ~ 127
  - curved 156
  - delay 125
  - ID 143
  - index point length 126

- index point migration 127
- probe on the wedge 125
- welds
  - austenitic welds 295
  - austenitic welds (small diameter) 280
  - copper canister 270
  - CRC-Evans 244
  - friction stir welds 205
  - inspections of coiled tubing 255
  - laser welds 287
  - pipe 216
  - pipe girth welds 249
  - piping 219
  - pressure vessel 230
  - reactor vessel nozzle-to-shell 220
  - tie-ins for pipeline 283
- wheel inspection 274

- width, beam 115
- width, element 112
- width, pulse 145

## **Y**

- Young's modulus ( $E$ ) 24

## **Z**

- zone discrimination 243
- zone, dead 118
- zone, heat-affected (HAZ) 216
- zones
  - far-field 39
  - near-field 39
  - transit-field 39
- zones, Fresnel 202

Introduction to Phased Array Ultrasonic Technology Applications

First edition, fourth printing, published in Waltham, United States of America, January 2017

Legal Deposit, National Library of Canada: August 2004

Produced and distributed by Olympus

